ABSTRACT

Title of Dissertation: HOLOGRAPHIC COSMOLOGICAL MODELS AND THE ADS/CFT CORRESPONDENCE

Stefano Antonini
Doctor of Philosophy, 2023

Dissertation Directed by: Professor Brian Swingle
Department of Physics

The formulation of a quantum theory of gravity is a central open problem in theoretical physics. In recent years, the development of holography—and in particular the Anti-de Sitter/Conformal Field Theory (AdS/CFT) correspondence—provided a new framework to investigate quantum gravity and led to consistent advancement. However, how to describe cosmology within holography remains an unanswered question whose solution could determine whether holography is able to capture physics in our universe.

This dissertation describes a new proposal for embedding cosmological physics in the holographic paradigm. This is articulated in two different but related approaches, both involving time-symmetric Big Bang-Big Crunch cosmologies with negative cosmological constant Λ. In the first approach, the cosmological universe is given by a four-dimensional end-of-the-world brane moving in a five-dimensional AdS black hole spacetime. The proposed holographic dual description is given by a boundary conformal field theory. Under specific conditions, gravity is localized on the brane and effectively four-dimensional: an observer living on the brane is unaware of the

existence of the extra dimension. In this dissertation, I show how these conditions can be met in an AdS-Reissner-Nordström background while retaining a holographic dual description.

The second approach focuses on spatially flat $\Lambda < 0$ cosmologies which analytically continue to Euclidean wormholes connecting two asymptotic AdS boundaries. The proposed dual theory is given by two holographic 3D CFTs coupled by non-holographic 4D degrees of freedom on a strip. A different analytic continuation of the Euclidean wormhole leads to a Lorentzian traversable wormhole. After discussing the general features of these holographic cosmologies, I describe how the traversable wormhole can be reconstructed from the dual theory and how the existence of the former constrains the latter. Finally, I show that these $\Lambda < 0$ cosmologies can undergo phases of accelerated expansion and match observational data for the scale factor evolution.

The results presented in this dissertation should be regarded as the initial steps on a new line of research which will hopefully lead to a description of quantum gravity in a cosmological universe via holography. Achieving this goal would render holography a viable candidate to describe quantum gravity in our universe.

HOLOGRAPHIC COSMOLOGICAL MODELS AND THE ADS/CFT CORRESPONDENCE

by

Stefano Antonini

Dissertation submitted to the Faculty of the Graduate School of the
University of Maryland, College Park in partial fulfillment
of the requirements for the degree of
Doctor of Philosophy
2023

Advisory Committee:
Professor Theodore Jacobson, Chair
Professor Brian Swingle, Research Advisor
Professor Zackaria Chacko
Professor Christopher Jarzynski, Dean's Representative
Professor Raman Sundrum

Acknowledgements

First and foremost, I would like to thank my advisor, Brian Swingle. Besides being a phenomenal physicist from whom I have learned much of what I know as well as the importance of transcending disciplines' boundaries and of recognizing a worthy battle, throughout these five years he has been a constant guide and support both academically and humanly. He suggested research directions and involved me in collaborations while trusting me with complete freedom to develop and pursue my own interests. I could not hope for a better advisor. I owe him very much and I hope we will have the opportunity for many more collaborations in the years to come.

Second, I would like to thank Mark Van Raamsdonk for a very fruitful, enjoyable, and on-going collaboration which propelled much of my research throughout these years. I learned very much from Mark's knowledge, ideas, and physical intuition. I am also grateful to Ted Jacobson, from whom I learned much not only about gravitational physics, but also about scientific rigor, the importance of teaching, and how the wonder for physical phenomena can feed an insatiable curiosity. I wish we had more chances to collaborate. I would also like to thank Giovanni Montani, who has been and will be an excellent collaborator, friend, and model of scientific integrity.

I am very grateful to all my collaborators, from whom I learned much and who made every project a special journey: Greg Bentsen, Charles Cao, Brianna Grado-White, Jonathan Harper, Shao-Kai Jian, Giulia Maniccia, Petar Simidzija, and Chris Waddell. I would also like to thank everyone in Brian's research group for contributing to create the wonderful work (and not only) environment it has been: besides those mentioned above, Chris Baldwin, Gong Cheng, Andrew Guo, Subhayan Sahu, Troy Sewell, Yixu Wang, Christopher White, Mike Winer, Yongchan Yoo, and everyone at Brandeis University.

I am also grateful to everyone in the UMD physics department and particularly in MCFP. A special mention goes to my fellow students and friends Batoul Banihashemi, Gong Cheng, Alireza Parhizkar, Pranav Pulakkat, Rodrigo Silva, and Yixu Wang, with whom I shared this voyage, discussed countless topics, and started friendships that will last for years to come. I would also like to thank Zackaria Chacko, Ted Jacobson, Christopher Jarzynski, and Raman Sundrum for spending the time to be part of my examination committee.

This dissertation would have been an impossible goal to achieve without the personal support and the affection of all the wonderful people around me. First, I would like to thank my family: my parents, my brother Marco Valerio, Elena, Paola, and Annamaria. Their constant, unconditional support and love have been a fundamental and powerful motivation to advance on my path in the last few years.

A special thanks goes also to all my friends back in Italy and scattered around the world, and in particular to Giovanni, Andrea, Simone, Federica, Alessandro, Alessandro, Daniele, Giuseppe, Francesco, Lollo, and Jose. Our friendships have been a stable anchor and an invaluable support in these first few years away from home, and will always be a fixed point in the flow of my life.

The last five years would have not been nearly as enjoyable without the incredible friends I made during my journey: Selu, Adam, Nick, Martin, Christos, Jake, Dhruvit, Zach, Alex, Anisha, Zach, Danny, Eleftheria, and Maytal. It is beautiful and reassuring to know that these have been just the first few steps into each other's lives, and that many more have yet to come.

Last, but not least, I want to thank Grace. She changed the rules of the game the day she entered my life. She has supported (and put up with) me every day with her kindness and love. She constantly inspires me to be a better person. I am very grateful to and for her. I simply can't wait to spend our lives together.

Summary of Research Contributions

The research presented in this dissertation has been conducted in the last few years by me in collaboration with several co-authors (my advisor Prof. Brian Swingle, Prof. Mark Van Raamsdonk, Petar Simidzija, and Chris Waddell), and published in the papers [1–4]. Strictly related research not included in this dissertation is published in the papers [5–10]. In compliance with the guidelines of the University of Maryland and of the Physics Department's Graduate Director, Chapters 2-5 reproduce the main papers in Refs. [1–4] verbatim. The appendices of the same papers [1–4] are reported in Appendices A-D verbatim. The only alterations—which are necessary to uniform Chapters 2-5 and Appendices A-D to the rest of the dissertation—are in the placement of floating objects and in the numbering system of sections, equations, floating objects, and references. I will now report in detail the contributions I made to each chapter of the dissertation.

Chapter 1 contains background material, a review of the two approaches to holographic cosmology, an overview of the results obtained in the rest of the dissertation, and discussion. I am the sole author of this chapter.

Chapter 2 and Appendix A were originally published in Ref. [1]. Both authors contributed to the conceptual development of the paper and to the writing of the main sections of the paper (reported in Chapter 2). I wrote most of Appendix A. I carried out all the analytic and numerical calculations and prepared Figures and Tables.

Chapter 3 and Appendix B were originally published in Ref. [2], which is a conceptual paper with not many explicit calculations. All authors contributed to developing the ideas reported in the paper and to the writing (although I did not write the core of the paper). Besides contributing to the conceptual development of the framework, my main contribution was to carry out calculations and numerical simulations showing the possibility of obtaining phases of accelerated expansion in the $\Lambda < 0$ cosmologies under exam thanks to the presence of rolling scalar fields. This analysis, which is not reported in the paper, is at the basis of the discussion about acceleration in Chapter 3 (which is one of the main novelties of Ref. [2] with respect to previous literature) and served as a starting point to obtain the results presented in Chapter 5.

Chapter 4 and Appendix C were originally published in Ref. [3]. All authors contributed to developing the ideas reported in the paper and to the writing (although the core of the paper was written by me and one other co-author). I conducted the analysis of the bulk gauge field spectrum reported in Sections 4.2.3 and C.1, contributed (equally along with one other co-author) to the development of the wormhole reconstruction algorithm reported in Sections 4.3.2-4.3.4 and C.2-C.3, and carried out the associated numerical analysis reported in Section 4.3.5.

Chapter 5 and Appendix D were originally published in Ref. [4]. All authors contributed to developing the ideas reported in the paper and to the writing. As mentioned above, I conducted the initial analytic and numerical study of examples of accelerating cosmologies (not reported in the paper) that motivated and is at the basis of the analysis in Ref. [4]. I also contributed to finding the necessary conditions the potential must satisfy to support the solutions of interest and carried out the analysis of the example reproducing the flat ΛCDM result reported in Sections 5.2.3 and D.1, although I did not find the explicit form of the potential (5.14)-(5.15).

Chapter 6 contains an overview of the main results, discussion, and a summary of future directions. I am the sole author of this chapter.

Note that in most of this dissertation I use plural pronouns “we/us/our” regardless of whether or not I am the sole author of that given section and/or analysis.

Table of Contents

List of Figures

List of Tables

List of Abbreviations

3D	Three-dimensional
4D	Four-dimensional
5D	Five-dimensional
AAdS	Asymptotically Anti-de Sitter
ADM	Arnowitt-Deser-Misner
AdS	Anti-de Sitter
AdS-RN	Anti-de Sitter-Reissner-Nordström
ANEC	Averaged null energy condition
BAO	Baryon acoustic oscillations
BBN	Big Bang Nucleosynthesis
BCFT	Boundary conformal field theory
BF	Breitenlohner-Freedman
CFT	Conformal field theory
CMB	Cosmic microwave background
CVac	Cosmology from the vacuum
dS	De Sitter
EE	E-mode polarization-E-mode polarization [correlation]
EFT	Effective field theory
ETW	End-of-the-world
FLRW	Friedmann-Lemaître-Robertson-Walker
FRW	Friedmann-Robertson-Walker
GHY	Gibbons-Hawking-York
GKPW	Gubser-Klebanov-Polyakov-Witten
HKLL	Hamilton-Kabat-Lifschytz-Lowe
HRT	Hubeny-Rangamani-Takayanagi
IR	Infrared
JT	Jackiw-Teitelboim
KK	Kaluza-Klein
ΛCDM	Lambda-Cold Dark Matter
LHS	Left hand side
ODE	Ordinary differential equation
QCD	Quantum Chromodynamics
QECC	Quantum error correcting code
QES	Quantum extremal surface
QFT	Quantum field theory
RG	Renormalization group

RHS	Right hand side
RS	Randall-Sundrum
RT	Ryu-Takayanagi
SCFT	Superconformal field theory
SNIa	Type Ia supernova
SUSY	Supersymmetry
SYK	Sachdev-Ye-Kitaev
SYM	Super-Yang-Mills
TE	Temperature-E-mode polarization [cross-correlation]
TFD	Thermofield double
TT	Transverse-traceless
TT (in CMB data)	Temperature-temperature [correlation]
UV	Ultraviolet
wCDM	w-Cold Dark Matter

Chapter 1: Introduction

In this dissertation I will describe the progress made in the last few years by me and my collaborators in developing a new framework to describe cosmology within holography [1–10]. In our work, two different (but related) approaches can be identified, which I will dub the "holographic braneworld cosmology" approach [1, 5] and the "holographic wormhole cosmology" approach [2–4, 7–10]. Both approaches describe a FLRW universe with negative cosmological constant $\Lambda < 0$, which, after an expansion phase, reaches a turning point and recollapses in a time-symmetric fashion. The description of negative Λ cosmologies is a natural first step to embed cosmology within the framework of the AdS/CFT correspondence. Moreover, as we will see, although having a positive cosmological constant is the simplest way to explain the current phase of accelerated expansion of our universe, it is not the only one, and $\Lambda < 0$ cosmologies are not in principle ruled out by current cosmological observations.

In the holographic braneworld cosmology approach, the cosmological universe is described by an end-of-the-world (ETW) brane embedded in a higher dimensional asymptotically AdS black hole spacetime. For the purposes of this paper, the ETW brane can simply be considered a codimension-1 timelike hypersurface on which Robin boundary conditions[1] are imposed and

[1] In the AdS/BCFT literature, see for example [11, 12] and Chapter 2 (published in [1]), the boundary conditions are referred to as "Neumann" rather than "Robin". However, they establish a relationship between the induced metric and its derivative at the location of the brane, and they are therefore more correctly characterized as Robin boundary conditions. In Chapter 2 we refer to them as "Neumann" for consistency with the published article [1].

beyond which the spacetime geometry is cut off. The holographic dual description of the whole spacetime, including the braneworld cosmology, is given in terms of an excited state of a 4D CFT prepared by a Euclidean path integral with a boundary in the Euclidean past where conformal boundary conditions are imposed. A more detailed overview of this approach is reported in Section 1.3.

In the holographic wormhole cosmology approach, we consider a 4D, flat, time-reversal-symmetric Big Bang-Big Crunch cosmology with a negative cosmological constant and, in the same spirit of the constructions of Maldacena and Maoz [13], notice that such spacetimes analytically continue to an asymptotically AdS Euclidean wormhole connecting two AdS boundaries. We then propose a holographic description of the Euclidean wormhole in terms of a pair of 3D holographic CFTs coupled by 4D non-holographic degrees of freedom on an interval, with the full microscopic theory confining in the IR. We also argue that a different analytic continuation of the Euclidean wormhole leads to a Lorentzian traversable wormhole dual to the vacuum state of the confining dual theory. In this second approach, the presence of "rolling" scalar fields is rather natural, as they are associated with (generically non-vanishing) relevant deformations in the Lagrangian of the two 3D CFTs, and can lead to phases of accelerated expansion in the cosmological universe. A more complete overview of this approach is given in Section 1.4, and a detailed analysis is reported in Chapter 3 (originally published in Ref. [2]).

Given that the challenges presented by a holographic description of cosmology are substantial and that our framework has been introduced only recently, the advancement reported here, although promising, should be regarded as just the first few seminal steps into a research program which will hopefully lead in the future to a full holographic quantum gravity theory in a cosmological spacetime. In order to achieve this goal, considerable progress is needed in several directions, including the construction of fully microscopic examples of our setups (which, in a phenomenologically viable realization, must lead to a bulk effective field theory including dark matter and the standard model of particle physics), the ability to reproduce, within our framework, all the phenomenological features observed in cosmological data, and understanding how typical interpretational problems arising in quantum cosmology are settled once a holographic description of the universe is obtained (see Chapter 6 for a more extensive discussion of future directions).

The background material necessary to describe our approach to holographic cosmology is vast, and a full review of it is beyond the scopes of this dissertation. Therefore, I will only give a broad overview of the fields of holography (with particular focus on the AdS/CFT correspondence) and cosmology (along with a brief explanation of the difficulties faced in embedding cosmology within the holographic framework) in Sections 1.1 and 1.2, respectively. In these sections I will not give many technical details, but I will try instead to lay down the main conceptual milestones needed to motivate and explain our work. Along the way, I will refer to the best of my knowledge to the existing literature, where the reader will be able to find any further detail. I will then move on to give an overview of our holographic framework for cosmology and of the results presented in the following chapters. The holographic braneworld cosmology approach—which was first introduced in Ref. [5] and is the subject of Chapter 2 (published in Ref. [1])—is reviewed in Section 1.3, where we also outline the results presented in Chapter 2. The holographic wormhole cosmology approach [2,7–9], which is the subject of Chapter 3 (published in Ref. [2]), is reviewed in Section 1.4. A brief explanation of the relationship between the two approaches can be found in Section 1.5. Section 1.6 outlines the results of Chapter 4 (published in Ref. [3]), which investigates, within the second approach, the relationship between the boundary theory and the Lorentzian traversable wormhole (related to the cosmology by double analytic continuation). Section 1.7 summarizes the results of Chapter 5 (published in Ref. [4]), where we show how cosmologies described by our second approach can undergo phases of accelerated expansion and in principle match the observational data constraining the evolution of the cosmological scale factor. Sections 1.3-1.7 also contain brief reviews of additional background material needed to understand the corresponding chapters. A general discussion of the results, a critical evaluation of the pros and cons of our two approaches, and an overview of future directions in this line of research are reported in Chapter 6. Finally, Appendices A, B, C, and D contain technical details related to Chapters 2, 3, 4, and 5 (and were published as appendices of the respective papers [1], [2], [3], and [4]).

In this dissertation, we work in units such that $\hbar = c = k_B = 1$ (where $\hbar$ is the reduced Planck's constant, c the speed of light, and k_B the Boltzmann constant). When additional choices of units are made throughout the dissertation for simplicity of notation—for example $\epsilon_0 = 1$ with ϵ_0 the vacuum dielectric constant in Chapter 2, or $8\pi G/3 = 1$, with G the Newton's gravitational constant in some sections of Chapter 5—they are explicitly stated.

1.1 Overview of holography and the AdS/CFT correspondence

The formulation of a theory able to reconcile quantum and gravitational physics is one of the prominent open problems in fundamental physics. In the last few decades, the Anti-de Sitter/Conformal Field Theory (AdS/CFT) correspondence has emerged as a promising framework for the description of quantum gravity [14–19]. The introduction of AdS/CFT was preceded by the realization that the entropy of a gravitational system is bounded by the area of its boundary, a discovery dating back to the work of Bekenstein [20–23] and Hawking [24–26][2]. These seminal works suggested that information in gravitational systems is stored in their boundary, an idea that was further developed and formalized in Refs. [30–33] becoming referred to as the "holographic principle". In its modern (and stronger) version, the statement of holography is that a full quantum gravity theory in $d+1$ dimensions is equivalent ("dual") to a non-gravitational[3] quantum theory in d dimensions.

The AdS/CFT correspondence, initially introduced by Maldacena in the context of string theory [14], was the first explicit realization of the holographic principle and it relates a quantum gravity theory in an asymptotically Anti-de Sitter (AAdS) spacetime (the "bulk")[4] to a non-gravitational conformal field theory [41] with one dimension less, which can be thought of as living on the (timelike) AdS conformal boundary, which is a conformal compactification of Minkowski spacetime [16].[5] Anti-de Sitter spacetime is a maximally symmetric, vacuum solution of Einstein's equations in the presence of a negative cosmological constant $\Lambda < 0$, and its metric in the so-called global coordinates (which cover the whole AdS manifold) is given by

$$ds^2 = -(1+\frac{r^2}{L^2})dt^2 + \frac{dr^2}{1+\frac{r^2}{L^2}} + r^2 d\Omega_{d-1}^2 \tag{1.1}$$

[2]See [27] for a covariant generalization of the entropy bound and [28, 29] for later developments.

[3]There are examples in which the dual lower dimensional theory is also coupled to gravity, for example in the context of the Randall-Sundrum model [34, 35] and of double holography [36–38]. However, for AdS/CFT and for the purposes of this dissertation, we can restrict to the case where the lower dimensional theory is non-gravitational.

[4]More precisely, the bulk manifold is given by AAdS$_{d+1} \times \mathcal{M}$, where AAdS$_{d+1}$ is a $(d+1)$-dimensional, asymptotically AdS spacetime and $\mathcal{M}$ is a compact manifold. In Maldacena's original example $\mathcal{M} = S^5$ [14]. Throughout this dissertation, we will assume the compactified dimensions to be very small, and their effect to be negligible in first approximation. We will therefore neglect their presence from now on. Whether UV-complete realizations of our setups with small extra dimensions can be constructed is an important open question. See Refs. [39, 40] for recent top-down constructions in which extra dimensions are significantly smaller than the AdS scale. Note that in our case the extra dimensions need to be very small compared to any scale relevant for the effective field theory description of a realistic cosmology, e.g. the big bang nucleosynthesis scale.

[5]Note that the AdS conformal boundary where the CFT is defined is an infinite coordinate distance away from any point in the bulk spacetime (but it can be reached in a finite proper time by light rays). For this reason, we will frequently refer to it as the "asymptotic" boundary.

for a $(d+1)$-dimensional AdS spacetime, where L is the AdS length[6], which is related to the cosmological constant by $L^2 = -d(d-1)/(2\Lambda)$, and $d\Omega_{d-1}$ is the line element of a $(d-1)$-dimensional unit sphere. In these coordinates, the (timelike) asymptotic boundary of AdS where the dual CFT is defined is given by $r \to \infty$.[7] The isometry group of AdS_{d+1} is given by $SO(2,d)$, which is also the conformal group associated with a d-dimensional CFT defined on a conformal compactification of Minkowski spacetime, i.e. on the AdS conformal boundary [16]. The fact that the bulk and boundary theories are invariant under the same symmetry group is clearly a necessary condition for the duality to hold, and is one of the hints that led to the development of the AdS/CFT correspondence.

In AdS/CFT, a given bulk geometry corresponds to a given state of the dual CFT. The pure AdS spacetime (1.1) corresponds to the vacuum state of the dual CFT, but more generic AAdS geometries—which asymptotically take the form (1.1) and can be non maximally-symmetric vacuum solutions or non-vacuum solutions of Einstein's equations with a negative cosmological constant—are described by different CFT excited states. For example, asymptotically AdS black holes are described by thermal states [18]. When the spacetime is only asymptotically AdS_{d+1}, $SO(2,d)$ becomes an asymptotic symmetry group; on the boundary side of the duality this corresponds to having a CFT state which breaks the conformal symmetry[8] and/or relevant deformations turned on in the CFT Lagrangian, so that the $SO(2,d)$ symmetry is unbroken only in the UV.[9]

In the original example of AdS/CFT [14], the bulk theory is given by Type IIb string the-

[6]Notation remark: throughout this dissertation, the AdS length, or AdS radius, is denoted by either L or L_{AdS}.

[7]Notice that the conformal boundary has a well-defined Lorentzian metric, which can be obtained from the AdS metric in the limit $r \to \infty$ after performing a conformal rescaling by a factor $\propto r^{-2}$.

[8]Only the vacuum state respects all symmetries of the theory. For example, the thermal states dual to AdS black holes clearly have a scale given by their temperature.

[9]We will make this statement more precise shortly.

ory on $AdS_5 \times S^5$, and the boundary theory is $\mathcal{N} = 4$ supersymmetric Yang-Mills (SYM), a maximally supersymmetric conformal field theory in four dimensions with gauge group $SU(N)$. Since Maldacena's initial work, several other explicit examples of AdS/CFT duality have been discovered (see for instance [42–44] for other examples in string theory and [45,46] for the lower dimensional duality between JT gravity in AdS$_2$ and the low-energy limit of the SYK model).

In most understood examples of AdS/CFT correspondence, when the UV completion of the bulk theory is known it is represented by a string theory. In the low-energy and weakly coupled limit—i.e. when the spacetime curvature is much smaller than the string scale and the string coupling constant is small—these string theories reduce to classical supergravities, which are supersymmetric theories encompassing general relativity coupled to quantum fields (see [47] for a review). Therefore, in this regime—which is frequently referred to as semiclassical holography and is the one we will focus on in this dissertation—the bulk dynamics is described by semiclassical Einstein's equations with a negative cosmological constant.

The semiclassical holography limit of our interest identifies a specific regime in the bulk theory (low-energy, weakly coupled), which corresponds to a specific regime in the boundary dual theory. In order to understand the latter, it is useful to focus on the specific example of the correspondence between $SU(N)$ $\mathcal{N} = 4$ SYM and Type IIb string theory [14]. In the bulk theory there are three parameters: the string length ℓ_s, the string coupling constant g_s, and the AdS length L; in the boundary theory there are two parameters: the coupling constant g_{YM} and the number of colors N. It is useful to further define the 't Hooft coupling $\lambda = g_{YM}^2 N$, which is a good perturbative expansion parameter in the large-N limit of the gauge theory. The parameters in the two theories are related by [18]

$$4\pi g_s = \frac{\lambda}{N}, \qquad\qquad \frac{L}{\ell_s} = \lambda^{\frac{1}{4}}. \tag{1.2}$$

As we have mentioned, the semiclassical gravity limit is obtained when both stringy and quantum corrections to the geometry are suppressed, i.e. $\ell/L \ll 1$ and $g_s \ll 1$ respectively. In terms of the dual boundary theory parameters, this corresponds to taking the large-N limit while keeping the 't Hooft coupling λ fixed but large, such that $N \gg \lambda \gg 1$. Therefore, the semiclassical holography limit corresponds to the large-N and strongly coupled limit of the boundary dual theory.[10]

Another important feature of holography is the correspondence between radial position in the bulk spacetime and energy scale in the dual CFT [18]. The idea—which in its more rigorous form takes the name of holographic renormalization group (RG) [48–50]—is that the "emergent" bulk radial coordinate is related to the RG flow parameter of the dual boundary theory. In particular, the asymptotic AdS region of the bulk geometry (the bulk "IR") is described by the UV physics in the dual theory, and the deeper we go into the bulk the lower the energy scale in the dual theory is.[11] This concept also helps us make sense of the correspondence between states and geometries explained above: all AAdS spacetimes look like pure AdS (and respect the same $SO(2, d)$ symmetries) in the asymptotic region, which corresponds to the well-known fact that all excited states look like the vacuum state (and therefore are invariant under the same $SO(2, d)$ symmetries) at sufficiently short distances. But there is more: the dual boundary theory

[10] This is the reason why quantum gravity corrections in the context of AdS/CFT are frequently dubbed as "finite-N effects". The fact that the regime where strings are weakly coupled in the bulk corresponds to the strongly coupled regime in the dual theory is instead the reason why AdS/CFT is frequently called a strong/weak duality.

[11] This property is the reason why AdS/CFT is also sometimes labeled as a "UV/IR duality".

does not even need to be a CFT at every energy scale, but it can be a more generic quantum field theory (QFT) whose RG flow has a UV fixed point. In other words, the most generic setup for a boundary theory is a CFT with relevant deformations turned on in its Lagrangian, which could flow in the IR to another CFT or to a gapped theory [7, 8, 51–53]. Note that the UV fixed point in the RG flow guarantees that the theory in the UV is invariant under the action of the conformal group $SO(2, d)$, matching the asymptotic symmetries of AAdS spacetimes. This idea that the most generic boundary theory is a QFT with a UV fixed point in its RG flow will be central in a subset of our constructions (see Section 1.4 and Chapter 3).

Holography is a useful tool from both the boundary theory's and the bulk theory's points of view. On one hand, it is possible to compute observables and learn new lessons in the boundary theory by performing bulk calculations in the semiclassical regime. For example, the fact that the semiclassical gravity regime in the bulk corresponds to the strongly coupled regime in the dual gauge theory encouraged the development of a research program aimed at using holography to shed light on the physics of the confined phase of non-abelian gauge theories (see [51–53] for a review of the topic). The goal in this case would be to use relatively simple semiclassical bulk calculations to make predictions in the strongly coupled regime of Quantum Chromodynamics (QCD), a task which is particularly hard to achieve by working directly in the gauge theory formalism due to the inapplicability of perturbative techniques. On the other hand, from the point of view of a quantum gravity theorist, it is particularly interesting to ask what the boundary theory can teach us about the bulk. In fact, the boundary theory is a well-defined and UV-complete quantum field theory, which we are able to study beyond the semiclassical holography regime.[12]

[12]Studying the boundary theory away from the semiclassical holography regime would actually be easier, because it would correspond to investigating the weakly coupled regime of the gauge theory.

Since the boundary theory is conjectured by AdS/CFT to be completely equivalent to the full bulk quantum gravity theory, studying its properties away from the semiclassical holography limit could give us invaluable insight into the structure of a quantum gravity theory at a non-perturbative level.

1.1.1 Holographic dictionaries

In the early days of AdS/CFT, a more conservative point of view was sometimes adopted [18], according to which the correspondence only held in the semiclassical holography regime explicitly analyzed in Maldacena's work [14] and in other string theory examples. It is now more widely believed that the correspondence holds exactly and at a non-perturbative level rather than only in the large-N and strongly coupled limit. Although this more general statement of the correspondence is hard to prove due to our limited understanding of non-perturbative quantum gravity, recent progress in lower-dimensional models have supported this point of view [54].

The general AdS/CFT statement is summarized by the so-called Gubser-Klebanov-Polyakov-Witten (GKPW) dictionary [15, 16], which posits the equivalence of the quantum gravity and the CFT generating functionals (i.e. their partition functions in the presence of sources):

$$Z_{QG}[\phi_0] = Z_{CFT}[\phi_0], \tag{1.3}$$

where from the bulk point of view $\phi_0(x)$ represents the boundary conditions for bulk fields at the AdS boundary, while from the boundary theory point view it represents the external sources coupling to deformations of the CFT Lagrangian. CFT correlation functions can be extracted from the dictionary (1.3), as is customary in quantum field theory, by differentiating with respect to ϕ_0

and then setting $\phi_0 = 0$. Although computing the quantum gravity partition function at a non-perturbative level is a hopeless task at the current stage of our knowledge, when working within the semiclassical holography regime, the Euclidean path integral defining Z_{QG} can be evaluated in the saddle point approximation. In other words, the partition function can be approximated by solving the semiclassical equations of motion and evaluating the bulk action S_E on-shell:

$$Z_{QG}[\phi_0] \approx \mathrm{e}^{-S_E[\phi_0]|_{\phi=\phi_{cl}}}. \tag{1.4}$$

A different (but equivalent [55]) statement of the correspondence can be made directly in terms of correlation functions. This is the so-called extrapolate dictionary [56, 57], which will be used mostly in Chapter 4:

$$\langle \mathcal{O}(x_1)...\mathcal{O}(x_n)\rangle_{CFT} = \lim_{r\to\infty} r^{n\Delta} \langle \phi(x_1, r)...\phi(x_n, r)\rangle_{bulk} \tag{1.5}$$

where $\mathcal{O}$ is a CFT operator of conformal dimension Δ, r is the bulk radial coordinate, and ϕ is the bulk field dual to $\mathcal{O}$.

1.1.2 Holography and quantum information

In the last two decades, much progress has been made in unveiling the properties of holographic dualities. Especially noteworthy has been the advancement in our understanding of the relationship between properties of the spacetime geometry in the semiclassical holography regime and quantum information theoretic aspects of the dual boundary theory. This includes (but is not limited to) the holographic interpretation of boundary entanglement entropy [19, 58–64], various proposals for the holographic dual of complexity [65–67], the idea that spacetime is an emergent property arising from entanglement in the boundary theory [68–70], and the quantum error correcting code (QECC) interpretation of holography [71, 72] explicitly realized in tensor network models of holography [68, 73, 74].

The most celebrated and largely accepted example is the holographic computation of the entanglement entropy of a subregion of the boundary theory, first carried out by Ryu and Takayanagi [58, 59] in the purely classical regime and in a static spacetime (see also [60] for a Euclidean path integral derivation). The Ryu-Takyanagi (RT) formula expresses the entanglement entropy of a subregion B of the boundary theory in terms of the area of a codimension-2 hypersurface γ_B which extremizes the area functional and is homologous to region B:

$$S(B) = \frac{\mathcal{A}(\gamma_B)}{4G}, \tag{1.6}$$

where G is Newton's gravitational constant and γ_B is referred to as the extremal surface. A covariant form of the RT prescription valid in non-static spacetimes was introduced soon after by Hubeny, Rangamani, and Takayanagi (HRT) [61] (see also [62] for a derivation of the HRT formula), while a generalization to include the contribution of bulk quantum matter is known as quantum extremal surface (QES) formula and was initially introduced by Faulkner, Lewkowycz, and Maldacena [63] and further generalized to its present form by Engelhardt and Wall [64] (see also [75–77]). The application of the QES prescription[13] to setups involving evaporating black holes led to new discoveries related to the black hole information paradox [78], pointing toward a resolution in favor of the unitarity of evaporation [76, 77, 79, 80].

[13] Since the explicit formulation of the QES prescription will not be relevant for the purposes of this dissertation, we refer the reader to the literature cited above for further details.

For the sake of the discussion in Section 1.4.3 and Chapter 3 about cosmological islands, it is useful to introduce here the notion of entanglement wedge of a subregion B of the boundary. This is defined as the bulk region given by the domain of dependence of the codimension-1 hypersurface bounded by the asymptotic AdS boundary and the QES associated with region B. Note that the QES does not need to be connected, and it can in fact contain a closed component without violating the homology constraint. Consequently, the entanglement wedge can contain disconnected closed regions known as "islands" [79–84]. Physics in the entanglement wedge of B is completely encoded in the subregion B of the boundary theory [72].

Although a more extensive review of these quantum information theoretic aspects of holography is beyond the scopes of this dissertation, these should be regarded as some of the most intriguing and revolutionary features of holography. They led to a change of perspectives in our interpretation of quantum gravity (at least in its semiclassical regime) and delivered some of the most striking results in support of the holographic framework.

1.1.3 The bottom-up approach

In this dissertation, we will restrict our attention to the semiclassical holography regime in which the saddle point approximation (1.4) holds, and work within the so-called "bottom-up" approach to holography. Instead of starting from either a string theory setting or a description in terms of a dual boundary theory and then taking the semiclassical holography limit (an approach generally referred to as "top-down"), we will work directly in a low-energy bulk effective field theory (EFT) given by general relativity in the presence of a negative cosmological constant and coupled to classical or quantum fields. The idea is that such an EFT can be obtained by taking an appropriate low-energy limit of some full quantum gravity theory with a holographic dual description.

The requirement of the existence of a dual microscopic description in the sense of AdS/CFT imposes constraints on the bulk EFT. For example, in any given setup the bulk spacetime solution of the (semi)classical Einstein's equation must have an asymptotically AdS boundary[14] where the dual CFT can be defined, and bulk fields must satisfy appropriate boundary conditions there in order for the holographic dictionary to make sense (see Chapter 4 for further details on this point). The purpose of the bottom-up approach is therefore to find solutions of the bulk (semi)classical equations of motion satisfying a set of necessary conditions for the existence of a dual boundary theory. One can then study relatively complicated bulk setups in the well-understood framework of (semi)classical gravity and check whether they are compatible in principle with the existence of a UV completion in terms of a dual theory.

There are several advantages in employing this approach. First, it helps us understand what kind of constraints the existence of a dual theory imposes on the low-energy bulk EFT. Second, one can study physically interesting setups (for instance, the one describing a cosmological universe, as it is the case in this dissertation) and check whether they can in principle be described within the holographic framework without initially tackling the cumbersome task of finding an appropriate UV-complete description which reduces to the setup of interest in the semiclassical holography limit. In fact, our limited understanding of nonperturbative quantum gravity (and in particular string theory) and the small number of exact dualities known at this stage can be a limiting factor on the types of low-energy setups we are able to obtain using a top-down ap-

[14] As we will see in Section 1.4, and more extensively in Chapter 3, it is possible for the Lorentzian spacetime of interest to not have an asymptotic AdS boundary, as long as a complexified version of the bulk geometry possesses one.

proach; and even if such a UV-complete description involving a string theory dual to a boundary theory can be constructed for a given setup, it is in general quite challenging to obtain. Third, the bottom-up approach can also help us constrain the properties of the dual boundary theory and therefore simplify the task of finding the dual microscopic description. We will see an explicit example of this last fact in Section 1.6 and in more detail in Chapter 4, where the presence of bulk fields in a specific traversable wormhole background implies that the dual boundary theory must be confining and with a specific mass spectrum.

There is also an evident drawback of the bottom-up approach: the fact that a set of necessary conditions for the existence of a dual microscopic description are satisfied does not imply that such a dual description actually exists. The bottom-up approach combined with intuition coming from known holographic dualities allows us to set expectations on whether a dual theory exists and what its properties may be. Nonetheless, only a fully microscopic construction—in terms of a dual boundary theory and/or a corresponding bulk quantum gravity theory—reducing to the setup of interest in the appropriate regime can confirm or prove wrong these expectations. Therefore, the construction of microscopic setups able to describe the phenomena studied in the bottom-up approach in this dissertation remains a very intriguing subject to be explored in future research.

1.2 Cosmology and holography

Any candidate quantum gravity theory aiming at capturing physics in our universe must be able to describe the cosmological phenomenology we observe in our skies.[15] In the context of holography, it is not immediately clear how such a requirement can be met. The purpose of this

[15] See for example [85] for a review of some possible approaches to quantum cosmology and of general issues arising in the field.

dissertation is to collect the progress—made in the past few years by me and my collaborators—in the development of a new approach to the description of cosmology in holography and in particular within the AdS/CFT framework.

Before moving on to describe the main features and results of this new approach, we need to render clear the challenges one faces when trying to holographically describe cosmology. This is the purpose of the present subsection, where we will first give a broad overview of the relevant features of standard Friedmann-Lemaître-Robertson-Walker (FLRW, or FRW) cosmology in four dimensions, and then outline the difficulties encountered when trying to describe a cosmological universe within holography.

1.2.1 Brief review of FLRW cosmology

Cosmological observations on the Cosmic Microwave Background (CMB) [86–88]—which appears extremely isotropic on large scales—combined with the Copernican Principle—which states that the universe should appear the same to any observer independently of their position (or, in other words, that we are not "privileged" observers)—lead to the conclusion that the universe is, to very good approximation, homogeneous and isotropic at large scales [89]. Its metric then takes the FLRW form[16]

$$ds^2 = -dt^2 + a^2(t)\left[\frac{dr^2}{1-kr^2} + r^2 d\Omega_2^2\right], \tag{1.7}$$

where $a(t)$ is the cosmological scale factor and k is proportional to the spatial curvature of a given time slice. Without loss of generality, the parameter k can be taken to be $k = 0$ (spatially flat

[16]For a complete review of standard cosmology and as a source for the review material on cosmology presented in this subsection we refer to [89].

universe, the one considered in Chapters 3, 4, and 5 and favored by cosmological observations), $k = 1$ (spherical or closed universe, the one considered in Chapter 2), or $k = -1$ (hyperbolic or open universe, not considered in this dissertation). t is called cosmic time; a different time coordinate that we will also employ in this dissertation is the so-called conformal time, defined by $d\eta = dt/a(t)$.

The FLRW metric is a solution of Einstein's equations (possibly in the presence of a non-vanishing cosmological constant Λ) sourced by the stress-energy tensor of a perfect fluid

$$T^{\mu\nu} = (\rho + p)u^\mu u^\nu + p g^{\mu\nu}, \tag{1.8}$$

where u^μ is the fluid's 4-velocity, ρ its energy density, and p its pressure. The evolution of the scale factor is determined by the two independent components of the Einstein's equations, which take the name of Friedmann equations and can be written in the form

$$\left(\frac{\dot{a}}{a}\right)^2 = \frac{\Lambda}{3} - \frac{k}{a^2} + \frac{8\pi G}{3}\rho, \tag{1.9}$$

$$\frac{\ddot{a}}{a} = \frac{\Lambda}{3} - \frac{4\pi G}{3}(\rho + 3p), \tag{1.10}$$

with a dot indicating a derivative with respect to the cosmic time. The second Friedmann equation is sometimes referred to as the acceleration equation, and the quantity $H \equiv \dot{a}/a$ is the Hubble parameter. Combining the two equations, it easy to show that the system (1.9)-(1.10) is equivalent to the first Friedmann equation (1.9) plus the conservation equation

$$\dot{\rho} = -3\frac{\dot{a}}{a}(\rho + p). \tag{1.11}$$

Given a fluid equation of state relating ρ and p, equation (1.11) yields ρ as a function of a, which can then be substituted in the first Friedmann equation to obtain the evolution of the scale factor $a(t)$ as a function of cosmic time. Note that the cosmological constant can be seen as a perfect fluid with equation of state $p = -\rho$. In the rest of this dissertation, we will assume knowledge of the equation of state for all species driving the cosmological evolution and therefore a specific dependence of ρ on the scale factor. The first Friedmann equation will then be enough to fully determine the evolution of the cosmological universe. Where a minimally coupled, homogeneous scalar field will also be included in our analysis, the first Friedmann equation[17] (1.9) and the Klein-Gordon equation for the scalar field in the FLRW background are enough to fully specify the dynamics.

ΛCDM model and naturalness puzzles

The simplest possible cosmological model matching observations (including the accelerated expansion currently ongoing in our universe) to good accuracy [88] is the Lambda-Cold Dark Matter (ΛCDM) model, also known as the standard model of cosmology. In the ΛCDM model, the universe is described by a flat FLRW metric and the cosmological evolution is driven by

- A positive cosmological constant $\Lambda > 0$, which is currently dominating on the right-hand side of the Friedmann equation. Λ accounts for the Dark Energy responsible for the present accelerated expansion (about 70% of the energy density of the universe at the present time);
- Non-relativistic matter, which satisfies the equation of state $p_m = 0$ (implying $\rho_m \propto a^{-3}$).

[17] From now on we will refer to the first Friedmann equation simply as the "Friedmann equation".

This contribution accounts for both visible matter and Dark Matter and it makes up about 30% of the energy density of the universe at the present time. Following the cosmological evolution backward in time, the cosmological constant Λ remains constant while the matter energy density ρ_m grows. Therefore, the latter becomes the dominant contribution on the right-hand side of the Friedmann equation for sufficiently early times, giving rise to a matter-dominated era which ended roughly 4 billion years ago;

- "Radiation", which satisfies the equation of state $p_r = \rho_r/3$ (implying $\rho_r \propto a^{-4}$). This contribution accounts for ultra-relativistic matter such as photons and neutrinos (and heavier particles as we approach the early universe, in which the average temperature of the universe was much higher). It represents a subleading contribution ($\approx 0.0001\%$) to the total energy density of the universe at the present time. Radiation was dominant on the right-hand side of the Friedmann equation in the early universe (before the matter-dominated era), giving rise to a radiation-dominated era which ended roughly 10^4 years after the Big Bang, i.e. more than 13 billion years ago.

If we extrapolate the ΛCDM model all the way to the early universe, we encounter three "naturalness" puzzles, that we briefly outline below as a reference for the related discussion in Chapter 3:

- *Flatness problem.* CMB observations suggest that the universe is flat to very good accuracy: the best fit for the curvature parameter $\Omega_k = k/(H_0^2 a_0^2)$, where H_0 and a_0 are the Hubble radius and scale factor today, is given by $\Omega_k = 0.0007 \pm 0.0019$ [90][18]. As we

[18]Note that this estimate, as most of the other estimates of the cosmological parameters, is model-dependent and obtained assuming the ΛCDM model. Cosmological parameters are in fact very loosely constrained in a model-independent way, see Chapter 5 for further discussion on this point.

follow the evolution backwards towards the early universe, the time dependent curvature k/H^2a^2 further decreases during the matter-dominated and the radiation-dominated eras, and vanishes approaching the Big Bang singularity. Obviously, it could be that the universe is simply flat (this is essentially the point of view taken in Chapter 3). However, if one starts from the more generic assumption of having a non-vanishing curvature, then one faces the puzzling situation of having an extremely small parameter in the initial conditions of the cosmological evolution. One would ideally like to explain this accurate fine-tuning on physical grounds.

- *Horizon problem.* The extreme isotropy of the CMB on very large scales gives rise to a second puzzle. In fact, it is easy to show that if only a matter-dominated and a radiation-dominated era preceded the current accelerated expansion, regions of the CMB whose angular separation in the sky is larger than a few degrees have never been in causal contact between the Big Bang and the present time. Therefore, no physical process could have smoothed out initial anisotropies on large scales. This, once again, implies that the initial state of the universe at early times must be very isotropic, and therefore very fine-tuned.

- *Magnetic monopoles.* For completeness, we briefly report a third puzzle traditionally considered in the literature, even though we will not discuss it further in this dissertation. Assuming the validity of grand unified theories at high energies, magnetic monopoles should be created in the early universe. Given their abundance in the early universe and their evolution during a radiation-dominated and a matter-dominated era, their abundance at the present day should be comparable to that of nucleons [89]. The absence of any experimental evidence for magnetic monopoles is therefore puzzling.

All these naturalness puzzles are resolved if an accelerated expansion period is postulated to take place before the radiation-dominated era. This led to the introduction of the inflationary paradigm. Starting from generic initial conditions, inflation naturally prepares the apparently fine-tuned initial conditions necessary to match observations using the ΛCDM model. Additionally, it also explains the mechanism leading to the scale-invariant cosmological perturbations observed in the CMB spectrum and ultimately leading to the formation of structures in the universe. A review of inflation is beyond the scopes of this dissertation, and we refer the reader to the relevant literature (see for instance [89], see also [91] for a recent review).

Finally, the ΛCDM model is also affected by an additional naturalness puzzle which arises independently of whether we extrapolate ΛCDM all the way to the early universe: the "cosmic coincidence" problem. This comes from the observation that the matter energy density and the cosmological constant have a very different dependence on the scale factor. Therefore, it is quite a coincidence that we live in a specific age of the universe where the two are of the same order of magnitude, and of a similar order of magnitude as the radiation density as well (which is the only other species driving the cosmological expansion in the ΛCDM model). Note that this puzzle is not solved by inflation.[19]

The ΛCDM model, augmented by inflation, is a simple and successful effective model [88] and the best cosmological theory available to us at the moment. However, even if it is the simplest option, it is not the only model able to explain cosmological observations (see [92, 93], and [94] for a recent review of an alternative class of models, known as quintessence models), nor is it free of troubling, unresolved issues such as the Hubble tension (see [95] for a complete review of

[19] As we will see in Chapter 3, having a negative cosmological constant leading to a recollapsing universe (a so-called Big Bang-Big Crunch universe) in the spatially flat case allows us to resolve the cosmic coincidence problem.

currently open problems in the standard model of cosmology).

$\Lambda < 0$ cosmologies

In this dissertation we will focus our attention on cosmologies with a negative cosmological constant $\Lambda < 0$. As we will explain in more detail in the next subsection, this is indeed a good starting point to achieve a description of cosmology within AdS/CFT. Let us then briefly review the main properties of $\Lambda < 0$ cosmologies.

Any kind of ordinary matter satisfies an equation of state $p(t) = w(t)\rho(t)$ with $w \geq -1$,[20] where we allowed a time dependence of the parameter w to include also matter with a non-constant equation of state, such as rolling scalars (which will play an important role in our analysis). The limiting case $w = -1$, as we have seen, is a cosmological constant. From equation (1.11) we can then conclude that all energy densities decrease as the universe expands, except for the cosmological constant. This in turn implies that at some stage in the expansion of the universe the cosmological constant will eventually become the dominant contribution on the right-hand side of the Friedmann equation and equal to the sum of all other contributions, independently of its value.[21]

What happens next depends on the sign of the cosmological constant. If $\Lambda > 0$, the universe keeps expanding, the cosmological constant becomes even more dominant, and the universe

[20] Only very exotic kinds of matter, which go under the name of phantom dark energy (see [96] for a review), have $w < -1$. In our discussion we will assume the absence of phantom dark energy sources.

[21] There are two caveats to this statement, which can be understood by inspecting the two Friedmann equations (1.9) and (1.10). The first one is a universe with positive curvature $k = 1$ and a very small cosmological constant. In this case, depending on the equation of state for the species driving the cosmological evolution and on the size of their energy densities relative to the curvature term and the cosmological constant, the curvature term can become of the same size as the sum of the other energy densities and cause the universe to stop expanding and start recollapsing before the cosmological constant becomes relevant. The second caveat is if sources of negative energy (other than a negative cosmological constant) are present. If this is the case, depending on the relative size of positive and negative energy densities and on the equations of state of the different species driving the cosmological evolution, the universe could start recollapsing while the cosmological constant is still negligible.

undergoes an accelerated expansion—frequently referred to as a de Sitter phase (although this terminology becomes proper only when all the other energy densities become negligible)—for the rest of its history. According to the ΛCDM model, our universe is in fact currently dominated by a positive cosmological constant. On the other hand, if $\Lambda < 0$ the right hand size of the Friedmann equation vanishes and the universe stops expanding and starts recollapsing. By a simple manipulation of the two Friedmann equations (1.9) and (1.10), it is in fact easy to see that the acceleration $\ddot{a}$ is negative at the turning point if the constraint $w \geq -1$ is satisfied.[22] If the first derivative of all fields also vanishes at the turning point, the evolution of the universe is time-reversal-symmetric with respect to the inversion point. In this case, if the universe emerged from a Big Bang singularity, it will recollapse to a Big Crunch singularity.[23]

As a simple example of a $\Lambda < 0$ Big Bang-Big Crunch cosmology we can consider a spatially flat FLRW universe whose evolution is driven by a negative cosmological constant and a radiation term. The Friedmann equation then reads

$$\left(\frac{\dot{a}}{a}\right)^2 = \frac{\Lambda}{3} + \frac{8\pi G}{3}\frac{\rho_r^0}{a^4} \tag{1.12}$$

where ρ_r^0 is the radiation energy density when $a = 1$. Equation (1.12) can be solved analytically, and the scale factor reads

$$a(t) = \left(-\frac{8\pi G \rho_r^0}{\Lambda}\right)^{\frac{1}{4}} \sqrt{\sin\left(2\sqrt{-\frac{\Lambda}{3}}t\right)}. \tag{1.13}$$

[22]The only slightly trickier case is the $k = 1$ one mentioned in footnote 21, but it is not hard to convince oneself that it also eventually ends up in a collapsing universe.

[23]It is understood that the validity of the gravitational effective field theory does not extend all the way to the singularities, and therefore the cosmological evolution we described can only be trusted until the spacetime curvature is much larger than the Planck length. A description of the very early universe (and of the very late universe in Big Bang-Big Crunch models) requires a UV-complete quantum gravity theory.

This is clearly a symmetric Big Bang-Big Crunch universe, with the Big Bang at $t = 0$, the inversion point at $t = \pi/\left(4\sqrt{-\Lambda/3}\right)$ and the Big Crunch at $t = \pi/\left(2\sqrt{-\Lambda/3}\right)$.

$\Lambda < 0$ cosmologies seem at first sight incompatible with observational data suggesting that the expansion of the universe is currently accelerating. In particular, within the ΛCDM model the cosmological constant must be positive in order to explain Dark Energy. However, a positive cosmological constant is not the only way to obtain an accelerated expansion. In fact, from the acceleration equation (1.10) it is clear that $\ddot{a} > 0$ whenever a source of positive energy density with equation of state $w < -1/3$ is dominant on the right-hand side of the Friedmann equation. For instance, a scalar field slowly rolling down the slope of a potential has an equation of state $w \gtrsim -1$: if its potential energy is dominant over other energy densities, the universe undergoes a phase of accelerated expansion regardless of the sign of the cosmological constant, as we will now briefly review. This is the mechanism at the base of quintessence models of Dark Energy [92–94] and of primordial inflation.

Slowly-rolling scalar fields

Consider a homogeneous[24] scalar field $\phi = \phi(t)$ in a potential $V(\phi)$ on a FLRW background. Its energy density and pressure are given by

$$\rho_\phi(t) = \frac{1}{2}\dot{\phi}^2 + V(\phi), \qquad p_\phi(t) = \frac{1}{2}\dot{\phi}^2 - V(\phi), \tag{1.14}$$

[24]This is the only possibility compatible with a FLRW cosmology. In principle, we can imagine that spatial gradients of the scalar field are small and can be treated perturbatively over the homogeneous background.

and therefore

$$w_\phi(t) = \frac{\frac{1}{2}\dot{\phi}^2 - V(\phi)}{\frac{1}{2}\dot{\phi}^2 + V(\phi)}. \tag{1.15}$$

In the presence of the scalar field, the bulk EFT equations of motion are given by a system of two coupled equations, i.e. the Klein-Gordon equation for the scalar field and the Friedmann equation governing the evolution of the scale factor:

$$\begin{cases} \ddot{\phi} + 3H\dot{\phi} + \frac{dV}{d\phi} = 0 \\ H^2 = \frac{\Lambda}{3} - \frac{k}{a^2} + \frac{8\pi G}{3}\left[\frac{1}{2}\dot{\phi}^2 + V(\phi) + \rho\right] \end{cases} \tag{1.16}$$

where we indicated with ρ the energy density of all other species present in the FLRW universe and we recall that $H = \dot{a}/a$. Note that the Klein-Gordon equation on the first line of equation (1.16) describes a damped particle moving in a potential V, with time-dependent damping factor proportional to the Hubble parameter H. If the universe is expanding, and therefore $H > 0$, the scalar field is damped, whereas if the universe is contracting, implying $H < 0$, the scalar is anti-damped in its motion.

From equation (1.15) it is clear that when $V(\phi) \gg \dot{\phi}^2$—implying that the scalar is slowly rolling down the slope of the potential—the scalar field approximately satisfies the equation of state of a cosmological constant $w_\phi \gtrsim -1$.[25] This can also be seen explicitly from the Friedmann equation on the second line of equation (1.16): when $\dot{\phi}$ is negligible, the effect of the presence of the scalar field is to shift the cosmological constant Λ by $8\pi G V(\phi)$, where $V(\phi)$ changes only adiabatically during the slow-roll phase. In particular, if the scalar potential term is positive

[25] Note that if $\dot{\phi}^2$ is small but not completely negligible, the scalar equation of state has $w > -1$. In this case, the scalar field can still drive an accelerated expansion as long as $w < -1/3$. For example, it is possible to approximate wCDM models in this way, see Section 5.2.4 and Appendix D.2 for additional details on this point.

and dominant on the right-hand side of the Friedmann equation, the universe undergoes a phase of accelerated expansion, regardless of the sign of the fundamental cosmological constant Λ. Clearly, the accelerated expansion in this case lasts only while the scalar potential is dominant and the slow-roll condition is satisfied, and will eventually come to an end. If $\Lambda < 0$, the universe will then eventually stop expanding and start recollapsing.

The slow-roll condition is often expressed (especially in the context of inflation) in terms of two slow-roll parameters depending only on the potential $V(\phi)$:

$$\begin{cases} \epsilon_V \equiv \frac{1}{16\pi G}\left(\frac{V_{,\phi}}{V}\right)^2 \ll 1 \\ |\eta_V| \equiv \frac{1}{8\pi G}\left|\frac{V_{,\phi\phi}}{V}\right| \ll 1 \end{cases} \tag{1.17}$$

where we indicated with , a derivative with respect to the scalar field. The first condition guarantees that the slow-roll condition $V(\phi) \gg \dot{\phi}^2$ is satisfied and therefore the universe accelerates if $V(\phi)$ is dominant on the right-hand side of the Friedmann equation. The second slow-roll parameter η_V controls how long the slow-roll phase (and therefore the accelerated expansion) lasts. From these two conditions we can conclude that a long phase of accelerated expansion is possible in the presence of rolling scalar fields if the potential's slope and its curvature are small with respect to the scale of the potential itself, i.e. if the potential is somewhat flat.

1.2.2 Challenges of a holographic description of cosmology

As we have seen in Section 1.1, holography is best understood within the framework of AdS/CFT, where the bulk spacetime is either pure AdS—see equation (1.1)—or more generically asymptotically AdS (AAdS). All known explicit examples of the duality are formulated in

AAdS spacetimes. Intuitively, the reason is that we need a timelike asymptotic AdS boundary on which to define the dual theory. As we have discussed, $SO(2, d)$ is both the asymptotic isometry group of AAdS_{d+1} and the conformal group associated with a d-dimensional CFT defined on the asymptotic AdS boundary, and the theories on the two sides of the duality need to be invariant under the same symmetry group. Therefore, if the bulk spacetime is not AAdS, the dual theory cannot be a CFT—or more generally a QFT described by a RG flow with a UV fixed point—defined on a conformal compactification of Minkowski spacetime.

Although holographic duality is believed to be more general than the AdS/CFT correspondence—see for instance [97–105] for some progress towards a holographic description of de Sitter spacetime, and [106] for a review of the current status of asymptotically flat (or "celestial") holography—it is not yet clear how to holographically describe theories in spacetimes that are not AAdS and so do not have a timelike asymptotic boundary and an asymptotic $SO(2, d)$ isometry group. This fact immediately renders clear what is the central problem in a holographic description of cosmology: cosmological spacetimes, even those with a negative cosmological constant, are never asymptotically AdS. One intuitive way to see this is that they are sourced by uniform energy densities, and therefore they are not "asymptotically empty" as it is the case for AAdS spacetimes, where only the negative cosmological constant is relevant in the asymptotic region.[26]

Several attempts have been made to address this issue and obtain a holographic description of cosmology. These include the holographic description of de Sitter spacetime [97–105] (which could be able to describe at least the late stages of evolution of our universe if it is driven by a positive cosmological constant), string theory constructions involving metastable de Sitter

[26] We are neglecting here the special case given by the solution of the Friedmann equation with negative spatial curvature $k = -1$, a negative cosmological constant $\Lambda < 0$, and no additional sources of energy density ($\rho = 0$). This is in fact a hyperbolic slicing covering part of pure AdS spacetime.

vacua [107–109], and more phenomenologically-oriented approaches such as [110]. Motivated by the observational evidence that our universe is currently accelerating and by the fact that the simplest explanation for such an acceleration is a positive cosmological constant $\Lambda > 0$, all these approaches aim at describing $\Lambda > 0$ cosmologies. This clearly rules out standard AdS/CFT, and requires new ingredients. In the three approaches mentioned above, these are a new framework such as dS/dS correspondence, an explanation of how special de Sitter vacua arise in string theory and how they can be described holographically, and a dual quantum field theory involving imaginary parameters, respectively. Although progress has been made in these approaches (especially the first two), a consistent holographic description of a cosmological universe has not been achieved yet.

In the last few years, my collaborators and I contributed to advance the field in a new direction starting from a different point of view. Given that our ability to holographically describe $\Lambda < 0$ spacetimes is much more developed at the current stage thanks to AdS/CFT, it seems like a natural first step to obtain a holographic description of cosmologies with a negative cosmological constant such as those described at the end of the previous subsection. Although this approach avoids the additional difficulty of developing a holographic framework able to describe $\Lambda > 0$ spacetimes, it is nonetheless affected by the main issue of the lack of an AdS asymptotic region. In order to deal with this problem, we developed two different but related approaches, which we will now review in Subsections 1.3 and 1.4, and explore in more detail in Chapters 2 and 3.

We would like to remark that, although the main purpose of this new approach is to obtain, as a starting point, a first holographic description of cosmology regardless of its viability as a model of our universe, $\Lambda < 0$ cosmologies are not in principle ruled out by observations. In Section 1.7, and in more detail in Chapter 5, we will in fact show that $\Lambda < 0$ cosmological universes in our holographic framework can undergo phases of accelerated expansion thanks to the presence of rolling scalar fields, and that their scale factor evolution can in principle match to good accuracy the one derived from cosmological data. Naturally, they predict that the current phase of accelerated expansion will eventually end before the universe reaches its turning point and starts recollapsing.

1.3 First approach: holographic braneworld cosmology

The first approach we employ to embed a $\Lambda < 0$ cosmology within the holographic framework is to consider a so-called braneworld cosmology [5, 34, 35, 111–115]. We will now briefly review the construction introduced in Ref. [5] (we refer to Chapter 2, Appendix A, and [5] for technical details) focusing first on the Lorentzian bulk EFT and then on the proposal for a holographic dual description. We will then explain the difficulties faced in the simplest possible model studied in Ref. [5] and summarize the results of Chapter 2 (published in Ref. [1]), in which such difficulties are overcome and a well-defined braneworld cosmology embedded in a spacetime admitting a holographic dual description is obtained. See [6, 116–119] for related work.

1.3.1 Braneworld cosmology in AdS-Schwarzschild black hole

Consider a maximally extended AdS-Schwarzschild black hole spacetime (sometimes referred to as double-sided black hole, eternal black hole, or non-traversable wormhole) in five dimensions [120].[27] Each one of the two exterior patches (the "left" and "right" asymptotic re-

[27] This choice of dimensions yields the desired four-dimensional cosmology. However, the analysis reported here can be generalized to other choices of dimension.

gions) is described in Schwarzschild coordinates by the metric

$$ds^2 = -f(r)dt^2 + \frac{dr^2}{f(r)} + r^2 d\Omega_3^2, \qquad f(r) = 1 + \frac{r^2}{L^2} - \frac{2\mu}{r^2} \tag{1.18}$$

where μ is a parameter proportional to the black hole mass (see equation (A.9) in Appendix A.1 for its explicit expression), and the event horizon radius is given by

$$r_H = \frac{L}{\sqrt{2}}\sqrt{\sqrt{1+\frac{8\mu}{L^2}} - 1}. \tag{1.19}$$

Consider now a codimension-1 (i.e. four-dimensional) spherically-symmetric "end-of-the-world" (ETW) brane living in the left asymptotic region (see Figure 1.1 (a) for a depiction of the Penrose diagram including the ETW brane). Although its existence and microscopic description is best understood in string theory constructions (see for instance [121–123] based on the idea first introduced in [124], see also [125, 126]), for the bottom-up purposes of this dissertation, the ETW brane can simply be regarded as a codimension-1 timelike hypersurface cutting off part of the left asymptotic region and on which Robin boundary conditions are imposed for bulk fields (including the metric). The ETW brane carries a stress-energy tensor

$$T_{ab}^{ETW} = -\frac{T}{4\pi G} h_{ab}, \tag{1.20}$$

where T is the tension parameter taking values in the range $T \in [0, 1/L)$[28] and h_{ab} is the induced metric on the brane. The trajectory of the ETW brane in the bulk spacetime is obtained by

[28]We restrict here to positive tension branes, see [5], Chapter 2, and Appendix A for a detailed explanation of the reason in the present context, and [127] for a discussion of the physical implications of negative tension branes.

imposing the Israel junction conditions [128], which can also be obtained by varying the Gibbons-Hawking-York (GHY) brane action (see Chapter 2 and [129, 130]):

$$K_{ab} - K h_{ab} = -2T h_{ab}, \tag{1.21}$$

where K_{ab} is the brane's extrinsic curvature and $K = h^{ab} K_{ab}$ its trace. By parametrizing the brane trajectory using the Schwarzschild time coordinate t, equation (1.21) yields a first order differential equation for the brane radius $r(t)$:

$$\left(\frac{dr}{dt}\right)^2 = \frac{f^2(r)}{T^2 r^2} \left(T^2 r^2 - f(r)\right). \tag{1.22}$$

We consider time-reversal-symmetric solutions by imposing the initial condition $r'(0) = 0$, where a prime denotes a derivative with respect to the Schwarzschild time t. This implies that our Lorentzian spacetime can be obtained by analytic continuation from a reflection-symmetric Euclidean geometry (see Figure 1.1), which should be regarded as a saddle point of a reflection-symmetric gravitational Euclidean path integral. Such a feature will allow us to make contact with the Euclidean path integral of the dual boundary theory by means of the GKPW dictionary (1.3). The symmetry condition $r'(0) = 0$ also uniquely determines the brane's maximum radius r_0. The brane therefore emerges from the past singularity, crosses the past horizon, expands in the left asymptotic region until the turning point at $t = 0$, then recollapses into the future horizon and finally into the future singularity in a time-symmetric fashion.

Let us now introduce the proper time λ along the brane trajectory, defined by $d\lambda =$

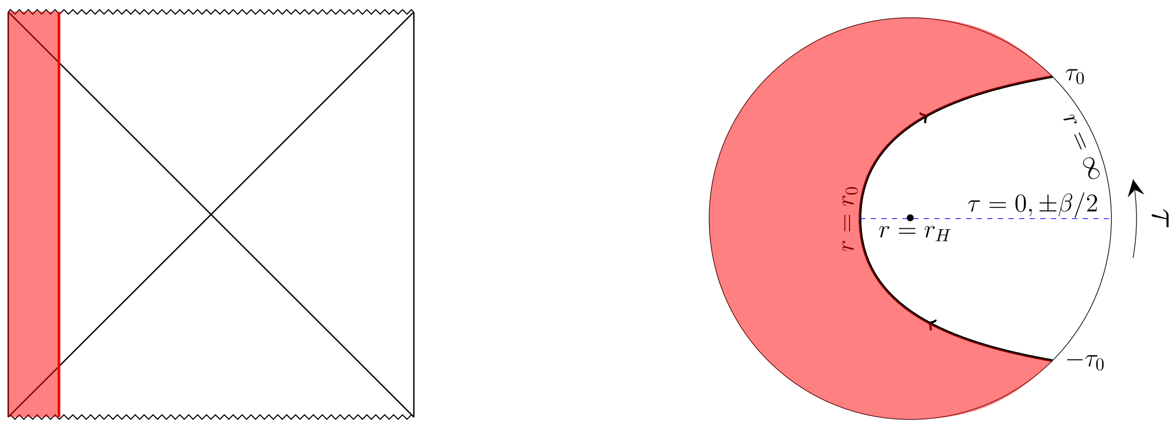

(a) (b)

Figure 1.1: AdS-Schwarzschild braneworld cosmology setup. (a) Schematic Penrose diagram of the Lorentzian geometry with the ETW brane (indicated by a red line) cutting off the part of the left asymptotic region shaded in red. The dual CFT whose pure excited state describes the Lorentzian spacetime lives on the right asymptotic boundary. (b) Corresponding Euclidean geometry. The part of geometry shaded in red is cut off by the ETW brane. The bulk time-reflection symmetric slice $\tau = 0, \pm\beta/2$ left invariant by the analytic continuation is indicated by a blue dashed line. The dual Euclidean BCFT is defined on $S^3 \times I$, where I is the interval $[-\tau_0, \tau_0]$ in Euclidean time and the S^3 is suppressed in this Figure.

$\sqrt{f(r) - r'^2/f(r)}dt$. The metric induced on the brane then takes the form

$$ds^2_{ETW} = -d\lambda^2 + r^2(\lambda)d\Omega_3^2, \tag{1.23}$$

which is the metric of a closed ($k = 1$) FLRW universe with the brane radius $r(\lambda)$ playing the role of the scale factor. In terms of the proper time, equation (1.22) takes the form of a Friedmann equation for a closed universe with a negative cosmological constant $\Lambda_4 = 3(T^2 - 1/L^2)$ and a radiation term proportional to the black hole mass:

$$\left(\frac{\dot{r}}{r}\right)^2 = \left(T^2 - \frac{1}{L^2}\right) - \frac{1}{r^2} + \frac{2\mu}{r^4}, \tag{1.24}$$

where we used a dot to indicate a derivative with respect to the brane's proper time.

The intuition is therefore that a four-dimensional comoving observer on the ETW brane would perceive the radial motion of the ETW brane in the higher dimensional black hole spacetime as the expansion and contraction of a Big Bang-Big Crunch FLRW universe. The Big Bang and Big Crunch singularities correspond to the past and future black hole singularities, respectively. Additional terms in the Friedmann equation beyond the simplest ones contained in equation (1.24) can be added by considering more complicated forms of the brane stress-energy tensor instead of the simple pure-tension contribution. Clearly, in order for this "braneworld cosmology" interpretation to make sense at least in principle as a description of our own universe, the 4D observer must be unaware of the existence of the extra fifth dimension. If, on one hand, one can consider a QFT simply living on the brane which would not "give away" the presence of the extra dimension to a brane observer [34, 35], having gravity localized on the brane and looking four-dimensional to a 4D observer is not as trivial. In fact, in the present setup gravity is intrinsically five-dimensional and 4D gravity on the brane can be obtained only via a particular localization mechanism discovered by Randall and Sundrum [34, 35].

1.3.2 Gravity localization: the Randall-Sundrum model

Gravitational fluctuations in a five-dimensional spherically symmetric spacetime can be expressed in terms of a superposition of modes, where each mode can be written as a product of a 4D mode and a one-dimensional wavefunction $\psi_m(r)$ in the extra fifth radial dimension (see Appendix A.5). These wavefunctions, which are called Kaluza-Klein (KK) modes, are eigenmodes of a one-dimensional Schrödinger equation with a specific potential $V(r)$ determined by the background geometry and with eigenvalues given by m^2.[29] Randall and Sundrum [34, 35] showed that, in the presence of a 4D brane with critical tension $T = 1/L$[30] embedded in pure AdS$_5$, there exists a "zero mode" with $m^2 = 0$ and ψ_m sharply peaked at the location of the brane, corresponding to a 4D massless graviton bound to the brane. The intuition behind the existence of the localized mode is that the presence of the brane introduces a term in the Schrödinger potential proportional to a negative delta function at the brane location (see Section 2.4 and Appendix A.5). Therefore, the Randall-Sundrum model yields a 4D gravitational description on the Minkowski brane even in the presence of a non-compact extra dimension. There is naturally also a tower of massive KK modes, but the correction to 4D general relativity arising from their presence is negligible at low energies [34, 35].

Our setup is slightly more complicated than the one considered in the original Randall-Sundrum model. First, the brane is sub-critical, and therefore there is a negative 4D cosmological constant $\Lambda_4 < 0$ (we have an "AdS brane" [111]). Second, the 5D bulk geometry is not pure AdS, but rather an AAdS black hole. Karch and Randall [111] showed that AdS branes embedded in pure AdS$_5$ support gravity localization if $|\Lambda_4| \ll 1$ (i.e. the brane is near-critical), but only locally. In fact, the Randall-Sundrum zero mode becomes an "almost zero" mode with mass m_0 bound on the brane, corresponding to a light (if Λ_4 is small) but massive 4D graviton. Therefore, as long as we probe the physics only at length scales smaller than $1/m_0$, ordinary 4D gravity is reproduced. Since AAdS black hole spacetimes are indistiguishable from pure AdS in the asymptotic region,

[29] This notation differs slightly from the one we use in Chapter 2, but is the one employed in Refs. [34, 35] in the case of a "Minkowski" brane (i.e. a brane with $T = 1/L$ embedded in pure AdS). For such a setup, $m^2 = \omega^2 - k^2$ where ω is the frequency and $k = |\vec{k}|$ with $\vec{k}$ the wave-vector in the three spatial directions of the brane.

[30] Note that the effective 4D cosmological constant Λ_4 vanishes for a critical tension brane, i.e. we have a "Minkowski" brane rather than an "AdS" brane [111]. Notice also that our definition of the tension differs by a multiplicative constant from the one in Refs. [34, 35, 111], and here we used our notation from Subsection 1.3.1 to define the critical tension.

we can expect the same local localization phenomenon to take place in our setup provided that the brane is far enough from the black hole horizon.

In an AdS-Schwarzschild background,[31] Clarkson and Seahra [131] showed that if the brane is far from the black hole horizon and deep into the AdS asymptotic region, gravity on the brane is indeed locally localized via a light but massive graviton similar to the Karch-Randall scenario. However, the presence of the black hole in the bulk implies that the bound almost zero mode becomes a "quasi-bound" mode with complex frequency $\omega = \bar{\omega} + i\Gamma$. In other words, the quasi-bound mode is exponentially suppressed in time, corresponding to a 4D massive graviton on the brane with a finite lifetime which will eventually "leak" into the bulk. Intuitively, the quasi-bound mode still exists thanks to the presence of the negative delta term in the Schrödinger potential at the brane location, but because the potential vanishes approaching the black hole horizon, the graviton wavefunction has a non-vanishing probability of tunneling towards the horizon and the probability for the graviton to be bound on the brane decays over time. Although the 4D graviton is metastable, the imaginary part of the frequency Γ becomes very small if the brane is far from the black hole horizon, signaling a long-lived (massive, but light) graviton.[32]

To summarize, an observer comoving with the brane will interpret the motion of the brane in the 5D AAdS black hole spacetime as the expansion and contraction of a 4D Big Bang-Big Crunch FLRW universe. If for some part of its evolution the brane is far from the black hole horizon and deep into the asymptotic AdS region, there the observer will also experience ordinary 4D gravity as long as they do not probe physics on very large scales (revealing the massive

[31] And limiting their analysis to the small black hole case $r_H \ll L$ and to the approximation in which the brane is moving adiabatically in the black hole spacetime, see Chapter 2. In Chapter 2 and Appendix A we extend their analysis to the large black hole case and to an AdS-Reissner-Nordström background.

[32] Note that the 4D massive gravitational description, although perturbatively well-defined [111], is only effective, with the full gravitational theory being higher dimensional. Therefore, the usual issues arising when trying to formulate a consistent massive theory of gravity [132] are not relevant to our setup.

nature of gravitons) or for a very long time (revealing the finite lifetime of the quasi-bound graviton). These length and time scales will be quantified in the case of our interest in Chapter 2 and Appendix A.

1.3.3 Holographic dual proposal via AdS/BCFT

Now that we have specified the bulk setup of interest, we can ask what a possible dual boundary theory would look like. With this goal in mind, let us focus on the saddle of the gravitational Euclidean path integral associated with the Lorentzian spacetime we just described, which is given by the Euclidean geometry in Figure 1.1 (b).

When performing the analytic continuation between the two geometries, the time-reflection symmetric slice $\tau = 0, \pm\beta/2$—where τ is the Euclidean time and β the inverse temperature of the black hole setting the periodicity of the Euclidean time coordinate—is left invariant. This is the Cauchy slice on which the Euclidean path integral "prepares" the state[33] of the bulk theory which is then evolved forward and backward in real time to yield the Lorentzian geometry in Figure 1.1 (a). Therefore, the brane radius on such a slice is still given by $r(\tau = \pm\beta/2) = r_0$ with $dr/d\tau|_{\tau=\pm\beta/2} = 0$. The brane equation of motion is analogous to equation (1.22), but with the opposite sign on the right-hand side. This implies that r_0—which in Lorentzian signature was the maximum radius reached by the brane during its evolution—becomes a minimum radius in Euclidean signature, with the brane expanding towards the asymptotic boundary as we leave the time-reflection symmetric slice.

For fixed values of the black hole spacetime parameters (i.e. the AdS length L and the black hole mass parameter μ in the Schwarzschild case), a choice of r_0—or equivalently of the brane

[33] See Appendix B.1 for further explanation of this point.

tension T—fully determines the brane trajectory, and in particular the two points where the brane intersects the asymptotic AdS boundary.[34] Since the trajectory is time-reflection symmetric, the two intersection points are also symmetric and we will identify them by $\tau = \pm\tau_0$ (see Figure 1.1 (b)), where τ_0 is called "preparation time" and will play a central role in our analysis in Chapter 2.

This construction suggests that the dual Euclidean boundary theory is defined on a manifold with a boundary in Euclidean time, given by $S^3 \times I$ where $I = [-\tau_0, \tau_0]$ is a finite interval. In order to consistently define a CFT on a manifold with a boundary, specific boundary conditions (known as conformal boundary conditions) must be imposed which preserve part of the conformal symmetry. The resulting theory is called boundary conformal field theory (BCFT) [134–137]. Each set of conformal boundary conditions can be described in terms of a specific "boundary state" (or Cardy state) $|B\rangle$[35] for the CFT at the corresponding boundary. Cardy states are characterized by a quantity called "boundary entropy" defined as $S_b = \log \langle 0|B\rangle$ with $|0\rangle$ the CFT vacuum, which gives an intensive contribution associated with the presence of the boundary to the entanglement entropy of subregions of a BCFT [137].

The fact that the bulk holographic dual of BCFTs is given by spacetimes cut off by ETW branes was first suggested by Takayanagi [11] and Fujita, Takayanagi, and Tonni [12]. In this AdS/BCFT proposal, which has been shown to yield results consistent with the physics of boundary conformal field theories in various setups, the ETW brane is homologous to the boundary manifold. In other words, the brane can be seen as an extension in the bulk of the boundary of the

[34] This statement is true for $d > 2$, and therefore in our $d = 4$ case. In lower dimensional examples, the brane anchoring points at the boundary are fixed and independent of the choice of parameters. For example, for $d = 2$ the brane always anchors at antipodal points of the thermal circle [127, 133]. Notice also that, as we will explain in the next subsection, not all combinations of parameters yield a "good" brane trajectory which hits the boundary, but sometimes the brane "overlaps" with itself preventing a dual description in terms of a BCFT.

[35] Note that boundary states are not normalized, and in fact non-normalizable [136, 137].

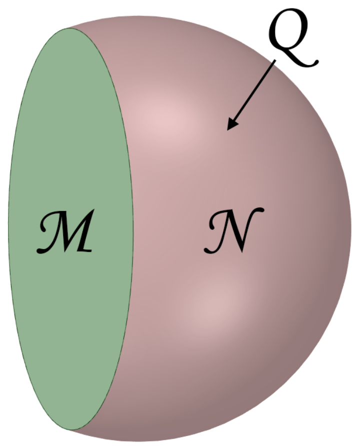

Figure 1.2: AdS/BCFT proposal. The bulk spacetime dual to a holographic BCFT defined on a manifold with boundary $\mathcal{M}$ in d dimensions is given by a $(d+1)$-dimensional manifold $\mathcal{N}$ cut off by a dynamic end-of-the-world brane, modeled by a d-dimensional manifold $\mathcal{Q}$ on which Robin boundary conditions for bulk fields are imposed. In the simplest model, the brane is characterized by a single parameter, the tension T. The brane $\mathcal{Q}$ is homologous to the manifold $\mathcal{M}$, i.e. it can be seen as a "bulk extension" of the boundary of $\mathcal{M}$. This figure appeared in Ref. [127].

manifold where the BCFT is defined (see Figure 1.2). In the simplest case where the ETW brane is characterized only by its tension, the value of the tension T is related to the boundary entropy of the specific Cardy state in the dual BCFT [11, 12].

According to the AdS/BCFT proposal, the Euclidean geometry in our braneworld setup is therefore dual to a Euclidean BCFT defined on a manifold with two boundaries in the Euclidean past and future. Since the setup is time-reflection symmetric, the two boundary conditions must be identical, implying that the two branes anchored at $\tau = \pm\tau_0$ have the same tension T, which allows them to smoothly join deep into the bulk to form a single brane.[36]

Given this duality between the Euclidean bulk saddle and the dual Euclidean BCFT, it is now interesting to ask which state of a correspondent Lorentzian CFT is the Lorentzian geometry

[36]It is worth noting that in the AdS-Schwarzschild case studied in Ref. [5] and reviewed here, the AdS-Schwarzschild Euclidean geometry is not the only saddle of the gravitational Euclidean path integral. There is in fact a competing saddle given by thermal AdS$_5$, in which there are two disconnected branes separately anchored at $\tau = -\tau_0$ and $\tau = \tau_0$. The two saddles switch dominance depending on the black hole mass and the brane tension, see [5] for further details. In the charged black hole case of Chapter 2 the two competing saddles are a sub-extremal and an extremal AdS-Reissner-Nordström black hole, with a single connected brane in both cases.

(including the braneworld cosmology) dual to. As we have seen, the Lorentzian geometry can be obtained by slicing open the gravitational Euclidean path integral along the time-reflection symmetric bulk slice $\tau = 0, \pm\beta/2$, and then evolving the resulting state on this Cauchy slice forward and backward in real time. The corresponding slice in the boundary theory is the $\tau = 0$ slice, on which the CFT Euclidean path integral prepares a highly excited pure state given by a finite amount τ_0 of Euclidean time evolution performed on the Cardy state $|B\rangle$.[37] Therefore, the conformal boundary conditions are a set of initial conditions in the Euclidean past for the Euclidean path integral preparing a specific excited state. This highly excited state looks thermal to good approximation [1, 5, 6, 138], which is the reason why the dual geometry is given by a black hole spacetime, but it is a pure state. It should therefore be regarded as a specific black hole microstate.

It is worth noticing that, in the Lorentzian geometry, the CFT dual to the whole 5D spacetime lives on the right asymptotic boundary, whereas the ETW brane moves between the black hole past and future interior and the left wedge (see Figure 1.1 (a)). As it is well known [67, 76, 77, 79, 80, 139–142], probing physics behind the horizon of a black hole from the dual CFT is an extremely complicated task. Consequently, probing the brane evolution, and therefore the cosmological physics, from the dual CFT in our setup is also a particularly tricky task. An intuitive way to understand this from the microscopic theory point of view is that, in order to probe the brane behind the horizon of the black hole, we need to detect deviations from the thermal behavior in a highly excited and highly thermalized state of the CFT. This task generally requires the computation of expectation values of very complicated or very fine-tuned operators (see for

[37] As we have mentioned, Cardy states are non-normalizable, and in fact they have infinite energy [136, 137]. The Euclidean time evolution "smooths out" this singularity, yielding a well-defined, finite-energy (but high-energy) state at $\tau = 0$ dual to the Lorentzian spacetime.

example [1,138]). Nonetheless, it was shown in Ref. [5] that specific observables (such as the entanglement entropy of large regions of the CFT near the time-reversal-symmetric slice [143] and the holographic complexity [66]) are able to probe the brane tension and therefore reconstruct the evolution of the associated braneworld FLRW cosmology.

1.3.4 Challenges of the approach and results of Chapter 2

In the spirit of the bottom-up approach to holography, we can now try and understand what properties the bulk effective field theory must have in order for a dual description of the cosmology to exist. From the discussion carried out in the previous subsections, we can identify two necessary conditions that need to be satisfied in order to obtain a holographic description of a well-defined cosmological universe:

1. At least for part of its trajectory, the ETW brane needs to be far from the black hole horizon and deep into the AdS asymptotic region, i.e. $r_0 \gg r_H, L$ must hold;

2. The preparation time τ_0 needs to be positive, which is equivalent to say that the brane must not overlap with itself.

The first condition is necessary in order for gravity to be locally localized on the brane at least for part of the brane trajectory, yielding a well-defined notion of a 4D cosmological universe in that part of the trajectory. The second condition guarantees the existence of a finite interval $I = [-\tau_0, \tau_0]$ on the boundary where the dual BCFT can be defined.

It was shown in Ref. [5] that in the simplest case considered there and in the previous subsections, where the black hole spacetime is AdS-Schwarzschild, the two conditions cannot be satisfied at the same time. In fact, whenever the tension is large enough to satisfy the condition

$r_0 \gg r_H$, the brane "overlaps" with itself and the preparation time becomes negative. This phenomenon can be detected by calculating, in the Euclidean bulk geometry, the amount $\Delta\tau$ of Euclidean Schwarzschild time needed for the brane to reach the asymptotic boundary from the turning point at $\tau = \pm\beta/2$. If $\Delta\tau > \beta/2$, where we recall that the inverse temperature β sets the periodicity of the Euclidean time coordinate, the brane overlaps itself before reaching the boundary. This result implies that gravity localization and a dual description in terms of a BCFT are mutually exclusive in the AdS-Schwarzschild case.

Motivated by this shortcoming, we investigated analogous questions in a slightly different setup in which the 5D spacetime is given by an AdS-Reissner-Nordström (AdS-RN) black hole. The resulting analysis was published in Ref. [1] and is reported in Chapter 2 and Appendix A.

AdS-RN [144–149] is a static, purely electrically charged solution of Einstein-Maxwell equations. The metric takes the same spherically symmetric form (1.18), with $f(r)$ now given by

$$f(r) = 1 + \frac{r^2}{L^2} - \frac{2\mu}{r^2} + \frac{Q^2}{r^4} \tag{1.25}$$

where the charge parameter Q (which from now on we will simply call charge) is proportional to the black hole electric charge (see equation (A.4) in Appendix A.1). This spacetime has a timelike singularity and two horizons: an outer horizon at $r = r_+$ and an inner horizon at $r = r_-$. Allowed values for the charge Q are upper-bounded by the "extremal charge" Q_e for which $r_+ = r_-$. The solution for which the two horizons coincide is known as extremal black hole and is generally considered non-physical (although only marginally) because it contains a naked singularity, violating the cosmic censorship conjecture [150]. Due to the timelike nature of the singularity, the double-sided AdS-RN black hole can be in principle further extended by gluing together multiple exterior and interior patches (see Figure 1.3). However, this picture is also believed to be non-physical due to the instability of the inner horizon which would cause the formation of a spacelike singularity under small perturbations of the geometry (see [151] and references therein).

Similar to the AdS-Schwarzschild case, a pure-tension ETW brane can be embedded in this spacetime cutting off part of the left asymptotic region of the maximally extended black hole spacetime. In Lorentzian signature, the brane in this case would emerge from the past inner and outer horizons, expands up to a maximum radius r_0, then recollapse in a symmetric way into the future outer and inner horizons. If we (naively) consider multiple patches glued together and trust the bulk EFT beyond the past and future inner horizons, the brane would then reach a minimum radius r_0^- before starting expanding again and emerging in a new exterior patch (see Figure 1.3). However, as we have mentioned, the instability of the inner horizon implies that our bulk EFT is valid only in a single exterior patch and only outside the past and future inner horizons.

The braneworld cosmology in this case is again given by a FLRW universe, where the Friedmann equation takes the form

$$\left(\frac{\dot{r}}{r}\right)^2 = \left(T^2 - \frac{1}{L_{AdS}^2}\right) - \frac{1}{r^2} + \frac{2\mu}{r^4} - \frac{Q^2}{r^6}. \tag{1.26}$$

The cosmological evolution is therefore analogous to the AdS-Schwarzschild case, except for the presence of an additional term proportional to the black hole charge and dominant for small values of the scale factor, i.e. in the early and late universe. This kind of energy density in the cosmology literature goes under the name of "negative energy stiff matter" [152, 153]. The stiff matter term is the one responsible for the existence of a minimum radius for the brane at

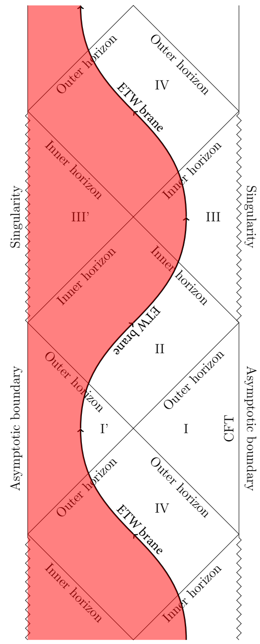

Figure 1.3: Schematic penrose diagram of the Lorentzian maximally extended AdS-RN black hole cut off by an ETW brane. The region shaded in red is cut off by the brane and not part of the geometry. Multiple interior and exterior patches have been glued together in this depiction, but the bulk EFT is reliable only in regions I, I', II, and IV due to the instability of the inner horizon. This figure appeared in Ref. [1].

$r = r_0^-$. Therefore, if we trust the braneworld cosmology evolution past the inner horizon, the cosmology undergoes a "Big Bounce" when the stiff matter term becomes dominant on the right-hand side of the Friedmann equation (1.26). However, the instability of the inner horizon causes the braneworld cosmology to become a Big Bang-Big Crunch cosmology under small perturbations of the background geometry [151].

As we have reviewed, the 4D braneworld cosmology interpretation is meaningful only if gravity has a 4D effective description on the brane, and this is possible only if the brane is outside the horizon and deep into the asymptotic AdS region.[38] In Ref. [1] (reported in Chapter 2 and Appendix A) we show that in the AdS-RN setup it is indeed possible for part of the brane trajectory to be arbitrarily far from the black hole horizon (i.e. $r_0 \gg r_+$) while preserving the

[38]Note that in this regime, which is the one we will mainly focus on in Chapter 2, the stiff matter term is negligible.

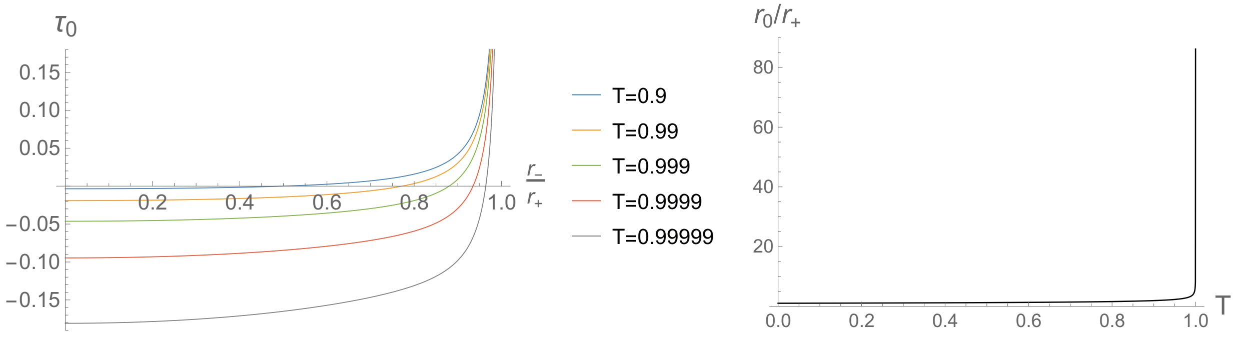

(a) (b)

Figure 1.4: Solutions with $\tau_0 > 0$ supporting gravity localization in a black hole spacetime with $L = 1$ and $r_+ = 100$. (a) For any given value of the tension T, the preparation time is positive if the black hole is sufficiently close to extremality, i.e. if the ratio r_-/r_+ is sufficiently close to 1. (b) For $r_- = 99.9$, corresponding to a near-extremal black hole, the inversion point r_0 of the brane trajectory can be very far from the black hole outer horizon r_+ if the brane is near-critical, i.e. if $T \lesssim 1$. This figure appeared in Ref. [1].

positivity of the preparation time (see Figure 1.4 and Section 2.2). This result can be achieved only in a specific region of the parameter space: in order for $r_0 \gg r_+$ to hold, the black hole must be large ($r_+ \gg L$) and the brane must be near-critical ($T \lesssim 1/L$); given two such values of r_+ and T, the preparation time is positive only if the black hole is near-extremal ($r_- \lesssim r_+$, implying a highly charged black hole). In this regime, the bulk construction admits a holographic dual description which can be built using the AdS/BCFT proposal as explained in Section 1.3.3. The pure excited state dual to the Lorentzian geometry will be a state of a 4D CFT with a $U(1)$ global symmetry.[39]

After identifying the region of interest in the parameter space, we explicitly study gravity localization on the brane by extending the analysis of Clarkson and Seahra [131] to the large and charged black hole case. We find that gravity is in fact locally localized on the brane in the part of its trajectory where it is far from the black hole horizon, thanks to the existence of a quasi-bound

[39]In AdS/CFT, gauge symmetries in the bulk theory (such as the $U(1)$ symmetry associated with bulk electromagnetism in our setup) correspond to global symmetries in the boundary theory [154].

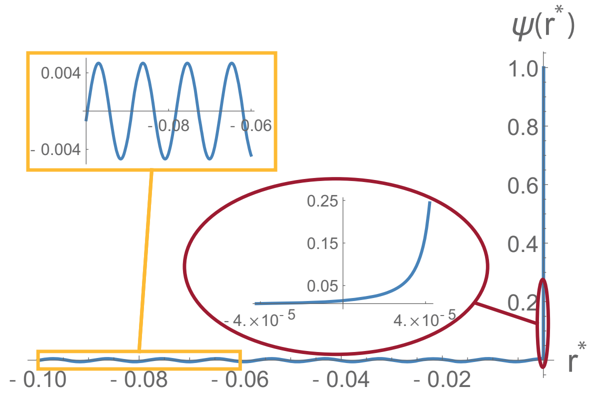

Figure 1.5: Quasi-bound mode wavefunction $\psi(r^*)$ as a function of the tortoise coordinate r^* defined as $dr^* = dy/f(y)$, with $y = r/r_+$. The black hole horizon is given by $r^* \to -\infty$. In this numerical evaluation we set $L = 1$, $r_+ = 100$, $r_- = 99.9$, and angular momentum $l = 5$ (see Section 2.4). The position of the brane is the one corresponding to the maximum radius r_0 of a brane with near-critical tension $T = 0.999999$. $\psi(r^*)$ is very sharply peaked near the brane location $r_b^* = 4.65 \cdot 10^{-5}$ and it oscillates near the horizon $r^* \to -\infty$. This behavior shows how the quasi-bound mode is well localized on the brane giving rise to effective 4D gravity, but it has a non-vanishing probability to "leak" into the bulk. This figure appeared in Ref. [1].

mode with a finite but long lifetime (see Figure 1.5 and Section 2.4). We also show that, in the regime of interest, the saddle of the Euclidean path integral given by the near-extremal Euclidean AdS-RN black hole cut off by the ETW brane is dominant in the fixed-charge ensemble over the other possible competing saddle, given by an extremal black hole with the same charge and preparation time (see Appendix A.3).

To summarize, the result of the analysis of Chapter 2 is that it is possible to construct a 4D braneworld Big Bang-Big Crunch cosmology embedded in a 5D AdS-RN black hole spacetime such that

- Gravity is effectively 4D on the brane for (a consistent) part of the cosmological evolution around the time-symmetric point (when probed on relatively short spatial and time scales);
- The associated Euclidean bulk geometry is the dominant saddle in the Euclidean gravitational path integral computing the partition function for the fixed-charged ensemble;

- The bulk Lorentzian setup admits the existence of a holographic description in terms of a pure excited state of a 4D CFT with a $U(1)$ global symmetry. Such a state is prepared by a BCFT Euclidean path integral with a boundary in the Euclidean past where conformal boundary conditions are imposed.

1.4 Second approach: holographic wormhole cosmology

In this subsection we will give an overview of our second approach to the holographic decription of $\Lambda < 0$ cosmology. This is inspired by ideas first introduced by Maldacena and Maoz [13] and further developed in Ref. [7], and it was formulated in its present form in Refs. [2, 8, 9]. Related ideas also appeared in Refs. [10, 155]. Chapter 3 (which was published in the seminal paper [2]) gives a complete introduction to the holographic wormhole cosmology approach, explaining in detail its properties and relationship with previous literature. Therefore, in this subsection we will summarize the main features of the construction and refer to Chapter 3 and Appendix B for further details.

1.4.1 The bulk setup: cosmology and AdS wormholes

The observation at the foundation of our second approach is that certain time-symmetric Big Bang-Big Crunch cosmologies with negative cosmological constant analytically continue to Euclidean wormholes connecting two asymptotically AdS regions [13]. The simplest example is the spatially flat FLRW cosmology driven by a negative cosmological constant and radiation studied at the end of Section 1.2.1. Let us consider the solution (1.13) of the Friedmann equation (1.12). For simplicity and without loss of generality, let us perform a translation of the time coordinate and set the inversion point to be $t = 0$, so that the geometry is time-reversal-invariant. The scale factor (1.13) then reads $a(t) = A\sqrt{\cos(Bt)}$, where we defined $A = (-8\pi G\rho_r^0/\Lambda)^{\frac{1}{4}}$ and $B = 2\sqrt{-\Lambda/3}$. The Big Bang is now at $t = -\pi/(2B)$ and the Big Crunch at $t = \pi/(2B)$.

By analytically continuing the time coordinate $t \to -i\tau$, we obtain the Euclidean flat FLRW metric

$$ds^2 = d\tau^2 + a_E^2(\tau)(dx^2 + dy^2 + dz^2) \tag{1.27}$$

where $a_E(\tau) = a(-i\tau) = A\sqrt{\cosh(B\tau)}$. The Euclidean scale factor is the solution of a Friedmann equation similar to (1.12), but with signs flipped on the right-hand side:

$$\left(\frac{a_E'}{a_E}\right)^2 = -\frac{\Lambda}{3} - \frac{8\pi G}{3}\frac{\rho_r^0}{a_E^4}, \tag{1.28}$$

where we indicated with a prime a derivative with respect to the Euclidean time τ. By inspecting the expressions for the two scale factors $a(t)$ and $a_E(\tau)$, it is immediate to see that the maximum value at $t = 0$ of the Lorentzian scale factor corresponds to the minimum value at $\tau = 0$ of the Euclidean scale factor. Furthermore, the Euclidean scale factor diverges exponentially for $\tau \to \pm\infty$, implying that the Euclidean geometry has two asymptotic AdS regions there. This can be easily understood by looking at the form of the metric when rewritten using the Euclidean conformal time coordinate (defined by $d\xi = d\tau/a_E(\tau)$ and setting $\xi(\tau = 0) = 0$):[40]

$$ds^2 = a_E^2(\xi)\left(d\xi^2 + dx^2 + dy^2 + dz^2\right), \tag{1.29}$$

[40]Notation remark: the coordinate labels used here are different from those used in Chapters 3, 4, and 5. In fact, each chapter uses the coordinate labels most suitable for its specific goals, but the relationship between different notations is straightforward to figure out.

with $a_E^2(\xi) = A^2 \cosh\left[-i2\mathrm{am}\left(iAB\eta/2, 2\right)\right]$, where $\mathrm{am}(u,m)$ is the Jacobi amplitude.[41] By expanding the Jacobi amplitude near the two poles at $u = \pm i\mathcal{K}(-1)$ corresponding to the asymptotic regions $\tau \to \pm\infty$ (where $\mathcal{K}(m)$ is the complete elliptic integral of the first kind), one can show that the metric takes the form

$$ds^2|_{\tau\to\pm\infty} = \frac{4/B^2}{\left(\xi \mp \frac{2\mathcal{K}(-1)}{AB}\right)^2}\left(d\xi^2 + dx^2 + dy^2 + dz^2\right). \tag{1.30}$$

Equation (1.30) is the pure Euclidean AdS metric in Poincarè coordinates with AdS radius $L = 2/B = \sqrt{-3/\Lambda}$, as expected. Therefore, the analytic continuation of the time-symmetric FLRW cosmology driven by a negative cosmological constant and radiation is an asymptotically AdS Euclidean wormhole with planar cross section and with the two asymptotic AdS boundaries located at $\xi = \pm 2\mathcal{K}(-1)/(AB)$.

The solution described above is just a simple example of a more generic class of solutions with similar properties. In general, given a Euclidean time-reflection symmetric AdS wormhole[42] with metric of the form (1.29), its analytic continuation yields a real time-symmetric FLRW metric. It is worth mentioning here that, away from the time-reversal-symmetric slice, the evolution of a FLRW universe obtained by analytically continuing a Euclidean wormhole depends on the specific EFT driving the cosmological evolution. In general, not all such FLRW metrics describe Big Bang-Big Crunch cosmologies. Note also that not all time-symmetric Big Bang-Big Crunch FLRW cosmologies have an analytic continuation given by a Euclidean wormhole (see Section

[41]Note that, between the two poles at $u = \pm i\mathcal{K}(-1)$, $\mathrm{am}(u,2)$ is purely imaginary for u purely imaginary, which correctly implies that the scale factor $a_E(\xi)$ is real.

[42]Only time-reflection symmetric Euclidean geometries analytically continue to real Lorentzian spacetimes [8]. In the presence of other bulk fields, they must also be time-reflection symmetric, i.e. their derivative must vanish at the center of the wormhole $\tau = 0$ (and therefore at the inversion point of the cosmology $t = 0$).

1.7 and Chapter 5 for further details). The class of solutions we are interested in are those in which the Euclidean geometry is given by an AdS wormhole and its Lorentzian continuation is a time-symmetric Big Bang-Big Crunch FLRW cosmology.

As we have seen in Section 1.2.2, one of the biggest challenges for obtaining a holographic description of cosmology within AdS/CFT is the absence in cosmological universes of an asymptotic AdS boundary on which to define the dual CFT. Intuitively, $\Lambda < 0$ cosmologies in the class we just identified escape this problem because asymptotic AdS boundaries are present in the Euclidean geometry obtained by analytically continuing the cosmology. More precisely, the gravitational Euclidean path integral with two AdS boundaries possesses a saddle (the Euclidean wormhole) whose analytic continuation gives rise to the FLRW cosmology. If such a Euclidean path integral is holographically dual to a Euclidean path integral for a microscopic, non-gravitational theory associated with the two asymptotic AdS boundaries,[43] the Big Bang-Big Crunch cosmology has a holographic description in terms of a specific state of the dual theory. The challenge of describing cosmology within holography therefore reduces to finding a microscopic boundary theory dual to a bulk theory whose Euclidean gravitational path integral admits Euclidean wormhole saddles with metric of the form (1.29) and with an associated Big Bang-Big Crunch cosmology. Our proposal for the general form of the dual theory and the state dual to the cosmological universe will be described in the next two subsections.

Before moving on to describe the proposed holographic dual theory, we would like to remark that planar Euclidean wormhole geometries with metric of the form (1.29) also admit a different analytic continuation. In fact, they also have a reflection symmetry along any of the non-

[43]We will see that the dual theory does not simply live on the two 3D disconnected AdS boundaries, but on a connected 4D manifold $\mathbb{R}^3 \times I$, where I is a finite interval and the two 3D AdS boundaries are identified with the endpoints of the interval.

compact $\mathbb{R}^3$ directions x, y, z. Analytic continuation of one of these coordinates, say $x \to iX$, yields a static spacetime

$$ds^2 = a_E^2(\xi)\left(-dX^2 + d\xi^2 + dy^2 + dz^2\right) \tag{1.31}$$

where $a_E(\xi)$ is the same conformal factor we had in Euclidean signature, which possesses two simple poles at the location of the two asymptotic AdS boundaries, which we generically indicate with $\xi = \pm\xi_0$. This is a static, horizon-less metric connecting two asymptotic AdS boundaries. Hence, it describes a Lorentzian AdS eternal traversable wormhole with planar cross section. From now on we will refer to this analytic continuation as the "wormhole picture" as opposed to the "cosmology picture" obtained by analytically continuing the ξ (or equivalently τ) coordinate.

The Lorentzian wormhole (1.31) is a solution of the same "Friedmann equation" describing the Euclidean wormhole (see equation (1.28) for the simple case driven by a negative Λ and radiation). This equation, however, describes now the spatial evolution of the conformal factor along the wormhole radial direction τ (we recall that $d\xi = d\tau/a_E(\tau)$) in the Lorentzian spacetime. The consistency of gravitational effective field theories leading to similar Lorentzian wormhole solutions is debatable. In fact, planar Lorentzian traversable wormholes must be sustained by a large amount of negative vacuum energy [2, 7, 8, 156], which seems to be inconsistent with typical QFT results. However, examples of mechanisms leading to negative energy enhancement in related setups have been recently found [157, 158]. In the simple EFT considered above, the negative energy is provided by the "radiation" term with the negative sign on the right-hand side of equation (1.28). The presence of this contribution, which is a very natural radiation term in the cosmology picture, must be justified in the wormhole picture in terms of some enhanced negative vacuum energy, see Chapter 3 for further details.

Although the existence and consistency of the wormhole picture are not necessary for a holographic description of cosmology, they give rise to interesting additional features which we will discuss in the next subsections. Therefore, while keeping in mind the caveats mentioned above, we will work under the assumption that EFTs giving rise to Lorentzian traversable wormholes of the form (1.31) can be consistently obtained.

1.4.2 The proposed holographic dual theory: a "Euclidean sandwich"

The existence of Euclidean wormhole solutions connecting multiple AdS boundaries is a rather puzzling feature from the AdS/CFT point of view [7, 13, 54, 159–164]. In fact, the partition function computed by the gravitational Euclidean path integral in the presence of Euclidean wormholes with n mouths does not factorize into a product of n partition functions associated with the n boundaries.[44] On the other hand, if the boundary dual theory were given by n decoupled theories living on the n boundaries, the boundary partition function would instead factorize. This problematic feature is known as factorization puzzle and led to the interpretation of the gravitational path integral as computing the average of the product of partition functions over an ensemble of boundary theories (see [7, 13, 54, 159–166] for a detailed discussion of the factorization puzzle in various settings).

In order to build a holographic dual of the Euclidean wormhole configurations discussed in the previous subsection, we suggest a different (although related) setup not involving an ensemble interpretation [2, 8]. Consider two copies of a holographic Euclidean 3D CFT defined on $\mathbb{R}^3$ with

[44]This is true at least perturbatively around the saddle point approximation. The full, non-perturbative quantum gravity partition function might instead factorize, and there are hints that this is indeed the case coming from lower dimensional models [165, 166].

an $AAdS_4$ dual bulk Euclidean spacetime, and a 4D Euclidean CFT with many fewer degrees of freedom (i.e. $c_{3D} \gg c_{4D}$ where c is the central charge) defined on $\mathbb{R}^3 \times I$, where I is a finite interval[45]. Let us then couple, via a relevant deformation, the two 3D CFTs to the 4D CFT at opposite ends of the interval I, so that the whole setup is symmetric under reflection about the midpoint of the interval.[46] In this way, we have constructed a Euclidean "sandwich" theory, consisting of the two 3D theories with the 4D theory with many fewer degrees of freedom in between, see Figure 1.6.[47] Note that the 4D theory does not necessarily need to be holographic in this setup.

The condition $c_{3D} \gg c_{4D}$ guarantees that a bulk dual description in terms of a 4D spacetime still exists when the 3D CFTs are coupled to the 4D CFT (intuitively, the coupling to the "few" degrees of freedom of the 4D CFT modifies only slightly the bulk EFT dual to the two 3D CFTs, at least in the UV). Additionally, the relevant coupling implies that the two 3D CFTs are unmodified in the UV, and therefore the asymptotic AdS regions of the two dual Euclidean $AAdS_4$ spacetimes are unaffected. On the other hand, the coupling induces a large amount of entanglement between the two 3D theories in the IR, and the region deep into the bulk dual spacetime can be radically modified. In particular, the two Euclidean $AAdS_4$ spacetimes can connect deep into

[45]To avoid confusion, we restricted here to the case where the 4D microscopic degrees of freedom are also described by a CFT, but in general they can be described by a more generic QFT [2, 8]. Additionally, this construction can be generalized to different choices of the boundary manifold. For instance $S^3 \times I$ leads to spatially closed cosmologies. However, we will see that the choice considered here, besides leading to a phenomenologically more realistic flat cosmology, also allows us to establish a duality between cosmological observables and the vacuum physics of a confining gauge theory on flat spacetime.

[46]More precisely, in order to obtain such a reflection symmetry we need to couple at the two ends of the interval the 3D CFT and its (CP)T-conjugate.

[47]To make contact with well-understood microscopic examples in String Theory, we can choose both the 3D CFT and the 4D CFT to be supersymmetric (for instance, we can choose the 4D theory to be $\mathcal{N} = 4$ Super-Yang-Mills). In this case, the boundary conditions at each extreme of the interval I preserve half of the generators of the 4D supersymmetry. However, the opposite orientation of the two 3D theories implies that the two sets of preserved generators are complementary. Therefore, supersymmetry is completely broken in the full "sandwich" theory. For additional details on this point see Chapter 3 and [2, 8].

Figure 1.6: Proposal for the Euclidean "sandwich" theory dual to the Euclidean wormhole. Two holographic 3D CFTs are coupled to a 4D CFT on an interval. Under appropriate conditions, the two Euclidean AAdS$_4$ spacetimes dual to the 3D CFTs join up to form a Euclidean wormhole. This figure appeared in Ref. [2] (describing in that case the Lorentzian theory dual to the associated Lorentzian wormhole).

the bulk to form a Euclidean wormhole.

When the 4D CFT is not holographic, we expect the 4D Euclidean bulk dual to the sandwich theory to be given, in the saddle point approximation, either by two disconnected AAdS$_4$ spacetimes dual to the two 3D CFTs, or by a 4D Euclidean wormhole connecting the two asymptotic AdS boundaries where the 3D CFTs live. The disconnected bulk configuration corresponds to a Euclidean sandwich theory which is gapless (i.e. a CFT), while the Euclidean wormhole corresponds to a Euclidean sandwich theory which is confined/gapped in the IR.[48] In fact, in a gapped theory there is no non-trivial physics in the deep IR; therefore, in the spirit of the holographic renormalization group [18, 48–50], a spacetime dual to a gapped theory must be cut off deep into the bulk [7, 8, 51–53]. Our proposal is that such a cutoff is naturally provided by the two AAdS$_4$ spacetimes joining up to form a Euclidean wormhole, so that every point in the Euclidean geometry is at a finite radial coordinate distance away from the asymptotic boundaries. On the other hand, physics is non-trivial at arbitrarily long wavelengths in a gapless theory, implying that its bulk dual description should extend arbitrarily far away from the AdS boundary, as it is the

[48]Note that the 4D sandwich theory is defined on a non-compact manifold $\mathbb{R}^3$ times a compact interval I; therefore, it flows in the IR to an effective 3D theory on $\mathbb{R}^3$, which can be either a 3D CFT, or more generically a 3D confining theory.

case for the disconnected bulk configuration suggested above. Further intuition on these points can be gained by considering a doubly-holographic setup [36–38] leading to a picture similar to the holographic braneworld cosmology approach discussed in Section 1.3 (see Section 1.5).

Since we are interested in a holographic dual description of the Euclidean wormhole saddles discussed in the previous subsection and related by analytic continuation to Big Bang-Big Crunch FLRW cosmologies, we will focus our attention here on sandwich theories which are confined in the IR. The bulk field content on the wormhole background (and therefore in the cosmology obtained by analytic continuation of the wormhole) will clearly depend on the details of the two 3D CFTs, of the 4D CFT coupling them, and of the specific coupling chosen. We remark that this proposal for the dual theory has been obtained within a bottom-up approach to holography, i.e. starting from a bulk EFT of interest in the semiclassical holography regime and inferring the possible form of the boundary theory based on known features of the AdS/CFT correspondence. In the same spirit, in our analysis we will assume the existence of a sandwich theory dual to our bulk setup and study the constraints imposed on it by the existence of a wormhole dual description, as well as the necessary conditions the bulk EFT must satisfy for such a dual description to exist. Clearly, the ideal end goal and one of the most important future directions in the field is to find an explicit microscopic sandwich theory realizing our proposal in a top-down setting.

Before moving on to describe the Lorentzian states associated with our cosmology and Lorentzian wormhole pictures, three important remarks are in order. First, the full bulk Euclidean saddle dual to a gapped sandwich theory such as the one described above is not given only by the Euclidean wormhole of the previous subsection: there is also a 4D non-gravitational EFT living on $\mathbb{R}^3$ times an interval, with the two endpoints of the interval identified with the two

AdS boundaries (see the central drawing in Figure 1.7). In fact, the Euclidean wormhole can be intuitively understood to be dual to the two 3D CFTs in the sandwich theory, whereas the non-gravitational "auxiliary" degrees of freedom on the interval connecting the two AdS boundaries correspond to the non-holographic 4D CFT connecting the two 3D CFTs in the sandwich theory. This feature will be important in our discussion of the bulk EFT in Chapter 3. Second, our proposal for the holographic dual of the Euclidean wormhole is related to the ensemble proposal [7, 13, 54, 159–166]. In fact, the partition function of our sandwich theory can be expressed as an ensemble average of the product of the partition functions of the two 3D CFTs, with the average taken over an ensemble of possible couplings with the 4D CFT [7]. Third, the stability of AdS Euclidean wormhole saddles is an important open problem [167, 168].[49] We will work here under the assumption that, for the theories of our interest, such saddles are stable (see the string theoretic model proposed in Ref. [8] for a partial justification of this assumption).

1.4.3 Lorentzian states, cosmological islands, and slicing duality

Lorentzian states from different slicings of the Euclidean path integral

We now have a microscopic Euclidean theory—the sandwich theory—dual to a Euclidean wormhole geometry with metric of the form (1.29) whose asymptotic boundaries are connected by an auxiliary non-gravitational theory on a strip. As we have seen in Section 1.4.1, there are two different analytic continuations of the Euclidean wormhole leading to the cosmology and the Lorentzian wormhole pictures. Note that the two corresponding time-reflection symmetric slices

[49] Euclidean wormhole saddles in UV-complete quantum gravity theories can be unstable e.g. under field theoretic perturbations or brane nucleation. Wormholes that are stable under the former but unstable under the latter are local minima of the Euclidean path integral and are therefore subdominant saddles in the Euclidean path integral [167].

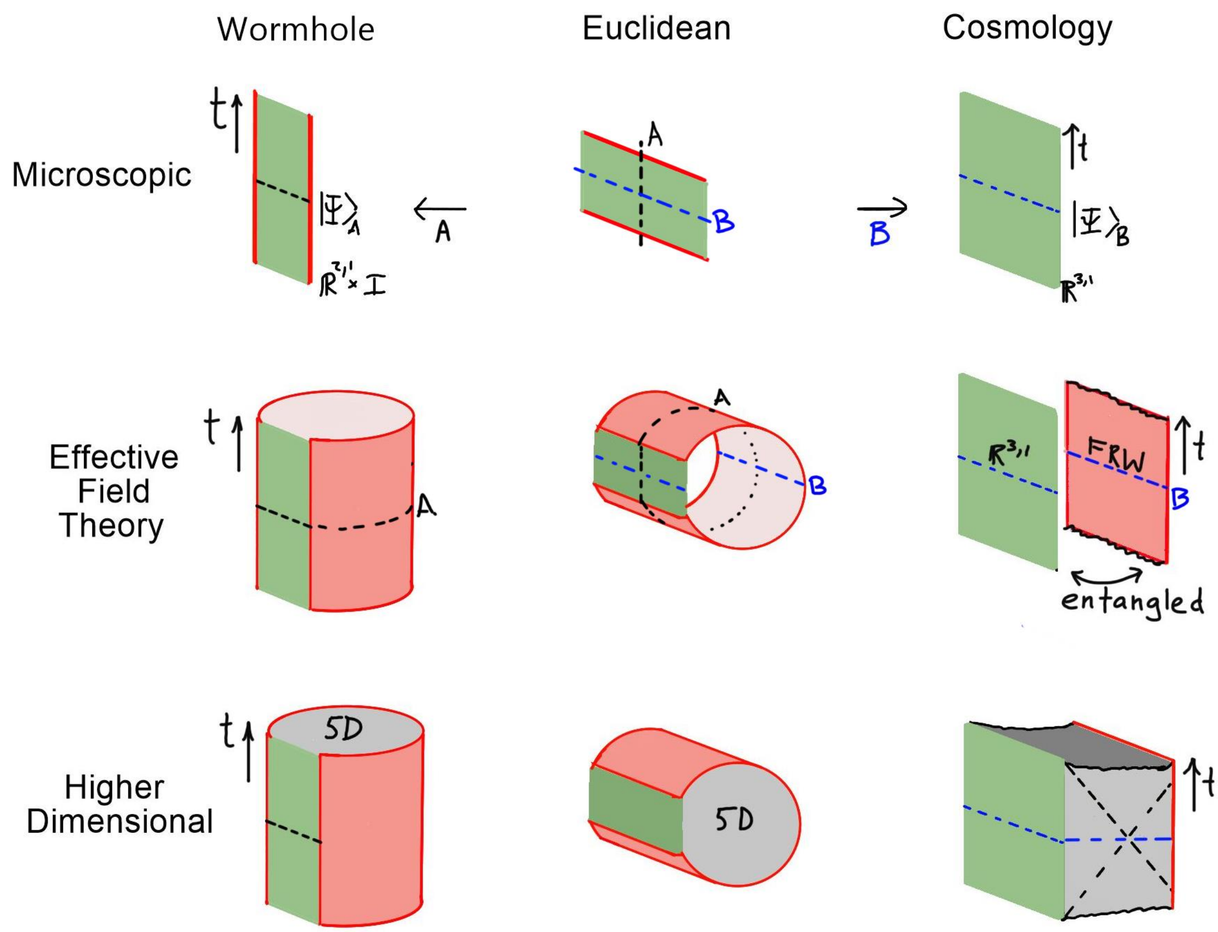

Figure 1.7: Different representations of the holographic wormhole cosmology setup. The equivalent theories are represented in the Euclidean picture in the central column, in the Lorentzian wormhole picture in the left column and in the cosmology picture in the right column. The first row corresponds to the microscopic setup, given by the Euclidean sandwich theory (center) and the associated Lorentzian theories—a Lorentzian confining theory in its vacuum state (left) and a 4D CFT in an excited state (right). The second row corresponds to the bulk effective field theory setup, with the Euclidean saddle given by the Euclidean wormhole (red) and the auxiliary non-gravitational degrees of freedom (green) coupling the AdS boundaries (center) and the associated Lorentzian theories—an eternal traversable wormhole with boundaries coupled by auxiliary degrees of freedom (left) and a Big Bang-Big Crunch FLRW cosmology entangled with a non-gravitational auxiliary bath (right). The third row depicts the corresponding doubly holographic setups described in Section 1.5. This figure appeared in Ref. [2].

($\tau = 0$ and $x = 0$)—where the bulk Euclidean path integral prepares the initial state to be evolved in Lorentzian time—intersect both the Euclidean wormhole and the auxiliary non-gravitational theory. Therefore, the latter is also involved in the bulk EFT analytic continuation.

The two full bulk Lorentzian EFT pictures are then those depicted on the right (cosmology) and left (wormhole) drawings of the central row in Figure 1.7. In the cosmology picture, we have a 4D flat Big Bang-Big Crunch FLRW universe together with a non-gravitational auxiliary theory living on a separate 4D Minkowski spacetime. Fields in the two spacetimes are decoupled but highly entangled to each other.[50] This can be understood intuitively by noticing that the bulk Euclidean path integral preparing the state at the time-reflection symmetric slice indicated by B in Figure 1.7 is analogous to the one preparing the thermofield double (TFD) state, with one theory given by the EFT in the FLRW cosmology and the other theory given by the auxiliary theory on Minkowski spacetime. We emphasize that this specific state for the cosmology prepared by the Euclidean path integral (similar to the construction of Hartle and Hawking [169]) is defined at the time-symmetric slice of the Big Bang-Big Crunch cosmology, i.e. at late times. This fact plays an important role in our discussion in the next subsections and in Chapter 3. In the wormhole picture, we have an AdS Lorentzian planar eternal traversable wormhole with the two asymptotic boundaries coupled by an auxiliary non-gravitational 4D theory on a strip. This was to be expected, because traversable wormholes in AdS/CFT can arise only if the two asymptotic boundaries are coupled to each other, otherwise the interaction between the two boundary theories taking place through the bulk spacetime would not have a correspondent microscopic description [170–173].

[50] Note that, given that the 4D CFT has many fewer degrees of freedom than the 3D CFTs, the amount of entanglement between fields in the cosmology and fields in the auxiliary theory is upper-bounded (up to a multiplicative constant) by the number of degrees of freedom in the 4D CFT.

These two different "slicings" of the bulk Euclidean path integral defining the two Lorentzian pictures correspond to two different slicings of the microscopic boundary Euclidean path integral for the sandwich theory. The cosmology slicing corresponds to identifying the interval I with the Euclidean time direction and slicing open the boundary Euclidean path integral in the middle of the interval (see the top-right drawing in Figure 1.7). The state prepared on such a slice is a highly excited pure state of the non-holographic 4D CFT on spatial $\mathbb{R}^3$. Note that, in the corresponding Lorentzian theory, the degrees of freedom associated with the two 3D CFTs in the sandwich theory are non-physical: they only appear on the boundary in the Euclidean past of the path integral preparing the state. On the other hand, the Lorentzian wormhole slicing corresponds to identifying one of the three non-compact directions, say x, with the Euclidean time coordinate and slicing open the boundary Euclidean path integral on the $x = 0$ slice, which has topology $\mathbb{R}^2 \times I$ (see the top-left drawing in Figure 1.7). Since the x direction is non-compact, this defines the vacuum state of the corresponding Lorentzian theory (see Appendix B.1), which is simply the Lorentzian version of the gapped sandwich theory described above. Note that the two slicings of the microscopic boundary Euclidean path integral not only define two different states, but these are actually states of two different theories: one is a pure excited state of a 4D CFT on Minkowski spacetime, and the other one the vacuum state of a confining theory on spatial $\mathbb{R}^2 \times I$.

Cosmology as an entanglement island

It is now interesting to discuss the relationship between the microscopic Lorentzian states and the dual bulk Lorentzian geometries. The wormhole picture is fairly straightforward: the vacuum state of the gapped theory given by the two holographic 3D CFTs coupled by the non-holographic 4D CFT is dual to a 4D AdS Lorentzian eternal traversable wormhole, which is a solution of the semiclassical Einstein's equations sourced by the vacuum expectation value of the stress-energy tensor of bulk fields, with the two boundaries coupled by non-gravitational 4D degrees of freedom. On the contrary, the cosmology picture is much more intricate. On the microscopic side, we have an excited state of a non-holographic 4D CFT; on the bulk side, we have a highly entangled state of two theories living in two disconnected spacetimes: another version of the same 4D CFT on Minkowski spacetime but in a mixed state, and a Big Bang-Big Crunch FLRW cosmology whose evolution is driven by bulk fields determined by the specific Euclidean sandwich theory we started with. Remarkably, the cosmological spacetime is holographically encoded in an a priori non-holographic theory, thanks to the presence of holographic 3D CFTs in the Euclidean past and future of the path integral preparing the microscopic state.

This seemingly counter-intuitive conclusion is actually not different from the kind of physics arising when studying the Page curve for evaporating black holes in holography [76,77,79,80]. In the so-called "East Coast model" [76,80], a 2D AdS black hole evaporates into a non-gravitational 2D CFT "bath" on a Minkowski background. The two spacetimes are "glued" at the asymptotic AdS boundary, where transparent boundary conditions are imposed. The corresponding microscopic theory is given by a 1D holographic quantum mechanical system coupled to a non-holographic 2D CFT. There are two main analogies between this setup and the one of our interest. First, there is a non-holographic 2D CFT appearing in both the microscopic and the bulk dual setups (where it plays the role of the bath), and its state is different in the two cases [174]. This is very similar to what happens with our 4D non-holographic CFT. Second, the black hole geometry can be seen as dual to the holographic quantum system just like our Euclidean wormhole geometry (and therefore the cosmology) can be seen as dual to the two holographic 3D CFTs in the sandwich theory. However, its interior is actually encoded at late times in the degrees of freedom of the non-holographic 2D CFT. In fact, the entanglement wedge of a large region R of the microscopic 2D CFT at late times is given by the same region in the 2D "bath" in the bulk EFT, plus an "entanglement island" in the black hole interior. This is similar to how our cosmology is encoded in the excited state of the microscopic non-holographic 4D CFT. This fact suggests that our cosmology is in some sense an entanglement island for the microscopic 4D CFT.

It turns out that this interpretation is indeed correct. Fields in the cosmology are highly entangled with fields of the 4D CFT on Minkowski spacetime in the bulk EFT, as we have seen. This large amount of entanglement guarantees that the entanglement wedge of large regions of the microscopic 4D CFT is given by the corresponding region in the 4D CFT in the bulk EFT, plus an entanglement island in the cosmological spacetime [175, 176], see Figure 1.8. Therefore, the cosmology can be seen as an island for the microscopic 4D CFT. This fact renders clear that reconstructing the cosmological physics from the dual excited state of the microscopic, non-holographic 4D CFT is a very non-trivial task: it is analogous to reconstructing the interior of a black hole in the late stages of its evaporation by having access only to its Hawking radiation, which is believed to be an extremely complex endeavor (see for instance [67, 141, 142] and references therein). Fortunately, our construction involving a wormhole in the analytic continuation of the cosmological spacetime suggests an interesting way to avoid this issue and have easier access to the cosmological physics from the microscopic setup, as we will now discuss.

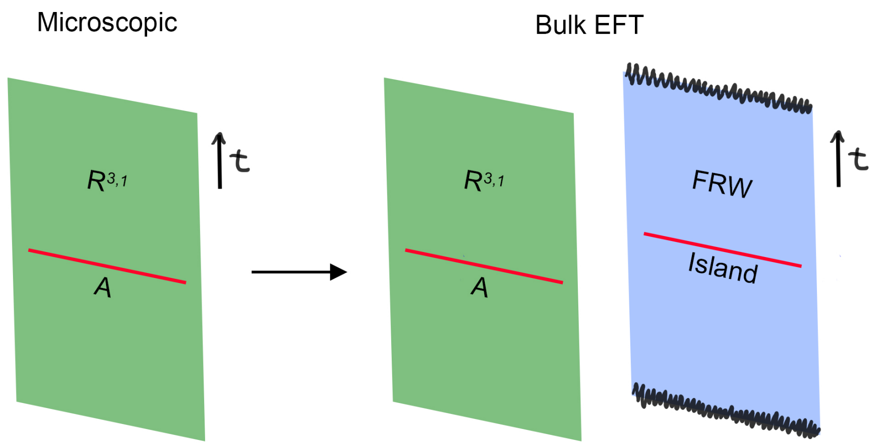

Figure 1.8: Cosmological islands. The entanglement wedge of a large region A of the microscopic 4D CFT includes the same region A in the bulk EFT version of the 4D CFT plus an entanglement island in the cosmological spacetime [175].

Slicing duality

The cosmological spacetime we obtain in our setup is related by analytic continuation to the Euclidean wormhole, and by double analytic continuation to the Lorentzian traversable wormhole. Specifically, the cosmology and wormhole scale factors are related to each other by analytic continuation. But there is more. Both analytic continuations leave the codimension-2 surface at $\tau = x = 0$ invariant. This corresponds to the $x = 0$ surface at the time-reversal-symmetric slice in the cosmology picture, and to the time-reversal-symmetric slice at the center of the wormhole in the wormhole picture. Consequently, correlators for given bulk fields computed on such a codimension-2 surface in the cosmology picture are equal to correlators for some bulk fields in the wormhole picture (see Figure 1.9). More generically, correlators in the cosmology which are time-dependent and are not restricted to $x = 0$ are related to some correlator in the wormhole picture by double analytic continuation (and to some Euclidean correlator by a single analytic continuation).

The same is true for the microscopic theories: correlators in the excited state of the non-

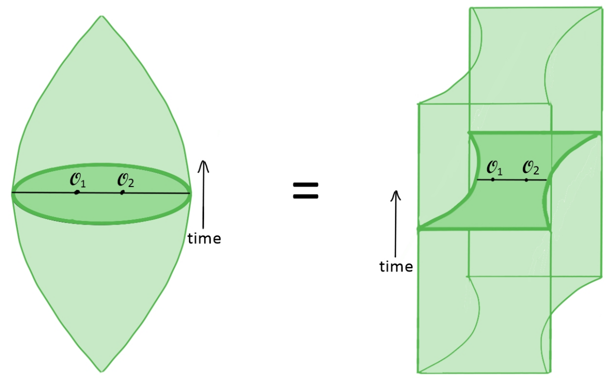

Figure 1.9: Correlators on the codimension-2 surface $\tau = x = 0$ left invariant by the double analytic continuation are equal in the cosmology (left) and wormhole (right) pictures. More generic correlators away from the invariant codimension-2 slice are related to each other by double analytic continuation. This figure appeared in Ref. [2].

holographic 4D CFT dual to the cosmological setting are related to correlators in the vacuum state of the Lorentzian gapped sandwich theory dual to the Lorentzian wormhole by double analytic continuation (and to Euclidean correlators in the Euclidean sandwich theory by a single analytic continuation). This is a somewhat surprising feature because they are correlators in different theories, and it is a consequence of the fact that both Lorentzian theories in their respective states arise from the same Euclidean path integral for the underlying Euclidean sandwich theory. This feature, which we dub "slicing duality" has important consequences both from a bulk phenomenological point of view (see Section 1.4.4) and for the problem of reconstructing the cosmological universe from the dual microscopic theory.

The latter consequence of the slicing duality is not hard to understand. As we have seen, reconstructing the cosmology from the dual excited state of the 4D non-holographic CFT is a very complicated task. Intuitively this is because the dual theory lives on a Minkowski spacetime which cannot be interpreted as the asymptotic AdS boundary of the bulk spacetime; the cosmological spacetime in fact does not have an asymptotic AdS boundary at all. On the other hand, the reconstruction of the Lorentzian wormhole from the dual vacuum state of the gapped theory is much easier, and it relies on the usual AdS/CFT tools. Intuitively, this is because the wormhole spacetime does have asymptotic AdS boundaries where the dual holographic 3D CFTs live.[51]

As we have seen, the slicing duality implies that, once we have full knowledge of the physics in the wormhole spacetime, the physics in the cosmological spacetime is also completely known, because its properties can be obtained by double analytic continuation. Therefore, the slicing duality gives us a way to "get around" the difficult issue of reconstructing the physics in the "cosmological island" directly from the exicted state of the non-holographic 4D CFT: we can (much more easily) reconstruct the physics in the Lorentzian wormhole from the vacuum state of the dual gapped theory, and then obtain the cosmological physics by double analytic continuation.

We would like to point out one interesting implication of the discussion above. In the cosmology picture the scale factor evolution is driven by the expectation value of the stress-energy tensor in some non-vacuum state, corresponding to the presence of a radiation term, a matter term, etc. on the right-hand side of the Friedmann equation. On the other hand, in the wormhole picture the source appearing on the right-hand side of the semiclassical Einstein's equations is the vacuum expectation value of the stress-energy tensor. Since the two expectation values are related to each other by double analytic continuation, assuming a given field content driving the cosmological evolution implies assuming a specific behavior of the vacuum stress-energy tensor in the Lorentzian wormhole spacetime. This is the feature motivating the title of the paper [2] (reported in Chapter 3 and Appendix B). One interesting open question is then to understand what generic vacuum energy patterns can be obtained in the Lorentzian wormhole

[51] A more accurate account of this statement about the easiness of reconstruction of the wormhole spacetime is the subject of Chapter 4 (see Section 1.6 for an overview of the results of Chapter 4).

picture; the answer to this question clearly constrains the possible cosmologies which can be described within our framework (see Chapter 6 for further discussion on this point).

1.4.4 The cosmological universe: naturalness puzzles and rolling scalars

Let us now focus on the cosmological spacetime and understand the generic features we can expect it to possess in our holographic wormhole cosmology approach. We will in particular discuss two main consequences of our setup on the phenomenology of the cosmological universe: the possible resolution of some of the naturalness puzzles without the need of inflation and the generic presence of rolling scalar fields which could give rise to phases of accelerated expansion (see the end of Section 1.2.1).

Naturalness puzzles

The cosmological spacetime described by our framework could naturally avoid, without the need of primordial inflation, three of the puzzles introduced in Section 1.2.1, namely the flatness problem, the horizon problem, and the cosmic coincidence problem.

- *Flatness problem.* As we have seen, the fact that the fundamental microscopic theory describing the cosmology is formulated on a spatially flat spacetime implies that the cosmology is a flat FLRW cosmology. Although this is not exactly a solution of the flatness problem—which arises when we consider a non-flat cosmology and notice that its spatial curvature radius must be very large to agree with observations—it suggests that, in our holographic setting, the spatial topology of the universe is just a consequence of the choice of specific microscopic dual theory. In the simple case we consider here in which the sandwich theory is defined on $\mathbb{R}^3 \times I$, the cosmology is just exactly flat.

- *Horizon problem.* The possible resolution of the horizon problem in our construction is much more subtle. This puzzle arises because we assume the initial state of the universe is defined at early times, slightly after the Big Bang. As we have explained in Section 1.2.1, such a state must be correlated at very large scales (much larger than the cosmological horizon) to justify the extreme isotropy of the CMB today. As we have pointed out, our construction gives a specific state for the cosmology, which is prepared by the gravitational Euclidean path integral defining our setup, similar to the analysis of Hartle and Hawking [169]. In particular, this state is not prepared at early times, but rather at the time-symmetric point where the cosmology stops expanding and starts recollapsing, i.e. at late times. If this "special" state happens to be correlated at large scales, clearly the horizon problem does not arise, because evolving backwards towards the Big Bang and forward towards the Big Crunch the state near the singularities will also be correlated on very large scales. What is interesting is that the slicing duality suggests that the special state prepared for the cosmology by the Euclidean path integral is indeed correlated at arbitrary large scales, even much larger than the cosmological horizon at late times. The argument goes as follows. Correlators in the Lorentzian wormhole spacetime (including those on the codimension-2 surface left invariant by the double analytic continuation) are non-vanishing at arbitrary large scales because bulk fields are in a vacuum state.[52] Since these correlators are related to cosmological correlators by double analytic continuation (or are just equal to them on the invariant codimension-2 surface), the special state of the cosmology at the time-symmetric

[52] One subtlety could be that, since the dual microscopic Lorentzian theory is gapped, correlations at very long scales might be suppressed in the wormhole. However, we show in Chapter 4 (published in Ref. [3]) that a massless sector is also present in the wormhole, guaranteeing the existence of correlations at arbitrary long scales.

slice also has correlations at arbitrary large scales. Therefore, the extreme isotropy of the universe at large scales is naturally built into the specific state of the cosmology arising within our framework.

- *Cosmic coincidence.* The fact that the cosmologies obtained within our framework are time-symmetric flat Big Bang-Big Crunch cosmologies automatically addresses the cosmic coincidence problem. In fact, at the time-symmetric point there is a single scale given by the cosmological constant $\Lambda < 0$, which is equal to the sum of all other contributions on the right-hand side of the Friedmann equation. This scale sets both the time scale for the variation of the energy densities other than the cosmological constant, and the time scale for the age of the universe. Therefore, for generic times in the cosmological evolution (i.e. provided that we do not live at very early stages of the cosmology) the cosmological constant and all other energy densities will roughly be of the same order of magnitude. Clearly, this argument works for the negative cosmological constant. However, it is reasonable to suppose that an effective positive cosmological constant arising at some point in the cosmological evolution (such as the one driving the current accelerated expansion of our universe)—possibly thanks to the presence of rolling scalar fields, as we will see shortly—is of the same order of magnitude as the fundamental, negative cosmological constant (see Section 3.3.6 for a discussion of this statement).

We remark that although our framework seems to escape at least some of the naturalness puzzles, this does not immediately imply that inflation is not necessary to describe a realistic cosmological universe. One of the greatest successes of inflation is the prediction of the spectrum of anisotropies in the CMB, and in particular of the scale invariance of cosmological perturbations.

Although there could be some alternative mechanism yielding the same result in our framework (we plan to investigate this possibility in the future), it is also possible that inflation is necessary in our setup to achieve it. Since, as we will now discuss, rolling scalar fields such as the ones driving inflation are generically present in our cosmologies, realizing the inflationary scenario within our models is a concrete possibility.

Generic presence of rolling scalar fields

We conclude the present section by remarking one more feature arising in the holographic wormhole cosmology approach, i.e. the generic presence of rolling scalar fields in the cosmological spacetime. In order to understand why this is the case, let us consider the Euclidean wormhole dual to the Euclidean sandwich theory. In general, the Euclidean bulk EFT contains scalar fields with small negative mass[53] dual to relevant scalar operators in the dual holographic 3D CFTs. In the most generic case, the Lagrangian of the 3D CFTs will be modified by the addition of relevant perturbations terms. In fact, the case where all relevant perturbation coefficients are vanishing and the 3D CFTs are CFTs at all energy scales can be seen as a fine-tuned special setup [9, 10]. In the presence of relevant perturbation in the 3D CFTs' Lagrangians, the expectation values of scalar fields in the wormhole background evolve as we move from the asymptotic boundary (where they are in the AdS vacuum) towards the center of the wormhole. This corresponds in the dual theory to the evolution of the expectation value of relevant operators under RG flow. This evolution can be expressed in terms of a scalar field ϕ (depending only on the wormhole "radial" coordinate τ) rolling in a classical potential $V(\phi)$.

[53] Scalar fields with negative mass can exist in AAdS spacetimes as long as the masss satisfies the Breitenlohner-Freedman (BF) bound [177, 178].

The generic existence of such rolling scalar fields in the Euclidean wormhole implies that the same scalars are also generically present in the cosmological spacetime, where they are homogeneous and time-dependent. In general, the scalar fields explore different regions of the potential $V(\phi)$ in the wormhole and in the cosmology,[54] see Section 3.3.6 for a complete description of their behavior. An interesting possibility is that these rolling scalar fields in the cosmology undergo a slow-roll phase along the slope of a positive region of the potential $V(\phi)$, driving a period of accelerated expansion for the cosmological universe. This mechanism could explain the current accelerated expansion observed in our universe in the spirit of quintessence models [92–94] (this is the subject of Chapter 5—published in Ref. [4]—which we will briefly review in Section 1.7), and also allow us to embed the inflationary paradigm within our framework if necessary.

1.5 Relationship between the two approaches

In order to make contact between the holographic braneworld cosmology and the holographic wormhole cosmology approaches, let us first focus on the Euclidean picture and consider a variation of the holographic wormhole approach where the microscopic sandwich theory lives on $S^3 \times I$ instead of $\mathbb{R}^3 \times I$ (the holographic 3D CFTs now live on S^3). As a consequence, a positive curvature term is present on the right-hand side of the Euclidean Friedmann equation, implying that the corresponding cosmology is closed instead of flat. Let us now consider the special case where the 4D CFT coupling the two holographic 3D CFTs in the sandwich theory is also holographic. The Euclidean bulk dual spacetime is then given by a 5D AAdS black hole spacetime dual to the holographic 4D CFT and cut off by an ETW brane anchored at the two

[54] We require the potential $V(\phi)$ to be analytic, so that the solutions of the cosmology and wormhole equations of motion are related by analytic continuation. See Section 1.7 for further details.

ends of the interval I, which can be interpreted as the dual of the two holographic 3D CFTs living there.[55] The ETW brane is now the "Euclidean wormhole" connecting the two 3D CFTs. Interpreting the interval I as the Euclidean time direction and analytically continuing the Euclidean setup, we obtain an excited pure state for the microscopic holographic 4D CFT and a dual Lorentzian spacetime given by an AAdS$_5$ black hole with the left asymptotic region cut off by an ETW brane. The cosmology is then a braneworld cosmology embedded in a higher dimensional black hole, analogous to the one considered in the holographic braneworld cosmology approach.

In this sense, in the special case in which the 4D degrees of freedom coupling the two 3D CFTs are also holographic, the two approaches can be seen as two equivalent descriptions of the same doubly holographic setup [36–38]. There are therefore a total of three descriptions of the same system (see Figure 1.7): the holographic braneworld cosmology is the highest-dimensional, doubly holographic description; the holographic wormhole cosmology is the intermediate bulk EFT description, in which the 5D bulk degrees of freedom are replaced by 4D non-gravitational auxiliary degrees of freedom; the microscopic picture (given, in Euclidean signature, by the sandwich theory) is the fundamental, UV-complete, and lowest-dimensional description without gravity involved. Note that if the 4D CFT coupling the two holographic 3D CFTs is not holographic, the highest dimensional (doubly holographic) description does not exist, whereas the holographic wormhole cosmology setup studied in the previous subsection and in Chapter 3 persists. Therefore, the holographic braneworld cosmology approach of Section 1.3 and Chapter 2 can be seen as a special case of the more general holographic wormhole cosmology framework.

[55]Note that there could be a competing saddle given by thermal AdS$_5$ cut off by two disconnected branes [5]. However, since we are considering a bulk Euclidean saddle which involves a wormhole in the 4D bulk description, we are implicitly assuming that the Euclidean black hole saddle cut off by the connected ETW brane is dominant in the 5D bulk path integral.

For a discussion of the pros and cons of the two approaches, we refer to Chapter 6.

Some remarks are in order. First, note that in the holographic braneworld cosmology obtained as a doubly holographic description of the holographic wormhole cosmology, gravity is automatically localized on the brane. In fact, we considered the setup in which $c_{3D} \gg c_{4D}$, which implies that an effective 4D gravity description must exist (and is indeed provided by the intermediate bulk EFT description) [8]. Therefore, this doubly holographic description cannot be obtained in the simplest bottom-up braneworld cosmology setup with a pure-tension brane embedded in a 5D AdS-Schwarzschild black hole, because such a construction does not support gravity localization on the brane as we have discussed in Section 1.3.4. It must be given instead within a construction allowing gravity localization, such as the one studied in Chapter 2 or more complicated setups involving more generic 5D spacetimes and branes which are not pure-tension. Understanding whether and how the 4D EFT breaks down in doubly holographic setups when gravity becomes delocalized is an interesting open question.

Second, in order to make contact with the holographic braneworld cosmology approach as we described it in Section 1.3, we considered a holographic wormhole cosmology setup where the sandwich theory lives on $S^3 \times I$. In this case, the "wormhole slicing" of the microscopic Euclidean path integral would define a state for a Lorentzian theory on spatial $S^2 \times I$, which should be similar to the Bunch-Davies state for de Sitter space [179]. The corresponding Lorentzian traversable wormhole has a spherical rather than a planar cross section. Although we have not explored this setup in detail, it would be interesting to understand whether some of the properties we explored in the previous subsection for the planar case (such as the possible resolution of the horizon problem in the holographic wormhole cosmology approach) are preserved in the spherical case.[56]

Note that there should also be no conceptual issue in formulating a doubly holographic description of the case where the sandwich theory is defined on $\mathbb{R}^3 \times I$. In this case, we would have a Euclidean 5D planar black hole [180] saddle cut off by an ETW brane which has the geometry of the planar Euclidean wormhole of interest, see the bottom-center drawing in Figure 1.7. In the cosmology picture we would obtain a planar 5D Lorentzian black hole and a spatially flat braneworld cosmology living in the left asymptotic region of the maximally extended black hole spacetime, see the bottom-right drawing in Figure 1.7. In the wormhole picture we would obtain a pure AdS_5 spacetime (we remind that the bulk geometry is a solution of the vacuum semiclassical Einstein's equations in this case) cut off by an ETW brane with the geometry of the planar Lorentzian traversable wormhole of interest, see the bottom-left drawing in Figure 1.7. This doubly holographic setup also shows clearly that probing the braneworld cosmology from the dual excited state of the 4D CFT is hard because it sits behind the horizon of the 5D black hole, whereas probing the Lorentzian traversable wormhole (i.e. the ETW brane) from the dual vacuum state of the gapped sandwich theory is easy and can be done by means of the "usual" AdS/CFT tools because there is no horizon in the 5D bulk dual.

Finally, using the doubly holographic setting described here we can also see more clearly why the sandwich theory needs to be gapped in order for the bulk spacetime to contain a 4D wormhole (or, equivalently, a connected ETW brane). In the doubly holographic case, the 4D Euclidean wormhole is identified with the ETW brane cutting off the region deep into the 5D bulk. This can be interpreted as a holographic realization of the fact that, in the dual 4D holographic

[56]Clearly, the resolution we presented for the flatness problem does not carry on to the spherical case, in which the FLRW cosmology is closed.

sandwich theory, physics at arbitrarily long wavelengths is trivial, i.e. the sandwich theory is confining.

1.6 Properties and reconstruction of the Lorentzian traversable wormhole

In Chapter 4 (published in Ref. [3]) we work within the holographic wormhole cosmology approach and focus entirely on the Lorentzian wormhole picture. The metric of the planar traversable wormhole is given by equation (1.31), which we report here:[57]

$$ds^2 = a^2(z)\left(-dt^2 + dx^2 + dy^2 + dz^2\right). \tag{1.32}$$

We recall that the conformal factor $a(z)$ has two simple poles at the location of the two asymptotic AdS boundaries at $z = \pm z_0$. We study two general questions that we report here:

1. Given a microscopic setup, what features of the observables signal the presence of a dual eternal traversable wormhole?

2. How can the wormhole geometry be reconstructed from microscopic observables?

In the spirit of the bottom-up approach to holography, the answer to the first question can help us constrain the microscopic theory dual to our bulk setup and therefore find explicit examples realizing our proposal. As we have already explained, the latter is a very important task that will need to be carried out in future research in order to obtain a fully microscopic description of cosmology within AdS/CFT. On the other hand, answering the second question would clarify how physics in the Lorentzian wormhole geometry can be probed if we have access to the dual gapped

[57]We uniform here the notation to the one used in Chapter 4. We therefore drop the subscript $_E$ on the conformal factor, label the Lorentzian time coordinate with t instead of x, and call the wormhole radial direction z instead of ξ.

"sandwich" theory in its vacuum state. Since observables in the Lorentzian wormhole geometry and in the cosmology are related by double analytic continuation (see Section 1.4.3), this would also give us a way to probe cosmological physics from the microscopic dual description.

Constraints on the boundary theory from wormhole physics

As a result of our analysis, we find a number of generic features the boundary microscopic theory must possess in order to be dual to the Lorentzian eternal traversable wormhole of our interest. Here we will briefly summarize such constraints, and refer to Chapter 4 for additional details.

- As we have anticipated in Section 1.4, we find that the boundary theory must be a confining gauge theory with a discrete mass spectrum. In fact, any bulk field can be written as a superposition of a discrete set of modes labeled by the (quantized) momentum along the wormhole radial direction $z \in [-z_0, z_0]$. This discrete set of modes corresponds to a tower of massive particles with discrete mass spectrum in the dual theory. For a test scalar field, the specific form of the spectrum depends on the wormhole's conformal factor $a(z)$ and is given by the eigenvalue spectrum of an auxiliary Schrödinger problem with potential

$$V(z) = \frac{a''(z)}{a(z)} + m^2 a^2(z), \tag{1.33}$$

  where a prime indicates a derivative with respect to the z coordinate and m is the mass of the bulk scalar field. Therefore, a specific wormhole geometry implies a specific mass spectrum for scalar particles in the dual confining theory. On the other hand, a bulk $U(1)$ gauge field has an associated evenly-spaced and a-independent discrete spectrum of momenta in the z direction, leading to an evenly-spaced spectrum of masses for vector particles in the dual theory. This is a consequence of the fact that the action for a $U(1)$ gauge field in 4D is conformally invariant, and therefore the associated spectrum contains no information about the wormhole's conformal factor. Interestingly, the $U(1)$ gauge field also gives rise to a massless sector in the dual confining theory, which guarantees the existence of correlations at arbitrary long scales in the wormhole geometry (a property used in Section 1.4.4 and Chapter 3 to argue in favor of a resolution of the horizon problem). Depending on the boundary conditions imposed on the bulk gauge field, the massless sector is given either by a massless scalar field—which can be interpreted as a Goldstone boson—or by a massless boundary gauge field, see Section 4.2.3 for further details on these points.

- Two-point functions for scalar operators in the confining theory must have a specific behavior, which can be obtained by calculating correlators for scalar fields in the bulk theory and using the extrapolate dictionary (1.5). For the two-point function of a scalar operator $\mathcal{O}$ with both operators inserted in one of the two holographic 3D CFTs living on the boundaries of the wormhole (indicated by $+$ for the boundary at $z = z_0$ and by $-$ for the boundary at $z = -z_0$) we find

$$\langle \mathcal{O}_\pm(t,x,y)\mathcal{O}_\pm(t',x',y')\rangle = \frac{1}{4\pi\sqrt{-\Delta t^2 + \Delta x_\perp^2}} \sum_{n=0}^{\infty} (u_n^+)^2 \exp\left(-k_n\sqrt{-\Delta t^2 + \Delta x_\perp^2}\right), \tag{1.34}$$

where $\Delta t = t - t'$, $\Delta x_\perp = \sqrt{(x-x')^2 + (y-y')^2}$, u_n^+ are normalization factors, and k_n are the discrete bulk momenta in the z direction. Note that both u_n^+ and k_n depend on the specific form of the wormhole's conformal factor. On the other hand, for the two-point function of a scalar operator $\mathcal{O}$ with one operator inserted in each one of the two holographic 3D CFTs, we obtain

$$\langle \mathcal{O}_{\pm}(t,x,y)\mathcal{O}_{\mp}(t',x',y')\rangle = \frac{1}{4\pi\sqrt{-\Delta t^2+\Delta x_\perp^2}}\sum_{n=0}^{\infty}(-1)^n(u_n^+)^2\exp\left(-k_n\sqrt{-\Delta t^2+\Delta x_\perp^2}\right). \tag{1.35}$$

- Finally, we expect to see a signature of the existence of the traversable wormhole in the entanglement entropy of subregions of the two holographic 3D CFTs living on the boundaries of the wormhole. For example, we expect the entanglement entropy of the union of two large identical regions A_L in the "left" CFT and A_R in the "right" CFT to exhibit a phase transition from a volume law to an area law as we increase the size of the regions. This corresponds to the transition between two possible candidate RT surfaces: the first one is the union of two disconnected surfaces homologous to A_L and A_R respectively, the second one is a single connected RT surface going through the wormhole.

Wormhole reconstruction

To answer the second question, we consider three different observables in the microscopic confining theory able to probe the traversable wormhole geometry.

- The first (and main) observables we consider are the two-point functions of scalar operators in the confining theory. Given such two-point functions, we can extract the discrete mass spectrum of scalar particles, corresponding to the spectrum of discrete momenta in the z direction for the corresponding bulk scalar field. We then build an explicit algorithm to reconstruct the potential (1.33) given its spectrum. This is an example of an inverse

Sturm-Liouville problem [181–183], which is not solvable in general. However, the symmetry of our setup (implying $V(z) = V(-z)$) and the assumption that the wormhole is asymptotically AdS (implying that $V(z) \sim C/(z_0 \pm z)^2$ near the boundaries at $z = \mp z_0$, with C constant) are enough to render the problem solvable. Finally, we show that given a single potential associated with a bulk massless scalar field or two potentials associated with two bulk massive scalar fields, the wormhole's conformal factor $a(z)$ can be reconstructed. Therefore, this procedure allows us to reconstruct the wormhole geometry either from a single two-point function of a scalar operator dual to a massless bulk scalar field, or from two two-point functions of scalar operators dual to massive bulk scalar fields. We also show that having access to only part of the scalar spectrum guarantees an approximate reconstruction of the wormhole geometry, and quantify the error in the reconstruction in terms of the number of eigenvalues available. See Figure 1.10 for the result of a numerical implementation of the reconstruction algorithm. Note that a similar reconstruction cannot be carried out starting from the momentum spectrum of a bulk gauge field because, as we have pointed out above, it does not contain any information about the wormhole's conformal factor.

- The wormhole geometry can also be more easily reconstructed from the two-point function of scalar operators with large scaling dimension in the holographic 3D CFTs living on the boundaries of the wormhole. In fact, such operators are dual to heavy scalar fields in the wormhole background, the correlators of which can be computed in the geodesic approximation [184]. This yields a functional dependence of the correlators on the wormhole's conformal factor, which can be inverted to reconstruct the wormhole geometry.

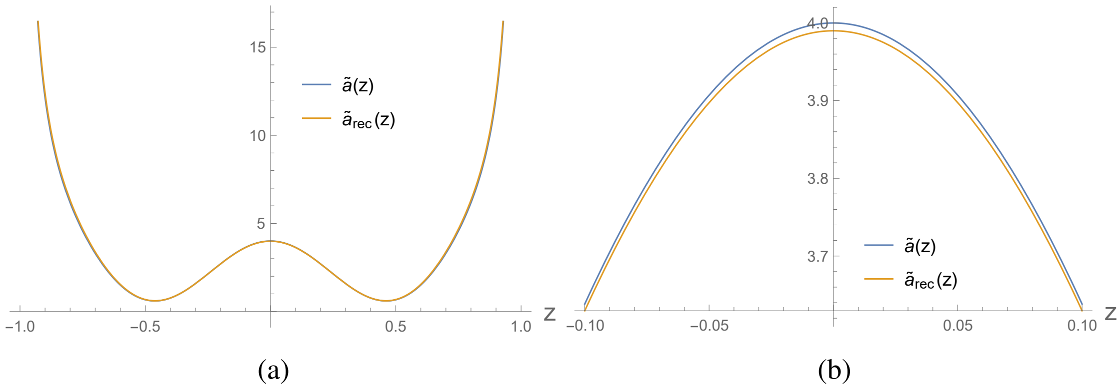

Figure 1.10: Numerical implementation of wormhole reconstruction algorithm from scalar spectra. We chose an analytic form for the wormhole's conformal factor (given in equation (4.79) and denoted here by $\tilde{a}(z) = a(z)/L$) and generated the corresponding spectra for two bulk scalar fields of masses $m_1 L = 1/2$ and $m_2 L = 3/2$. We then numerically reconstructed the scale factor from the first $j_{max} = 50$ eigenvalues of such scalar spectra using our algorithm. The true scale factor $\tilde{a}(z)$ and the reconstructed scale factor $\tilde{a}_{rec}(z)$ are depicted as a function of z. (a) The reconstructed scale factor approximates the true scale factor to good accuracy. (b) Due to the fact that we used a finite amount ($j_{max} = 50$) of eigenvalues, the reconstruction is only approximate and accurate up to corrections of order $1/j_{max} \sim 10^{-2}$. This figure appeared in Ref. [3].

- Finally, the entanglement entropy of a strip-shaped subregion of one of the two holographic 3D CFTs living on the boundaries of the wormhole is also able to probe the wormhole geometry. In fact, the area of the corresponding RT surface also has a functional dependence on the wormhole's conformal factor, which can be inverted to reconstruct the wormhole geometry.

1.7 Accelerating cosmologies in the holographic wormhole cosmology approach

In Chapter 5 we work within the holographic wormhole cosmology approach and study the bulk EFT in the presence of a scalar field in a classical potential sourcing Einstein's equations. In particular, we focus on the cosmology picture and show that:

- Homogeneous scalar fields slowly rolling in a potential V can lead to phases of accelerated expansion in the time-symmetric, $\Lambda < 0$ Big Bang-Big Crunch cosmology. In fact, a phase of accelerated expansion occurs quite generically for simple potentials, without the need to fine-tune the initial conditions and the parameters of the model.

- The evolution of the cosmological scale factor including the phase of accelerated expansion can be in accordance with observational data for an appropriate choice of potential, parameters, and initial conditions.

- These solutions admit analytic continuations to a Euclidean AdS wormhole with the scalar field satisfying the BF bound at the two asymptotic boundaries and varying throughout the wormhole.

- The scalar potential supporting the solutions of our interest can arise from a superpotential in a supergravity theory, i.e. our solutions are compatible with a supersymmetric bulk EFT which would represent a low energy description of a UV-complete string theory construction.

We will now explain how these results are obtained in some more detail.

We consider a bulk EFT in which the evolution of the FLRW universe is driven by a negative cosmological constant, a homogeneous scalar field ϕ in a potential $V(\phi)$, radiation with energy density ρ_R/a^4, and matter with energy density ρ_M/a^3.[58] By choosing units such that $8\pi G/3 = 1$ and by absorbing the negative cosmological constant in the definition of the poten-

[58]We are uniforming our notation to the one employed in Chapter 5. ρ_R and ρ_M are the radiation and matter energy densities when $a = 1$, which are indicated by ρ_r^0, ρ_m^0 in the notation of Section 1.2.1.

tial, the equations of motion in the cosmology picture then take the form

$$\begin{cases} \ddot{\phi} + 3H\dot{\phi} + \frac{dV}{d\phi} = 0 \\ \\ H^2 = \frac{1}{2}\dot{\phi}^2 + V(\phi) + \frac{\rho_R}{a^4} + \frac{\rho_M}{a^3} \end{cases} \tag{1.36}$$

The corresponding analytically continued equations of motion[59] for the Euclidean EFT are given by

$$\begin{cases} \phi_E'' + 3H_E\phi_E' - \frac{dV}{d\phi_E} = 0 \\ \\ H_E^2 = \frac{1}{2}(\phi_E')^2 - V(\phi_E) - \frac{\rho_R}{a_E^4} - \frac{\rho_M}{a_E^3} \end{cases} \tag{1.37}$$

where $\tau = -it$, $a_E(\tau) = a(i\tau)$, $\phi_E(\tau) = \phi(i\tau)$, $H_E(\tau) = H(i\tau)$. We remark that the scalar field is homogeneous and varies over time in the cosmology picture; on the other hand, it is time-independent and varies spatially along τ (which is the wormhole radial direction in a wormhole solution) in the Euclidean picture. Note that the Klein-Gordon equation in the cosmology picture describes the evolution of a damped particle in a potential V, whereas in the Euclidean picture it describes the evolution of a damped particle in an inverted potential $-V$. For wormhole solutions of the Euclidean EFT equations of motion (1.37), we can assume without loss of generality that $\phi_E = 0$ at the two asymptotic AdS boundaries in the wormhole geometry, i.e. for $\tau \to \pm\infty$. This corresponds to the identification $V(0) = \Lambda/3$, where Λ is the fundamental negative cosmological constant.

Within our holographic wormhole cosmology approach, we are interested in solutions of these equations of motion given by $a(t)$, $\phi(t)$ such that (we set $t = 0$ at the time-reversal-

[59]Note that this terminology, which we use here and throughout the rest of this dissertation, is somewhat imprecise for the Euclidean and the Lorentzian wormhole pictures. In fact, these equations do not describe time evolution, but the spatial behavior of the scale factor and the scalar field along the radial direction of the wormhole.

symmetric slice in the cosmology picture, and therefore $\tau = 0$ at the reflection-symmetric slice in the Euclidean geometry)

- The evolution of the scale factor $a(t)$ in the cosmology picture presents a phase of accelerated expansion, and possibly matches the scale factor evolution in our universe as described by cosmological data.

- The cosmological solution is time-reversal-symmetric: $a(t) = a(-t)$, $\phi(t) = \phi(-t)$, implying $\dot{\phi}(0) = 0$ at the time-reversal-symmetric slice where $\dot{a}(0) = 0$. We denote $a(0) = a_0$ and $\phi(0) = \phi_0$. As we have explained, this guarantees the existence of an associated real and reflection-symmetric (for $\tau \to -\tau$) Euclidean geometry.

- The associated Euclidean geometry is given by a Euclidean AdS wormhole, with the two asymptotic boundaries at $\tau \to \pm\infty$.

- The BF bound is satisfied at the two asymptotic AdS boundaries, guaranteeing that the AdS solution is stable to scalar perturbations and the dual microscopic theory well-defined.[60]

These requirements translate into a series of six necessary conditions the potential V has to satisfy in order to be able to support the solutions of our interest (see Figure 1.11 for the shape of a typical potential in this class):

1. The potential must have a positive region "flat enough" to support a slow-roll phase corresponding to the accelerated expansion phase of the universe.

2. The potential at the symmetric point $t = \tau = 0$, which is $V(\phi_0)$, must be negative in order

[60]In particular, having the scalar field satisfy the BF bound ensures that the scaling dimension of the scalar operator dual to the bulk scalar field is real.

for the right-hand side of the Friedmann equation (in both pictures) to vanish. We remind that we absorbed the negative cosmological constant Λ into the definition of the potential.

3. Because in the cosmology picture $\dot{\phi}(0) = 0$ and the scalar field satisfies the equation of motion of a damped particle in a potential V, the scalar must be ascending the potential at $t = 0$. Therefore, $0 > V(\phi_0) > V(\phi_{min})$ where ϕ_{min} is a local minimum of the potential through which the scalar field must pass during its evolution between the slow-roll phase and the symmetric point.

4. In the Euclidean picture, the requirement of having AdS boundaries implies that $V(\phi_E(\tau)) \to \Lambda/3 < 0$ for $\tau \to \pm\infty$, and we chose without loss of generality $\phi_E(\pm\infty) = 0$. Because in the Euclidean picture the spatial evolution of the scalar field throughout the wormhole is described by the equation of motion of a damped particle in a potential $-V$ with initial conditions $\phi'(0) = 0$, $\phi(0) = \phi_0$, this implies that $-V$ must have a local minimum at $\phi = 0$ where the scalar field can settle as $\tau \to \pm\infty$, and therefore $V(0) < 0$ must be a local maximum of the potential V with $V(0) > V(\phi_0)$. This in turn implies that $d^2V/d\phi^2|_{\phi=0} < 0$, i.e. the scalar field has negative mass and is dual to a relevant operator in the dual CFT, as we would expect from the discussion in Section 1.4.4.

5. The potential must satisfy the BF bound at the two AdS asymptotic boundaries: $d^2V/d\phi^2|_{\phi=0} \geq 9V(0)/4$.

6. The potential $V(\phi)$ must be analytic.

Given a potential satisfying these necessary conditions, it is in general possible to find appropriate values for the remaining parameters and the initial condition ϕ_0 yielding a solution involving an

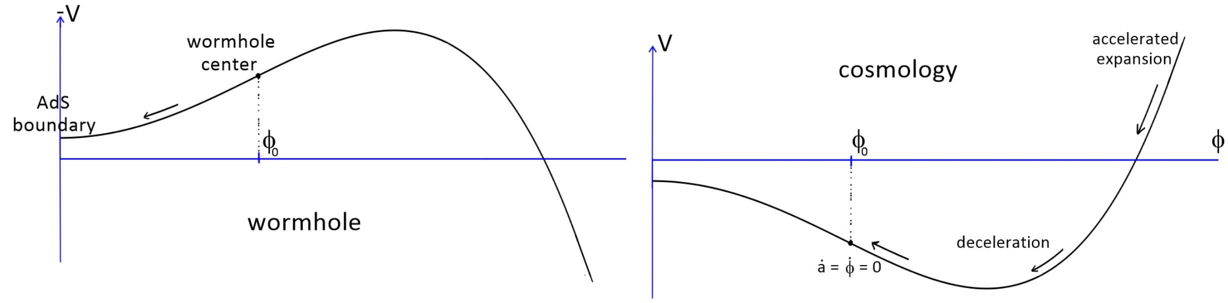

Figure 1.11: Typical scalar potential supporting an accelerating solution with a well-defined Euclidean wormhole analytic continuation. The evolution of the scalar field in the potential $V(\phi)$ in the wormhole picture (left) and cosmology picture (right) is also shown. This Figure appeared in Ref. [2] and [4].

accelerating, time-symmetric cosmology with a well-defined AdS Euclidean wormhole analytic continuation. Note that different parts of the potential are explored in the cosmology and wormhole pictures, see Figure 1.11. A discussion of why potentials of this form could arise naturally within a bulk EFT with a holographic dual Euclidean sandwich theory can be found in Section 3.3.6.

We remark that the solutions of the cosmology and wormhole equations of motion are related by analytic continuation only if the potential $V(\phi)$ is analytic, hence condition 6. In fact, if this is not the case it would be possible, for instance, to find different well-behaved solutions to the wormhole equations of motion corresponding to the same cosmological solution by simply changing the part of potential explored by the scalar field in the wormhole solution, while leaving the rest of the potential untouched. This is clearly impossible if the potential $V(\phi)$ is analytic. In this dissertation, we will therefore require the potential to be analytic.

We would like to remark that the choice of initial conditions and parameters is crucial to obtain solutions of the desired form. Suppose we are given a potential with a positive region able to support an accelerated expansion of the cosmological universe, and a set of parameters and initial conditions at the time-symmetric point. In the cosmology picture, we can then evolve the solution backwards towards the Big Bang or (equivalently) forward towards the Big Crunch. The accelerated expansion will then take place only if the initial conditions and parameters are such that the scalar field reaches the "slow-roll region" of the potential before the scale factor shrinks to zero (i.e. before we hit the singularity). Whether or not this happens is strongly dependent on the initial conditions and parameters of the model. Similarly, in the Euclidean picture, having a potential with the desired properties outlined above is not enough to obtain a wormhole solution. For instance, if the derivative of the potential at the symmetric point $|V'(\phi_0)|$ is too large, the potential will increase fast away from ϕ_0 and towards $\phi = 0$. This in turn will cause the $(\phi_E')^2/2$ term in the wormhole Friedmann equation (1.37) to increase. However, the quantity $(\phi_E')^2/2 - V(\phi_E)$ decreases because the scalar field is damped. Consequently, if the scale factor is not too large, the matter or the radiation terms could become dominant again on the right-hand side of the Euclidean Friedmann equation, causing the Euclidean solution to reach another turning point instead of expanding indefinitely towards the asymptotic AdS boundaries. Thus, in this case we do not obtain a Euclidean wormhole solution. This behavior was observed in our numerical analysis.

Genericity of acceleration

As a first step, we set for simplicity $\rho_M = 0$ and consider a simple two-parameters family of potentials of the form

$$V(\phi) = -2 + \frac{1}{2}m^2\phi^2 + e^{g\phi^2} - g\phi^2, \tag{1.38}$$

where $0 > m^2 > -9/4$ is the scalar field's mass (satisfying the BF bound) near the AdS asymptotic boundaries of the wormhole, and g is a free parameter. Given an initial condition at the

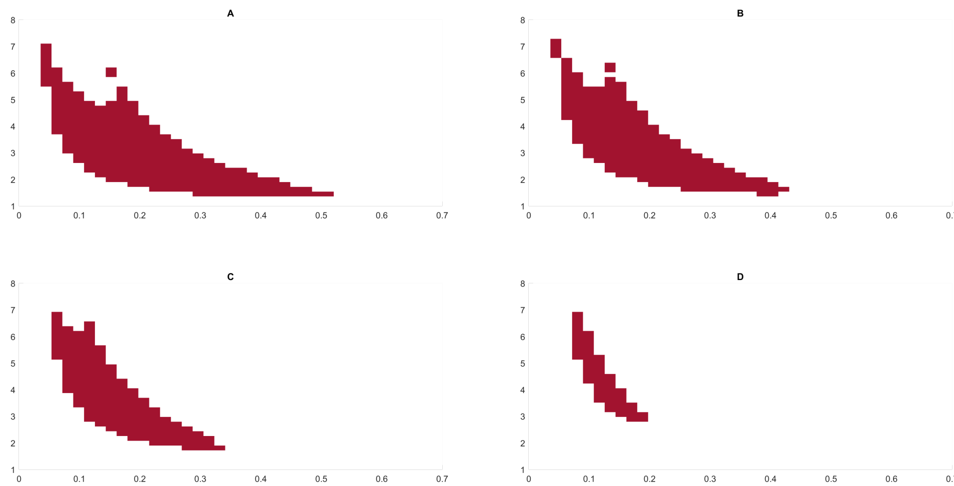

Figure 1.12: Genericity of acceleration in the cosmology picture for a simple scalar potential. On the y axis is the parameter g, on the x axis the initial condition ϕ_0. The red region is the region of parameter space for which acceleration occurs at some stage in the cosmological evolution. Clearly, there is a codimension-0 region of the parameter space for which acceleration takes place. (A) $m^2 = -9/4$, i.e. the BF bound is saturated. (B) $m^2 = -2$. (C) $m^2 = -7/4$. (D) $m^2 = -3/2$. Having a phase of accelerated expansion becomes less generic as we increase $m^2 < 0$ away from the BF bound. This Figure appeared in Ref. [4].

symmetric point $\phi(0) = \phi_0$ for the scalar field, ρ_R/a_0^4 is uniquely fixed by the Friedmann equation at the turning point, i.e. $\rho_R/a_0^4 = -V(\phi_0)$. Therefore, for any given value of m, a solution is parametrized by a pair (g, ϕ_0). We can then study in what region of the $g - \phi_0$ parameter space the cosmological solution undergoes a phase of accelerated expansion between the singularity and the turning point. Our numerical analysis (displayed here in Figure 1.12) shows that, at least for the simple potential studied here, no particular fine-tuning of the parameters and initial conditions is needed in order for a phase of accelerated expansion to take place. It also shows that for smaller (in absolute value) masses, an accelerated expansion phase is less likely to happen.

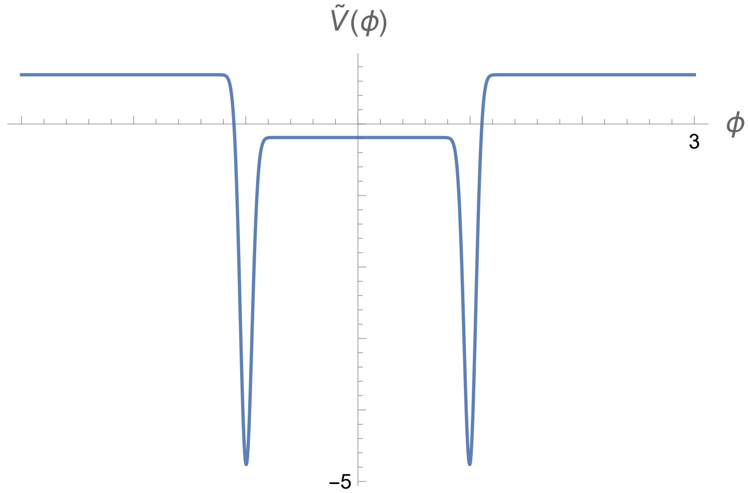

Figure 1.13: Potential supporting holographic wormhole cosmology solution reproducing ΛCDM scale factor evolution. The potential is rescaled by the Hubble constant (which is the Hubble parameter at the present time) H_0, i.e. $\tilde{V} = V/H_0^2$. When the scalar field slowly rolls on the plateau region, the potential contribution to the Friedmann equation is effectively a positive cosmological constant which can drive an accelerated expansion. This Figure appeared in Ref. [4].

Reproducing ΛCDM and wCDM models

Next, we study potentials able to reproduce to arbitrary accuracy the scale factor evolution predicted by the ΛCDM (with $\Lambda > 0$) and wCDM[61] models between the early universe and the present time. Clearly, our model describes Big Bang-Big Crunch cosmologies and the evolution of the scale factor in the future will be different from the one predicted by ΛCDM or wCDM (which corresponds to an eternal accelerated expansion). We report here the main results for the ΛCDM case and refer to Section 5.2.4 and Appendix D.2 for the wCDM analysis.

Consider a symmetric FLRW universe driven by radiation, matter, and a homogeneous scalar field in a five-parameters potential satisfying the necessary conditions outlined above and presenting a very flat positive "plateau" region for large values of the field. An example of the

[61]The wCDM model is a generalization of the ΛCDM model in which the dark energy is not given by a cosmological constant, but by some other form of energy density with a constant equation of state parameter w in the range $-1/3 > w > -1$.

potential of interest is depicted in Figure 1.13. Its explicit analytic expression is not particularly informative and can be found in equations (5.14) and (5.15). If the scalar field rolls very slowly on the plateau region and the potential term is dominant over radiation and matter, the universe undergoes an accelerated expansion during which the potential is nearly constant. Hence, during the slow-roll phase this model can reproduce the phenomenology of a ΛCDM model with positive cosmological constant (whose value is set by the height of the plateau) to good accuracy. By choosing the height of the plateau to match the best experimental value for $\Lambda > 0$ (obtained by assuming the ΛCDM model [90, 185]), and setting the radiation and matter densities to match their experimental values (again obtained assuming ΛCDM), we were indeed able to reproduce the scale factor evolution obtained in the corresponding ΛCDM model to arbitrary accuracy between the early universe and the present time, see Figure 1.14. In order to achieve this result, one of the five parameters in the potential needs to be accurately fine-tuned (see Section 5.2.3 and Appendix D.1). Naturally, the future evolution of the scale factor differs between our model and ΛCDM: in the former the accelerated expansion ends, the universe reaches its turning point, and it starts recollapsing in a symmetric fashion; in the latter, the universe undergoes an eternal de Sitter phase. We also show that the same solutions able to reproduce cosmological data to good accuracy have a well-defined Euclidean wormhole analytic continuation.

We would like to remark that this result was obtained using a specific kind of potential—whose naturalness in the context of AdS/CFT remains an open question—and by fine-tuning one of the parameters. Nonetheless, this should be regarded as a proof of principle that, although they are not the simplest models for our universe, $\Lambda < 0$ cosmologies can match observational data to good accuracy, and that a realistic cosmology described within our holographic wormhole cosmology approach is possible. Finding other classes of potentials achieving this result and

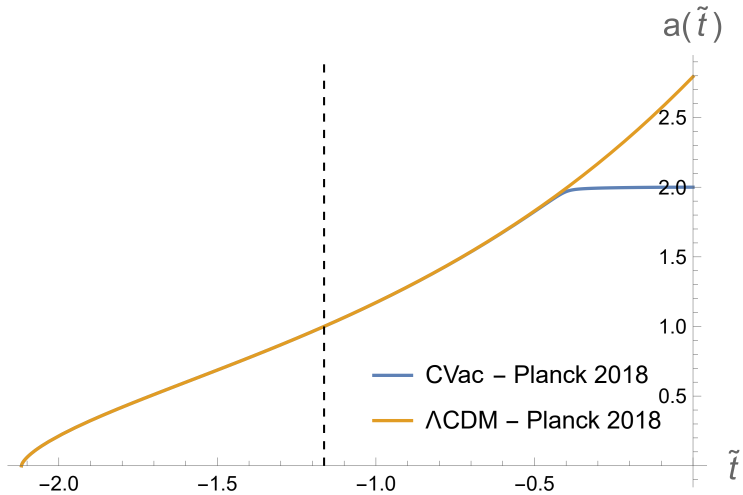

Figure 1.14: Comparison between scale factor evolution in holographic wormhole cosmology model with scalar potential with a flat region (denoted by "CVac") and corresponding ΛCDM model. For both models, the scale factor was obtained choosing the cosmological parameters to be the best fit (assuming ΛCDM) to the *Planck* 2018 data [90]. The two scale factors are indistinguishable between the early universe and the present day (indicated by the black dashed line). The future evolution will be different: in the holographic wormhole cosmology model the accelerating phase will end and the universe recollapse symmetrically (here we depict only the expansion phase), whereas in the ΛCDM model the universe will undergo an eternal de Sitter phase. The time on the x axis is measured in units of the Hubble time, i.e. $\tilde{t} = H_0 t$. This Figure appeared in Ref. [4].

arising naturally within our holographic framework is an interesting direction for future research.

Scalar potentials from superpotentials

Finally, we show that any kind of scalar potential we can consider in our analysis can be obtained from an associated superpotential in a $\mathcal{N} = 1$ supergravity theory [47, 186]. In particular, we restrict to the gravity and scalar sectors only, consider a single chiral superfield (and therefore a single complex scalar field), and take a Kähler potential of the form $K(\phi, \bar{\phi}) = \bar{\phi}\phi$, where the bar indicates complex conjugation. With these specific choices, the scalar field's potential $V_W(\phi)$ is related to the superpotential $W(\phi)$ by

$$V_W(\phi) = e^{\phi\bar{\phi}} \left(|W'(\phi) + \bar{\phi}W(\phi)|^2 - 3|W(\phi)|^2 \right) . \tag{1.39}$$

Since we focus on the single scalar case in our bulk EFT, we can further simplify the problem by restricting to the case of a real scalar field, i.e. $\phi = \bar{\phi}$.

We can then ask: given a form of the potential $V_W(\phi)$ (which is the potential of interest in our cosmological EFT), is it possible to build a superpotential $W(\phi)$ giving rise to that potential via equation (1.39)? We find that the answer is yes, and derive an explicit algorithm to construct the superpotential given any form of the scalar potential $V_W(\phi)$. This result implies that the models involving rolling scalar fields studied in Chapter 5 can in principle be obtained in the context of supergravity theories which could have a string theoretic UV completion.

This completes the overview of the results presented in this dissertation. We will now explain in detail such results in Chapters 2, 3, 4, and 5 (published in Refs. [1–4] respectively) before giving our concluding remarks and an outline of future directions in Chapter 6.

Chapter 2: Holographic braneworld cosmology from $U(1)$ charged BCFT

Authors:[1] *Stefano Antonini, Brian Swingle.*

Abstract: In the last two decades the Anti-de Sitter/Conformal Field Theory correspondence (AdS/CFT) has emerged as focal point of many research interests. In particular, it functions as a stepping stone to a still missing full quantum theory of gravity. In this context, a pivotal question is if and how cosmological physics can be studied using AdS/CFT. Motivated by string theory, braneworld cosmologies propose that our universe is a four-dimensional membrane embedded in a bulk fivedimensional AdS spacetime. We show how such a scenario can be microscopically realized in AdS/CFT using special field theory states dual to an "end-of-the-world brane" moving in a charged black hole spacetime. Observers on the brane experience cosmological physics and approximately four-dimensional gravity, at least locally in spacetime. This result opens a new path towards a description of quantum cosmology and the simulation of cosmology on quantum machines.

[1]Originally published as *Cosmology at the end of the world*, Nature Phys. 16 (2020) 8, 881-886, e-Print: 1907.06667, [1]. The Supplementary Material of Nature Phys. 16 (2020) 8, 881-886 (also available in the appendices of e-Print: 1907.06667) is reported in Appendix A.

2.1 Introduction

The achievement of a quantum mechanical description of spacetime is one of the most challenging issues facing modern physics. The Anti-de Sitter/Conformal Field Theory (AdS/CFT) correspondence provides a promising starting point to accomplish this goal. As a concrete realization of the holographic principle [30, 187], it relates the observables of a full quantum gravity theory living in a $(d+1)$-dimensional spacetime (the bulk) to those of a d-dimensional dual field theory without gravity associated to the boundary of the bulk spacetime [17]. However, at this stage AdS/CFT must still be regarded as a toy model of the physical world, since the asymptotically AdS spacetimes it describes are different from the universe we observe. In this paper we exhibit a viable way to study certain Friedmann-Lemaître-Robertson-Walker (FLRW) cosmologies using the AdS/CFT correspondence, realizing a recently proposed new perspective on braneworld cosmology and quantum gravity in a cosmological universe [5].

AdS/CFT associates different states of the CFT to different geometries of the bulk spacetime. In particular, certain highly excited pure states of the CFT have a dual geometry hosting a black hole and a dynamical end-of-the-world (ETW) brane [11, 12, 112, 133, 138]. This bulk configuration is built from a two-sided wormhole spacetime by replacing the left boundary with the ETW brane (see Figure 2.1). The original wormhole spacetime describes an entangled state of two CFTs, and the ETW brane corresponds to a complete measurement of one CFT to leave a pure state of the remaining CFT. Hence, observables in the CFT must probe the physics behind the horizon of the black hole, including the remaining part of the left asymptotic region [188–191] and the evolution of the ETW brane [5, 143].

Although we do not know how to do the decoding in general, some CFT observables have been explicitly shown to probe the physics behind the horizon in similar setups. The entanglement entropy of large regions of the CFT [5, 143] and the holographic complexity [5] exhibit a time-dependent behaviour containing information about the evolution of the ETW brane and its tension. Although we will not evaluate explicitly the mentioned quantities in this paper, they can be calculated in our setup by directly generalizing the techniques employed in ref [5].

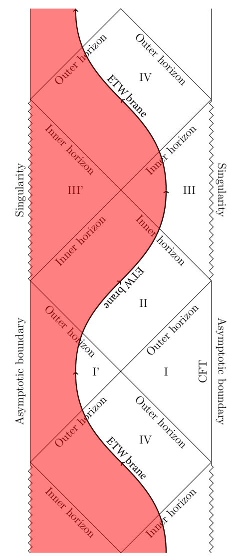

Figure 2.1: Brane trajectory. Maximally extended Penrose diagram for the AdS-Reissner-Nordström black hole. Only the time and radial directions are represented, while the other spatial dimensions are suppressed. Light rays move at an angle of $45°$. More patches of the AdS-RN spacetime are glued together here. Region I is the exterior of the black hole and the CFT lives on the asymptotic boundary associated with it. Region I' is the corresponding second asymptotic region, typical of maximally extended black holes. In Regions II and IV, which are bounded by the outer and inner horizons, the radial coordinate is timelike, while the time coordinate is spacelike. Regions III and III' are the interior regions of the maximally extended black hole. The ETW brane oscillates inside and outside the two horizons of the black hole, cutting off the left asymptotic region I'. The red region, generally part of the maximally extended charged black hole, is not present in our spacetime.

The presence of the brane opens an interesting scenario: when the bulk spacetime is 5-dimensional, an observer living on the 4-dimensional ETW brane would interpret the motion of the brane as the evolution of a FLRW universe, where the radial position plays the role of the scale factor [114, 115, 153, 192–194]. Hence, holographic duality allows to describe such "braneworld cosmologies" using CFT observables associated with the right asymptotic region of the black hole [5]. Holographic cosmologies have been considered previously [110, 195, 196], also in the context of de Sitter holography [99] and braneworld holography [153, 193, 194, 197]. However, in the latter cases the holographic CFT lives on the brane and is coupled to gravity, whereas we are proposing a non-perturbative CFT description of the entire spacetime including the brane.

Now, a braneworld cosmological model can only be realistic if, for an observer living on the brane, gravity is effectively 4-dimensional and localized on the brane. The Randall-Sundrum model [34,35] provides a mechanism for gravity localization on 4-dimensional branes embedded in AdS_5 bulk, and the mechanism can be generalized to different brane geometries [111] and to the presence of black holes [198, 199]. If the brane is not too close to the black hole horizon, gravity is localized, but only locally in spacetime: an experimentalist on the brane would observe ordinary gravity only on non-cosmological scales, and for a limited range of time. In this work we show that, in the presence of a charged black hole in the bulk (AdS-Reissner-Nordström) [144–149], such gravity localization is achievable without losing the dual CFT description of the spacetime. This proof-of-principle result, not attainable in the simplest setup of an AdS-Schwarzschild black hole and a pure tension brane [5], opens the door to a new formulation of cosmology within AdS/CFT. Our choice of units is $\hbar = c = \varepsilon_0 = k_B = 1$.

2.2 Euclidean analysis

The spacetime described above is dual to a CFT state that can be prepared in principle using a quantum computer. Theoretically, it is convenient to describe it starting from a Euclidean path integral. Extending previous works [5,200], the dual state is a fixed charge boundary state of the CFT on a spatial sphere $\mathbb{S}^{d-1}$ evolved for an amount τ_0 of imaginary (Euclidean) time, called preparation time:

$$|\Psi\rangle = \mathrm{e}^{-\tau_0 H}\,|B,Q\rangle\,. \tag{2.1}$$

The ETW brane is associated to the past boundary condition in the path integral. The preparation time τ_0 of the CFT state must be positive, because otherwise the state is not normalizable and hence not in the CFT Hilbert space.

In Euclidean signature, the brane is the bulk extension of the CFT boundary [5, 11, 12]. Its trajectory starts at the asymptotic boundary $r = \infty$ at $\tau = -\tau_0$, reaches a minimum radius $r = r_0$ and ends again on the boundary at $\tau = \tau_0$. Because the state is highly excited, the bulk geometry will also typically contain a black hole. The total Euclidean periodicity is given by the inverse temperature β of the black hole, determined by its size and charge. The brane trajectory excises part of this total range of Euclidean time, leaving only the interval $[-\tau_0, \tau_0]$ where the CFT is defined. Thus, the preparation time, which is a property of the CFT state we are considering, can be written in terms of bulk quantities as $2\tau_0 = \beta - 2\Delta\tau$ for positive-tension branes, where $\Delta\tau$ is the total Euclidean time needed for the brane to cover half of its trajectory. As noted above, the preparation time must be positive to have a sensible CFT state. Therefore, only the Euclidean geometries with a positive preparation time will be dual to a CFT state of the type described in equation (2.1) [5]. We call such geometries “sensible Euclidean solutions”. Alternatively, if $\tau \leq 0$, the brane overlaps itself and there is no Euclidean time interval $[-\tau_0, \tau_0]$ on the boundary where to define the CFT [5] (see Figure 2.2).

The bulk physics is specified by the Euclidean action, which for the Einstein-Maxwell system considered here is $I = I_{bulk} + I_{ETW}$. I_{bulk} is the Einstein-Maxwell action with a negative

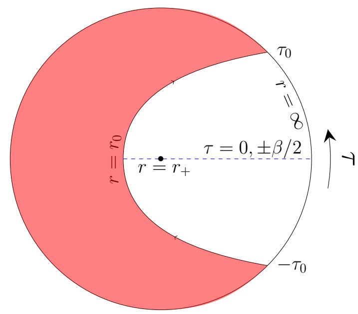

Figure 2.2: Euclidean brane trajectory. The Euclidean path integral on this spacetime computes the norm of the CFT state. The radial coordinate is the radius r, with the outer horizon $r = r_+$ at the center and the asymptotic boundary $r = \infty$ at the circumference. The other spatial dimensions are suppressed. The angular coordinate is the Euclidean time τ, which has a periodicity β. The blue dashed line represents the $\tau = 0, \pm\beta/2$ slice, where the brane reaches its minimum radius r_0. The red region is cut off by the ETW brane. The portion of asymptotic boundary not excised by the brane gives twice the preparation time τ_0 of the CFT state.

cosmological constant $\Lambda = -d(d-1)/(2L_{AdS}^2)$, including a Gibbons-Hawking-York term and an electromagnetic boundary term (needed if the charge is held fixed [201–203]) for the asymptotic boundary. The brane action reads:

$$I_{ETW} = -\frac{1}{8\pi G}\int_{ETW} d^d x\sqrt{h}\,[K - (d-1)T] + I_{ETW}^{em}, \tag{2.2}$$

where G is the $(d+1)$-dimensional Newton constant, K is the trace of the extrinsic curvature of the brane, T is the tension, h is the determinant of the metric induced on the brane and I_{ETW}^{em} is an electromagnetic boundary term. The variation of the bulk action leads to the Einstein-Maxwell equations with a negative cosmological constant, whose solution is the AdS-Reissner-Nordström (AdS-RN) metric (in Euclidean signature):

$$ds^2 = f(r)d\tau^2 + \frac{dr^2}{f(r)} + r^2 d\Omega_{d-1}^2 \tag{2.3}$$

with (for $d > 2$)

$$f(r) = 1 + \frac{r^2}{L_{AdS}^2} - \frac{2\mu}{r^{d-2}} + \frac{Q^2}{r^{2(d-2)}} \tag{2.4}$$

where μ and Q are the mass and charge parameters of the black hole. They can be expressed as a function of the inner (Cauchy) and outer (event) horizons of the black hole, solutions of the equations $f(r_+) = f(r_-) = 0$. The black hole is called extremal when $r_- = r_+$, corresponding to the maximum admissible charge for a fixed mass.

Varying the brane action and imposing Neumann boundary conditions [11,12], the equation

$$K_{ab} - Kh_{ab} = (1-d)Th_{ab} \tag{2.5}$$

is obtained, with $a, b = 0, ..., d-1$. By parametrizing the trajectory of the brane with $r = r(\tau)$, the $\tau\tau$ component of equation (2.5) yields

$$\frac{dr}{d\tau} = \pm\frac{f(r)}{Tr}\sqrt{f(r) - T^2r^2} \tag{2.6}$$

where the sign depends on if the brane is expanding or contracting. The other components of equation (2.5) give an equation for $d^2r/d\tau^2$, which can also be obtained from equation (2.6) (more details are reported in Appendix A.2). For $d > 2$ and $|T| < T_{crit} = 1/L_{AdS}$, the equation $f(r) = T^2r^2$, which gives the zeros of equation (2.6), has always two solutions (which can be computed numerically): $r_0^+ > r_+$ and $r_0^- < r_-$. Between the two solutions the square root takes imaginary values. Since the brane is contracting from and expanding to $r = \infty$, the minimum radius that it reaches at the inversion point is $r_0 = r_0^+$ and is always outside the event horizon r_+. The role of the solution r_0^- will be clear later. Since we are interested in time-symmetric solutions, we require r_0 to sit on the $\tau = 0, \pm\beta/2$ line. In this paper we will consider only positive tensions, corresponding to the geometry in Figure 2.2.

For negative tension branes, the part of geometry retained is the one shaded in red in Figure 2.2 and does not include the black hole horizon. Furthermore, the preparation time in such a case is defined as $\tau_0 = \Delta\tau$ [12]. Although these solutions are interesting, it is not clear if they correspond to a dual CFT state [5] and if they can support gravity localization. Therefore we leave their study to future work. From the CFT point of view, this is justified because we can set the charge, preparation time, and boundary condition via the path integral. The boundary condition determines the tension, hence we may restrict to positive tension. Given values of

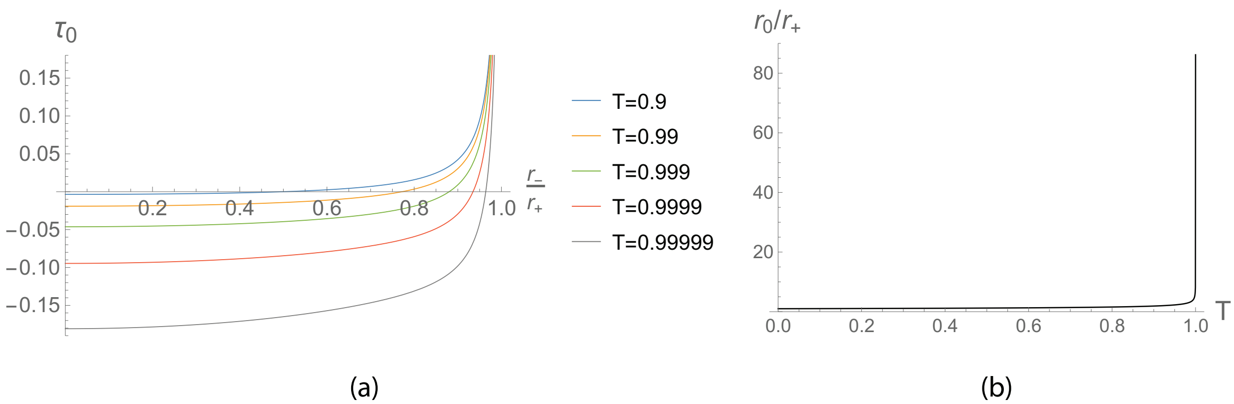

Figure 2.3: Euclidean sensible solutions. (a) Preparation time τ_0 as a function of the ratio between inner and outer horizon radii r_-/r_+ for different values of the tension T. The larger the ratio, the closer the black hole to extremality. The preparation time is positive for every value of the tension if the black hole is sufficiently close to extremality. We chose four spatial dimensions ($d = 4$), $r_+ = 100$ and we set the AdS radius to be $L_{AdS} = 1$. (b) The ratio between the minimum radius of the brane r_0 and the outer horizon radius r_+ grows with the tension T. Our choice of parameters is $d = 4$, $r_+ = 100$, $r_- = 99.9$, $L_{AdS} = 1$. When the brane is near-critical ($T \to 1/L_{AdS}$), it is far from the black hole horizon at the inversion point, and in the Lorentzian picture gravity can be locally localized on it.

d, r_+, r_- and T, it is possible to evaluate the Euclidean time $\Delta\tau$ and therefore the preparation time τ_0 (see Appendix A.2). We find that, for a black hole sufficiently close to extremality, i.e. for $r_- \to r_+$, it is possible to approach the critical value of the tension T_{crit} while retaining a sensible Euclidean solution, i.e. with $\tau_0 > 0$. At the same time, when $T \to T_{crit}$ the ratio between the minimum radius of the brane and the outer horizon radius becomes very large. We further remark (see Appendix A.3) that this non-extremal black hole solution is always dominant in the thermodynamic ensemble when $\tau_0 > 0$. This result was not feasible in the AdS-Schwarzschild case [5] and is first main result of this work.

As noted above, the CFT states we consider can be prepared given full quantum control of the CFT. Euclidean evolution is not unitary and cannot be deterministically implemented. However, by preparing the thermofield double state [172, 204, 205] and measuring the left side in a simple basis [138], a random such state can be prepared.

2.3 Lorentzian analysis and braneworld cosmology

In order to study cosmological physics, we must find the Lorentzian geometry associated with the Euclidean picture outlined above. Consider the state (2.1), obtained taking the $\tau = 0, \pm\beta/2$ slice of the thermal circle (where the brane reaches its minimum radius r_0), and evolve it in real time. The corresponding geometry is a maximally extended AdS-RN black hole with the ETW brane cutting off part of the left asymptotic region. The effect of the transition to Lorentzian signature on equation (2.6) is to flip the sign of the radicand, thus the RHS is now real only if $r_0^- < r < r_0^+$. The minimum radius in Euclidean signature is a maximum radius in Lorentzian signature. Therefore the brane expands and contracts crossing the two horizons of the black hole, but, differently from the AdS-Schwarzschild case, it never reaches the singularity (see Figure 2.1).

Defining the brane proper time $d\lambda^2 = [f(r) - r'^2/f(r)]dt^2$, the metric induced on the brane takes the form

$$ds^2_{ETW} = -d\lambda^2 + r^2(\lambda) d\Omega^2_{d-1} \tag{2.7}$$

which is a closed FLRW metric where the brane radius $r(\lambda)$ plays the role of the scale factor, ranging between r_0^- and r_0^+ and satisfying the Friedmann equation

$$\left(\frac{\dot{r}}{r}\right)^2 = -\frac{1}{r^2} + \frac{2\mu}{r^d} - \frac{Q^2}{r^{2d-2}} + \left(T^2 - \frac{1}{L^2_{AdS}}\right) \tag{2.8}$$

where the dot indicates a derivative with respect to the proper time. For $d = 4$, this result (already obtained in refs. [115, 153]) shows that an observer comoving with the brane interprets the motion of the brane in the bulk as the expansion and contraction of a closed FLRW universe in the presence of radiation (with energy density proportional to the mass of the black hole), a negative cosmological constant $\Lambda_4 = 3(T^2 - 1/L^2_{AdS})$ (which is very small when $T \to T_{crit}$) and stiff matter [152, 153] with negative energy density (proportional to the charge of the black hole).

From the bulk point of view, the existence of a minimum radius is due to the repulsive nature of the RN singularity, while from the braneworld point of view, the (repulsive) stiff matter term is responsible for the absence of the cosmological singularity, replaced by a Big Bounce [152]. In principle, gluing together more patches of the AdS-RN bulk spacetime, we can obtain a cyclical cosmology. However, the instability of the Cauchy horizon against even small perturbations suggests that, in the region near the bounce, the present description of the brane evolution is not reliable. [151] When the charge of the black hole vanishes, we recover the AdS-Schwarzschild description of a Big Bang-Big Crunch braneworld cosmology. We emphasize that the cosmological interpretation is not appropriate in the region where the Big Bounce takes place, because a 4-dimensional description of gravity localized on the brane is achievable only when the brane sits far from the black hole horizon.

2.4 Gravity localization

The remaining issue is whether observers on the brane see approximately four-dimensional gravity. Randall and Sundrum showed [34, 35] that a 4-dimensional Minkowski brane embedded in a warped AdS$_5$ spacetime supports a normalizable graviton zero-mode bound on the brane, reproducing 4-dimensional gravity. The bound mode is lost in the presence of an AdS-Schwarzschild black hole in the bulk [198], but a resonant quasi-bound mode with a finite lifetime persists when the brane is static and far from the black hole horizon [199]. This is a metastable mode that, after a finite lifetime, "leaks" into the bulk and falls into the black hole horizon. The shorter the spatial scale of the gravitational perturbation, the longer it is bound on the brane. Gravity is therefore locally localized both in space and in time, meaning that it will look 4-dimensional to an observer living on the brane, but only on spatial and time scales smaller than the cosmological ones.

Clarkson and Seahra [199] focused their attention mainly on the small black hole case ($r_H < L_{AdS}$). Since sensible Euclidean solutions with $r_0/r_+ \gg 1$ are achievable only if the black hole is large, our generalization of their work to the AdS-RN spacetime is focused on the $r_+ \gg L_{AdS}$ case (see Appendix A.5).

Let us consider a linear perturbation of the metric $\delta g_{\mu\nu} = g_{\mu\nu} - g^0_{\mu\nu}$, $\mu, \nu = 0, ..., d$. As a tensor on a spatial slice at constant radius ($t = const$, $r = const$), it can be decomposed into scalar, vector and tensor components [206]. The graviton mode of interest is the tensor component which has $\delta g_{t\mu} = \delta g_{r\mu} = 0$. We also use the transverse-traceless (TT) gauge condition $\delta g^{\mu}_{\mu} = 0 = \nabla^{\mu}\delta g_{\mu\nu}$. It is useful to introduce the adimensional coordinates and parameters $y = r/r_+$, $\tilde{t} = t/r_+$, $\gamma = L_{AdS}/r_+$, $q = Q/r_+^{d-2}$ and to decompose the metric perturbation in terms of tensor harmonics $\mathbb{T}^{(k)}_{ij}$ (with $i, j = 1, ..., d-1$) on the unit $(d-1)$-sphere. They satisfy $\Delta_{d-1}\mathbb{T}^{(k)}_{ij} = -k^2\mathbb{T}^{(k)}_{ij}$, where Δ_{d-1} is the $(d-1)$-dimensional covariant Laplacian on the unit $(d-1)$-sphere and $k^2 = l(l+d-2)-2$, with $l = 1, 2, ...$ generalized angular momentum.

Defining the tortoise coordinate $dr^* = dy/f(y)$ and studying the problem in the frequency domain, the linearized Einstein equations can be recast in the form of a one-dimensional Schrödinger equation for each tensor mode:

$$-\partial^2_{r^*}\psi_{k,\omega}(r^*) + V_k\left[y(r^*)\right]\psi_{k,\omega}(r^*) = \omega^2\psi_{k,\omega}(r^*) \tag{2.9}$$

where the potential reads:

$$V_k(y) = f(y)\left[\frac{d^2-1}{4\gamma^2} + \frac{d^2-4d+11+k^2}{4y^2} + \frac{(d-1)^2\left(1+\frac{1}{\gamma^2}+q^2\right)}{4y^d} - \frac{(d-1)(3d-5)q^2}{4y^{2d-2}}\right]. \tag{2.10}$$

This potential diverges for $r^* = r^*_\infty$ (where $y(r^*_\infty) = \infty$) and vanishes exponentially for $r^* \to -\infty$, at the black hole horizon.

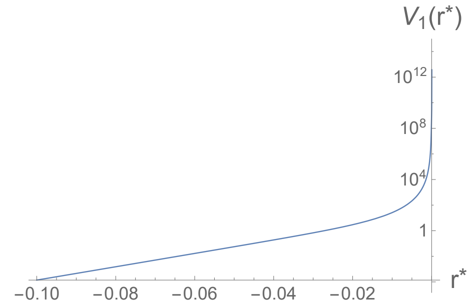

Figure 2.4: Potential $V_k[y(r^*)]$ - Large black hole. Potential (2.10) as a function of the tortoise coordinate r^* in four spatial dimensions ($d = 4$). We chose the values $r_+ = 100$, $r_- = 99.9$ for the outer and inner horizon radii respectively, setting the AdS length to be $L_{AdS} = 1$ and the angular momentum (and therefore the eigenvalue k) to be $l = k = 1$. The potential diverges for $r^*_\infty = 4.94 \cdot 10^{-5}$ and vanishes exponentially at the horizon $r^* \to -\infty$.

Now we need to find a boundary condition on the ETW brane, which cuts off the radial coordinate at $r^* = r^*_b < r^*_\infty$. If the brane is moving in the bulk, this is a non-trivial task. We assume that the brane is moving adiabatically with respect to the time scale of the perturbation, and consider it effectively static at a position $r^* = r^*_b$, verifying later the reliability of the adiabatic approximation. Under this assumption, the linearized version of equation (2.5) provides the (Neumann) boundary condition $\partial_{r^*}\psi_{k,\omega}|_{r^*=r^*_b} = (d-1)f(y)/(2y) \cdot \psi_{k,\omega}|_{r^*=r^*_b}$, with $y = y(r^*)$. Requiring this boundary condition is equivalent to add to the potential (2.10) a negative delta at the position of the brane, whose depth is $(d-1)f(y)/y$. In the original Randall-Sundrum model, such a delta guarantees the existence of the zero bound mode. The rapid vanishing behaviour of the potential (2.10) at the black hole horizon implies that only a metastable, quasi-bound mode with complex frequency $\omega = \bar{\omega} + i\Gamma/2$ and pure infalling boundary condition at the black hole horizon (typical of quasi-normal modes) can be present in our setup. In the large black hole case ($\gamma \ll 1$) this is the only resonant mode [199].

Focusing on the $d = 4$, $\gamma \ll 1$ case of interest, we use the trapping coefficient method [199] (see Appendix A.5) to find the real and imaginary parts of the frequency of the quasi-bound mode.

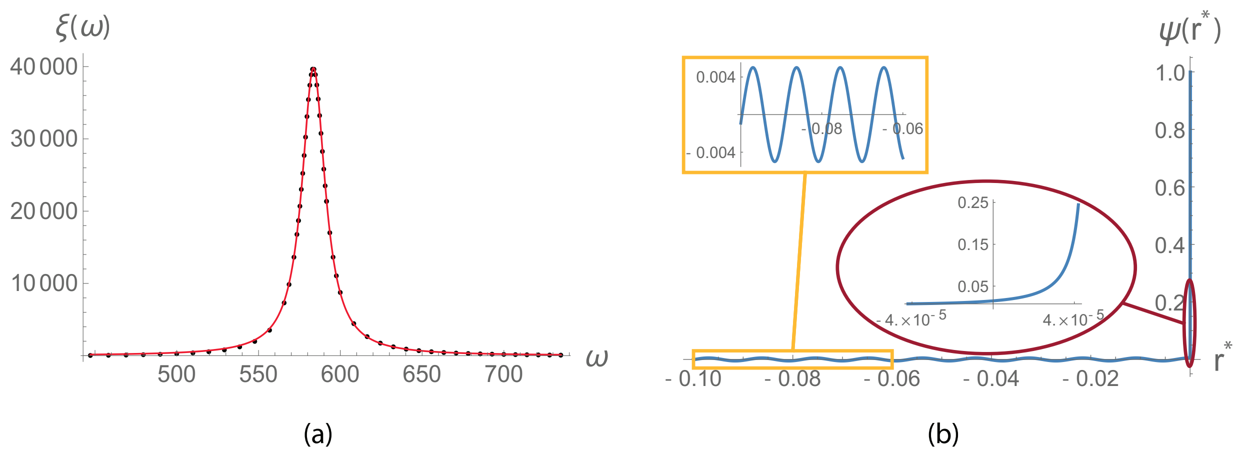

Figure 2.5: Quasi-bound mode. Results for four spatial dimensions ($d = 4$), with outer and inner horizon radii given by $r_+ = 100$ and $r_- = 99.9$ respectively. We set the AdS length to be $L_{AdS} = 1$, giving $\gamma = L_{AdS}/r_+ = 0.01 \ll 1$. The choice for the angular momentum is $l = 5$, while the position of the brane is taken to be $y_b = 34.62$ (corresponding to the maximum radius of a brane with tension $T = 0.999999$). (a) Squared trapping coefficient $\xi(\omega)$ as a function of frequency ω. $\xi(\omega)$ presents a Breit-Wigner peak centered at the real part $\bar{\omega}$ of the frequency of the quasi-bound mode, while its imaginary part $\Gamma/2$ is given by the half-width at half-maximum. The fit gives $\bar{\omega} = 583.6$, $\Gamma = 17.28$. The adjusted coefficient of determination for the fit is $R^2 = 0.999978$, showing the accuracy of the Breit-Wigner approximation for the peak of the squared trapping coefficient for this choice of parameters. (b) Quasi-bound mode wavefunction $\psi(r^*)$ as a function of the tortoise coordinate r^*. $\psi(r^*)$ oscillates in the near-horizon region, as shown in the top-left inset, and grows very fast near $r^*_b = 4.65 \cdot 10^{-5}$, as it is evident from the right-bottom inset. Therefore, the quasi-bound mode is very well localized on the brane, but has a non-vanishing probability to leak into the bulk and fall into the black hole.

For a given value of the charge of the black hole, there are three control parameters: the size of the black hole γ, the position of the brane $r^*(y_b)$, and the angular momentum l. We find that, when the brane is sufficiently far from the horizon of the black hole, $\bar{\omega} \gg \Gamma$ (i.e. the mode is long-lived) and the graviton is very well localized on the brane (see Figure 2.5). Such a localization is lost if the brane radius becomes too large. Increasing the size of the black hole, the brane must sit farther from the horizon to retain the long-lived quasi-bound mode. Gravity localization is also more efficient for higher values of the angular momentum l. Increasing l means probing shorter distances on the brane. Therefore, this result is in accordance with our expectation to obtain a 4-dimensional effective description of gravity only locally. The last step is to verify that the adiabatic approximation is reasonable. One must compare the time scale of oscillation $t_o = 1/\bar{\omega}$ with the "Hubble time" $T_H = y(t)/y'(t)$, determined by the Lorentzian version of equation (2.6). The adiabatic approximation is reliable if $t_o \ll T_H$ and if the condition $(y')^2/f^2(y) \ll 1$ (used to derive the boundary condition at the brane, see Appendix A.5.1) is satisfied. For given values of charge and tension, the approximation is arbitrarily good when approaching the inversion point in the trajectory of the brane, where y' vanishes. But it holds also for a significant portion of the trajectory of the brane, as quantified by the ratio between the proper time spent to cover the part of trajectory where the approximation is reliable and the total amount of proper time for the entire trajectory. As an example, for the set of parameters considered in Table 2.1, if we accept $t_o \sim T_H/10$ as the threshold for the validity of the adiabatic assumption, the latter holds for $\sim 55\%$ of the total amount of brane proper time. The decay time $t_d = 2/\Gamma$ is almost always considerably larger than the Hubble time, meaning that our analysis loses significance before the quasi-bound mode leaks into the bulk. We finally remark that the time of oscillation of the mode is very close to the one expected for a 4-dimensional metric perturbation of the Einstein-static universe $t_{GR} = y_b/\sqrt{f(y_b)(l+2)l}$. The local localization of gravity on the Euclidean-sensible braneworld solution is the second main result of this work.

2.5 Discussion

In this work we proved that it is possible to build a holographic braneworld cosmology model which admits locally a 4-dimensional effective description of gravity. An interesting open question is if this framework can be extended to different cosmological models, eventually including a de Sitter phase that could match our current observational data, and if gravity localization

y_b	T_H	t_o	t_d	$(y')^2 / [f(y)]^2$	$\lambda(y_b)/\lambda_{tot}$
30	$1.762 \cdot 10^{-3}$	$9.172 \cdot 10^{-4}$	0.08370	$3.581 \cdot 10^{-6}$	0.9764
45	$2.698 \cdot 10^{-3}$	$9.190 \cdot 10^{-4}$	0.1880	$6.786 \cdot 10^{-7}$	0.9465
60	$3.716 \cdot 10^{-3}$	$9.229 \cdot 10^{-4}$	0.3342	$2.012 \cdot 10^{-7}$	0.9035
75	$4.875 \cdot 10^{-3}$	$9.282 \cdot 10^{-4}$	0.5226	$7.484 \cdot 10^{-8}$	0.8459
90	$6.282 \cdot 10^{-3}$	$9.350 \cdot 10^{-4}$	0.7516	$3.129 \cdot 10^{-8}$	0.7713
105	$8.178 \cdot 10^{-3}$	$9.432 \cdot 10^{-4}$	1.026	$1.356 \cdot 10^{-8}$	0.6748
120	0.01124	$9.530 \cdot 10^{-4}$	1.339	$5.495 \cdot 10^{-9}$	0.5462
135	0.01895	$9.645 \cdot 10^{-4}$	1.713	$1.527 \cdot 10^{-9}$	0.3540
145.1 (max)	∞	$9.733 \cdot 10^{-4}$	1.956	0	0

Table 2.1: Adiabatic approximation: time scales comparison. Results for four spatial dimensions ($d = 4$) and a large, near-extremal black hole with outer and inner horizon radii given by $r_+ = 100$ and $r_- = 99.9$ respectively. We set the AdS radius to be $L_{AdS} = 1$ (i.e. $\gamma = L_{AdS}/r_+ = 0.01$). We further chose the value $l = 10$ for the angular momentum and $T = 0.999999999$ for the brane tension, which is clearly near-critical. With this choice of parameters, the maximum radius reached by the brane is $y_b^{max} = 145.1$ (reported in the last line of the first column). In the first column we show the position of the brane in adimensional coordinates $y_b = r_b/r_+$. In the second, third and fourth columns the time scales of motion of the brane (T_H) and of oscillation (t_o) and decay (t_d) of the quasi-bound mode are reported, respectively. When $T_H \gg t_o$ is satisfied (for example in the last three lines), the adiabatic approximation holds. If $t_d \gg T_H$, the adiabatic approximation breaks down before the mode leaks into the bulk. The fifth column shows the ratio $(y')^2 / [f(y)]^2$, where $y' = dy/dt$ and $f(y)$ is the absolute value of the 00 component of the metric (given by equation (2.4)) expressed in terms of the adimensional coordinates and parameters. This ratio must be small in order for our analysis to be consistent. In the last column we report the fraction between the proper time $\lambda(y_b)$ needed for the brane to expand from y_b to y_b^{max} and shrink back to y_b, and the total amount of proper time needed to complete the brane trajectory. The Euclidean solution corresponding to this choice of parameters is sensible and dominant in the thermodynamic ensemble.

is achievable on even larger scales in such setups. Understanding gravity localization beyond the adiabatic approximation would also be interesting.

The holographic dual description presents many non-trivial issues to be explored. Determining which CFT observables are able to probe the physics behind the horizon of the black hole, and therefore the braneworld cosmology, is crucial. If the brane is not too far from the black hole horizon, one possibility is the entanglement entropy of large spatial regions of the

CFT [5,59,207], while additional information can be extracted from the holographic complexity, even if its CFT interpretation is not completely clear yet. It is also important to identify field theories with the right boundary states to make our construction work and verify the stability of the solutions in the full theory. For example, one should check that scalar fields do not condense in the near-extremal black hole background (or that the desired properties persist in such a condensed state). Explicit realizations of AdS/BCFT in top-down stringy models have been proposed in refs [12,208]. Given a CFT, it should be possible to simulate it on an quantum computer [138,172,204,205], thereby opening up the possibility to experimentally study holographic braneworld cosmology.

Although many questions still need to be answered, the model presented in this paper shows the possibility to holographically describe a FLRW cosmology using AdS/CFT, bringing us one step closer to the understanding of quantum gravity in a cosmological universe.

Acknowledgements

This work was supported in part by the U.S. Department of Energy, Office of Science, Office of High Energy Physics QuantISED Award DE-SC0019380 and by the Simons Foundation via the It From Qubit collaboration. We thank M. Van Raamsdonk, C. Waddell, D. Wakeham, M. Rozali, S. Cooper, R. Sundrum, R. Bousso, S. Kumar, Y. Wang and J. Maldacena for useful discussions.

Chapter 3: The holographic wormhole cosmology approach

Authors:[1] *Stefano Antonini, Petar Simidzija, Brian Swingle, Mark Van Raamsdonk.*

Abstract: We argue that standard tools of holography can be used to describe fully non-perturbative microscopic models of cosmology in which a period of accelerated expansion may result from the positive potential energy of time-dependent scalar fields evolving towards a region with negative potential. In these models, the fundamental cosmological constant is negative, and the universe eventually recollapses in a time-reversal symmetric way. The microscopic description naturally selects a special state for the cosmology. In this framework, physics in the cosmological spacetime is dual to the vacuum physics in a static planar asymptotically AdS Lorentzian wormhole spacetime, in the sense that the background spacetimes and observables are related by analytic continuation. The dual spacetime is weakly curved everywhere, so any cosmological observables can be computed in the dual picture via effective field theory without detailed knowledge of the UV completion or the physics near the big bang. In particular, while inflation may explain the origin of perturbations in the cosmology picture, the perturbations can be deduced from the dual picture without any knowledge of the inflationary potential.

[1]Originally published as *Cosmology from the vacuum*, e-Print: 2203.11220 (under review, JHEP), [2]. The appendices of the paper are reported in Appendix B.

3.1 Introduction

Holographic models from string theory [14–17] have been extremely successful in describing a great variety of quantum gravitational phenomena, including the physics of high-energy scattering processes where gravitational effects are important, the formation, dynamics, and evaporation of black holes, and even the emergence of spacetime and gravitation from intrinsically quantum mechanical phenomena. However, it remains a significant open challenge to find a quantum gravitational description of the physics in cosmological spacetimes like our own universe.

Cosmology with $\Lambda < 0$

A possible misconception is that the obstruction to describing realistic cosmological physics using holography is that holographic models naturally describe spacetimes with a negative cosmological constant while our own universe appears to have a positive cosmological constant. However, the observational evidence [209, 210] tells us not that there is a positive cosmological constant, but that the expansion of the universe is currently accelerating, i.e. that $\ddot{a} > 0$ where a is the scale factor. Einstein's equations then imply that $3p + \rho < 0$ where p and ρ are the pressure and energy density. This could be explained *either* by a positive cosmological constant, *or* by the potential energy associated with time-dependent scalar fields that are currently at a positive value of their potential [92, 93, 211] (see also [212, 213] for more recent discussions).[2] While the ΛCDM model with $\Lambda > 0$ provides a good fit to cosmological data, the possibility of $\Lambda < 0$ with

[2] In the latter case, there are also constraints on how quickly the scalar can be changing. There may be additional possibilities based on strongly coupled quantum fields or modified gravity.

time-dependent scalars is not ruled out (see [213–217] for recent discussions). Time-dependent scalars are also natural to consider from an effective field theory point of view since they preserve the same symmetries as an FRW spacetime. In this case, there is no particular reason why the scalars can't be evolving towards a minimum or extremum of the potential with a value (which we can define to be the fundamental cosmological constant in the effective theory) that is zero or negative.

In the absence of current observations that can tell us more definitively whether the fundamental cosmological constant is positive, negative, or zero, we might ask which possibility is most natural from a theoretical perspective. The current situation in string theory is that we have (via holography) a wealth of deeply understood models that describe quantum gravitational physics with a negative cosmological constant[3] and no fully microscopic models of four-dimensional quantum gravity with zero or positive cosmological constant.[4] Even at the level of effective field theory, it is still controversial whether metastable string compactifications with $\Lambda > 0$ exist (see e.g. [219, 220] for recent discussions). So at present, the possibility that seems most likely to admit a fully non-perturbative theoretical description based on our current understanding is $\Lambda < 0$.[5]

Given that we already have a good theoretical understanding of other types of spacetimes with $\Lambda < 0$ through holography, a natural next step toward understanding cosmology from a quantum gravity point of view is to try to understand $\Lambda < 0$ cosmologies microscopically, espe-

[3]More specifically, we have models where the magnitude of this is similar to the observed magnitude and the size of the extra dimensions are acceptably small. Furthermore, these models typically have scalars whose potential has derivatives of scale similar to that of the cosmological constant - this is equivalent to having one or more scalar operators of low dimension in the dual CFT. Thus, there are likely to be nearby points on the potential with small positive values and a small enough slope so that the scalars change acceptably slowly.

[4]See [97, 98, 100–102, 107, 109, 110, 218] for various approaches to describing $\Lambda > 0$ cosmology.

[5]Of course, it could just be a historical accident that we understood quantum gravity with $\Lambda < 0$ at least 25 years before $\Lambda > 0$.

cially since it seems possible that our universe could have $\Lambda < 0$.[6]

Why it is hard to describe $\Lambda < 0$ cosmological models holographically

Even if we presume $\Lambda < 0$, there is still a significant obstacle in using holography to describe models of cosmology: cosmological models assume a homogeneous and isotropic universe filled with matter and radiation, while usual holographic models describe spacetimes that are *asymptotically empty*. While holography has no trouble describing spacetimes with black holes, gravitational waves, radiation, etc... these interesting features are always in the interior of a spacetime that asymptotically looks just like pure AdS.[7] This rigid asymptotic behaviour is related to the fact that any finite energy state of the dual field theory has the same UV physics (e.g. short distance correlators).

A complementary way to view the difficulty is that cosmological spacetimes with $\Lambda < 0$ are typically big-bang / big-crunch geometries with no asymptotically AdS regions that could be associated with a dual field theory.

Asymptotically AdS regions in complex time

A hint for how to make progress is that these $\Lambda < 0$ cosmological spacetimes often do have asymptotically AdS regions if we consider complexifying the coordinates. In an expanding universe with $\Lambda < 0$, the negative cosmological constant eventually comes to dominate the evolution, and this causes the scale factor to decelerate and eventually turn around. In cases where

[6] This was also emphasized recently in [215]. It is certainly still interesting to understand whether string theory can produce $\Lambda > 0$ models and whether these can be given a non-perturbative description, but it seems to us that comparatively little effort has been expended exploring what may be a simpler possibility.

[7] We can also have other types of rigid asymptotic behaviors in models where the dual field theory is not conformal in the UV.

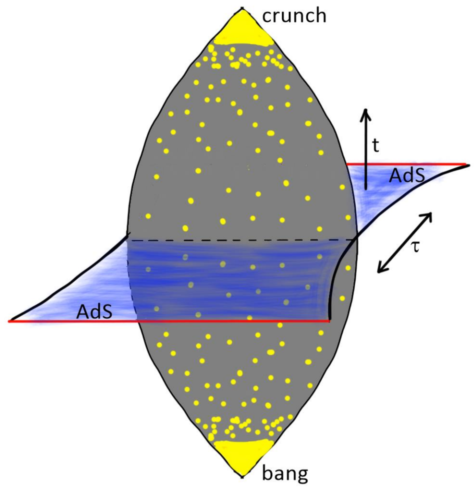

Figure 3.1: Asymptotically AdS regions in the analytic continuation of a time-symmetric $\Lambda < 0$ cosmology. The asymptotically AdS Euclidean gravity theory can be given a microscopic holographic description, and this can be used to define a special state for the cosmology.

any scalar fields also have zero time derivative at this point, the full solution for the background geometry is time-reversal symmetric about this turn-around point. In such time-symmetric geometries, we can analytically continue the time direction to obtain a real Euclidean geometry.[8] This analytically continued geometry has a pair of asymptotically AdS regions at Euclidean time $\tau = \pm\infty$ (see Figure 3.1) provided that the scalar fields asymptote to some value with a negative potential. In the special case of a flat cosmology (that we will focus on), we can perform a further analytic continuation of one of the spatial directions to obtain a *static* Lorentzian geometry with a pair of asymptotically AdS regions.

So far, this is a mathematical curiosity: starting from a time-reversal symmetric $\Lambda < 0$ flat cosmological spacetime, we can associate via analytic continuation a Euclidean geometry and a static horizon-free Lorentzian geometry each with a pair of asymptotically AdS regions.

However, the observation suggests a path forward to find a microscopic description of the

[8]The scale factor is typically analytic around the time-reversal symmetric point since it is a solution of the Friedmann equation, and the analytically continued Friedmann equation is sensible for typical equations of state.

$\Lambda < 0$ cosmology:

1. Find a microscopic description for the physics of the associated spacetimes with asymptotically AdS regions using holography.
2. Use this microscopic description of the Euclidean theory to define a special state for the Lorentzian cosmology and to give a holographic description of the physics of this state.

Before turning to the holographic descriptions, let us further motivate the second point here.

A special state for cosmology

In quantum field theory, if we have a time-reversal symmetric background Lorentzian spacetime related by analytic continuation to a reflection-symmetric Euclidean spacetime, the quantum field theory on this Euclidean spacetime[9] defines a special state of the Lorentzian theory, obtained by slicing the path integral defining the Euclidean theory (see Appendix A for a review). Observables for this state in the Lorentzian theory are related by analytic continuation to observables in the Euclidean theory. For example, for a field theory in Minkowski space, the state defined by the associated Euclidean field theory is the vacuum state.

In our case, the spacetimes are dynamical, but we will argue that the Euclidean version of the gravitational theory describing the Lorentzian cosmology can still be used to define a preferred quantum state for the cosmology. This is similar to the idea of Hartle and Hawking [169], who argued that a natural state for cosmology is provided by a Euclidean gravitational path integral with no boundary in the Euclidean past.

[9] The Euclidean field theory may require additional boundary conditions for fields to complete its definition, e.g. if the analytically continued spacetime has asymptotically AdS regions. In this case, we have a family of states, each associated with a choice of boundary conditions.

In our case, the Euclidean spacetimes we consider do have a boundary in the Euclidean past, namely an asymptotically AdS boundary. This is important for us as it will permit us to define the gravitational path integral non-perturbatively using holography.

Holographic description of spacetimes with two asymptotically AdS regions

We now return to the question of how to holographically describe the physics of these spacetimes. For our discussion, we focus on the most phenomenologically relevant case of four-dimensional flat cosmology; we comment on the generalization to other cases in the discussion.

We have seen that for a large class of $\Lambda < 0$ flat cosmological spacetimes, analytic continuation gives a Euclidean geometry of the form

$$ds^2 = d\tau^2 + a^2(\tau)(dx^i dx^i) \tag{3.1}$$

with asymptotically AdS regions for $\tau \to \pm\infty$. A further analytic continuation gives a Lorentzian static spacetime

$$ds^2 = d\tau^2 + a^2(\tau)(dx_\mu dx^\mu) \; . \tag{3.2}$$

Such geometries are sometimes described as asymptotically AdS planar *wormholes*, since they have two asymptotically AdS regions connected by a "throat" with a planar cross section. The two asymptotically AdS regions here suggest a dual holographic description that involves a pair of three-dimensional CFTs,[10] where the coordinates labeled by x correspond to the directions on which the field theory lives, and the τ direction is the emergent radial direction.

[10]The AdS/CFT description of Euclidean wormholes was first discussed in [13], where the possible connection to cosmological physics via analytic continuation was also pointed out. More recent discussions of the holographic description of the types of wormholes we are discussing here appears in [156, 221].

Figure 3.2: Left: two non-interacting 3D CFTs are dual to a pair of disconnected AdS spacetimes. Right: two 3D CFTs interacting via a non-holographic 4D CFT, proposed to be dual (in some cases) to a Lorentzian wormhole with two asymptotically AdS boundaries.

For the Lorentzian wormhole, since it is possible to go (causally) from one asymptotically AdS region to the other through the geometry, the two CFTs in the holographic description must be interacting somehow.[11] The physical separation between the boundaries in the wormhole geometry indicates that the interactions between the two CFTs are not instantaneous and do not induce arbitrarily strong correlations [7, 221]. These features suggest that the interaction is not a local field theory interaction; in [7], we argued that the interaction likely involves some auxiliary degrees of freedom and that a natural possibility is for these extra degrees of freedom to take the form of a four-dimensional quantum field theory on $\mathbb{R}^3$ times an interval, to which the two CFTs are coupled at the edges of the interval (see Figure 3.2).[12] The proposed dual for the asymptotically AdS wormhole geometry is the vacuum state of this 3D-4D-3D theory.

To preserve the four-dimensional character of the dual gravitational theory, the four-dimensional field theory should have many fewer local degrees of freedom than the 3D CFTs so that it rep-

[11]For Euclidean wormhole solutions in general, it has been suggested that the dual description may be in terms of some type of ensemble of CFTs, since the connected geometry suggests correlations between the two sides, but such correlations will be absent for a single pair of non-interacting CFTs [13, 54, 163, 222–224]. In the special case where the wormhole cross-section has a translation-invariant direction so that we can analytically continue to a static Lorentzian wormhole, we can make the stronger statement that the CFTs must be interacting [3, 7]. As discussed in [7], when this interaction is mediated via auxiliary degrees of freedom, integrating these degrees of freedom out in the Euclidean picture does give rise to something like an ensemble of CFTs, where the ensemble is over possible sources for local operators.

[12]More generally, the two 3D CFTs could be boundaries or defects in a higher-dimensional quantum field theory. This seems to be the most general possibility consistent with Lorentz invariance, local quantum field theory, and the absence of instantaneous interactions and diverging correlators between the two 3D theories.

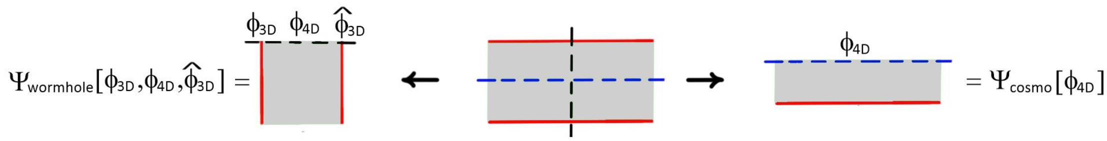

Figure 3.3: Two different slicings of the same microscopic Euclidean path integral give states dual to the Lorentzian wormhole and the cosmology. The pictures on the left and right indicated a Euclidean path integral over field configurations with the specified boundary conditions at the top surface. See also Figure 6 for the gravity interpretation of these states.

resents a small perturbation to the physics in the UV. Nevertheless, via a long RG flow, this perturbation leads to a large amount of entanglement between the 3D CFTs in the IR, giving rise to the connected dual geometry [7]. We review some additional motivations and evidence for this construction in section 2 below.

Holographic description of the cosmological physics

Assuming this dual description of the Lorentzian wormhole spacetime, we can now try to understand the dual of the cosmological physics.

The proposed dual for the Euclidean wormhole is the Euclidean version of the same field theory: a pair of Euclidean 3D CFTs on $\mathbb{R}^3$ coupled via a Euclidean 4D CFT on $\mathbb{R}^3$ times an interval.[13]. This Euclidean theory can be used to construct the Lorentzian vacuum state dual to the Lorentzian wormhole by slicing the path integral perpendicular to the direction that is to be analytically continued (one of the $\mathbb{R}^3$ directions), as shown in Figure 3.3.[14]

To define a state associated with the cosmological spacetime, we slice the same path integral in a different way, perpendicular to the direction between the two 3D CFTs, along the surface fixed by the reflection symmetry that exchanges the two 3D CFTs. We can understand this via the

[13]More precisely, the wormhole is the dominant saddle point geometry in a gravitational path integral dual to this field theory path integral.

[14]See Appendix B.1 for a review of how quantum states can be defined by slicing Euclidean path integrals.

right-hand figure of figure 2: the sliced CFT path integral corresponds to the sliced gravitational path integral that constructs a state for the cosmology at the time-symmetric point.

This second slicing defines a state of the 4D CFT on spatial $\mathbb{R}^3$. The 3D CFT appears only in the Euclidean path integral used to construct the state, not in the physical degrees of freedom. Even though the 4D CFT is not conventionally holographic, the presence of the holographic 3D CFT in the Euclidean past of the path integral produces a state that is sufficiently complex to encode the semiclassical physics of the cosmological spacetime.

The physics here is similar to how black hole interiors can be encoded in auxiliary radiation systems [79,80,225,226], or of how bubbles of spacetime associated with a holographic CFT can be encoded in the state of a different CFT [227] or a collection of non-interacting BCFTs [228].

Extracting cosmological observables

The 4D CFT state that encodes the cosmological spacetime is a high-energy state that will look almost completely thermal. Thus, extracting the cosmological observables from this state would appear to be extremely difficult, similar to extracting local behind-the-horizon physics from a CFT state describing a single-sided black hole.[15] Indeed, in the special case where the 4D CFT is holographic, the cosmological physics can be understood as living on an end-of-the-world (ETW) brane behind a black hole horizon.[16]

However, because we are considering a special state that arises from a Euclidean path integral, observables in the Lorentzian cosmology can be extracted in a simple way from this Euclidean theory, or alternatively from the vacuum physics of the Lorentzian wormhole. Since both

[15] The entanglement wedge of a large enough subsystem of the 4D CFT will include part of the cosmological spacetime, so entanglement entropy for such large subsystems does provide one direct probe of the cosmology.

[16] This was the case in the first examples of models of this type [1,5], where the approach was dubbed "Black hole microstate cosmology". See section 2.1 for a review

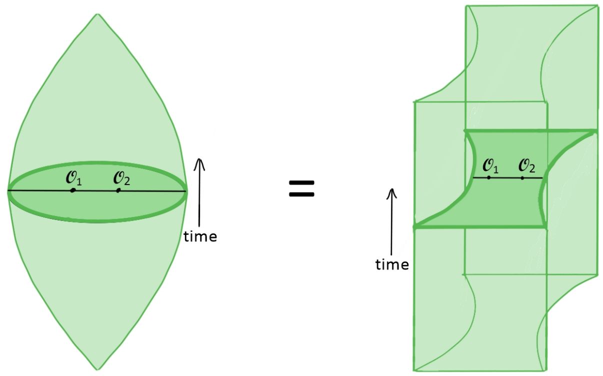

Figure 3.4: Observables restricted to an $\mathbb{R}^2$ at the time-reflection symmetric surface in the cosmology (black line) are equal to corresponding observables on the $\mathbb{R}^2$ in the middle of the Lorentzian wormhole. More general observables are related by double analytic continuation.

the cosmology and the Lorentzian wormhole arise from the same Euclidean path integral through different slicings, there is a precise relationship between observables in the cosmology picture and observables in the wormhole picture. We have already seen that the scale factors in these two pictures are related by analytic continuation. But the correlation functions of local operators in the cosmology (which include all standard cosmological observables) will also be related by analytic continuation to the correlation functions in the wormhole picture. The wormhole geometry is static and horizon-free, so local observables in this picture are related in a much simpler way (e.g. by an HKLL procedure [229]) to the dual quantum field theory, which is in its vacuum state. Thus, we can understand cosmological observables by calculating the *vacuum* observables in the wormhole picture (via effective field theory or using the vacuum observables of the dual QFT), and then analytically continuing these to the cosmology picture. As a special case, correlation functions in the cosmology at $t = 0$ (the turn-around point) in which all operators live in a single 2D plane are simply equal to some corresponding vacuum correlation functions at the midpoint of the wormhole, as shown in Figure 3.4.

In the wormhole picture, there is no big bang or big crunch, and the spacetime is weakly curved everywhere. Thus, an effective field theory description should be valid everywhere. This should permit a computation of cosmological observables without having to explicitly understand physics in the vicinity of the Big Bang, and without having to use the underlying microscopic description. A shorter version of the present paper emphasizing the effective field theory point of view is the companion paper [9].

Naturalness problems in cosmology

If this framework can support realistic models of cosmology it may help resolve various naturalness problems. Extrapolating our present observations of the universe back to early times we find that the universe at early times must have been extremely flat and extremely homogeneous, and must have contained correlations between regions that were apparently never in causal contact since the big bang. Thus, the required initial state would appear to be finely tuned and/or unnatural in various ways. Inflation seeks to explain how such an initial state could have arisen naturally by postulating an earlier period of exponential expansion with many e-foldings.

In our framework, the Euclidean theory constructs a state at the time-symmetric point, and the initial state close to the big bang is most naturally understood as the result of quantum evolution backwards to the big bang.[17] Thus, features of the state in the early universe are natural provided that they arise from the backward evolution of a state at the time-symmetric point that is produced by the Euclidean path integral.

The construction of the state via a Euclidean theory with $\mathbb{R}^3$ symmetry naturally produces a universe that is flat and very homogeneous. Also, since correlations in the cosmology picture at

[17] We can consider the quantum evolution of the state with either direction of time. We discuss below in Section 3.4.2 how the arrow of time experienced by observers might emerge.

the time-symmetric slice are equal to vacuum correlators in the wormhole picture, we *naturally have correlations in the cosmology picture between regions of the universe that were never in causal contact*, since all points in the static wormhole picture have intersecting past light cones.

While the model appears to alleviate many of the problems that inflation was introduced to explain, it remains to be seen whether it can reproduce the detailed quantitative results for the cosmological perturbations that arise from inflationary models and that agree with observations. An interesting point is that inflationary physics may still be present in our framework and may provide a dual explanation for the origin of perturbations/correlations, but since we can also compute these via the wormhole picture, *no explicit knowledge of the inflationary potential or any other early universe physics is required to compute the perturbations*.

Generic cosmological predictions

In this paper, we focus on the generic predictions of this class of models. In all cases, the underlying $\mathbb{R}^3$ symmetry gives rise to a cosmology that is flat, homogeneous, and isotropic. The background is always time-symmetric so that the universe will eventually recollapse. For models based on 3D CFTs with relevant operators, we generically have time-dependent scalar fields whose potential energy decreases from a positive value to a negative value before rising to a larger negative value at the time-symmetric point (so we have time dependent dark energy). In some cases, the positive potential *leads to a phase of accelerated expansion before the collapse*. The models could have inflation in the early universe, but it is not clear whether this is generic. However, as we emphasized above, direct knowledge of the physics of the early universe is not needed to extract the physics of cosmological perturbations from the model, and these perturbations naturally contain correlations at all scales. Further, the standard flatness and horizon problems (explaining why the universe is so flat and why the temperature is nearly the same in all directions) are explained by the symmetries of the model and the fact that the state of the cosmological spacetime is naturally defined at the time-symmetric point rather than at the big bang. Thus the setup may solve the standard problems that inflation addresses without the need for inflation. However, it remains to be seen whether the possibilities for the scale factor evolution and the details of the cosmological perturbations are realistic.

The specific predictions of the model will depend on the 4D effective field theory, which is in turn determined by our choice of 3D and 4D QFTs in the microscopic setup. This choice is the only input for the physics of the model. The curvature scale in the universe is related to the number of degrees of freedom in the 3D holographic CFT[18], and the gauge group in the 4D effective theory is related to the global symmetry group of the 3D CFT. Some of this gauge symmetry (and supersymmetry) may be broken by the time-dependent scalars, whose values would set the scale of the symmetry breaking.

Outline

In the following sections, we flesh out these basic observations and explore their consequences. In section 2, we review the basic setup and motivations for this class of models and explain how the cosmological observables are related to vacuum observables in the dual wormhole picture. In section 3, we explore the general properties and predictions for the background cosmology, making explicit the relation between cosmological observables and vacuum physics

[18]As we explain below, avoiding large quantum corrections to the cosmological constant in the effective field theory picture may require that the underlying theories are supersymmetric, but this supersymmetry may not be apparent in the 4D effective description of the cosmology because it is broken by the state, e.g. by time-dependent scalar field expectation values.

of the wormhole. We show that the simplest toy model gives rise to a standard $\Lambda < 0$ plus radiation cosmology with a big bang and a big crunch, but that more generic models (described in detail in section 3.6) will include time-dependent scalar fields that can naturally yield a phase of accelerated expansion before the collapse. In section 4, we discuss fluctuations about the background geometry and how cosmological perturbations (including physics of the CMB) are related to vacuum correlators in the wormhole. We conclude in section 5 with a discussion, including the steps necessary to verify that fully microscopic models of this scenario can work. Even if the models we consider turn out not to be viable to describe realistic cosmology, they have a number of interesting general features that might be employed in future microscopic models of cosmology based on string theory and/or holography. We summarize these features in section 5.3 of the discussion.

Relation to earlier work

This paper represents the present stage of evolution of a class of cosmological models originally proposed in [5], and further developed in [1, 6–8] (see also [230, 231]). In the original models, the 4D CFT was assumed to be holographic, and the cosmological physics was on an ETW brane behind the horizon of a black hole.[19] The present manifestation of the models with specific suggestions for microscopic realizations appeared in [7, 8]. The present paper is the first to explicitly consider in detail the phenomenological consequences and point out that examples making use of 3D CFTs with relevant operators can lead to accelerated expansion.

Related models of cosmology for low dimensions were discussed in [77, 155, 233]. The “holographic cosmology” of [110] has similarities to our model in that they propose to relate

[19] These models built on the AdS/BCFT proposal, see [11, 12, 113], see also [138, 232].

cosmological physics to geometry associated with a 3D RG flow. However in that case, the transformation relating the geometries involves an analytic continuations of parameters as well as coordinates, and it is not clear whether the cosmology picture can be directly associated with an underlying physical theory. The paper [234] discussed a different approach to relating accelerated expansion to $\Lambda < 0$ physics. The recent model of [235] also assumes a time-symmetric universe with an associated special state, but in that case, the point of time-reflection symmetry is the big bang, and $\Lambda > 0$ is considered.

3.2 Basic setup

In this section, we explain our basic holographic construction, focusing on the physically relevant case of flat $\Lambda < 0$ four-dimensional cosmology.

Our starting point is a three-dimensional holographic superconformal[20] field theory on $\mathbb{R}^{2,1}$ dual to gravity on an asymptotically AdS$_4$ spacetime. For a realistic cosmology, we want to choose an example with many degrees of freedom so that the curvature scale very small relative to the Planck scale, i.e. $L^2_{AdS}/G \ll 1$. We would also like the size of the extra dimensions to be small.[21] We can choose the global symmetry group $\mathcal{G}$ of the SCFT to correspond to some desired gauge group for the matter in the four-dimensional gravitational theory.[22]

[20] We could also start with a non-supersymmetric conformal field theory if there exists an example dual to a spacetime with small L^2_{AdS}/G and small extra dimensions. However, as we discuss below, supersymmetry at this stage may be required in order to avoid a cosmological constant problem. We will end up breaking supersymmetry in any case.

[21] The recent papers [39, 40] provide an explicit construction of supersymmetric AdS string vacua with negative cosmological constant whose magnitude is less than 10^{-123} in Planck units and whose extra dimensions are very small. These 3D SCFTs dual to these solutions may be an appropriate starting point for our construction.

[22] As we discuss below, this gauge symmetry may be further broken by time-dependent scalar field expectation values in the cosmology.

The Lorentzian wormhole and its dual

The next step promotes the asymptotically AdS_4 geometry to a Lorentzian traversable wormhole with two asymptotically AdS_4 regions. To do this, we consider a second copy of the 3D SCFT, but with reversed orientation, so that the new copy preserves a complementary set of supersymmetries [8]. This is dual to gravity on a second asymptotically AdS_4 spacetime. To connect these two asymptotically AdS spacetimes, we couple the two three-dimensional theories weakly, via an intermediate four-dimensional CFT with relatively few degrees of freedom [7], as in Figure 3.2. The coupling introduces a scale (the distance between the 3D CFTs), and in the examples we require, the theory confines at lengths much larger than this scale. The vacuum state has a large amount of entanglement between the two 3D CFTs, and this leads to the connected wormhole geometry in the gravity dual.[23] Models with the correct vacuum structure will exhibit a symmetry breaking $\mathcal{G} \times \mathcal{G} \to \mathcal{G}$ corresponding to the fact that the bulk gauge field in one asymptotically AdS region is the same as the one in the other asymptotically AdS region [237]. The IR field theory will have massless Goldstone bosons associated with this symmetry breaking.

The main evidence that this 3D-4D-3D field theory construction can give a holographic description of the Lorentzian wormhole is [3, 7, 8]:

1. In examples where the 4D theory is also holographic, the dual geometry has the interpretation of a geometrical brane and its corresponding anti-brane separated at the asymptotic boundary of a 5D spacetime. Parallel brane-antibrane systems are typically unstable, and the natural endpoint of the instability in this case is for the branes to connect up, forming the wormhole. We expect that the basic field theory physics responsible for this effect

[23] See [3, 7, 8] for a detailed discussion of this claim, and [236] for more recent discussion of the idea.

continues to apply even when the four-dimensional CFT is not holographic.

2. By coupling the two 3D CFTs with a 4D CFT, we break conformal invariance and supersymmetry. The resulting theory will have an RG flow, and it is natural that the degrees of freedom in the two 3D CFTs will become more and more entangled as we go to the IR. It is also generic that the IR theory should be confining rather than having a non-trivial IR fixed point. The wormhole dual is consistent both with the large amount of entanglement between the two 3D theories and with the confinement (since the middle of the wormhole gives an IR end to the spacetime at a finite proper distance from any point in the geometry).

3. As we review below, the effective field theory description of the wormhole requires an unusual quantum field theory phenomenon (anomalously large negative Casimir energies) that had not previously been understood. Motivated by the models, this phenomenon was searched for and found to exist in a holographic quantum field theory setup [8, 157].

4. The basic mechanism of coupling two holographic CFTs to generate a traversable wormhole is similar to that used in [170, 172], though our mechanism crucially involves auxiliary degrees of freedom to achieve the coupling.

Going forward, we will assume that this holographic description is correct; in the discussion we comment on ways that this could be verified explicitly in microscopic examples.

The Euclidean wormhole and its dual

So far, we have the vacuum state of a 3D-4D-3D QFT dual to a geometry with a four-dimensional planar Lorentzian wormhole. The wormhole geometry can be described using a metric

$$ds^2 = d\tau^2 + A^2(\tau)(-d\zeta^2 + dx_i dx_i) \ . \tag{3.3}$$

Here, $A(\tau)$ is symmetric under reversal of τ and grows exponentially for $\tau \to \pm\infty$ corresponding to the two asymptotically AdS boundaries. The ζ and x^i coordinates are the coordinates of the original 3D CFT.

The vacuum state of our Lorentzian field theory is naturally associated with a Euclidean version of this theory, where the 3D CFTs are on $\mathbb{R}^3$ and the 4D theory is on $\mathbb{R}^3$ times an interval I. Specifically, the vacuum wavefunctional is obtained by slicing the path integral defining the Euclidean theory perpendicular to one of the $\mathbb{R}^3$ directions, as reviewed in appendix A.

The Euclidean theory is dual to the analytically continued wormhole geometry, with metric:

$$ds^2 = d\tau^2 + A^2(\tau)(dw^2 + dx_i dx_i) \ . \tag{3.4}$$

More precisely, this is the saddle point geometry for the gravitational path integral of the dual theory.

The cosmology and its dual

The cosmological spacetime that we desire is obtained from this Euclidean wormhole spacetime by analytic continuation of the τ coordinate, which gives the planar FRW geometry

$$ds^2 = -dt^2 + a^2(t)(dw^2 + dx_i dx_i) \ . \tag{3.5}$$

In this case, the function $a(t)$ is time-symmetric and will generally correspond to a big-bang / big-crunch cosmology, though other time-symmetric scale factors might be possible.[24]

The holographic construction gives rise to a special state describing the quantum physics of this cosmology. This is obtained by slicing the path integral for the Euclidean theory in a different way, at the midpoint of the interval I, as shown in Figure 3.3. This new slicing does not intersect the 3D CFTs at all, so the interpretation is that we have an excited state of the 4D CFT on $\mathbb{R}^3$ produced by a path integral that has the "insertion" of a 3D holographic CFT in the Euclidean past.

Unlike usual examples of holography, the underlying degrees of freedom are not associated with any boundary of the cosmological spacetime. We will understand this better presently.

3.2.1 Higher dimensional description with a 4D holographic CFT

To develop intuition for this class of models, it is useful to understand a special case, where the 4D auxiliary theory is also holographic. This was the case considered in [1, 5] where such models were originally proposed.

Here, each geometry described above is now the geometry of an end-of-the-world (ETW) brane that lives at the boundary of a five-dimensional spacetime (bottom row of Figure 3.6).

For the Lorentzian and Euclidean wormhole geometries, the five-dimensional geometry is asymptotically AdS with boundary geometry $\mathbb{R}^{2,1} \times I$ or $\mathbb{R}^3 \times I$, and the ETW brane reaches the asymptotically AdS region at the boundaries of I. In the cosmology picture, the higher-dimensional geometry is asymptotically AdS with boundary geometry $\mathbb{R}^{3,1}$, and the ETW brane does not intersect the boundary. The dual state is a high-energy excited state of the 4D CFT, so the

[24] See [1] for a possible construction of bouncing cosmology.

geometry can be interpreted as a particular planar black hole microstate. The ETW brane housing the FRW geometry lives behind the horizon of this black hole. The cosmological singularities of the FRW spacetime are part of the past and future singularities of the black hole.

This last picture provides intuition for how the 4D cosmological spacetime can be described by some state of the 4D CFT which is not associated with any boundary in the cosmology. From the 5D point of view, the cosmology and the asymptotically AdS boundary are separated in the 5D radial direction. In examples where the 4D theory is not holographic, there is no 5D geometrical space, so the cosmology is like an island (using the terminology of [79,80,225,226]). Other examples where a holographic theory in the Euclidean past is used to encode a geometrical spacetime in a quantum theory that is not necessarily holographic were discussed recently in [227] and [228]. This is also similar to the way that black hole interiors can be encoded in auxiliary radiation systems [79,80,225,226].

3.2.2 Auxiliary systems in the effective field theory description

We now return to the generic case to better understand the effective field theory description in the cosmology, wormhole, and Euclidean pictures. We will see that the 4D CFT plays an important role as a non-gravitational auxiliary system in the effective descriptions.

Single 3D theory: The 3D holographic CFT that we start with is dual to some gravitational theory whose 4D effective description has gravity with a negative cosmological constant and matter with gauge symmetry given by the global symmetry group of the 3D CFT.

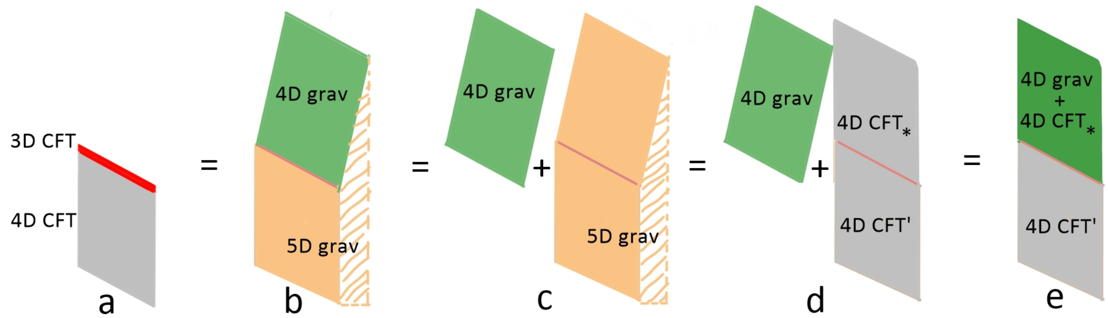

Figure 3.5: Effective field theory description of holographic 3D-4D coupled theories with $c_{3D} \gg c_{4D}$. a) Microscopic picture b) Higher-dimensional gravity picture: 4D gravitational physics of the 3D theory appears as the physics of an ETW brane near the AdS boundary. c) Isolating the 5D bulk gravitational physics. d) 5D gravitational physics is equivalent to physics of the dual 4D CFT with a cutoff (indicated by *) on half the space. e) Final effective description: a 4D CFT coupled to a 4D gravity theory + cutoff CFT. The state of the lower 4D CFT in the final picture is different than the state in the micoscopic picture.

Single 3D theory + 4D theory: Next, we would like to understand the effect of coupling a single copy of the 3D CFT to a 4D CFT on a half-space.

This can be understood most easily by thinking about the case where the 4D CFT is holographic (see Figure 3.5). Here, we have a higher-dimensional dual description where the 4D gravity theory dual to the 3D CFT now gives the effective description of physics on an ETW brane in a 5D asymptotically AdS spacetime whose boundary geometry is a half space.[25] In the limit of interest where the 3D theory has many more local degrees of freedom than the 4D CFT, the ETW brane makes an angle close to $\pi/2$ with the bulk radial direction and lies on a surface that cuts off the would-be second half of the asymptotic region.

From the higher-dimensional perspective, the extra physics that we have added via the 4D CFT is a gravitational theory on asymptotically AdS spacetime with a cutoff surface that removes one half of the asymptotic region. In field theory language, this should correspond to the 4D CFT

[25] Such models were considered originally in [111–113]. Microscopic examples starting with $\mathcal{N} = 4$ SYM theory were discussed in [238], and explicit gravity dual solutions were found in [239–242], based on the general $OSp(2,2|4)$-symmetric solutions of type IIB supergravity found in [239, 240]. The limit of $c_{3D} \gg c_{4D}$ was considered in [117, 243, 244].

on Minkowski space with a UV cutoff on half of the spacetime.[26] In this half of the spacetime the cutoff 4D CFT is coupled locally to the 4D gravitational theory dual to the 3D CFT (Figure 3.5e).[27] While we have motivated this final picture by higher-dimensional holography, we expect it to hold also when the 4D CFT is not holographic.

Two 3D theories + 4D theory: In the full construction for the Lorentzian wormhole, we have two boundary 3D CFTs that are coupled together by a 4D CFT. In this case, we have two copies of the four-dimensional gravitational theory just described, each with an asymptotically AdS region, but these join up in the IR to give the wormhole geometry. The fields at the two asymptotically AdS boundaries are coupled via the auxiliary non-gravitational 4D CFT on an interval. This is depicted in the middle-left picture of Figure 3.6.[28]

This auxiliary 4D theory coupling the two asymptotically AdS boundaries is an essential part of the construction. Without it, the vacuum state of the quantum fields on the wormhole would be significantly different and would not exhibit the type of vacuum energy to support the wormhole in the first place. We will discuss this further in section 3.

Euclidean picture: The effective field theory description of the Euclidean picture is essentially the same as that in the Lorentzian wormhole picture, but with the translation-invariant time direction replaced by a spatial direction (Figure 3.6, middle).

[26]Here, "cutoff" really indicates some UV modification that allows the theory to be coupled in to the gravitational theory in way that preserves supersymmetry.

[27]According to [245], this coupling can also be understood as a modification to the gravitational effective action, in which the graviton develops a small mass, related to the ratio c_{4D}/c_{3D} of degrees of freedom, and certain higher curvature terms are induced.

[28]This discussion has been somewhat heuristic. It would be nice to understand better the extent to which the effects of the higher-dimensional bulk geometry can be captured by a local effective field theory. The discussion below assumes that any effects that are non-local from the four-dimensional point of view can be neglected.

Cosmology picture: The Euclidean effective field theory (Figure 3.6, middle) has a reflection symmetry in the direction between the two asymptotically AdS boundaries of the wormhole. The surface fixed by this reflection (labeled B in the center picture of Figure 3.6) has two disconnected parts, one in the gravitational theory at the midpoint of the wormhole, and one in the 4D CFT. This surface corresponds to the $t = 0$ surface in the cosmology picture, so that picture also includes a gravitational theory (housing the cosmology) and an auxiliary 4D CFT. These do not interact with each other directly, but are entangled. The connection between these two parts in the lower half of the Euclidean picture leads to entanglement between the two parts in the cosmology picture, similar to how a thermofield double path integral connects two quantum systems in the Euclidean past.

When we have a 5D gravity description, we can think of the state of the 4D CFT as describing the physics outside the black hole horizon and the 4D gravitational theory as describing the physics inside the black hole including the physics of the ETW brane.

The role of the 4D CFT in the effective description (Figure 3.6, middle-right) is different from its role in the microscopic description (Figure 3.6, top-right). In the micsrocopic picture of the cosmology, we only have a complicated pure state of the 4D CFT. The physics of the ETW brane is encoded in the IR physics of this state. In the effective field theory picture, we have a simpler mixed state of the 4D CFT that encodes the physics outside the horizon, and this is purified by the state of the 4D gravitational theory that describes the cosmological physics. As we describe in the discussion, this implies the presence of "islands" and explains the appearence of cosmological islands in the work of [175].

As summarized in Figure 3.6, the different analytic continuations, together with the holographic duality and the possibility of a higher-dimensional holographic description give up to

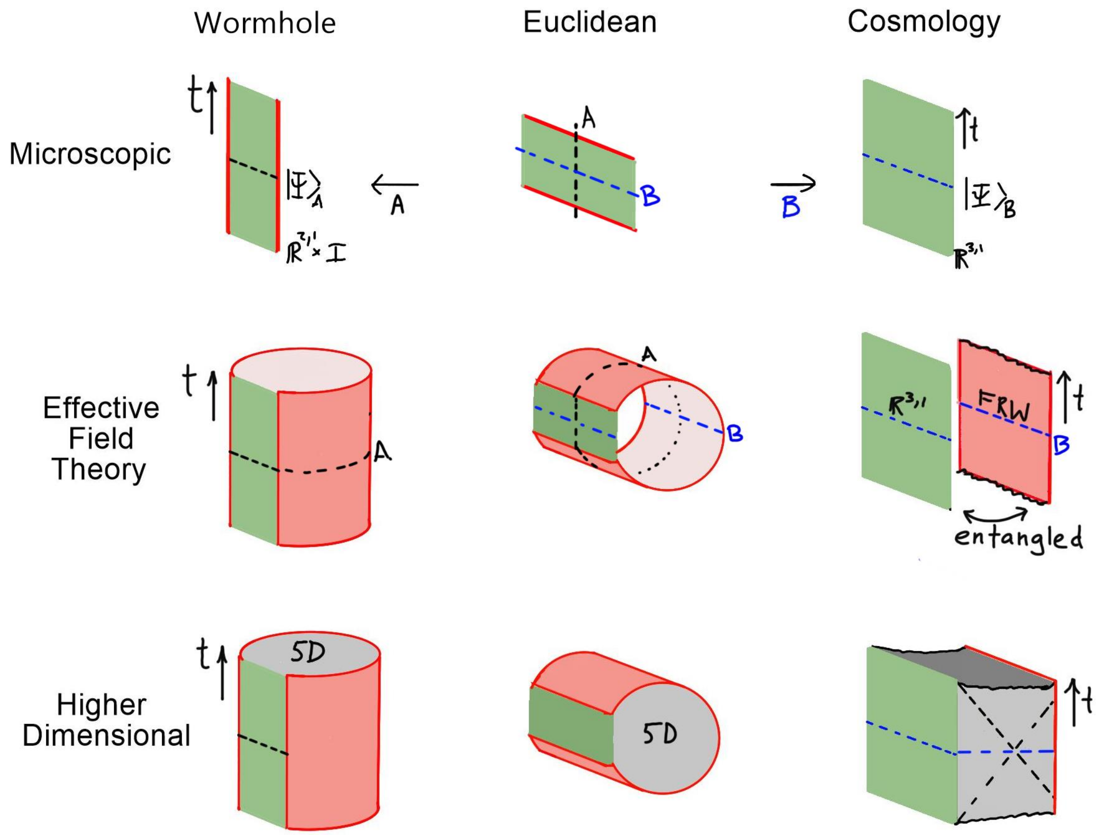

Figure 3.6: Top row: the Euclidean path integral for the 3D-4D-3D theory (middle-top) can be sliced in two different ways to the vacuum state of the Lorentzian 3D-4D-3D theory or a complex excited state of the 4D CFT. The middle row shows the holographic dual descriptions of these pictures in the general case where the 4D theory is not holographic. The Euclidean description (center) can be understood as a gravitational path integral that can be sliced to define the static Lorentzian wormhole or the cosmology, entangled with an auxiliary 4D CFT. When the 4D CFT is holographic, we have a higher-dimensional gravity description (bottom row).

nine different pictures of the physics.

3.2.3 Cosmology from vacuum physics

In our setup, we have two Lorentzian spacetimes, the cosmology and the Lorentzian wormhole, whose holographic descriptions arise from slicing the same Euclidean path integral in two different ways. This "path integral slicing duality" implies an exact equivalence between certain observables for the two Lorentzian states. The Euclidean path integral with operators inserted on the intersection of the two slices will have an interpretation as the expectation value of some observables in one Lorentzian picture and some closely related observables in the other Lorentzian picture; these are equal since they are computed in exactly the same way.

In our application, the Euclidean path integral in the 3D-4D-3D QFT corresponds to a Euclidean gravitational path integral that includes contributions from a dominant saddle point geometry (the Euclidean wormhole) and fluctuations around this. The geometry and fluctuations here determine the background geometry and quantum states in the two Lorentzian pictures. To the extent that we can describe the Lorentzian physics in terms of quantum field theory on a background saddle-point geometry, we can say that the field theory observables in the cosmology picture will be directly related to field theory observables in the wormhole picture, since again they arise from the same Euclidean path integral.[29]

The simplest case is to consider some observables that live at the intersection of the two slices. For example, we can consider in the Euclidean effective field theory picture some correlation function of local operators restricted to an $\mathbb{R}^2$ in the $\mathbb{R}^3$ that forms the midpoint of the wormhole. This Euclidean correlation function is equal to some correlation function in the cosmology at the time-reflection symmetric surface, and also equal to a vacuum correlation function of operators at the midpoint of the wormhole in the Lorentzian wormhole picture. In this way, any cosmological observable that lives in an $\mathbb{R}^2$ at the time-symmetic point is equal to a vacuum observable in the wormhole picture, as shown in Figure 3.4.

More generally, time-dependent observables in each Lorentzian theory are related by analytic continuation to observables in the Euclidean theory, so time-dependent observables in the

[29]Going beyond the field theory approximation, we run into the question of how to precisely define bulk gravitational observables; it may be that for the precisely defined gravitational observables associated to a naive local observables in the QFT picture, we have slight differences between the observables in the wormhole and the cosmology picture.

two Lorentzian theories will be related by a double analytic continuation. We have already seen that this applies to the scale factor in the background geometry. But it should also apply to other observables, such as the equal time correlation functions of the stress-energy tensor that encode the physics of the CMB. Thus, by understanding the vacuum observables in the Lorentzian wormhole picture, we should be able to answer almost any question about the physics of the cosmology.

In the remainder of this paper, we focus on the effective field theory description, and the relation between the cosmological observables in the FRW universe and vacuum observables in the wormhole geometry dual to the vacuum state of the 3D-4D-3D theory.

3.3 Implications for background cosmology

In this section, we focus on the background cosmology, describing how the scale factor evolution and stress-energy tensor evolution are related in the cosmology and wormhole pictures.

Assuming the validity of four-dimensional effective field theory, we expect that it should be a good approximation when discussing the background geometry to use the semiclassical Einstein equation,

$$R_{\mu\nu} - \frac{1}{2} g_{\mu\nu} R - \frac{3}{L^2} g_{\mu\nu} = 8\pi G \langle T_{\mu\nu} \rangle \ , \tag{3.6}$$

where L is the AdS length associated with the underlying 3D CFTs. It will be useful to begin by explicitly describing the background geometries and evolution equations in the two pictures.

Background geometry and stress-energy tensor: cosmology

In the cosmology picture, we have a background geometry

$$ds^2 = -dt^2 + a^2(t)(dw^2 + dx_i dx_i) \ , \tag{3.7}$$

where $a(t)$ is time-reversal symmetric.

The homogeneous part of the stress-energy tensor takes the form[30]

$$T^{tt} = \rho(t), \qquad T^{ij} = \frac{p(t)}{a^2(t)}\delta^{ij}, \qquad T^{ww} = \frac{p(t)}{a^2(t)} \ . \tag{3.8}$$

where ρ and p are the conventionally defined energy density and pressure. These will also be time-reversal symmetric. In terms of the Hubble parameter $H = \dot{a}/a$, the covariant conservation equation $\nabla_\mu T^{\mu\nu} = 0$ gives

$$\dot{\rho} = -3H(\rho + p) \tag{3.9}$$

which can be used to express p in terms of ρ and a. Finally, Einstein's equations relate ρ and a by the Friedmann equation

$$H^2 + \frac{1}{L^2} = \frac{8\pi G}{3}\rho \ . \tag{3.10}$$

Taking the time derivative of (3.10) and using (3.9), we have also that

$$\dot{H} = -4\pi G(p + \rho) \ . \tag{3.11}$$

[30]Here and below, quantum expectation values are implied when writing components of the stress-energy tensor.

In this cosmology picture, we expect that the stress-energy tensor has various contributions, including vacuum energy of fields as well as matter and radiation.

Background geometry and stress-energy tensor: wormhole

Let us now see how the scale factor and stress-energy tensor in the cosmology are related directly to those in the Lorentzian wormhole spacetime.

In the wormhole picture, we can describe the metric as

$$ds^2 = d\tau^2 + a_E^2(\tau)(-d\zeta^2 + dx_i dx_i) \ . \tag{3.12}$$

Here, $a_E(\tau)$ is obtained from $a(t)$ by analytic continuation $t^2 \leftrightarrow -\tau^2$. It is symmetric under reversal of τ and grows exponentially for $\tau \to \pm\infty$ corresponding to the two asymptotically AdS boundaries.

In this picture, the stress-energy tensor is

$$T^{\tau\tau} = -\rho_E(\tau), \quad T^{ij} = \frac{p_E(\tau)}{a^2(t)}\delta^{ij}, \quad T^{\zeta\zeta} = -\frac{p_E(\tau)}{a_E^2} \ , \tag{3.13}$$

where ρ_E and p_E are related to ρ and p by analytic continuation $t^2 \leftrightarrow -\tau^2$.

The energy conservation equation gives

$$\frac{d\rho_E}{d\tau} = -\frac{3}{a_E}\frac{da_E}{d\tau}(\rho_E + p_E) \tag{3.14}$$

and the analogue of the Friedmann equation gives

$$-\left(\frac{1}{a_E}\frac{da_E}{d\tau}\right)^2 + \frac{1}{L^2} = \frac{8\pi G}{3}\rho_E \ . \tag{3.15}$$

3.3.1 Energy from vacuum energy

We see that the time evolution $\rho(t)$ of the cosmological energy density, is directly related to a component of the vacuum stress tensor in the wormhole picture as

$$\rho(t) = -T_{\tau\tau}(\tau = it) \tag{3.16}$$

where the right side is real because of the $\tau \to -\tau$ symmetry.

The pressure in the cosmology picture is

$$p(t) = T^{\zeta}{}_{\zeta}(\tau = it) \ , \tag{3.17}$$

where the right side is minus the proper energy density in the wormhole picture. Here, $p(t)$ is also real by the τ-reflection symmetry. While $T_{\tau\tau}$ and $T^{\zeta}{}_{\zeta}$ represent components of the vacuum stress energy tensor in the wormhole picture (i.e. a Casimir stress-energy tensor in the system with two boundaries), the functions $\rho(t)$ and $p(t)$ represent the full stress-energy tensor in the cosmology, including both vacuum and non-vacuum contributions. Thus, in a realistic example, the stress-energy tensor from matter, dark matter, and vacuum in the cosmology picture would all arise from vacuum energy in the wormhole picture. They could be computed from knowledge of the effective field theory in the wormhole and are thus determined without specific knowledge of the big bang or the initial state in the cosmology picture.

3.3.2 Analytic structure of the scale factor

The $\tau \to -\tau$ reflection symmetry and AdS asymptotics in the wormhole picture imply that the wormhole scale factor $a_E(\tau)$ is an even function of τ (defining $\tau = 0$ to be the middle of the wormhole) that grows exponentially for $\tau \to \pm\infty$.[31]

The Lorentzian scale factor $a(t)$ is obtained from $a_E(\tau)$ by analytic continuation $\tau \to it$, so it will also be an even function of t. That $a_E(\tau)$ has the asymptotics of a $\cosh$ function suggests an oscillatory piece in the real time scale factor $a(t)$ (since $\cosh$ continues to a cosine), but this does not necessarily imply a periodic cosmology. For example, in the simple example $a_E^2(\tau) = \cosh(2\tau/L)$ that arises from a $\Lambda < 0$ + radiation cosmology, we find $a^2(t) = \cos(2t/L)$ which goes to zero for $t = \pm\pi/(2L)$. Thus, we get a big-bang/big-crunch.

For other choices of $\hat{a}_E(z)$ with AdS asymptotics, we can have big-bang/big-crunch scale factors with different functional form or periodic scale factors. However, the physically allowed scale factors will be determined by the dynamics of the theory.

3.3.3 Vacuum energy in the wormhole picture

To understand the possibilities for the scale factor and stress-energy tensor evolution in the cosmology picture, we need to understand the possibilities for the vacuum energy in the wormhole picture.

Here, it is important that the metric is dynamical, so one needs to understand the vacuum

[31] Alternatively, the scale factor $\hat{a}_E(z)$ in conformal coordinates (see appendix B) has simple poles at $\pm z_0$, with no other poles in $[-z_0, z_0]$.

configuration of a dynamical metric coupled to quantum fields (including the metric itself).

Assuming the validity of four-dimensional effective field theory, we expect that it should be a good approximation to self-consistently solve the semiclassical Einstein equation (3.6) where $\langle T_{\mu\nu} \rangle$ represents the vacuum energy of the fields (presumably, including metric fluctuations) in our effective theory on the background with metric g.[32] That is, we find the vacuum energy of the effective field theory on a fixed geometry of the form (3.12), giving some functional of the scale factor $\hat{a}_E(z)$, and then include this functional on the right-hand side of the Einstein equation. In this calculation, it is important to take into account the 4D CFT coupling fields in the two asymptotically AdS regions.

The vacuum energy calculation will generally be divergent in the continuum QFT limit, but it is natural in the gravitational context to assume a cutoff at the Planck scale, $M_{UV} = 1/\sqrt{G}$. In this case, for a renormalizable quantum field theory, the divergent pieces of the stress-energy tensor should take the form of local terms that may involve the curvature.

The cosmological constant problem

The leading potential divergence takes the form $\langle T_{\mu\nu} \rangle = \hat{\Lambda} g_{\mu\nu}$, giving a quantum correction to the cosmological constant. Here, $\hat{\Lambda}$ could have contributions of order $1/G^2$, M^2/G, or $M^4 \log(M^2 G)$ for some mass scale M associated with the effective theory. Any of these would be problematic for realistic cosmology: this is the usual cosmological constant problem.[33] However, there is reason to believe that such contributions will cancel in our setup.

An acceptably small cosmological constant / curvature scale in the 4D geometry dual to

[32] It is probably useful to keep in mind the alternative possibility that the four-dimensional effective field theory is not adequate to understand the background geometry, e.g. because the effects of the higher-dimensional bulk cannot be adequately reproduced by local terms.

[33] The last term could be acceptable in the case that the mass scale is similar to that expected for neutrino masses.

a single 3D CFT can be arranged by making an appropriate choice of CFT. Supersymmetric AdS compactifications of string theory with acceptably small curvature scale and small extra dimensions have been argued to exist recently in [39, 40]. These should correspond to some dual superconformal theory where the smallness of the curvature / cosmological constant relative to the Planck scale is related to the large number of degrees of freedom. Evidently, any $\langle T_{\mu\nu} \rangle \propto g_{\mu\nu}$ contributions to the stress-energy tensor in the effective field theory description of the 4D bulk must cancel. This can likely be understood as a result of supersymmetry in the bulk effective theory.

Coupling in a 4D theory with many fewer local degrees of freedom in a way that preserves supersymmetry and conformal invariance should not affect the dual geometry significantly; this is known to be true in various examples where the dual geometries are known explicitly [243].

In the full setup for the cosmology picture, we break supersymmetry by introducing another boundary theory; this preserves supersymmetry on its own, but the two boundaries together break supersymmetry. There is a well known example where such non-local breaking of supersymmetry in the CFT does not lead to large contributions to the bulk stress-energy tensor. For a supersymmetric holographic conformal field theory compactified on a circle with antiperiodic boundary conditions for fermions, supersymmetry is broken by the boundary conditions on the circle, but the vacuum state is believed to be dual to a geometry with the same scale of curvature as in the dual of the theory with supersymmetric (periodic) boundary conditions for fermions [180]. From an effective field theory point of view, the point may be that the same cancellations that avoided large contributions to the stress-energy tensor in the supersymmetric case persist here.[34]

[34] A useful example may be the calculation of Casimir energy density in a supersymmetric theory where the supersymmetry is broken by boundary conditions. In general Casimir energy calculations, after introducing a regulator, the energy density for infinite volume is subtracted from the energy density with boundaries, and then the regulator is removed to yield a finite result. For a supersymmetric theory, energy density in infinite volume would vanish, so

An alternative argument for the absence of corrections to the cosmological constant is that in the cosmology picture, the dual theory is just the 4D CFT with unbroken supersymmetry. However, the effective theory in the cosmology also then has an underlying supersymmetry but may look non-supersymmetric because of our choice of state (e.g. due to the time-dependent scalar fields). In this case, the leading divergent contributions to the stress-energy tensor should be absent since they are independent of the state and vanish for the vacuum state of a supersymmetric theory.

Renormalization of the Newton constant

The next potential divergence comes at order $1/G$ and is proportional to the Einstein tensor, $\langle T_{\mu\nu}\rangle \sim 1/G(R_{\mu\nu}-g_{\mu\nu}R)$. Since this is multiplied by $8\pi G$ in the Einstein equation, it comes in at the same order as the Einstein tensor on the left side. Thus, we can think of it as renormalizing the Newton constant by an order one amount. Such contributions can occur even for supersymmetric theories.

R^2 terms

The final possibility for divergent terms are R^2 corrections with coefficients of order $\log(M^2G)$. Since they come into the Einstein equations multiplied by G, they will only be comparable to the Einstein term in regions of the geometry where the curvature is close to the Planck scale, e.g. near the initial and final time in the cosmology picture. We expect that they can be ignored in the wormhole picture.

the full energy density should also be finite, even though the boundary conditions break supersymmetry.

Finite terms

The remaining part of the stress-energy tensor, finite in the $G \to 0$ limit, can be understood as a Casimir energy density associated with the fields. This part is essential for ending up with a wormhole geometry that can give rise to a cosmological spacetime, since the other significant terms are the Einstein term and cosmological constant term that together give rise to a single-sided pure AdS spacetime.

If the scale of curvature is of order the AdS scale L throughout the geometry, the Einstein term and the cosmological constant term in the Einstein equations will both be of order $1/L^2$. In this case, the Casimir energy density must be of order $1/(GL^2)$ to have a comparable effect. Naively, the scale of the energy density for a field theory with c_0 fields in a geometry with length scale L would be c_0/L^4. The number of fields in our effective theory is expected to be relatively small, so we require that the Casimir energy density is larger than its "natural" value by a factor of $L^2/(Gc_0) \sim c_{3D}/c_0$. Thus, we have the unusual situation of needing a vacuum energy that is anomalously *large*.

A more specific quantitative connection between the Casimir energy density and the scale of curvature in the geometry is provided by evaluating the $++$ component of the Einstein equation at the middle of the wormhole where $\hat{a}'_E = 0$. For this component, the cosmological constant term does not contribute, so the connection between the curvature scale and the energy density is more direct. We have that

$$T_{++} = \frac{1}{8\pi G} R_{++} = -\frac{1}{4\pi G} \frac{\hat{a}''_E}{\hat{a}_E} \sim -\frac{\ell^2}{G} \frac{1}{\ell^4} \ . \tag{3.18}$$

Choosing coordinates where $a(0) = 1$, the left side gives the proper null energy density and ℓ gives the length scale associated with the curvature at the midpoint of the wormhole. Thus, to get $\ell \gg \sqrt{G}$, we need negative null Casimir energy that exceeds the geometrical scale $1/\ell^4$ by a large factor $\frac{\ell^2}{G}$.[35]

Since such a large factor is absent for the Casimir energy density of a field on a space with a periodic spatial direction[36], the interface in the effective field theory picture between the fields on the wormhole and the non-gravitational 4D CFT fields must play an essential role. To understand whether certain interfaces can give rise to such enhancement, [8,157] studied holographic models of interface quantum field theories. Remarkably, it was found that the needed enhancement of Casimir energy appears (and, within the model studied, can be arbitrarily large) for special choices of the interface physics.[37]

The somewhat surprising appearance of this energy enhancement provides some evidence for the viability of the class of models we are studying.[38] However, it will be important to understand better how general this enhancement is (e.g. whether it requires strongly coupled field theory) and whether we can exhibit it in microscopic quantum field theories. See appendix D for additional comments related to the understanding of enhanced Casimir energies in quantum field theory.

---

[35]In appendix B, we show that the integrated null-energy along a null path from one asymptotically AdS boundary to the other must also be negative. Thus, the averaged null energy condition is also violated, but this is typical for Casimir energies.

[36]There, the Casimir null energy density is equal to the negative of the thermal null energy for the same theory at temperature $1/\ell$, as we review in Appendix D.

[37]In the holographic model, the interface between CFTs is associated with a bulk interface brane that separates regions of the geometry associated with the two CFTs. The enhancement of Casimir energy occurs when the tension of this interface brane is taken to some lower critical value.

[38]Specifically, the general arguments for the existence of solutions together with the assumption that the solutions could be understood within the context of four-dimensional effective field theory required/predicted a seemingly unlikely quantum field theory effect, and that effect was later found to be present in holographic models.

Classical scalar field contributions

Another possible contribution consistent with the symmetries of the wormhole geometry is to have one or more scalar fields with a non-trivial classical profile $\phi(\tau)$. We will see below that having non-trivial scalars is generic when the 3D CFT that we start with has relevant or marginally relevant operators, as the variation of these scalars reflect possible RG flows that we might have with this 3D CFT in the UV [246].

With varying scalars, potential terms and derivative terms will both contribute to the stress-energy tensor and back-react on the geometry. In the cosmology picture, we will in this case have a time-dependent scalar field; we will see below that this can give rise to a phase of accelerated expansion before the recollapse. We will discuss this in more detail in section 3.6 below.

The presence of a non-trivial scalar field does not remove the need for a large Casimir energy. For example, in the wormhole picture with conformal distance coordinate z, we have that the contribution of the scalar field to the null energy is

$$T_{++} = \partial_z \phi \partial_z \phi > 0 \ . \tag{3.19}$$

This gives a positive contribution to the left side of equation (3.18), so the large negative Casimir energy is still required to agree with the right side of the equation.

3.3.4 Example: CFT matter

We now describe a few simple examples of our scenario at the level of effective field theory. To begin, we review the case where the matter in the gravitational part of our effective field theory is taken to be a CFT [8]. This is not what is expected from the microscopic models, but it has the advantage of being analytically tractable. In particular, the form of the stress-energy tensor is determined up to an overall constant by conformal invariance.

To find the form of stress-energy tensor, we can make use of conformal coordinates (see Appendix B.2) and perform a conformal transformation to flat space $\mathbb{R}^{2,1} \times [-z_0, z_0]$. Conformal invariance and 2+1 Poincaré symmetry imply that the vacuum stress tensor in this conformal frame takes the form

$$T_{zz} = -\frac{3}{z_0^4}F(z_0) \qquad T_{\mu\nu} = \eta_{\mu\nu}\frac{1}{z_0^4}F(z_0) \tag{3.20}$$

where F is a dimensionless constant that could depend on the ratio between z_0 and any other parameter with dimensions of length.[39]

We recall that the field theory in the wormhole geometry is coupled at its boundaries via a 4D CFT on a strip. The constant F can depend on our CFT, the non-gravitational CFT that couples the fields at the boundaries of the wormhole, and the physics of the interface between the two CFTs.

In the original conformal frame, the stress tensor using conformal coordinates becomes

$$T_{zz} = -\frac{1}{\hat{a}_E^2}\frac{3}{z_0^4}F + T_{zz}^{CA} \qquad T_{\mu\nu} = \eta_{\mu\nu}\frac{1}{\hat{a}_E^2}\frac{1}{z_0^4}F + T_{\mu\nu}^{CA} \tag{3.21}$$

where T_{zz}^{CA} and $T_{\mu\nu}^{CA}$ are terms due to the 4D conformal anomaly. In general, these are a specific combination of curvature squared terms whose coefficients depend on our choice of CFT. As in our discussion above, we expect that these can be ignored when the curvature of the geometry is

[39]This could be the width of the strip of 4D CFT that couples the two asymptotically AdS regions, or some parameter associated with the interface.

much larger than Planck scale, i.e. away from the big bang/big crunch. We will drop them for now in our discussion of the wormhole picture.[40]

Ignoring the conformal anomaly, the zz component of Einstein's equation gives

$$\left(\frac{\hat{a}_E'}{\hat{a}_E}\right)^2 - \frac{\hat{a}_E^2}{L^2} = -\frac{8\pi G}{z_0^4} F \frac{1}{\hat{a}_E^2} \ , \tag{3.22}$$

where L is the AdS radius. So we have

$$\int_{a_0}^{\hat{a}_E(z)} \frac{da}{\sqrt{\frac{a^4}{L^2} - \frac{8\pi GF}{z_0^4}}} = z \tag{3.23}$$

where a_0 is the minimum value of $\hat{a}_E$ where $\hat{a}_E' = 0$,

$$a_0 = \frac{1}{z_0}(8\pi GFL^2)^{\frac{1}{4}} \ . \tag{3.24}$$

For $z = z_0$, we have $\hat{a}_E \to \infty$, so we get

$$\int_{a_0}^{\infty} \frac{da}{\sqrt{\frac{a^4}{L^2} - \frac{8\pi GF}{z_0^4}}} = z_0 \tag{3.25}$$

which gives

$$F = \frac{\mathcal{I}^4 L^2}{8\pi G} \ . \tag{3.26}$$

where

$$\mathcal{I} = \int_1^{\infty} \frac{dx}{\sqrt{x^4 - 1}} = \frac{\Gamma\left(\frac{3}{2}\right)\Gamma\left(\frac{1}{4}\right)}{\Gamma\left(\frac{3}{4}\right)} = \frac{\sqrt{2}}{2} K\left(\frac{\sqrt{2}}{2}\right) \approx 1.311 \ . \tag{3.27}$$

[40] We will see that this assumption implies $F \sim L^2/G$, so that the conformal anomaly term is indeed smaller than the term we keep by a factor of $1/F \ll 1$.

We recall that F represents the energy density in units of the geometrical length scale in the conformal frame, where we have a CFT Minkowski space between two boundaries separated by z_0. As we discussed above, this would normally be expected to be of order the central charge c_0 of the CFT we are considering, but here we need it to take a much larger value $L^2/G \sim c_{3D}$, i.e. comparable to the central charge of the underlying holographic 3D CFT. However, such anomalously large values can arise with appropriate boundary physics, at least in certain holographic CFTs; see Appendix B.4 for more discussion.

Lorentzian solutions with CFT matter

It is straightforward to work out the Lorentzian cosmology that arises from this example. Again ignoring the conformal anomaly term, and using (3.26), the Friedmann equation gives (in proper time coordinates)

$$\left(\frac{\dot{a}}{a}\right)^2 + \frac{1}{L^2} = \frac{\mathcal{I}^4 L^2}{z_0^4}\frac{1}{a^4} \ . \tag{3.28}$$

This is equivalent to standard cosmological evolution with radiation and a negative cosmological constant. The universe expands from a big bang to a maximum scale factor and then contracts again. We can choose coordinates so that the maximum scale factor is $a = 1$ when $\dot{a} = 0$. This gives $z_0 = \mathcal{I}L$. Defining $t = Ls$ so that s is the time in units of the curvature scale L, the evolution equation simplifies to

$$\left(\frac{\dot{a}}{a}\right)^2 + 1 = \frac{1}{a^4} \ , \tag{3.29}$$

with solution $a = \sqrt{\cos(2s)}$. In terms of the comoving time variable t, the metric is thus simply

$$ds^2 = -dt^2 + \cos\left(\frac{2t}{L}\right) d\vec{x}^2 \ . \tag{3.30}$$

so we have a big-bang / big-crunch cosmology with total proper age $L\pi/2$ determined by the AdS scale in the wormhole picture.

As discussed in [8], the conformal anomaly terms can alter the behavior near the big bang and big crunch. For example, the special case where the conformal anomaly contributes only first-derivative terms to the Friedmann equation leads to an equation whose solution cannot be extended back past an initial time with energy density $T_{00} \sim 1/(c_0 G^2)$ where c_0 is a measure of the number of degrees of freedom in the effective field theory.

3.3.5 Non-conformal effective field theory

In microscopic examples, we expect that the effective field theory describing quantum fields in our setup will be some non-conformal field theory.

Here, the stress-energy tensor computed on a fixed background will be some more complicated functional of the scale factor; in conformal coordinates we can represent this as

$$T_{zz} = -\frac{1}{a^2}\frac{3}{z_0^4}F_a(z) \ . \tag{3.31}$$

The dependence of F on a may be complicated and non-local. In the cosmology picture, the resulting stress tensor evolution will also be more complicated and reflect the RG behavior of the field theory. In later work, we hope to investigate further the varieties of cosmological evolution associated with the vacuum stress tensors of more interesting field theories.

3.3.6 Evolution with a scalar field

It is natural to consider the possibility of one or more scalar fields with classical values that depend on time in the cosmology picture or on the τ coordinate of the wormhole. Such scalar field configurations preserve the spacetime symmetries of the setup and lead to models with time-dependent dark energy. In order to explain the current observations of an accelerating universe using our framework, having a time-dependent scalar field at some positive value of its potential is required, or at least is the simplest possibility.

The presence of scalar fields is generic in the gravitational effective field theories that correspond to our microscopic models. According to the AdS/CFT correspondence, we have a light bulk scalar field for each low-dimension scalar operator in the CFT, with the scalar field mass related to the operator dimension (for the case of a 3D CFT) by[41]

$$m^2 L^2 = \Delta(\Delta - 3) \ . \tag{3.32}$$

If the CFT is chosen so that the 4D cosmological constant $1/L^2$ is small, the scalar masses (which set the scale of the derivatives of the potential near the origin) will also be small; the result is that when these scalar fields vary, it is natural for them to be changing non-trivially throughout the spacetime.

If the CFT has both relevant and irrelevant scalar operators, the asymptotic values of the scalar fields will correspond to a saddle of the potential with both positive and negative directions.

[41]This gives a constraint $m^2L^2 > -9/4$, which is the Breitenlohner-Freedman bound for 4D gravity theories with stable AdS vacua. It is not completely clear that such stability is required on our setup; it might be interesting to explore whether models based on more general gravitational theories (perhaps dual to unstable or non-unitary 3D CFTs) could be sensible.

Generically, the potential will also have higher order terms, and these tend to make the potential positive for large values of the fields (assuming the AdS solution dual to our 3D CFT is stable). For example, in the 4D gauged supergravity models associated with 3D SCFTs with extended supersymmetry, the scalar potential is a quartic polynomial [247]. In models with less supersymmetry, the potential can be much more complicated (see e.g. [248] and references therein for examples).

For solutions of the dual gravitational theory that are controlled by our 3D CFT in the UV, the most generic situation is to have scalar fields associated with the relevant or marginally relevant operators of the theory vary from the saddle-point values as we move away from the AdS boundary. These solutions correspond to taking the dual quantum field theory to be an RG flow obtained by perturbing the CFT with a relevant operator.[42] The strict CFT is a special case where all such perturbations are set to zero.

In this section, we will describe the physical effects of such varying scalar fields in some generality, showing that they can lead to a phase of accelerated expansion. A more detailed analysis of these setups will be published elsewhere.

Scalar field evolution in the wormhole picture

It is convenient to start with the radial evolution of the scalar field in the wormhole picture. Here, using proper distance coordinates, the equation of motion for scalar fields ϕ_i with potential $V(\vec{\phi})$[43] is

$$\phi_i'' + 3H_E\phi_i' - \partial_i V(\vec{\phi}) = 0 \tag{3.33}$$

[42] Even if we start with the strict 3D CFT, such perturbations might be induced by the coupling to other 3D CFT via the 4D CFT.

[43] It will be convenient to absorb the cosmological constant into the definition of the scalar potential; we will assume this throughout this section.

(where $H_E \equiv a'_E/a_E$) and the field makes a contribution

$$\rho_E^\phi = -\frac{1}{2}(\partial_\tau \vec{\phi})^2 + V(\vec{\phi}) \tag{3.34}$$

to the right side of the scale factor evolution equation (3.15). In this picture, the evolution of $\vec{\phi}$ with τ is equivalent to the time evolution of a particle in a potential $-V(\vec{\phi})$ with damping coefficient $3H_E$ that becomes constant in the asymptotically AdS regions. We are interested in time-symmetric solutions, so the derivative of $\vec{\phi}$ should vanish at the midpoint of the wormhole. Moving away from the time-symmetric point, a_E increases,[44] so the evolution of $\vec{\phi}$ going away from this point will correspond to ordinary damped motion in the inverted potential.

For a given potential, the possible time-symmetric solutions will be in one-to-one correspondence with the value $\vec{\phi}_0$ of the scalar field at the midpoint of the wormhole. If $\vec{\phi}_0$ corresponds to an extremum of $V(\vec{\phi})$ the scalar will be constant throughout the geometry, and $V(\vec{\phi}_0)$ will be the cosmological constant. Otherwise, $\vec{\phi}$ will move downward (initially along the steepest path) in the inverted potential as we move toward the AdS boundary, as shown in Figure 3.7 (left).

Behavior at the AdS boundary

As we have explained above, having a varying scalar field as we go to the asymptotically AdS regions corresponds to the underlying 3D CFT being deformed in the UV by a relevant or marginally relevant scalar operator.[45] In this case, the scalar will descend to a value $\vec{\phi}_B$ corresponding to an extremum of $-V$ (or rise to an extremum of V) at the boundaries where $V(\vec{\phi})$ is

[44]The second time derivative of the scale factor is negative at the time-reversal symmetric point of the cosmology, so the second τ derivative is positive at the midpoint of the wormhole

[45]We ignore the case where the scalar blows up at the asymptotically AdS boundary, since we are assuming that the UV behavior corresponds to some well-defined CFT.

still negative.[46] Alternatively, going away from the boundary, the scalar rolls down a direction in the potential $V(\vec{\phi})$ with negative second derivative, corresponding to a massless or negative mass-squared scalar that still satisfies the Breitenlohner-Freedman bound [178].

Scalar field evolution in the cosmology picture

In the cosmology picture, the scalars will take the values $\vec{\phi}_0$ at the time-symmetric point and have vanishing time derivatives here.

The equation of motion in the cosmology picture with comoving (proper time) coordinates is

$$\ddot{\phi}_i + 3H\dot{\phi}_i + \partial_i V(\vec{\phi}) = 0 \tag{3.35}$$

and the field makes a contribution

$$\rho^\phi = \frac{1}{2}(\partial_t \vec{\phi})^2 + V(\vec{\phi}) \tag{3.36}$$

to the energy density appearing on the right side of the Friedmann equation (3.10).

As is familiar from discussions of inflationary cosmology, the dynamics of the scalar field is that of a particle in a potential $V(\vec{\phi})$ with time-dependent damping coefficient $3H$, such that we have usual damping in the expanding phase of the universe and anti-damping in the contracting phase (or evolving backwards towards the big bang).

In order to be stationary at the time-symmetric point, the scalars should be rolling up the

[46] In some cases, it might be that the scalar will oscillate before settling to this extremum. However, the relation (3.32) gives a lower bound $m^2L^2 \geq -9/4$. At least in the asymptotic region where $a'/a = 1/L$, the equation (3.33) for the scalar evolution corresponds to overdamped or critically damped motion, so there won't be oscillations in this region.

potential before this. As we described above, a typical potential in a theory supporting a stable AdS vacuum will have interaction terms that make the potential bounded below and positive for large values of the field.

Thus, in the anti-damped motion going back toward the big bang, a typical situation would be for the scalar to descend to some lower value of the potential before rising again to positive values (time-reverse of Figure 3.7, right).[47]

A phase of accelerated expansion

Going backward from the time-symmetric point, we have a phase of decelerated expansion while the scalar potential is negative. But at earlier times when the scalar potential reaches positive values, we can have a phase of accelerated expansion. Whether or not such a phase exists depends on the details of the potential, and in particular whether the scale factor reaches $a = 0$ going backwards in time before the scalar potential reaches large enough values to dominate over the matter and radiation.

If the accelerated expansion in our universe is explained in this way, the scalar must be rolling sufficiently slowly at the $V > 0$ point corresponding to the present time to be consistent with the observations. In later work, we plan to investigate in detail whether there exist potentials giving rise to evolution that satisfies the observational constraints.

[47]The minimum value that the potential passes through might correspond to the endpoint of the RG flow discussed above, but with multiple scalars, the minimum value of the potential reached via the scalar field dynamics does not necessarily correspond to an extremum of the potential.

Inflation at early times?

In our setup, the potential takes small values in the wormhole solution and for the late time cosmology (near the time-symmetric point) by construction (choosing an appropriate 3D CFT). However, in the surrounding "landscape" of string theory, the more generic values for the potential are expected to be closer to Planck scale. It is possible that the initial conditions for the matter/radiation dominated phase were set up by an early period of inflation where the scalar potential took much larger values, but it is not clear that such a phase is generic in our models or that it would happen at an energy scale where effective field theory is valid.

However, as we have emphasized above, it appears to be unnecessary in our model to understand the details of the early universe physics in order to compute cosmological perturbations. Cosmological observables in our model are computed most naturally in the wormhole picture where the effective field theory should be valid everywhere and the quantum state is time-independent. Here, the scalar field only explores a small region of the potential near the saddle that corresponds to the dual 3D CFT.

So while there may be inflation in the early universe of the cosmology picture, and the physics of inflation may provide an explanation for the origin of perturbations, etc... in that picture, understanding the details of this early universe physics is not necessary to extract the predictions of the model. The wormhole picture provides in some sense a dual picture of the physics, with a different explanation for the origin of correlations relevant to cosmological observables. We will discuss this further in section 4 below.

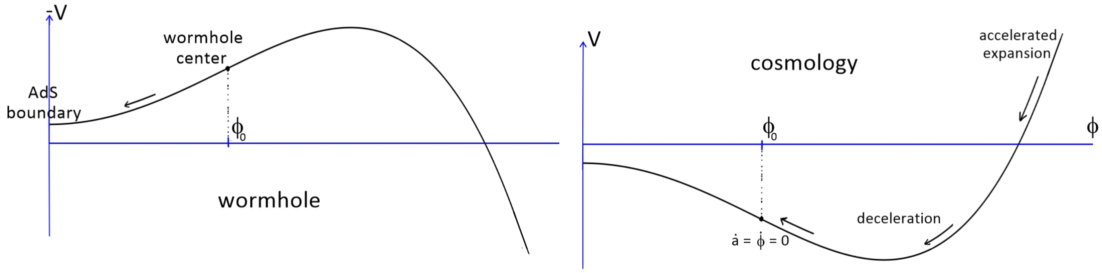

Figure 3.7: Left: evolution of the scalar from the wormhole center to the asymptotically AdS region corresponds to damped motion in the inverted potential $-V$ with damping "constant" $3a'_E/a_E$. The evolution of the scalar is dual to the RG flow induced by perturbing the dual CFT by a relevant operator. Right: Evolution of the scalar field in the cosmology from early times to the time-reversal symmetric point corresponds to damped motion in the potential V with damping constant $3\dot{a}/a$. The initial positive values of the potential typically give rise to a phase of accelerated expansion before deceleration and collapse.

Evolution from the initial time

In our scenario, it is most natural to consider the evolution of the scalar field from the asymptotically AdS boundary to the midpoint of the wormhole and then backward in time to the early universe as we have described. But it is also helpful to envision the evolution in the other direction, since this corresponds to more intuitive ordinary damped motion in the potential.

The evolution is summarized in Figure 3.7. Starting from a positive value of the potential and some large density of matter and radiation (that may have come from an inflationary phase) the scalar will roll down[48] to some negative value of the potential V before rising again. The potential might oscillate up and down multiple times due to the motion of the scalar in the vicinity of a minimum. At the time-symmetric point, the scalar comes to rest at a point $\vec{\phi}_0$ between two extrema, approaching this point along an upward trajectory of steepest increase.

The scalar field also takes the value $\vec{\phi}_0$ at the midpoint of the wormhole in the dual picture, but going away from this point evolves via damped motion in the inverted potential $-V$,

[48]A more general possibilitiy is that the scalar will move up the potential before rolling down, or have various oscillations.

eventually descending to the extremum that corresponds to our dual 3D CFT.

The initial conditions required to get a time-symmetric scale factor (i.e. $\dot{\vec{\phi}} = 0$ when $\dot{a} = 0$) and end up in the wormhole picture at a non-minimal extremum of $-V$ would appear to be finely tuned in the cosmology picture, but the microscopic setup guarantees these will arise.

Symmetry breaking

Having a non-zero scalar field expectation value away from the asymptotically AdS regions may be associated with a breaking of gauge symmetry and/or supersymmetry, such that the low-energy effective field theory relevant to the description of physics near the middle of the wormhole or in the cosmology picture is different than the effective field theory describing physics in the asymptotically AdS regions (which would be supersymmetric in microscopic models built from a 3D SCFT). If there is supersymmetry in the effective theory for the asymptotically AdS regions, a challenge is to explain why the scale of SUSY breaking is so much larger than the scale of the vacuum energy in the low energy effective description of the cosmology. This might be explained fairly naturally if it is the value of the scalar field that sets the supersymmetry breaking scale, since the typical potentials in 4D gravity theories dual to CFTs remain of order $8\pi GV \sim 1/L^2$ when the scalar fields themselves have Planck scale variations.[49] As we have described above, if such scalar field expectation values and other features of the state are the only thing that breaks supersymmetry in the cosmology picture, the supersymmetric cancellations that prevent a large quantum correction to the cosmological constant may persist.

It would be useful to understand the possibilities for the low energy physics of theories

[49]For example, a typical Lagrangian density would be $(\partial\phi)^2 - c_0/(GL^2) + c_2/L^2\phi^2 + c_4 G/L^2\phi^4$, with c_i order one, so $8\pi GT$ will stay of order $1/L^2$ as ϕ takes values of order $1/\sqrt{G}$.

obtained by starting from a supersymmetric 4D gravity with an AdS vacuum and breaking symmetries via expectation values for scalars in directions corresponding to relevant operator deformations in the CFT.

3.4 Fluctations about the background

The Euclidean path integral that defines our model corresponds to a gravitational path integral; we have been assuming this will be dominated by a saddle-point configuration that corresponds to the background geometry we have been discussing. However, the path integral also includes fluctuations about the background geometry. In the cosmology picture, these fluctuations correspond to different possible realizations of structure in the universe. Thus, the microscopic wavefunction describes an ensemble of possible cosmologies, rather than a single instance.

We can ask about the size of the perturbations (e.g. via the variance of various quantities in the ensemble) and also about the correlations between perturbations in typical elements of the ensemble. Information about these cosmological perturbations is contained in the correlation functions of the stress-energy tensor and other fields, and ultimately in the Euclidean QFT path integral that defines the microscopic state.

For example, we can consider the two-point function of the difference of the energy density from background $\langle(\rho(x) - \bar{\rho})(\rho(0) - \bar{\rho})\rangle$; the $x = 0$ case gives the variance at a point. While the overall energy density expectation value $\bar{\rho}$ is spatially constant (since our setup preserves translation invariance), the individual configurations contributing to the wavefunction of the universe will be inhomogeneous, and the quantitative information about these inhomogeneities can be extracted from the two-point function.

As we have emphasized above, since the same microscopic Euclidean path integral that defines the state of the cosmology is associated with the vacuum state of the confining gauge theory, the fluctuations that give rise to cosmological structure have an alternative interpretation as vacuum fluctuations in the wormhole picture. Correlations in the cosmology picture are related directly to the vacuum correlations in the wormhole picture.

For example, in a realistic cosmology with a Maxwell field, correlation functions of the energy density of this field (which would tell us about CMB observables) are related by analytic continuation to correlations of the stress tensor component $T_{\tau\tau}$ for the same field in the wormhole picture. In particular, any energy density correlators at the time-symmetric point of the cosmology are simply equal to the vacuum correlators $T_{\tau\tau}$ at the midpoint of the wormhole, provided all the operators sit in the same two dimensional plane.[50]

In the wormhole picture, correlation functions of bulk fields should be related in a relatively simple way to the correlation functions of operators in the microscopic field theory, using an HKLL-type prescription appropriate to our background geometry. That is, the bulk operator should correspond to a linear combination of local operators in the underlying field theory (mostly localized to the pair of 3D CFTs). So one could in principle use the microscopic field theory to calculate cosmological observables, though in practice, employing the effective field theory description in the wormhole picture should be adequate for most questions.

In future work, we plan to investigate the behavior of the correlators in our model and understand the predictions for cosmology. However, there is already one promising qualitative feature.

[50] This is the plane formed by the two coordinates in $\mathbb{R}^3$ that are spatial in both pictures.

An alternative to inflation or a dual description?

A distinctive feature in the density perturbations observed via the CMB is that there are correlations between regions of the universe that would have never been in causal contact if we assume simple cosmological evolution since the big bang. The theory of inflation naturally explains these correlations by introducing an early period of accelerated expansion. However, in our model, these correlations can be explained in a different way. They arise naturally since the cosmological correlators are directly related to vacuum correlators in the wormhole picture, and in a vacuum state on a static geometry, it is natural to have correlations at all scales (e.g. any two points have been in causal contact).[51]

We note also that the standard horizon and flatness problems addressed by inflation are naturally explained by the $\mathbb{R}^3$ symmetry of the model and the fact that the natural "initial" state lives at the time-symmetric surface. On the other hand, we don't know whether perturbations in our model agree with cosmological observations at the quantitative level.

While one possibility is that our model provides an alternative to inflation, it also seems possible that the wormhole picture provides a dual description of the same physics. It may be that in the cosmology picture there is inflation and that this generates the density perturbations in the usual way. In this case, the results must agree with the calculations in the wormhole picture where no knowledge of the early-universe physics or the inflationary potential is required. In this scenario, the inflationary physics would be dual to the vacuum physics of the wormhole in a similar way to how field theory and gravity can provide different explanations for the same

[51] Here, it may be important that while the dual quantum field theory is confining, it still has massless Goldstone bosons associated with the breaking of global symmetry $G \times G \to G$. In a theory with electromagnetism, one of these light degrees of freedom corresponds to the integral $\int A$ of the electromagnetic field between the asymptotic boundaries. So the infrared description still has long-range correlations beyond the confinement scale.

phenomenon in AdS/CFT.

3.4.1 The wavefunction of the universe in the effective field theory description

While the microscopic quantum state describing the cosmology is constructed using a CFT path integral, we can also think about the state of the universe from the effective field theory point of view as arising from a certain Euclidean gravity path integral in the effective field theory picture.

It is interesting to contrast this path integral with the one that Hartle and Hawking considered [169]. Hartle and Hawking suggested that the wavefunction of the universe most naturally arises from a wavefunction $\Psi[g_0]$ where the probability amplitude for a field configuration g_0 is given by a Euclidean gravitational path integral over all four-dimensional Euclidean geometries / field configurations having g_0 as the data at a boundary, with no other boundaries allowed.

In our approach, the state of the universe may also be naturally understood as arising from a Euclidean path integral. In the effective field theory description, the gravitational configurations contributing to the path integral used for computing observables have asymptotically AdS boundaries in the Euclidean past and future, and the fields in these asymptotic regions are coupled together via a non-gravitational CFT, as shown in Figure 3.8. This non-gravitating field theory serves as an anchor for the fluctuting geometries contributing to the gravitational path integral. The holographic picture suggests that these geometries should be homologous to the fixed geometry of the non-gravitational field theory.

A qualitative difference between our case and the Hartle/Hawking picture is that the fields in our cosmological spacetime are in a mixed state, entangled with the fields in the non-gravitational

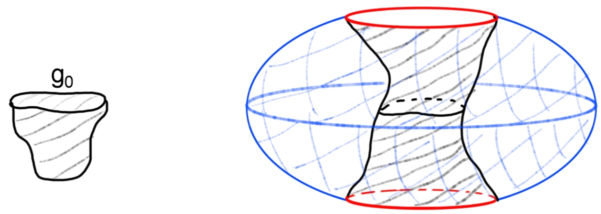

Figure 3.8: Left: A contribution to the Hartle-Hawking wavefunction of the universe. Right: A contribution to the gravitational path integral in our setup. In this case, the Euclidean gravity configurations have asymptotically AdS boundaries in the Euclidean past and future, and the fields at these boundaries are coupled together. The pictures correspond to the case of a closed universe; the flat universe we are focusing on can be obtained by taking the sphere volume to infinity.

quantum field theory. Tracing out these auxiliary fields may play a role in understanding how an ensemble of classical cosmologies arises from the wavefunction of the universe in our model.

3.4.2 The arrow of time

The special state in our cosmology is time-symmetric, so one must understand how the arrow of time emerges for observers in the model. The same issue arises for the Hartle-Hawking proposal, and there have been a number of previous discussions (see e.g. [249]). In [7], following Page [249] we suggested that the model might describe an ensemble of different cosmologies, some of which have arrows of time in one direction and some of which have arrows of time in the other direction. Here, we point out an interesting alternative, motivated by the idea that i) the arrow of time relates to the classical physics experienced by observers ii) the emergence of classicality involves decoherence and iii) that the physics of decoherence should occur either with forward quantum evolution or backward quantum evolution. The idea is that there might be two complementary bases of states, for which the basis elements are not time-reversal invariant, but the two bases are related by time-reversal. The in and out bases of states in discussions of scattering in quantum field theory provide an example. The full state can either be expressed in terms of the forward basis or the backward basis. Using the forward basis and tracing over some unobserved environmental degrees of freedom, we get an ensemble of states that might represent possible cosmologies with a forward arrow of time. Doing the same starting with the backward basis, we would then get an ensemble of possible cosmologies with a backward arrow of time. This picture has the intriguing property that each possible forward cosmology could be mathematically represented as a complicated superposition of backward cosmologies. However, further work is required to understand whether this possibility is sensible.

3.5 Discussion

In this paper, we have described a possible framework for cosmology motivated by two guiding principles (where the second was suggested by the first):

- There should be a fully non-perturbative microscopic description of the theory.
- There should be a preferred state.

In other words, we are exploring the most optimistic possible scenario for understanding the large-scale physics of our universe.

The first principle, together with our current understanding of string theory, led us to focus on the possibility that the fundamental cosmological constant in the effective theory describing our universe is negative. The existence of an asymptotically AdS analytic continuation suggested both a fundamental description involving 3D CFTs and a preferred state constructed using a Euclidean path integral. An unexpected consequence is the existence of a dual physical system whose vacuum state encodes most of the cosmological physics.

The resulting universe has a number of attractive features. Homogeneity, isotropy, and flatness are consequences of the symmetry of the model (and the fact that the present state of the universe is most naturally understood via backward evolution from the time-symmetric point). The equivalence between cosmological observables and vacuum observables in the dual wormhole system provides a natural explanation for the existence of correlations at all scales. This relation also means that any cosmological observables can be computed in principle without knowledge of the physics near the big bang, and without detailed knowledge of the UV completion. In particular, even if there is inflation at early times in the cosmology description, we can compute cosmological perturbations in the dual picture without knowledge of the inflationary potential.

The simplest toy example of our setup (with CFT matter) gives the simplest nontrivial $\Lambda < 0$ cosmology with radiation and cosmological constant leading to a big-bang / big crunch universe. This universe does not have an accelerating phase, but more generic examples of our setup have time-dependent scalar fields leading to time-dependent dark energy. These may exhibit a phase of accelerated expansion before the collapse and a phase of matter/radiation domination before that.

The small cosmological constant is related to the large number of degrees of freedom in the underlying 3D CFTs and (likely) the presence of supersymmetry in the fundamental description. The gauge group for the effective theory is controlled by the global symmetry group of the underlying 3D CFT; microscopic supersymmetric examples with almost any global symmetry group are known. Finally, both the model and the state are completely specified by our choice of 3D and 4D CFTs.

A natural next step (that we are currently pursuing) is to investigate in detail the cosmological evolution and cosmological correlation functions predicted by specific examples of this type of model, using an effective field theory approach, in order to understand whether realistic examples can be obtained.

3.5.1 Challenges

We emphasize that it is still an open question to demonstrate definitively that there are fully microscopic examples of this cosmological scenario, and a further challenge to understand whether examples of such models make predictions that are consistent with observations at a quantitative level. An important question is to verify that 3D-4D-3D quantum field theory systems of the type we have described can be dual to a Lorentzian wormhole. To demonstrate the viability of these models more directly, there are various options. For the fully microscopic examples suggested in [8], a classical type IIB supergravity calculation (or alternatively, a strongly coupled field theory calculation) is required to verify that the dual geometries have the right properties. Alternatively, one could try to understand precisely the four-dimensional effective gravitational theory for a microscopic example and understand how this can support a wormhole. Better understanding when and how quantum field theories can exhibit the appropriate vacuum energies to support a static Lorentzian planar wormhole is clearly an important step.

To understand whether our scenario can give rise to realistic examples of cosmology, there are many things to check. These include: whether the accelerated expansion from scalar potentials of the type we have described can satisfy the observational constraints on the time variation of dark energy,[52] whether the cosmological perturbations in our models can have the right magni-

[52]As we have explained, for the effective gravitational theories arising from holography, it is natural for the derivatives of the scalar potential to be small when the cosmological constant is small, so this is somewhat plausible.

tude and correlations, and whether we can satisfy numerous other phenomenological constraints, e.g. obtaining Standard Model as an effective theory, getting the right amount of dark matter and baryon asymmetry,[53] etc... . Since accelerated expansion in our models relies on having one or more time-dependent scalar fields with a very flat potential, it must be understood why other effects of such light scalar fields (e.g. long range forces or time-dependent couplings) have not been observed.[54]

Regardless of whether the scenario is realistic, it may still allow us to make progress on fundamental questions about quantum cosmology, just as we have learned about the quantum description of black holes through AdS/CFT.

3.5.2 Cosmological Islands

The fact that the effective field theory description of our cosmology includes an auxiliary system with which the fields in the cosmological spacetime are entangled is related in an intriguing way to observations in [175]. There, the authors asked when regions of cosmological spacetimes could be "entanglement islands", regions whose degrees of freedom are entangled with some other disconnected system in the effective field theory such that the two parts together form a proper quantum subsystem with a generalized entropy (and thus potentially dual to a quantum subsystem of a microscopic theory). They found that for certain $\Lambda < 0$ flat cosmologies, large enough spatial systems at times close enough to the recollapse point satisfy the criteria to be an island. In that analysis it was not clear what the complementary disconnected system or

[53]The time-dependent scalar fields that are generic in this class of models may be helpful in explaining the baryon asymmetry [250].

[54]A simple possibility is that these scalar fields are in the dark sector; fermions coupling to the scalar via $\phi\bar{\psi}\psi$ couplings in the underlying theory will have large masses when ϕ has large expectation values. For a more detailed discussion, see e.g. [251, 252].

the microscopic description could be. Our analysis suggests that exactly in the case where [175] found islands, we can give a microscopic description, and the microscopic description indeed involves an auxiliary system with which the fields in the cosmology picture are entangled.

We can also argue directly that large enough subsystems of our cosmology are islands. Consider a ball-shaped region of radius R in the microscopic 4D CFT. For large enough R, this will encode not only the physics of the same region in the 4D CFT in the effective description, but also part of the cosmology. To see this, consider a ball of radius R in the auxiliary system on the time-symmetric slice. This will have thermal entropy scaling like R^3. When R is much larger than the thermal scale, the fields in this region will be mostly purified by fields in the cosmology picture. It should thus be possible choose a similar ball-shaped region of the cosmology (also on the time-symmetric slice) with size proportional to R such that the entropy of the combined system now scales as R^2, coming from degrees of freedom near the boundaries of the two balls. Thus, for large enough R, this combined system with a cosmological island has smaller generalized entropy and provides the correct dual description of the microscopic CFT region.

This is even clearer when the 4D CFT is holographic. In this case, an RT surface for a ball-shaped region in the microscopic theory that remains outside the horizon will have area scaling like R^3 for large R, while an RT surface that enters the horizon and ends on a spherical region of the ETW brane will have area that scales like R^2 for large R.[55] So for large enough R, the latter surface is preferred, and the entanglement wedge includes part of the cosmology. This transition in entangling surfaces and the appearance of islands on the cosmological brane was originally observed and studied in [5].

[55]This R^2 may come with a large factor, since the ETW branes with localized gravity are associated with regions of the internal space with large volume in a higher-dimensional picture. So in the RT formula in the effective five dimensional theory, there will be terms proportional to the three-dimensional area of the intersection with the ETW brane, with a large coefficient.

We can also take the limit where the 4D CFT region size goes to infinity, in which case the entire time-symmetric slice in the cosmology is an island. Hence, the 4D CFT state at the time-symmetric point already has enough data to encode the entire cosmological evolution without any CFT time evolution. This is consistent with the cosmological time evolution being emergent and unrelated to the 4D CFT time evolution.[56] Moreover, in the special case where the 4D CFT is holographic, the Wheeler-DeWitt patch of the time-symmetric point includes the entire end-of-the-world brane trajectory, in agreement with the general analysis.

It is interesting to ask which other cosmological spacetimes can support islands - this may give us a hint whether any other types of cosmologies might have a holographic description similar to the one we are considering. This question was considered in some generality in [175] and [176, 253, 254]. For $\Lambda < 0$ ball-shaped islands continue to be possible for closed or open universes (i.e. where the spatial curvature is positive or negative), provided that the radius of curvature is sufficiently large [176]. This is consistent with the fact that the microscopic approach suggested in this paper can be generalized to positive or negative spatial curvature by replacing the $\mathbb{R}^3$ in the construction with S^3 or H^3. The curvature scale for these must be sufficiently large compared to the size of the interval separating the 3D CFTs to end up with the desired confining phase [5].

For $\Lambda \geq 0$, it was found that no islands are possible in flat [175] or open [176] cosmologies. For closed cosmologies (i.e. with positive spatial curvature), a new island candidate is given by the whole cosmological universe, regardless of the sign of Λ. Thus, it is interesting to ask whether some special state of a 4D CFT on S^3 might also encode the physics of cosmological spacetimes

[56] The disconnection between cosmological time evolution and CFT time evolution is even more evident if we consider that islands at the time-symmetric point $t = 0$ of the cosmology can be part of the entanglement wedge of regions R of the 4D auxiliary CFT even at late CFT times $t_{CFT} > 0$ [175].

with S^3 spatial geometry and $\Lambda \geq 0$. It is not clear how such a state could arise from a Euclidean path integral, though.

3.5.3 Summary of features

Whether or not the models we are describing turn out to be viable for realistic cosmology, they have a number of interesting features that might be useful in future approaches. To conclude the paper, we highlight some of the particular features that appear and that might inform future research.

First, we have various motivations to consider $\Lambda < 0$ cosmology:

- We take the existence of a complete, non-perturbative microscopic description as a guiding principle for describing cosmology. Given the present state of our understanding of string theory, this suggest that we focus more on the $\Lambda < 0$ possibility.

- Specifically, with $\Lambda < 0$, we avoid the vacuum instabilities and complicated bubbling multiverse picture that appears in $\Lambda > 0$ discussions. While this picture may dynamically give rise to anthropically allowed positive values of Λ if enough $\Lambda > 0$ string vacua exist [255], it seems difficult to establish that the required landscape of vacua exists (see e.g. [220]), and difficult to imagine what a microscopic description of such a scenario could look like.

- Considering models with time-dependent scalar fields (which can lead to an accelerated expansion phase even if $\Lambda < 0$) is natural in that this is the most general situation consistent with the symmetries of cosmological spacetimes. It is also natural from the string theory point of view, since the best understood regions of the string landscape with small positive potential energy are regions near AdS minima where we have excited some scalar fields.

An interesting feature of $\Lambda < 0$ is that it suggests there may be a natural state for the cosmology constructed from a Euclidean theory:

- Many natural $\Lambda < 0$ cosmological backgrounds have time-reversal symmetry about the $\dot{a} = 0$ point, and these time-symmetric geometries have an analytic continuation to a reflection-symmetric Euclidean geometry. The corresponding Euclidean gravity theory can be used to define a natural state for the cosmology. For this choice:

- The time-reversal symmetry of the background spacetime extends to the quantum state.

- The cosmological observables (for the full quantum state describing the ensemble of possible cosmologies) are analytic functions of coordinates.

- The late time cosmological observables can be calculated precisely without a detailed knowledge of the big bang or initial conditions in the cosmology picture.

- The cosmological observables are related to the vacuum observables in a dual picture. This naturally implies correlations between regions of the universe that were never in causal contact.

There are interesting features related to the holographic description:

- Three-dimensional holographic quantum field theories play an essential role in the description of the physics. Since these provide descriptions of vacuum AdS solutions, it is natural that they would continue to play an important role if we add a non-zero density of matter/radiation/scalar potential, etc... . In our construction, the three-dimensional theory no longer appears in the physical degrees of freedom of the holographic description, but still appears in the path integral that constructs the state.

- The fundamental microscopic degrees of freedom housing the quantum state of the universe are not conventionally holographic. In our example, they are a small N CFT. These holographic degrees of freedom are not "at the boundary" of the cosmological spacetime. Using the language of recent discussions of black hole evaporation, the cosmological spacetime is an "island." Related to this, we have that:

- The particles/fields in the effective description of cosmology are entangled with an auxiliary system that does not interact directly with the cosmology. Tracing out these auxiliary degrees of freedom, we have a mixed state of the cosmological effective field theory, describing an ensemble of different cosmologies.

- The full history of the universe is encoded in the state of the underlying 4D CFT at a single time, and should not be affected by changes to the CFT Hamiltonian at earlier or later times. Thus, time evolution in the cosmology seems unrelated to time evolution in the underlying CFT. We can say that time in the cosmology is emergent.

- Finally, the scalar field potential in the effective theory is directly related to properties of the underlying 3D CFT. Taking the number of CFT degrees of freedom to be very large (as would seem appropriate for describing the entire universe) naturally leads to both a small cosmological constant and small derivatives for the scalar potential.

In special cases where the 4D field theory may also be holographic, we have that:

- The cosmological spacetime lives behind the horizon of a black hole, and the cosmological singularities are related to the black hole initial and final singularities.

- In our specific setup, the cosmological physics lives on a brane in a higher-dimensional spacetime.
- Gravity is localized to the brane because the 3D CFTs associated with the four-dimensional physics have many more local degrees of freedom than the 4D CFT associated with the five-dimensional phsyics.

Finally, the models have some interesting consequences for phenomenological issues:

- The only input to the model is the choice of the underlying coupled 3D/4D field theory. The gauge group of the effective theory for the cosmology is determined by the global symmetry of the 3D CFT.
- The quantum state in the cosmology, and thus the cosmological perturbations are fixed given the choice of Euclidean effective field theory.
- Correlations between regions of the universe that were never in causal contact arise naturally because they are related to vacuum correlators in a dual picture.
- If the microscopic 4D CFT (and the dual gravity theory) is supersymmetric, this supersymmetry is only broken by the state in the cosmology picture. This may allow supersymmetric cancellations in the leading contribution to the cosmological constant to persist and explain why the cosmological constant can remain small. In the wormhole picture, supersymmetry is broken explicitly, but only by nonlocal effects (the incompatibility of the two boundary conditions). Again, this seems to avoid large corrections to the cosmological constant.

- The Friedmann equation implies that the total energy density at the time-symmetric point vanishes, so the magnitude of the (negative) dark energy is equal to the magnitude of the remaining energy. The time scale for the variation of these quantities is the age of the universe, so the dark energy and other sources of energy are expected to have a similar order of magnitude for most of the age of the universe. This may help explain the cosmological coincidence problem.

Acknowledgements

We would like to thank Panos Betzios, Matt Kleban, Lampros Lamprou, Henry Maxfield, Yasunori Nomura, Liam McAllister, Douglas Scott, Eva Silverstein, Chris Waddell, David Wakeham, and Aron Wall for helpful discussions and comments. This work is supported in part by the National Science and Engineering Research Council of Canada (NSERC) and in part by the Simons foundation via a Simons Investigator Award and the "It From Qubit" collaboration grant. PS is supported by an NSERC C-GSD award. SA is partially supported by a Leon A. Herreid Science Graduate Fellowship Award. This work is partially supported by the U.S. Department of Energy, Office of Science, Office of Advanced Scientific Computing Research, Accelerated Research for Quantum Computing program "FAR-QC" (SA) and by the AFOSR under grant number FA9550-19-1-0360 (BS).

Chapter 4: Wormhole reconstruction and constraints on the dual theory

Authors:[1] *Stefano Antonini, Petar Simidzija, Brian Swingle, Mark Van Raamsdonk.*

Abstract: A large class of flat big bang-big crunch cosmologies with negative cosmological constant are related by analytic continuation to asymptotically AdS traversable wormholes with planar cross section. In recent works (arXiv:2102.05057, arXiv:2203.11220) it was suggested that such wormhole geometries may be dual to a pair of 3D holographic CFTs coupled via auxiliary degrees of freedom to give a theory that confines in the infrared. In this paper, we explore signatures of the presence of such a wormhole in the state of the coupled pair of 3D theories. We explain how the wormhole geometry is reflected in the spectrum of the confining theory and the behavior of two-point functions and entanglement entropies. We provide explicit algorithms to reconstruct the wormhole scale factor (which uniquely determines its geometry) from entanglement entropies, heavy operator two-point functions, or light operator two-point functions (which contain the spectrum information). In the last case, the physics of the bulk scalar field dual to the light operator is closely related to the quantum mechanics of a one-dimensional particle in a potential derived from the scale factor, and the problem of reconstructing the scale factor from the two-point function is directly related to the problem of reconstructing this Schrödinger potential from its spectrum.

[1]Originally published as *Can one hear the shape of a wormhole?*, JHEP 09 (2022) 241, e-Print: 2207.02225, [3]. The appendices of the paper are reported in Appendix C.

4.1 Introduction

In this paper, we study the possible holographic description of Lorentzian geometries with two asymptotically AdS planar boundaries, with metric of the form

$$ds^2 = a^2(z)(dz^2 - dt^2 + dx^2 + dy^2), \tag{4.1}$$

where $z \in (-z_0, z_0)$ and $a(z)$ has simple poles at the locations $z = \pm z_0$ of the two asymptotic AdS boundaries. Such geometries make an intriguing appearance as the double analytic continuation of time-reversal symmetric $\Lambda < 0$ big-bang big crunch cosmologies. In [2, 8, 9], following [13] we argued that understanding the holographic description of such wormholes may lead to microscopic models of cosmological physics, perhaps even relevant to our universe.

In this paper, we will assume that gravitational solutions of this type exist[2] and can be described holographically, and we will attempt to understand the required properties of this holographic description. The pair of asymptotically AdS boundaries in the wormhole suggests a holographic description involving a pair of CFTs. These must be highly entangled with each other in the state corresponding to the wormhole since the two asymptotic regions are connected in the interior. Since it is possible to travel from one boundary to the other causally through the spacetime, these CFTs must also be interacting.

Various recent works [156, 170–173] have suggested specific ways to obtain traversable wormholes by coupling a pair of holographic CFTs. In [2,8] it was proposed that four-dimensional

[2]Planar traversable wormholes require an anomalously large amount of negative energy to exist [2, 8, 156]. An example mechanism leading to such enhanced negative energy was given in [157], and additional evidence for the existence of the solutions of our interest was presented in [2].

examples with geometry (4.1) might arise by coupling a pair of 3D CFTs via an auxiliary four-dimensional field theory. The 4D theory has many fewer local degrees of freedom than the 3D theories, but (via a renormalization group flow) strongly modifies the IR physics so that the IR theory is confining, with a ground state in which the two 3D CFTs are strongly entangled.

In this paper, we will be somewhat agnostic about how the CFTs associated with the two asymptotically AdS regions are coupled and ask instead how the wormhole physics is reflected in the state of the CFT degrees of freedom. We ask two general questions about the relationship between planar traversable wormhole geometries and observable properties in the dual field theory.

Question 1: *Given a microscopic setup, what features of the observables signal the presence of a dual eternal traversable wormhole?*

This first question is the subject of discussion in Section 4.2. We identify multiple signatures of the presence of a wormhole on the observables of the dual microscopic theory.

First, the theory has a discrete mass spectrum of particles characteristic of a confining gauge theory. In the wormhole geometry, the two asymptotic boundaries correspond to the UV of the field theory, while the middle of the wormhole corresponds to an IR "end" of the geometry that is a finite distance from any interior point. Having an IR end characterizes a geometry whose dual field theory is confining.[3] With this feature, the various bulk fields exhibit a discrete set of modes that correspond to towers of particles (glueballs, etc...) with a discrete set of masses in the dual field theory.

[3]See e.g. [180, 256] for previous models of holographic confining gauge theories. In Witten's original model, we have an internal S^1 contracting smoothly to zero at the IR end; in the wormhole geometry, we have an S^0 that contracts smoothly to zero.

In sections 4.2.1 and 4.2.3, we study in detail the spectra that arise from scalar fields and gauge fields in the wormhole and how these depend on the scale factor $a(z)$. Scalar fields in the wormhole geometry with normalizable boundary conditions can be decomposed into components associated with a discrete set of radial wavefunctions $u_i(z)$. These solve an auxiliary Schrodinger problem with potential

$$V(z) = \frac{a''(z)}{a(z)} + m^2 a^2(z) \; . \tag{4.2}$$

The associated eigenvalues λ_i give the values of the mass squared for the associated scalar particles in the 3D theory.

When a $U(1)$ gauge field is present in the bulk theory, it gives rise to an evenly-spaced discrete mass spectrum of vector particles in the dual field theory as well as a massless sector. Depending on the boundary conditions for the gauge field, the massless sector is given either by a massless scalar field (which can be interpreted as the Goldstone boson for the spontaneous breaking of a global $U(1) \times U(1)$ symmetry down to a single $U(1)$ symmetry, induced by the coupling between the two 3D CFTs), or by a massless gauge field (associated to a gauged residual $U(1)$ symmetry in the 3D CFTs). The existence of the massless sector non-trivially implies the existence of long-range correlations in the vacuum state of our confining theory.

In Section 4.2.2 we describe how the wormhole geometry implies a specific behavior for the two-point functions of scalar operators in the confining field theory, providing expressions for the one-sided and two-sided two-point functions in terms of the wormhole scale factor.

The wormhole geometry also has implications for the behavior of entanglement entropies of subregions of the microscopic theory, as we describe in Section 4.2.4. For example, considering the entanglement entropy for a region that includes a ball of radius R in each CFT, we expect a phase transition as the radius is increased past some critical radius where the RT surface changes from being disconnected to being connected.

The second question that we ask is the following:

Question 2: *How can the wormhole geometry be reconstructed from microscopic observables?*

We address this question in Section 4.3, where we identify three different observables from which to retrieve the behavior of the scale factor $a(z)$ appearing in equation (4.1).

In Sections 4.3.1 -4.3.5 we show how to reconstruct the scale factor using the mass spectra of scalar particles in the confining gauge theory arising from scalar fields in the bulk geometry. The spectrum associated with a given scalar field can be extracted from the two-point function of the corresponding scalar operator, as explained in Section 4.3.1. Using the spectral information associated with a single massless scalar,[4] or any two scalar fields of arbitrary different masses[5], we can reconstruct the scale factor.[6] The problem of reconstructing the wormhole geometry from mass spectra reduces to the question of whether, given the discrete spectrum of a Schrödinger equation, we can reconstruct the potential $V(z)$ which generates it. This is a particular case of an inverse Sturm-Liouville problem [181, 182], a well-known mathematical question which, in its two-dimensional version, is frequently formulated as "can one hear the shape of a drum?" [183]. Although the answer to this question is negative for generic potentials, the symmetry of our configuration and the AdS asymptotics turn out to be enough to render the inverse problem solvable. We provide an explicit algorithm in Section 4.3.4, first to reconstruct the Schrödinger

[4]The spectrum from a single scalar with $m^2 < 0$ (and satisfying the Breitenlohner-Freedman bound) may also be sufficient, though we only have numerical evidence for this.

[5]The spectrum of any scalar is enough to reconstruct the potential $V(z)$ in 4.2, but there can be multiple scale factors that result in this same potential. Having spectra from scalar fields with two different masses is always enough to fix $a(z)$ uniquely, though the ambiguity can likely be resolved with much less additional information, for example by looking at the short-distance behavior of a CFT two-point function or regularized entanglement entropy.

[6]The reconstruction is precise in the limit where the bulk theory is free.

potential appearing in (4.2) and then using the potentials for a pair of different mass scalars (or a single potential for $m^2 \leq 0$) to reconstruct the scale factor. We give an explicit example in section 4.3.5.

The second microscopic observable we can use to reconstruct the wormhole geometry is the two-point function of 3D CFT operators with large scaling dimension, corresponding to heavy bulk scalar fields (see Section 4.3.6). Such correlators can be evaluated in the geodesic approximation [184] leading to a functional dependence on the scale factor $a(z)$. Inverting this relationship by solving an integral equation allows us to reconstruct the wormhole metric in terms of microscopic correlators.

The third observable we consider, in Section 4.3.7, is the entanglement entropy of a strip-shaped subsystem in one of the two 3D CFTs. Similarly to the analysis for heavy correlators, the area of the Ryu-Takayangi (RT) surface [59] associated with such subregions has a functional dependence on the scale factor. Once inverted, this relationship yields the wormhole scale factor in terms of the entanglement entropy of the dual microscopic theory.

Applications to cosmology

As we have discussed above, the holographic description of planar asymptotically AdS wormhole geometries studied in this paper is an essential part of the framework introduced in [2, 8, 9] for describing certain time-symmetric $\Lambda < 0$ Big Bang-Big Crunch cosmologies holographically. In that setup, the quantum state encoding the cosmological spacetime and the quantum state encoding the wormhole spacetime arise from two different slicings of the same Euclidean field theory path integral, and the observables in the two pictures are related by an analytic continuation of two spacetime coordinates. In particular, the cosmological scale factor in conformal time is the analytic continuation of the wormhole scale factor $a(z)$, and so a complete knowledge of the wormhole geometry implies a complete knowledge of the cosmological evolution. Therefore, the wormhole reconstruction procedures developed in Section 4.3 imply that the cosmological scale factor can be reconstructed from simple confining field theory observables as well.[7] We will comment further on these aspects in Section 4.3.4 and in Section 4.4, where we give our concluding remarks.

4.2 From the wormhole to the microscopic theory

Let us consider a planar traversable wormhole geometry

$$ds^2 = a^2(z)(-dt^2 + dx^2 + dy^2 + dz^2), \tag{4.3}$$

with $t, x, y \in R$, and $z \in (-z_0, z_0)$ a coordinate with finite range. We assume that the wormhole connects two asymptotically AdS regions at $z = \pm z_0$, near which the scale factor $a(z)$ has the asymptotic form

$$a(z) \sim \frac{L}{z_0 \pm z} = \frac{\sqrt{-3/\Lambda}}{z_0 \pm z} \tag{4.4}$$

where $\Lambda < 0$ is the cosmological constant and L is the AdS radius. We will also assume that the wormhole is symmetric, $a(z) = a(-z)$. As explained above and discussed in detail in [2, 9],

[7] Probing the cosmological evolution without relying on the connection to the wormhole is a highly complex task [1, 2, 5, 8] (see also [6, 133] for lower-dimensional examples, and [118, 119] for related discussions), so this approach gives an explicit example of the power of the "slicing duality" introduced in [2, 8, 9]

such a geometry arises via a double analytic continuation from a large class of spatially flat, time-reversal symmetric Friedmann-Roberston-Walker (FRW) cosmologies with $\Lambda < 0$.

Interestingly, while the state of the cosmological effective field theory in these models is highly excited and thus generally difficult to study, the corresponding state in the wormhole picture is simply the canonical vacuum state. This allows one to study a wide class of cosmological observables (e.g. density perturbations, the CMB spectrum, etc.) by studying the vacuum physics in the traversable wormhole background. Moreover, since the wormhole connects two asymptotically AdS regions, we expect the physics in the wormhole to be dual to a pair of non-gravitational, microscopic 3D CFTs living on the two AdS boundaries $\mathbb{R}^{1,2}$.[8] Our goal in this paper will be to better understand how the effective low energy physics in the wormhole is related to the underlying microscopic physics of the two coupled 3D CFTs. As such, this question does not refer to the cosmology picture, and thus could be of interest outside the cosmological context.

4.2.1 Scalar particle spectrum from bulk scalar field

Let us begin by considering the simple situation in which the effective field theory in the wormhole consists of a single free scalar field ϕ of mass m.[9] The vacuum of the scalar field corresponds to the vacuum state of the dual microscopic theory. We will compute the excitation spectrum of the scalar in the wormhole, and thus obtain the mass spectrum of particles in the microscopic theory.

The excitation spectrum of the field ϕ on the wormhole background can be found by canon-

[8]Since the two boundaries are causally connected in the bulk via the traversable wormhole, the microscopic 3D CFTs must be coupled in such a way that allows information to pass from one theory to the other. In [2, 8] such a coupling is provided by a 4D theory with many fewer degrees of freedom, where the extra dimension is a compact interval. The resulting theory flows in the IR to a gapped 3D theory.

[9]This would be expected to hold precisely in a strict large N limit of the dual field theory and approximately for large but finite N.

ically quantizing ϕ. We begin by finding a complete set of mode solutions to the wave equation $(\Box - m^2)\phi = 0$. Translation invariance in the x, y, and t directions ensures a basis of solutions of the form

$$f_{k_x,k_y,i}(t,x,y,z) = \frac{1}{2\pi\sqrt{2\omega}a(z)} e^{-i\omega t} e^{ik_x x} e^{ik_y y} u_i(z), \tag{4.5}$$

which, after substituting into the wave equation, gives a Schrödinger equation for the modes u_i, namely

$$-u_i''(z) + V(z)u_i(z) = \lambda_i u_i(z). \tag{4.6}$$

The frequencies ω are related to the transverse momenta k_x, k_y and the eigenvalues λ_i via

$$\omega = \sqrt{k_x^2 + k_y^2 + \lambda_i}, \tag{4.7}$$

and the Schrödinger potential $V(z)$ is defined in terms of the wormhole scale factor $a(z)$ by

$$V(z) \equiv \frac{a''(z)}{a(z)} + m^2 a^2(z). \tag{4.8}$$

Since the scale factor, by assumption, has the symmetry $a(z) = a(-z)$, the same is true for the potential, $V(z) = V(-z)$. Furthermore the scale factor has the asymptotic AdS form (4.4) near the boundaries, and so the potential is of the asymptotic form

$$V(z) \sim \frac{\alpha}{(z_0 \pm z)^2}, \tag{4.9}$$

$$\alpha \equiv 2 - 3m^2/\Lambda. \tag{4.10}$$

From the Schrödinger equation we see that the two possibilities for the asymptotic behavior of $u(z)$ are either $u(z) \sim (z_0 \mp z)^{\Delta_+}$ or $u(z) \sim (z_0 \mp z)^{\Delta_-}$, where

$$\Delta_\pm \equiv \frac{1 \pm \sqrt{1+4\alpha}}{2}. \tag{4.11}$$

We call the former solutions *normalizable*, and the latter *non-normalizable*[10].

The canonical quantization of the scalar field is obtained by writing it as a mode sum

$$\hat{\phi}(t,x,y,z) = \sum_i \int dk_x \int dk_y \Big[f_{k_x,k_y,i}(t,x,y,z)\hat{a}_{k_x,k_y,i} + f^*_{k_x,k_y,i}(t,x,y,z)\hat{a}^\dagger_{k_x,k_y,i} \Big], \tag{4.12}$$

where $\hat{a}_{k_x,k_y,i}$ and $\hat{a}^\dagger_{k_x,k_y,i}$ are canonically commuting creation and annihilation operators for the modes $f_{k_x,k_y,i}$, and the vacuum state of the theory is defined as the state $|0\rangle$ which is annihilated by all the annihilation operators. We will assume that the modes appearing in the sum are normalizable, so that the excitations created by the creation operators are normalizable excitations.[11] Since we have chosen the modes f to be positive frequency with respect to the timelike Killing vector field ∂_t, this canonical vacuum state is the lowest energy state with respect to the

[10] Note that such denomination is meaningful only for $\alpha \geq 3/4$. For $-1/4 < \alpha < 3/4$, both solutions are normalizable in the L^2 norm, and there are two non-equivalent quantizations of the scalar field denominated "standard" and "alternative" quantizations, depending on whether we quantize the "normalizable" or "non-normalizable" part of the scalar field. When this ambiguity is present, we will focus here on the standard quantization scheme.

[11] This implies that the states created by acting on the vacuum with the creation operators have position space wavefunctions which are L^2 normalizable.

Hamiltonian generating time translations in t.

In order for the field ϕ to canonically commute with its conjugate momentum field, it is necessary and sufficient that the mode functions $f_{k_x,k_y,i}$ are orthonormal in the Klein-Gordon inner product. This implies the normalization condition

$$\int_{-z_0}^{z_0} dz\, u_i(z) u_j(z) = \delta_{ij}. \tag{4.13}$$

Since the z coordinate has a finite range, the set of normalizable solutions u_i to the Schrödinger equation is discrete, justifying the use of the discrete label $i = 0, 1, 2, \ldots$.

Having canonically quantized the scalar field, we can read off its energy spectrum. The Hamiltonian for a free scalar field is

$$\hat{H} = \sum_i \int dk_x \int dk_y\, \omega_{k_x,k_y,i} \left(\hat{a}^\dagger_{k_x,k_y,i} \hat{a}_{k_x,k_y,i} + \frac{1}{2} \right), \tag{4.14}$$

and thus, from Eq. (4.7), the energy spectrum of single particle excitations of the field ϕ is given by $\omega = \sqrt{k_x^2 + k_y^2 + \lambda_i}$. Since this is a free theory, the multi-particle spectrum is simply obtained by adding together single particle excitations.

We expect that the spectrum of excitations in the wormhole is equal to the spectrum of excitations in the dual microscopic theory. The dispersion relation $\omega = \sqrt{k_x^2 + k_y^2 + \lambda_i}$ suggests that in the (2+1)-dimensional microscopic theory[12] the particle excitations have momenta $\vec{k} = (k_x, k_y)$ and a discrete spectrum of squared masses $m_i^2 = \lambda_i$. Indeed, in the particular construction

[12]Note that the dual microscopic theory is (3+1)-dimensional (two 3D CFTs coupled by 4D auxiliary degrees of freedom), as we have pointed out. However, it flows in the IR to a gapped effective (2+1)-dimensional theory [2]. When, here and in the rest of the paper, we refer to the full dual theory as being (2+1)-dimensional, we have in mind such an effective gapped theory. This should not be confused with the two 3D CFTs living at the two asymptotic boundaries, and coupled by the auxiliary 4D degrees of freedom.

considered in [2, 8], the dual microscopic theory flows in the infrared towards a confining gauge theory on $\mathbb{R}^{1,2}$, which we expect to exhibit a discrete particle spectrum.

Therefore we find that the wormhole scale factor, and hence the corresponding FRW scale factor, determines the mass spectrum of scalar particles in the underlying microscopic theory. It would be interesting to understand which microscopic theories correspond to FRW cosmologies with realistic scale factors. We will not pursue this question here, but it could be an interesting area for future work. Instead we will now discuss correlators of scalar operators in the microscopic theory, and how they are related to the geometry of the bulk wormhole.

4.2.2 Scalar two-point functions

We would like to understand, given the geometry of the wormhole, what are the correlation functions of the CFT operator dual to a bulk scalar field. Then in Section 4.3 we will study the converse problem: how to reconstruct the wormhole geometry from a knowledge of the microscopic correlators.

Computing CFT correlators from a knowledge of the bulk geometry is straightforwardly done using the extrapolate dictionary of AdS/CFT: we compute the bulk correlators, and extrapolate them to the boundary to obtain correlators of 3D CFT operators in the dual confining theory. Let us work this out for the two-point function.

From (4.12), the bulk vacuum Wightman function evaluates to[13]

$$G^+(x,x') \equiv \langle 0|\,\phi(x)\phi(x')\,|0\rangle = \sum_n \int dk_x \int dk_y f_{k_x,k_y,n}(x) f^*_{k_x,k_y,n}(x'). \qquad (4.15)$$

[13] In the rest of the paper we will omit the ˆ on quantum operators.

Using the expression (4.5) for the mode functions, this can be simplified to

$$G^+(x,x') = \frac{1}{4\pi a(z)a(z')} \sum_n u_n(z)u_n(z') \int_{k_n}^{\infty} d\omega e^{-i\omega\Delta t} J_0\left(\Delta x_\perp \sqrt{\omega^2 - k_i^2}\right), \tag{4.16}$$

where $\Delta t \equiv t - t'$, $\Delta x_\perp \equiv \sqrt{(x-x')^2 + (y-y')^2}$, and we recall that $u_n(z)$ are eigenfunctions of the Schrödinger equation (4.6), with corresponding eigenvalues $k_n^2 \equiv \lambda_n$. Finally, the ω integral can be evaluated to give [257]

$$G^+(x,x') = \frac{1}{4\pi a(z)a(z')\sqrt{-\Delta t^2 + \Delta x_\perp^2}} \sum_{n=0}^{\infty} u_n(z)u_n(z') \exp\left(-k_n\sqrt{-\Delta t^2 + \Delta x_\perp^2}\right), \tag{4.17}$$

with the square roots taking values on their principal branch.

Consider now the CFT two-point function of the operator $\mathcal{O}$ which is dual to the field ϕ. This can be obtained by taking the points z and z' to the boundary, and removing powers of $z_0 \pm z$ and $z_0 \pm z'$ so that the expression is independent of z and z'. Concretely, $a(z) \sim 1/(z_0 - |z|)$ as $z \to \pm z_0$. Meanwhile the mode functions are of the form $u_n(z) \sim u_n^+(z_0+z)^{\Delta_+}$ near $z = -z_0$, where u_n^+ is the normalizable coefficient, chosen such that the modes are normalized as in (4.13). Since $u_n(z)$ is even if n is even and odd if n is odd, near $z = +z_0$ the mode functions are of the form $u_n(z) \sim (-1)^n u_n^+(z_0 - z)^{\Delta_+}$.

Since the wormhole has two boundaries, at $z = \pm z_0$, we have two types of insertions of the operator $\mathcal{O}$ into correlation functions. We denote an insertion of $\mathcal{O}$ at position (t,x,y) at the boundary $z = -z_0$ by $\mathcal{O}_-(t,x,y)$, and similarly for an insertion at the boundary $z = +z_0$. Thus there are two types of two-point functions: $\langle \mathcal{O}_\pm \mathcal{O}_\pm \rangle$ and $\langle \mathcal{O}_\pm \mathcal{O}_\mp \rangle$. The extrapolation procedure gives

$$\langle \mathcal{O}_{\pm}(t,x,y)\mathcal{O}_{\pm}(t',x',y')\rangle = \frac{1}{4\pi\sqrt{-\Delta t^2+\Delta x_\perp^2}}\sum_{n=0}^{\infty}(u_n^+)^2 \exp\left(-k_n\sqrt{-\Delta t^2+\Delta x_\perp^2}\right), \tag{4.18}$$

for the one sided correlators, and

$$\langle \mathcal{O}_{\pm}(t,x,y)\mathcal{O}_{\mp}(t',x',y')\rangle = \frac{1}{4\pi\sqrt{-\Delta t^2+\Delta x_\perp^2}}\sum_{n=0}^{\infty}(-1)^n(u_n^+)^2 \exp\left(-k_n\sqrt{-\Delta t^2+\Delta x_\perp^2}\right), \tag{4.19}$$

for the two sided correlators. Given the wormhole scale factor, the mode functions $u_n(z)$ and normalizations u_n^+ can be computed, and the $\mathcal{O}\mathcal{O}$ two-point functions can be evaluated. Therefore, the behavior of scalar operator correlators in the dual confining theory is uniquely fixed by the wormhole geometry.

4.2.3 Vector particle spectrum and massless sector from bulk gauge field

Let us now consider the quantization of a free $U(1)$ gauge field in the wormhole background (4.3). We will report here our main results, while a complete, detailed analysis can be found in Appendix C.1. For simplicity of notation, in this section we define $\ell = 2z_0$ and shift $z \to z - z_0$; the two boundaries are therefore at $z = 0, \ell$. The action for a massless gauge field is given by[14]

$$S_{gauge} = -\frac{1}{4}\int d^4x\sqrt{-g}F_{IJ}F^{IJ} \tag{4.20}$$

[14] In this section we will use latin indices $I, J = 0, 1, 2, 3$ to indicate 4D components, and greek indices $\mu, \nu = 0, 1, 2$ for 3D components t, x, y.

leading to the equations of motion (which, together with the Bianchi identity for F_{IJ}, provide the four Maxwell's equations)

$$\partial_I \left(\sqrt{-g} F^{IJ}\right) = 0. \tag{4.21}$$

As a result of the conformal invariance of the gauge field action (4.20) in 4D, the equations of motion are independent of the wormhole scale factor $a(z)$. In particular, we will work in Lorenz gauge $\eta^{IJ}\partial_I A_J = 0$, where they take the simple form

$$\eta^{IJ}\partial_I\partial_J A_K = 0. \tag{4.22}$$

We must now specify boundary conditions for the gauge field at the two boundaries. Unlike the scalar field case, the gauge field has two normalizable components, and the choice of boundary conditions leads to non-equivalent quantizations schemes (see Appendix C.1 and [258–262]). We will focus here on two (customary) possible choices of boundary conditions[15]: Dirichlet (also known as "magnetic"), where we fix $F_{\mu\nu}|_{z=0,\ell}$, and Neumann (also known as "electric"), where we fix $F_{\mu z}|_{z=0,\ell}$. The first choice, which leads to the "standard" quantization of the gauge field, is equivalent (in Lorenz gauge) to fixing the leading term of A_μ and the subleading term of A_z at the boundary, i.e. fixing $A_\mu|_{z=0,\ell}$ and $\partial_z A_z|_{z=0,\ell}$, up to a residual gauge transformation; the second choice, which leads to the "alternative" quantization of the gauge field, is equivalent to fixing the subleading term of A_μ and the leading term of A_z at the boundary, i.e. fixing $\partial_z A_\mu|_{z=0,\ell}$ and $A_z|_{z=0,\ell}$, up to a residual gauge transformation. The part of the bulk gauge field which is not fixed by the boundary conditions is quantized. Note that, motivated by the reflection symmetry of the microscopic theories of our interest [2], we are choosing identical boundary conditions at the

[15] See [262] for a detailed study of other possible choices of boundary conditions.

two asymptotic boundaries; in general, it is possible to consider different boundary conditions at the two boundaries. Let us now analyze the result of the quantization of the bulk gauge field in the two schemes.

Standard quantization

Let us start with Dirichlet boundary conditions. After fixing the residual bulk gauge freedom, we can quantize the bulk gauge field, obtaining

$$
\begin{aligned}
\hat{A}^D_\mu &= \sum_{n=1}^{\infty} \int \frac{dk_x dk_y}{2\pi\sqrt{\omega_n}\sqrt{\ell}} \sum_{j=a,b} \left[\tilde{\varepsilon}^{(j)}_\mu(k,\rho_n)\sin(\rho_n z)\mathrm{e}^{-(i\omega_n t - k_x x - k_y y)}\hat{a}^{(j)}_{k,\rho_n} + h.c.\right] \\
\hat{A}^D_z &= \int \frac{dk_x dk_y}{2\pi\sqrt{2\omega_0}\sqrt{\ell}} \left[\mathrm{e}^{-(i\omega_0 t - k_x x - k_y y)}\hat{a}_k + h.c.\right]
\end{aligned}
\tag{4.23}
$$

where $\omega_n = \sqrt{k_x^2 + k_y^2 + \rho_n^2}$, $\rho_n = n\pi/\ell$, $\hat{a}$ and $\hat{a}^\dagger$ are creation and annihilation operators satisfying the canonical commutation relations, and we defined the polarization vectors

$$
\begin{aligned}
\tilde{\epsilon}^{(a)}_\mu(k,\rho_n) &= \frac{1}{\sqrt{k_x^2+k_y^2}}(0,-k_y,k_x) \\
\tilde{\epsilon}^{(b)}_\mu(k,\rho_n) &= \frac{1}{\rho_n\sqrt{k_x^2+k_y^2}}(-(k_x^2+k_y^2),\omega_n k_x,\omega_n k_y).
\end{aligned}
\tag{4.24}
$$

The quantization of the 4D gauge field in the wormhole background with Dirichlet boundary conditions gives rise to a set of Kaluza-Klein modes. There is a zero mode, which can be interpreted as a massless 3D scalar field (the z component of the gauge field, uniform in the z direction), and an infinite tower of 3D massive vector fields, with discrete mass spectrum $m_n = \rho_n$. The $\tilde{\varepsilon}^{(a)}_\mu$ and $\tilde{\varepsilon}^{(b)}_\mu$ polarizations correspond to the transverse and longitudinal polarizations of such 3D massive vector fields, respectively. In the boundary dual confining theory, this bulk field content corresponds to a massless scalar particle and and a tower of massive vector bosons.

We would like to point out two features emerging from the present analysis. First, unlike the spectrum of a scalar field analyzed in Section 4.2.1, the spectrum of a 4D gauge field (or, equivalently, the mass spectrum of the dual vector particles) gives no information about the wormhole geometry besides the range of the z coordinate.[16] Since a free 4D gauge field is conformal, this feature is in fact to be expected. This means that the wormhole geometry cannot be reconstructed by starting from the mass spectrum of such vector fields.

Second, the presence of the massless scalar field indicates that, although the dual theory is confining, a massless sector is still present in a such theory. In order to understand how such a massless sector can arise, consider two copies of a 3D CFT with a global $U(1)$ symmetry group, whose respective bulk dual theories will then possess a $U(1)$ gauge symmetry. Let us now couple the two theories using 4D auxiliary degrees of freedom as described in [2, 8], such that the resulting theory is confining in the IR, and the holographic dual of its ground state is given by an eternal traversable wormhole of the form (4.3). The bulk theory will now contain a single $U(1)$ gauge field, associated with the $U(1) \times U(1)$ global symmetry of the boundary theory. This is suggestive of the fact that the boundary global symmetry is spontaneously broken by the coupling: $U(1) \times U(1) \to U(1)$. The massless scalar field $\hat{A}_z$ arising in the present analysis can be interpreted as a Goldstone boson associated to this spontaneous symmetry breaking [2]. The presence of the massless sector guarantees the existence of correlations at arbitrarily long scales (in the non-compact directions) in the ground state of the confining theory, and therefore in the wormhole. This feature can help with solving the horizon problem in the FRW cosmology related to our wormhole by double analytic continuation [2, 9].

[16]The same would be true of a massless scalar with a conformal coupling to the Ricci scalar.

Alternative quantization

With Neumann boundary conditions, after fixing the residual bulk gauge freedom, we obtain the bulk quantum field

$$\begin{aligned}\hat{A}^N_\mu = &\int \frac{dk_x dk_y}{2\pi\sqrt{2\omega_0}\sqrt{\ell}}\left[\tilde{\varepsilon}^{(0)}_\mu(k)\mathrm{e}^{-(i\omega_0 t-k_x x-k_y y)}\hat{a}^{(0)}_k + h.c.\right]\\ &+\sum_{n=1}^{\infty}\int \frac{dk_x dk_y}{2\pi\sqrt{\omega_n}\sqrt{\ell}}\sum_{j=a,b}\left[\tilde{\varepsilon}^{(j)}_\mu(k,\rho_n)\cos(\rho_n z)\mathrm{e}^{-(i\omega_n t-k_x x-k_y y)}\hat{a}^{(j)}_{k,\rho_n} + h.c.\right]\end{aligned} \tag{4.25}$$

with $\tilde{\varepsilon}^{(0)}_\mu(k) = (0,-k_y,k_x)/\sqrt{k_x^2+k_y^2}$ and $\tilde{\varepsilon}^{(a,b)}_\mu(k,\rho_n)$ as in equation (4.24). The quantization of the 4D gauge field in the wormhole background with Neumann boundary conditions also gives rise to a set of Kaluza-Klein modes. However, in this case there is a 3D massless gauge field with only one transverse physical polarization, and an infinite tower of 3D massive vector fields with mass $m_n = \rho_n$. No 3D massless scalar field is present. The 3D massless gauge field is uniform in the z direction. In the boundary dual confining theory, this bulk field content corresponds to a boundary massless gauge field, and a tower of massive vector fields. The presence of a single bulk gauge field again suggests a $U(1)\times U(1) \to U(1)$ symmetry breaking pattern. The existence of a 3D massless gauge field and the absence of a Goldstone boson associated with the symmetry breaking suggests that the $U(1)$ symmetries of the two original 3D CFTs (and the remaining $U(1)$ after symmetry breaking) are now gauged. Once again, the presence of the massless sector associated with the 3D massless gauge field guarantees the existence of correlations at arbitrarily long scales in the non-compact directions.

Therefore, we can conclude that the presence of a $U(1)$ gauge field in the wormhole geometry implies the existence of massive vector particles (with an evenly-spaced discrete spectrum of masses $m_n = n\pi/\ell$ ($n = 1, 2, 3, ...$)) and of a massless sector in the dual confining theory. For the standard quantization of the bulk gauge field, the massless sector is given by a massless scalar field, to be regarded as a Goldstone boson for the spontaneous breaking of a global $U(1) \times U(1) \to U(1)$ symmetry due to the coupling between the two 3D CFTs; for the alternative quantization, the spontaneously broken $U(1) \times U(1) \to U(1)$ symmetry is gauged, and the massless sector is given by the associated remaining boundary gauge field.

Additional particles in the dual confining gauge theory arise from fluctuations of the metric and other fields in the geometry; their mass spectra can be obtained via a similar analysis.

4.2.4 Entanglement entropy

Another boundary observable in which we expect to see a clear signature of the presence of the wormhole is the entanglement entropy of subregions of the dual microscopic theory. For example, consider the behavior of the entanglement entropy for a region $A = A_L \cup A_R$ — where A_L and A_R are identical-sized subregions of the left and right 3D CFTs respectively — as we vary the size of A. In the presence of a wormhole, we expect to observe a phase transition in the entanglement entropy related to a bulk transition from a disconnected RT surface (dominant for small A) to a connected RT surface going through the wormhole (dominant for large A). The transition occurs because the disconnected surfaces have a regulated area that eventually grows like the volume of the boundary region, while the connected surface has an area that eventually grows like the area of the boundary region. In the absence of a wormhole geometry connecting the two 3D theories living on the two boundaries, there is no such phase transition. We leave further investigation of the properties of holographic entanglement entropies in our setup to future work.

4.3 Reconstructing the wormhole

So far we have discussed how properties of the microscopic theory, such as its particle spectrum and correlators, are related to the geometry of the wormhole. Now let us ask the converse question: can we reconstruct the wormhole geometry from properties of the underlying confined microscopic theory? We will find that such a reconstruction is indeed possible if we have access to certain observables of the microscopic theory.

The first example of such an observable is given by the two-point functions $\langle \mathcal{O}_1 \mathcal{O}_1 \rangle$ and $\langle \mathcal{O}_2 \mathcal{O}_2 \rangle$ in the confining theory of two 3D CFT scalar operators $\mathcal{O}_1$ and $\mathcal{O}_2$ of different scaling dimensions[17]. Our wormhole reconstruction algorithm from these two-point functions can be summarized as follows.

First, in Section 4.3.1, we show how a knowledge of the scalar two-point function $\langle \mathcal{O} \mathcal{O} \rangle$ in the microscopic confining theory allows one to obtain the mass spectrum of the associated scalar particle excitations, which is equal to the spectrum of modes of a bulk scalar field with some mass m. Then, in Section 4.3.2, we show how the mass spectrum associated with an operator $\mathcal{O}_i$ can be used to reconstruct the Schrödinger potential which gives rise to this spectrum. From (4.8) we know that this potential is given directly in terms of the wormhole scale factor and the mass of the scalar field ϕ_i dual to the operator $\mathcal{O}_i$. In Section 4.3.3 we show how a knowledge of two such potentials, associated with two scalar operators $\mathcal{O}_1$ and $\mathcal{O}_2$ of different dimensions, allows one to invert this relationship and obtain the scale factor.[18] We summarize the entire algorithm in Section

[17] The operators $\mathcal{O}_1, \mathcal{O}_2$ are operators associated with the two 3D CFTs living at the two asymptotic boundaries, but their expectation value is computed in the full confining theory obtained by coupling the two 3D CFTs by auxiliary 4D degrees of freedom.

[18] Note that a single potential associated with a massless bulk scalar field is sufficient to reconstruct the scale factor. For $m^2 < 0$ (but above the BF bound) a single potential may also be enough to reconstruct the geometry, though we only have numerical evidence for this. For $m^2 > 0$, a single potential is not sufficient.

4.3.4 and provide an example of reconstruction in Section 4.3.5. The reconstruction algorithm for the wormhole geometry from boundary scalar two-point functions should be regarded as one of the main results of this paper. Finally, in Section 4.3.6 and 4.3.7 we explain how the wormhole scale factor can be reconstructed from correlators of 3D CFT operators with large scaling dimension, and from the entanglement entropy of strip-shaped subregions of one of the two 3D CFTs.

4.3.1 Mass spectrum from two-point function

In equation (4.18) and (4.19) we wrote down the CFT two-point functions $\langle \mathcal{O}_\pm \mathcal{O}_\pm \rangle$, in which both insertions of the operator $\mathcal{O}$ are inserted into the same same wormhole boundary, and $\langle \mathcal{O}_\pm \mathcal{O}_\mp \rangle$, where one insertion is into the CFT at $z = +z_0$ and the other insertion into the CFT at $z = -z_0$. Namely

$$G_{++}(s) \equiv \langle \mathcal{O}_\pm(x) \mathcal{O}_\pm(x') \rangle = \frac{1}{4\pi s} \sum_{n=0}^{\infty} (u_n^+)^2 \exp\left(-k_n s\right), \tag{4.26}$$

$$G_{+-}(s) \equiv \langle \mathcal{O}_\pm(x) \mathcal{O}_\mp(x') \rangle = \frac{1}{4\pi s} \sum_{n=0}^{\infty} (-1)^n (u_n^+)^2 \exp\left(-k_n s\right), \tag{4.27}$$

where $s \equiv \sqrt{-(t-t')^2 + (\boldsymbol{x} - \boldsymbol{x}')^2}$.

Let us consider these correlators in the regime where s is imaginary, $s = i\xi$, namely

$$G_{++}(\xi) = \frac{1}{4\pi i \xi} \sum_{n=0}^{\infty} (u_n^+)^2 \exp\left(-i k_n \xi\right), \tag{4.28}$$

$$G_{--}(\xi) = \frac{1}{4\pi i \xi} \sum_{n=0}^{\infty} (-1)^n (u_n^+)^2 \exp\left(-i k_n \xi\right). \tag{4.29}$$

Multiplying by $i\xi$ and taking the Fourier transform gives

$$G_{++}(k) \equiv \int_{-\infty}^{\infty} d\xi \, i\xi G_{++}(\xi) e^{ik\xi} = \frac{1}{2} \sum_{n=0}^{\infty} (u_n^+)^2 \delta(k - k_n), \tag{4.30}$$

$$G_{+-}(k) \equiv \int_{-\infty}^{\infty} d\xi \, i\xi G_{+-}(\xi) e^{ik\xi} = \frac{1}{2} \sum_{n=0}^{\infty} (-1)^n (u_n^+)^2 \delta(k - k_n), \tag{4.31}$$

and so we see that the spectrum of scalar excitations, $k_n^2 = \lambda_i$, is simply obtained from the peaks in the Fourier transforms of the two-point correlators, while the normalizations u_n^+ are obtained from the amplitudes of the peaks. Interestingly, it is possible to obtain this information either from the one-sided or two-sided correlators. Notice that to obtain the spectrum above a given scale k_0, we need to probe the two-point function on distance scales $\xi < 1/k_0$. From the analysis of Section 4.2.1, we can identify this spectrum of scalar excitations with the discrete spectrum of modes associated with a bulk scalar field.

4.3.2 The inverse Sturm-Liouville problem

Suppose now that, perhaps starting from CFT correlators as in the previous section, we obtain the spectrum λ_i of scalar excitations associated with a given operator $\mathcal{O}$ in the microscopic theory, which we can identify with the discrete spectrum of modes for a bulk scalar field. We know from the analysis in Section 4.2.1 that the λ_i are eigenvalues to the Schrödinger equation (4.6),

$$-u_i''(z) + V(z) u_i(z) = \lambda_i u_i(z), \tag{4.32}$$

where the potential $V(z)$ is related to the scale factor of the wormhole. Given the potential, the problem of finding the eigenvalues λ_i (i.e. diagonalizing the Hamiltonian) is called a Sturm-Liouville problem. Here, we are interested in the inverse Sturm-Liouville problem problem: finding the potential $V(z)$ from a given spectrum λ_i.[19]

Under the assumption of a generic potential the solution to the inverse Sturm-Liouville problem is not unique [181, 182]. However the potentials that are of interest to us are not completely generic; we are assuming that the wormhole geometry is even $a(z) = a(-z)$, and so the potential is also even, $V(z) = V(-z)$. In the context of wormholes that arise from cosmological models [2], this symmetry of the geometry arises from the $\mathbb{Z}_2$ symmetry present in both the Euclidean CFT path integral used to define the theory, as well as the choice of slicing of this path integral which defines the state of the theory. It has been shown in [182] that if the potential is even and integrable, $\int_{-z_0}^{z_0} V(z) < \infty$, then the inverse Sturm-Liouville problem can be solved. Namely, there exists an efficient algorithm which allows one to reconstruct the potential $V(z)$ given its spectrum.

Unfortunately we cannot directly apply these results to solve our inverse Sturm-Liouville problem, because our potential diverges as $1/z^2$ near the AdS boundaries (see Eq. (4.9)) and hence is not integrable. In this section we will upgrade the reconstruction algorithm in [182] to allow for potentials with AdS asymptotics. We will make the following assumptions:

Assumptions

1. The domain of z is $(-z_0, z_0)$ for some $z_0 > 0$;

[19] The question "can one hear the shape of a drum?" [183] — i.e. "Can one determine the geometry of a two-dimensional manifold from a knowledge of the spectrum of the Laplace operator?" — is a higher dimensional analog to the inverse Sturm-Liouville problem.

2. The potential is symmetric, $V(z) = V(-z)$;

3. The potential diverges as $\frac{\alpha}{(z_0-|z|)^2} + \frac{\beta}{(z_0-|z|)}$ at $z = \pm z_0$, with $\alpha > -1/4$ and $\beta \in \mathbb{R}$;

4. The normalizable spectrum $\{\lambda_j\}$ to the Schrödinger equation (4.32) is known.

Let us make some comments about these assumptions. From equation (4.9) we see that the parameter α characterizing the leading divergence of the potential is given by $\alpha = 2 + m^2L^2$, where L is the AdS length in the asymptotically AdS regions, and m is the mass of the scalar field. The assumption $\alpha > -1/4$ is therefore equivalent to the Breitenlohner-Freedman (BF) bound $m^2L^2 > -d^2/4$, with $d = 3$ the spatial dimension of the wormhole [177, 178]. We are also allowing for a subleading divergent term in $V(z)$ proportional to some other constant β.[20] We see from (4.8) that such a term in the potential is expected to arise from general scale factors with boundary asymptotics of the AdS form.

As we have already seen, for a potential with leading divergence of the form in assumption 3, the series expansion near $z = -z_0$ of a solution to the Schrödinger equation (4.32) is

$$u(z) = u^{(-)}(-z_0)(z+z_0)^{\Delta_-}\left(1+\ldots\right) + u^{(+)}(-z_0)(z+z_0)^{\Delta_+}\left(1+\ldots\right), \tag{4.33}$$

where

$$\Delta_\pm \equiv \frac{1}{2} \pm \bar{\Delta}, \tag{4.34}$$

$$\bar{\Delta} \equiv \frac{1}{2}\sqrt{1+4\alpha}, \tag{4.35}$$

[20] In principle, we could also have some subleading divergent term with a different non-integer power, but we will restrict our analysis to this case.

and $u^{\pm}(-z_0)$ are numerical coefficients. The omitted terms in the above expansion are of subleading order in the distance $z+z_0$ from the boundary. We say that the term proportional to $u^{(+)}(-z_0)$ is normalizable at $z = -z_0$, and the term proportional to $u^{(-)}(-z_0)$ is non-normalizable at $z = -z_0$. We have a similar expansion at $z = +z_0$, with normalizable and non-normalizable coefficients $u^{(+)}(z_0)$ and $u^{(-)}(z_0)$. We define the *normalizable eigenfunctions* of the Schrödinger equation (4.32) to be those eigenfunctions for which the non-normalizable component vanishes at both endpoints, $u^{(-)}(-z_0) = u^{(-)}(z_0) = 0$. The *normalizable spectrum* is the set of eigenvalues associated with the normalizable eigenfunctions.

Note that the normalizable eigenfunctions are indeed normalizable in L^2 norm. Perhaps somewhat confusingly, if $\alpha < 3/4$, eigenfunctions which are non-normalizable at one or both endpoints are also normalizable in L^2 norm. This is related to the ambiguity — which arises when a scalar field in AdS has a mass in the range $-d^2/4 < m^2L^2 < -d^2/4 + 1$ — in deciding which part of the field to identify with the expectation value of the dual CFT operator, and which part to identify with the source of the dual CFT operator. For simplicity we will always associate the normalizable eigenfunctions with the expectation values of the dual operators, which in the bulk is the statement that, as we have done in Section 4.2.1, we will expand the scalar field in terms of a complete set of normalizable eigenfunctions of the wave equation.

We will now show how to reconstruct the potential $V(z)$ from its spectrum, subject to these assumptions. The main idea is to reconstruct the unknown potential $V(z)$ from some known "test" potential $\tilde{V}(z)$ which has the same asymptotic spectrum as $V(z)$. Our first task is to determine the test potential $\tilde{V}(z)$.

Finding the test potential

We want to find a test potential $\tilde{V}(z)$ such that the eigenvalues $\tilde{\lambda}_j$, $j = 0, 1, 2, \ldots$, of the eigenvalue problem

$$-u''(z) + \tilde{V}(z)u(z) = \tilde{\lambda}u(z), \tag{4.36}$$

$$u^{(-)}(\pm z_0) = 0, \tag{4.37}$$

are asymptotically equal to λ_j for $j \to \infty$. To find such a $\tilde{V}(z)$, let us consider solving the equation $-u''(z) + V(z)u(z) = \lambda u(z)$ on the interval $z \leq 0$, in the limit $\lambda \to \infty$. If $V(z)$ contains terms which are bounded on $z \leq 0$, then the term proportional to λ dominates over these terms and we can simply replace these bounded terms by their average value over $z \leq 0$. Besides this constant, the only terms which remain are the divergent pieces of $V(z)$ on $z \leq 0$, which we know by assumption to be $\frac{\alpha}{(z_0+z)^2} + \frac{\beta}{z_0+z}$, although we do not know the values of α and β a priori. By making the same argument for $z > 0$, we conclude that in the limit $\lambda \to \infty$, the potential $V(z)$ can effectively be replaced by

$$\tilde{V}(z) \equiv \frac{\alpha}{(z_0 - |z|)^2} + \frac{\beta}{z_0 - |z|} + c, \tag{4.38}$$

where α, β, c are unknown constants. Our goal is to determine these constants. We will do this by equating the asymptotic spectrum $\tilde{\lambda}_j$ associated with this $\tilde{V}(z)$ with the asymptotic part of the given spectrum λ_j.

The potential $\tilde{V}(z)$ is simple enough that we can explicitly compute its asymptotic spectrum. As we show in Appendix C.2, up to terms that go to zero as $j \to \infty$, the spectrum at large j is

$$\tilde{\lambda}_j \sim Zj^2 + Aj + B\log(j) + C, \tag{4.39}$$

where Z, A, B, C are given by

$$Z = \left(\frac{\pi}{2z_0}\right)^2, \tag{4.40}$$

$$A = \left(\frac{\pi}{2z_0}\right)^2 2\Delta_+, \tag{4.41}$$

$$B = \frac{\beta}{z_0}, \tag{4.42}$$

$$C = \left(\frac{\pi}{2z_0}\right)^2 \left(\Delta_+^2 - \frac{4\alpha}{\pi^2}\right) + \frac{\beta}{z_0}\left[\log(\pi) - \psi(\Delta_+)\right] + c, \tag{4.43}$$

with $\psi(x)$ being the digamma function and Δ_+ was defined in (4.34). Notice that $Z > 0$. As we saw, the Breitenlohner-Freedman bound requires $\alpha > -1/4$, and so $A > 0$ as well. Meanwhile, B and C can take on any real values. These restrictions on Z, A, B, C, together with equation (4.39), constitute the necessary asymptotic conditions on the sequence λ_j in order for it to correspond to the spectrum of a scalar field in a symmetric wormhole geometry which connects two asymptotically AdS regions. We will assume that the spectrum from which we are trying to reconstruct the wormhole geometry is of this form. In this case we know that there exists a solution to the inverse Sturm-Liouville problem; we will try to find this solution.

Recall that our current goal is to obtain the test potential $\tilde{V}(z)$ defined in (4.38). Given the spectrum λ_j we can deduce the values Z, A, B, C, and then we can invert equations (4.40)-(4.43) to give z_0, α, β and c in terms of Z, A, B, C:

$$z_0 = \frac{\pi}{2\sqrt{Z}}, \tag{4.44}$$

$$\alpha = \frac{A}{4Z}\left(\frac{A}{Z} - 2\right), \tag{4.45}$$

$$\beta = \frac{\pi B}{2\sqrt{Z}}, \tag{4.46}$$

$$c = -\frac{A}{4\pi^2}\left[\frac{(\pi^2-4)A}{Z} + 8\right] - B\left[\log(\pi) - \psi\left(\frac{A}{2Z}\right)\right] + C. \tag{4.47}$$

Therefore, given a spectrum λ_j with the correct asymptotic form, we can obtain the test potential $\tilde{V}(z)$. The spectrum $\tilde{\lambda}_j$ associated with the test potential will be asymptotically equal to λ_j, as desired.

Notice that, solely from this asymptotic analysis, we can already make several conclusions about some large scale features of the wormhole geometry, and the associated Schrödinger potential $V(z)$. For instance, from (4.40) we see that the leading (quadratic in j) term in the asymptotic expansion of the spectrum λ_j determines z_0, the coordinate width of the wormhole geometry. Meanwhile the term linear in j determines the leading (α/z^2) divergence of the potential near the AdS boundaries, and hence the cosmological constant. The subleading $\log(j)$ term gives the β/z divergence of the potential, and the term constant in j gives the average value c of the non-singular terms in the potential.

It is in accordance with our intuition from AdS/CFT that the values α and β, which are related to the AdS asymptotics of the wormhole geometry, are associated with the UV asymptotics of the spectrum λ_j. Interestingly we also see that what might be considered the two most extremely IR features of the wormhole — the size of the wormhole z_0 and the average value c

— are also determined by the asymptotic form of the spectrum. Heuristically we can say that the asymptotic spectrum encodes the large scale features of the wormhole.

In order to determine the finer details of the wormhole, and in particular the potential $V(z)$, we will need to make use of our knowledge of the spectrum λ_k at finite k. In fact we will find that the eigenvalue λ_k encodes the features of the potential on coordinate distance scales of the order z_0/k, and so if we are only interested in reconstructing the features of the potential (and thus of the scale factor) on scales larger than z_0/N, then to a good approximation it is enough to only know the finite subset $\{\lambda_1, \lambda_2, \ldots, \lambda_N\}$ of the full spectrum.[21] Let us now work out the details of this reconstruction.

Reconstructing the true potential from the test potential

Having obtained the test potential $\tilde{V}(z)$ from the asymptotic spectrum, let us now discuss how to reconstruct the true potential $V(z)$. The main idea of the reconstruction algorithm is based on the study of inverse Sturm-Liouville problems by Ref. [182], but adapted to allow for singular potentials such as ours.

We begin by defining $u(z, \lambda)$, $\tilde{u}(z, \lambda)$, $v(z, \lambda)$ and $\tilde{v}(z, \lambda)$ as the solutions to the following

[21] Of course we also need the asymptotic form of λ_j in order to obtain the large scale structure of the potential.

initial value problems on $z \in (-z_0, z_0)$:

$$u : \begin{cases} u''(z,\lambda) = \big[V(z) - \lambda\big] u(z,\lambda) \\ u^{(+)}(-z_0,\lambda) = \frac{1}{2\bar{\Delta}} \\ u^{(-)}(-z_0,\lambda) = 0 \end{cases} \qquad v : \begin{cases} v''(z,\lambda) = \big[V(z) - \lambda\big] v(z,\lambda) \\ v^{(+)}(+z_0,\lambda) = \frac{1}{2\bar{\Delta}} \\ v^{(-)}(+z_0,\lambda) = 0 \end{cases} \tag{4.48}$$

$$\tilde{u} : \begin{cases} \tilde{u}''(z,\lambda) = \big[\tilde{V}(z) - \lambda\big] \tilde{u}(z,\lambda) \\ \tilde{u}^{+}(-z_0,\lambda) = \frac{1}{2\bar{\Delta}} \\ \tilde{u}^{-}(-z_0,\lambda) = 0 \end{cases} \qquad \tilde{v} : \begin{cases} \tilde{v}''(z,\lambda) = \big[\tilde{V}(z) - \lambda\big] \tilde{v}(z,\lambda) \\ \tilde{v}^{(+)}(+z_0,\lambda) = \frac{1}{2\bar{\Delta}} \\ \tilde{v}^{(-)}(+z_0,\lambda) = 0 \end{cases} \tag{4.49}$$

Here primes denote z derivatives and recall that $\bar{\Delta} = \sqrt{\alpha + 1/4}$. As before we are using the notation $u^{(\pm)}(z_0, \lambda)$ for the normalizable $(+)$ and non-normalizable $(-)$ parts of $u(z, \lambda)$ at $z = z_0$, and similarly at $z = -z_0$. The reason for the choice of normalization $1/(2\bar{\Delta})$ is explained in Appendix C.3. Notice that while u and $\tilde{u}$ are by definition always normalizable (and hence non-diverging) at the left boundary $z = -z_0$, in general they are non-normalizable (and thus in general diverging) at the right boundary $z = +z_0$. Similarly the v and $\tilde{v}$ are normalizable at the right boundary, but non-normalizable at the left one. However the discrete set of functions $u_j(z) \equiv u(z, \lambda_j)$ and $v_j(z) \equiv v(z, \lambda_j)$ are eigenfunctions of the Schrödinger equation with potential V and normalizable boundary conditions at the left *and* right boundaries, and so these functions are completely regular on the entire wormhole. Analogously, $\tilde{u}_j(z) \equiv \tilde{u}(z, \tilde{\lambda}_j)$, $\tilde{v}_j(z) \equiv \tilde{v}(z, \tilde{\lambda}_j)$ are also regular in $[-z_0, z_0]$.

With this in mind, we define the *Wronskian* $\omega(\lambda)$ as the non-normalizable part of $u(z, \lambda)$ at the right boundary, namely

$$\omega(\lambda) \equiv -\lim_{z\to z_0} \frac{u(z,\lambda)}{(z_0-z)^{\Delta_-}}, \tag{4.50}$$

so that $\omega(\lambda)=0$ if and only if λ is a normalizable eigenvalue of the Schrödinger equation (4.32) with potential $V(z)$. The following lemma, which we prove in Appendix C.3, will play a crucial role in our reconstruction of $V(z)$ from $\tilde{V}(z)$:

Lemma 1 *For any L^2 integrable function $f(z)$ on $z\in(-z_0,z_0)$ the following identity holds:*

$$f(z) = \sum_{j=0}^{\infty} \frac{\tilde{v}_j(z)\int_{-z_0}^{z} dy\, u_j(y)f(y) + \tilde{u}_j(z)\int_{z}^{z_0} dy\, v_j(y)f(y)}{\omega'(\lambda_j)}. \tag{4.51}$$

Let us set $f(z)$ equal to $u_0(z)$, the eigenfunction of the Schrödinger equation corresponding to the lowest eigenvalue λ_0. A basic fact from Sturm-Liouville theory states that $u_j(z)$ has j roots, and so $u_0(z)>0$. Using the orthonormality of the $u_j(z)$ in the L^2-norm, the lemma gives

$$u_0(z) = \tilde{u}_0(z) + \frac{1}{2}\sum_j \tilde{y}_j \int_{-z_0}^{z_0} dx\, u_j(x)u_0(x), \tag{4.52}$$

where

$$\tilde{y}_j(z) \equiv 2\frac{\tilde{v}_j(z) - (-1)^j\tilde{u}_j(z)}{\omega'(\lambda_j)}, \tag{4.53}$$

Differentiating (4.52) twice and using the differential equations satisfied by $u_0(z)$ and $\tilde{u}_0(z)$, we obtain

$$V(z)u_0(z) = \tilde{V}(z)u_0(z) + \sum_j \left[\tilde{y}_j(z)u_j(z)\right]' u_0(z). \tag{4.54}$$

Finally, since $u_0(z) > 0$ this implies

$$V(z) = \tilde{V}(z) + \sum_j \big[\tilde{y}_j(z)u_j(z)\big]'. \tag{4.55}$$

Equation (4.55) relates the unknown, true potential $V(z)$ to the test potential $\tilde{V}(z)$, the latter having already been determined in the previous section. However this formula is not sufficient for determining $V(z)$, because the eigenfunctions $u_j(z)$ appearing inside this formula implicitly depend on $V(z)$ through the Schrödinger equations

$$u_j''(z) = \big[V(z) - \lambda_j\big]u_j(z). \tag{4.56}$$

Instead, we should think of (4.55) together with the Schrödinger equations (4.56) as a coupled system of non-linear ODEs for the unknown functions $V, u_0, u_1, u_2, \dots$.

If we restrict j to the interval $0, 1, \dots, j_{\text{max}}$, then

$$\begin{cases} V(z) = \tilde{V}(z) + \sum_{j=0}^{j_{\text{max}}} \big[\tilde{y}_j(z)u_j(z)\big]', \\ u_j''(z) = \big[V(z) - \lambda_j\big]u_j(z), \quad j = 0, 1, \dots, j_{\text{max}} \end{cases} \tag{4.57}$$

forms a closed system of $j_{\text{max}} + 2$ equations for $j_{\text{max}} + 2$ unknown functions $V, u_0, u_1, \dots, u_{j_{\text{max}}}$. For a given value of j_{max}, denote $V_{j_{\text{max}}}(z)$ as the solution for $V(z)$ obtained by solving this finite system of equations. Since $\tilde{y}_j \to 0$ as $j \to \infty$[22], we expect that the corrections to $V_{j_{\text{max}}}$ become smaller and smaller as we increase j_{max} to larger and larger values, and that in the limit $j_{\text{max}} \to \infty$

[22]To see this note that as $j \to \infty$ we have that $\lambda_j \to \tilde{\lambda}_j$ and hence in this limit $\tilde{u}_j$ and $\tilde{v}_j$ both approach the jth eigenfunction of the Schrödinger equation with potential $\tilde{V}$. Since the jth eigenfunction of a symmetric Sturm-Liouville problem has parity $(-1)^j$ we see that $\tilde{v}_j = (-1)^j \tilde{u}_j$ and hence $\tilde{y}_j \to 0$.

we obtain the true potential $V(z)$.

In practice, we will restrict to a finite j_{max} and thus obtain an approximation to the true potential $V(z)$. Since the functions u_j and $\tilde{y}_j$ oscillate on scales of order z_0/j, we can think of this as being a good approximation to the true potential on coordinate distance scales larger than $z_0/j_{max} \sim 1/(\sqrt{Z}j_{\text{max}})$.[23] We will explicitly see this feature in the example reconstruction presented in Section 4.3.5.

Let us briefly comment on a subtlety which arises when we attempt to solve the truncated system of ODEs (4.57). The issue is that in order to obtain $\tilde{y}_j$ via equation (4.53), we need to compute the derivatives of the Wronskian, $\omega'(\lambda_j)$. However the Wronskian is defined in (4.50) in terms of the mode function $u(z,\lambda)$, which depends on the potential $V(z)$, and so it appears that $\omega'(\lambda_j)$ must be solved for simultaneously with the system of equations for $V(z)$ and u_j. Although this is possible, there is an elegant approach due to [182] which allows us to independently and efficiently compute $\omega(\lambda_j)$ prior to computing $V(z)$ and u_j.

The main idea is to observe that, from its definition, the function $\omega(\lambda)$ is equal to zero if and only if $\lambda = \lambda_j$. It can then be shown [182] that $\omega(\lambda)$ is an entire function of order $1/2$ and thus by the Hadamard factorization theorem can be written as $\omega(\lambda) = A\prod_i(1-\lambda/\lambda_i)$, where A is some normalization constant which can be determined by considering the large λ limit, in which $\lambda_j \to \tilde{\lambda}_j$ and $u_j \to \tilde{u}_j$. Differentiating and setting $\lambda = \lambda_j$ gives

$$\omega'(\lambda_j) = -\frac{\tilde{u}_j^{(-)}(z_0)}{\lambda_j - \tilde{\lambda}_j}\prod_{i\neq j}^{\infty}\frac{(\lambda_j-\lambda_i)}{(\lambda_j-\tilde{\lambda}_i)} \approx -\frac{\tilde{u}_j^{(-)}(z_0)}{\lambda_j - \tilde{\lambda}_j}\prod_{i\neq j}^{j_{\text{max}}}\frac{(\lambda_j-\lambda_i)}{(\lambda_j-\tilde{\lambda}_i)}, \tag{4.58}$$

[23]The *scale independent* features of the potential $V(z)$, namely the amplitudes of the $1/z^2$ and $1/z$ AdS divergences at the AdS boundaries and the average value of the non-diverging piece of $V(z)$, were determined from the asymptotic (large j) part of the spectrum.

where we have approximated $\lambda_j \approx \tilde{\lambda}_j$ for $j > j_{\text{max}}$. This formula allows us to approximate $\omega'(\lambda_j)$ from quantities that we are given (λ_j) and quantities which we can easily compute ($\tilde{\lambda}_j$ and $\tilde{u}_j$).

4.3.3 Solving for the scale factor from $V(z)$

Having reconstructed the potential V, we now want to obtain the wormhole scale factor by solving the non linear ODE (4.8) for $a(z)$. It is convenient to define the scale factor in AdS units $\tilde{a}(z) = a(z)/L$, in terms of which the ODE takes the form

$$\tilde{a}''(z) + (\alpha - 2)\tilde{a}^3(z) - V(z)\tilde{a}(z) = 0 \tag{4.59}$$

where we used $m^2L^2 = \alpha - 2$, and α is the parameter entering the definition of the test potential. In order to find a unique solution for $\tilde{a}(z)$, we need to impose initial conditions for $\tilde{a}(z)$ and its derivative at some point $z \in (-z_0, z_0)$. However, we only know that the scale factor is symmetric (and therefore $\tilde{a}'(0) = 0$), and that its asymptotic behavior is given by equation (4.4), which in AdS units becomes

$$\lim_{z \to \mp z_0} \tilde{a}(z) = \frac{1}{z_0 \pm z}. \tag{4.60}$$

In general settings and without further assumptions, this information is not enough to uniquely determine the scale factor from a single reconstructed potential. Let us understand this in some more detail.

If the bulk scalar field is massless, which implies $\alpha = 2$, there is a unique symmetric solution to the ODE (4.59) with the correct asymptotics (4.60). In fact, in this case the ODE reduces to a linear ODE. Therefore, given a symmetric solution of the ODE with some initial condition

$\tilde{a}(0)$, all other solutions differ by a multiplicative constant. Only one solution in such family has the correct coefficient (i.e. 1) for the divergent term. We conclude that a single potential associated to a bulk massless scalar field is enough to reconstruct the wormhole geometry. On the other hand, for $\alpha \neq 2$ (corresponding to $m^2 \neq 0$) it is non-trivial to understand whether there is a unique symmetric solution to (4.59) with the correct asymptotics.

In order to shed light on this problem, it is useful to consider the generic ansatz[24]

$$\tilde{a}(z) = \frac{1}{z_0 + z} + \frac{1}{z_0 - z} + R(z) \tag{4.61}$$

where $R(z)$ is a symmetric function, regular in $z \in [-z_0, z_0]$. Suppose we have a solution $\tilde{a}_1(z)$ to the ODE (4.59) of the form (4.61). Let us consider a second solution of the form $\tilde{a}_2(z) = \tilde{a}_1(z) + f(z)$ where $f(z)$ is a symmetric function, regular in $z \in [-z_0, z_0]$. $\tilde{a}_2(z)$ is by construction symmetric and of the form (4.61), i.e. it has the correct asymptotic behavior. Substituting $\tilde{a}_2(z)$ in the ODE (4.59) and using the fact that $\tilde{a}_1(z)$ is also a solution, we find that $f(z)$ must satisfy

$$\begin{cases} \frac{f''(z)}{f(z)} - \frac{\tilde{a}_1''(z)}{\tilde{a}_1(z)} + (\alpha - 2)[f(z) + 2\tilde{a}_1(z)][f(z) + \tilde{a}_1(z)] = 0 \\ f'(0) = 0 \\ f(\pm z_0) < \infty \end{cases} \tag{4.62}$$

For $\alpha = 2$ (massless bulk scalar field), the problem (4.62) has no non-trivial solutions, because all the candidate solutions of (4.62) are proportional to $\tilde{a}_1(z)$, which is divergent at $z = \pm z_0$, and

[24] Note that this is the most generic ansatz giving rise to a potential of the form we are considering (specified in Assumption 3 in Section 4.3.2). In particular, it implements the symmetry of the scale factor and the AdS asymptotic behavior at the two boundaries, while introducing no further divergences in the potential besides the quadratic and linear ones appearing in our assumptions.

therefore violate $f(\pm z_0) < \infty$. This result is supported by our numerical analysis, and confirms our expectation that there is a unique symmetric solution of the ODE (4.59) with asymptotic behavior (4.60) when $\alpha = 2$: the spectrum of a massless scalar field is sufficient to reconstruct the wormhole geometry.

For $\alpha > 2$ (massive, non-tachyonic bulk scalar field, $m^2 > 0$), our numerical analysis suggests that, in general, there are infinitely many solutions to the system (4.62). For example, consider the scale factor[25]

$$\tilde{a}(z) = \frac{1}{z_0 + z} + \frac{1}{z_0 - z} + \cos\left(\frac{2\pi z}{z_0}\right) + \exp\left[-\frac{1}{(z_0^2 - z^2)}\right], \tag{4.63}$$

from which we can easily compute the corresponding potential $V(z)$. However, the system (4.62) then has multiple solutions, only one of which corresponds to the scale factor $\tilde{a}(z)$ which we started with (see Figure 4.1). Without additional information it is not possible to pick out the correct scale factor over the other valid solutions, $\tilde{a}_1, \tilde{a}_2$, etc. Therefore, the solution of the ODE (4.59) is not uniquely determined by symmetry and by the asymptotic behavior (4.60). We can conclude that, for $m^2 > 0$ and without further assumptions on the properties of the scale factor, we cannot reconstruct the wormhole geometry from a single potential $V(z)$, i.e. from a single scalar field spectrum[26].

[25] Note that this form of the scale factor has no particular physical meaning. We included the last term to emphasize that the presence of non-perturbative contributions (at $z = \pm z_0$) does not prevent the existence of multiple solutions. The same result was obtained for several different forms of the scale factor.

[26] If we assume that the regular part of the scale factor $\tilde{a}(z)$ has a convergent asymptotic expansion around $z = \pm z_0$, and that such an expansion converges to $\tilde{a}(z)$ itself, then we can reconstruct the scale factor uniquely by matching its asymptotic expansion with an asymptotic expansion for the reconstructed potential. Numerically, only the first few terms are needed in order to obtain initial conditions at a point $\tilde{z} = -z_0 + a$ (with small but finite a), and then the ODE (4.59) can be solved with such initial conditions. Note that the assumption of a convergent asymptotic series alone is not enough: there might be non-perturbative contributions to the scale factor $\tilde{a}(z)$ (e.g. of the form included in equation (4.63)) which cause the asymptotic expansion to converge to a function $g(z) \neq \tilde{a}(z)$. When this is the case, the asymptotic expansion leads to a wrong reconstructed scale factor.

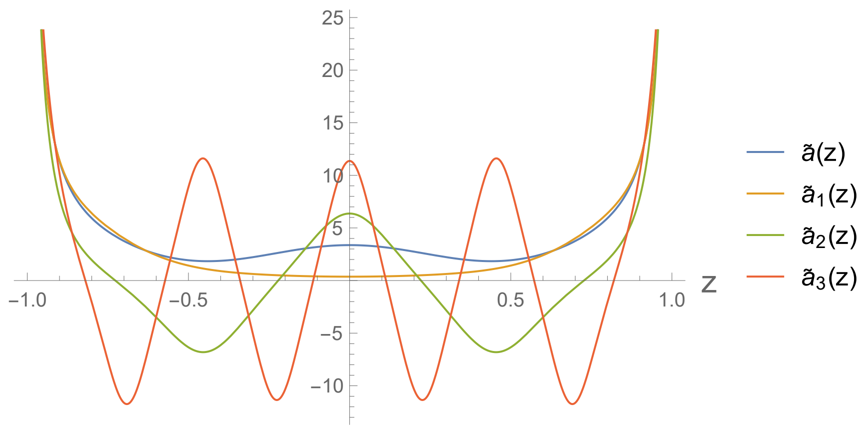

Figure 4.1: Multiple solutions of the ODE (4.59) with potential $V(z)$ defined by the scale factor (4.63), with $z_0 = 1$ and $mL = 3/2$. The solutions displayed are the original scale factor (4.63) $\tilde{a}(z)$, and additional solutions of the form $\tilde{a}_i(z) = \tilde{a}(z) + f_i(z)$, where $f_i(z)$ is a solution of (4.62). In particular, they are solutions of (4.62) with initial conditions $f_1(0) = -3$, $f_2(0) = 3$, $f_3(0) = 8$. The solutions $\tilde{a}_i(z)$ are symmetric and display the asymptotic behavior (4.60). In general, there are infinite solutions of this form.

Finally, for $\alpha < 2$ (tachyonic bulk scalar field, $m^2 < 0$), our numerical analysis suggests that there is no solution of (4.62). Although we have no mathematical proof for the non-existence of a solution of the problem (4.62), the numerical evidence and the fact that multiple solutions of the ODE (4.59) exist for any $\alpha > 2$ but a unique solution exists for $\alpha = 2$ points towards the existence of a unique symmetric solution of the ODE (4.59) with the correct asymptotics (4.60) when $\alpha < 2$. Therefore, we expect that the spectrum of a single tachyonic scalar field is sufficient to reconstruct the wormhole geometry.

From the discussion above we can conclude that, without making additional assumptions about the sign of m^2 or the analyticity of the scale factor, it is not possible to reconstruct the wormhole geometry from a single scalar spectrum. In particular, although for $m^2 \leq 0$ one spectrum is sufficient to reconstruct the scale factor, for $m^2 > 0$ additional data is required to perform the task.

To understand this better, it is useful to look at how multiple solutions differ from each other asymptotically, when they exist (i.e. for $m^2 > 0$). This means to study the form of equation (4.62) when keeping only leading terms near one of the boundaries. Using the ansatz (4.61) for $\tilde{a}_1$ and focusing on the left boundary at $z = -z_0$, we get

$$f''(z) + \frac{2\alpha - 6}{(z + z_0)^2} f(z) = 0. \tag{4.64}$$

Using a power law ansatz $f(z) \sim (z + z_0)^\gamma$ in equation (4.64) we find

$$\gamma_\pm = \frac{1}{2} \pm \frac{\sqrt{9 - 8(\alpha - 2)}}{2} \tag{4.65}$$

where we remind that $\alpha - 2 = m^2L^2$ and that $f(z)$ must be regular at the boundary (i.e. only $\Re(\gamma) \geq 0$ leads to meaningful solutions). An analogous result can be obtained for the right asymptotic boundary at $z = z_0$.

For the $m^2 > 0$ case of interest (where multiple solutions to the ODE (4.59) exist), we can distinguish three cases:

1. For $2 < \alpha < 3$ ($0 < m^2L^2 < 1$) or $\alpha = 25/8$ ($m^2L^2 = 9/8$), there is only one non-negative real value of γ. Therefore in general we get the asymptotic behavior $f(z) \sim c_+(z + z_0)^{\gamma_+}$. This represents a one-parameter family of solutions, and a given solution is determined by a specific value of c_+.

2. For $3 \leq \alpha < 25/8$ ($1 \leq m^2L^2 < 9/8$), there are two non-negative real values of γ. The asymptotic behavior of the general solution is then given by $f(z) \sim c_+(z+z_0)^{\gamma_+} + c_-(z+z_0)^{\gamma_-}$, and we have a two-parameter family of solutions parametrized by (c_+, c_-).

3. For $\alpha > 25/8$ ($m^2L^2 > 9/8$), there are two complex values of γ with positive real part

$\Re(\gamma) = 1/2$. The corresponding asymptotic behavior of the general solution can be written as

$$f(z) \sim c_1(z+z_0)^{\frac{1}{2}} \cos\left[\frac{\sqrt{9-8(\alpha-2)}}{2}\log(z)\right] + c_2(z+z_0)^{\frac{1}{2}} \sin\left[\frac{\sqrt{9-8(\alpha-2)}}{2}\log(z)\right]. \tag{4.66}$$

This represents a two-parameter family of solutions, parametrized by (c_1, c_2).

Since the near-boundary limit of the bulk theory corresponds to the UV limit of the dual microscopic field theory, we expect the short-distance expansions of various field theory quantities (short-distance two-point functions or regularized entanglement entropies for small regions) should contain enough information about the near-boundary behavior of the scale factor to distinguish the possible solutions. In particular, it should be possible to obtain the value of the parameters $c_\pm$ (or $c_{1,2}$) from such short-distance behavior. This would allow one to uniquely reconstruct the wormhole geometry for $m^2 > 0$ using a single scalar spectrum and the UV behavior of the corresponding boundary scalar two-point function. We leave a detailed analysis of this possibility to future work.

Taking a different route, we will now show that if we have access to two scalar field spectra for two non-interacting bulk scalar fields of different mass (for any sign of m^2), the wormhole geometry can be uniquely reconstructed. Note that two spectra are always sufficient to reconstruct the scale factor, but the discussion in the previous paragraphs suggests that they might not be necessary.

Reconstructing the wormhole from two scalar spectra

Let us now assume that we have access to two distinct mass spectra of scalar particles in the dual confining gauge theory, corresponding to two non-interacting scalar fields with different masses in the same wormhole geometry. Suppose that, given the knowledge of the two spectra, we reconstructed the two associated potentials $V_1(z)$ and $V_2(z)$ using the procedure described in the previous subsections. We can then evaluate the ODE (4.59) for the two potentials at $z = 0$, and take their difference. Since $\tilde{a}(z)$ is the same in both equations, and we can obtain the values of α_1, α_2 from the asymptotic spectra, this yields an initial condition for the scale factor at the center of the wormhole:

$$\tilde{a}(0) = \tilde{a}_0 \equiv \sqrt{\left|\frac{V_1(0) - V_2(0)}{\alpha_1 - \alpha_2}\right|}. \tag{4.67}$$

We can now solve the ODE (4.59) for any of the two potentials imposing initial conditions at the center of the wormhole: $\tilde{a}(0) = \tilde{a}_0$, $\tilde{a}'(0) = 0$. This uniquely determines the wormhole scale factor.

It is worth noting that this procedure holds for any form of the scale factor (even in the non-physical case where it is not positive everywhere) and for both signs of m^2. Moreover, since in generic settings we expect to have multiple scalar fields in the wormhole geometry [2, 9], it is reasonable, and in fact to be expected, that we can have access to multiple spectra of scalar particles in the dual confining gauge theory.

4.3.4 Wormhole reconstruction algorithm

Let us summarize the algorithm that allows us to reconstruct the wormhole geometry from two scalar mass spectra in the underlying microscopic theory.[27] These spectra may be given as input data, or they may be obtained from a knowledge of the microscopic correlators, as explained in Section 4.3.1. We will assume that the spectra are of the asymptotic form $\lambda_j \sim Zj^2 + Aj + B\log j + C$, with $Z, A > 0$ and B, C arbitrary. As we have seen, this is a necessary condition for a microscopic spectrum to have a dual description in terms of a free scalar field in a wormhole background. The reconstruction algorithm is as follows:

1. Start with the first spectrum; call it λ_j. Fit the asymptotic values of λ_j to the curve $Zj^2 + Aj + B\log j + C$ and determine the constants Z, A, B, C.

2. Using (4.44)-(4.47) determine z_0, α, β, c, and from (4.38) construct $\tilde{V}(z)$.

3. Choose an integer $j_{\text{max}} > 0$. The wormhole scale factor will be accurately reconstructed on scales larger than z_0/j_{max}.

4. Compute the lowest $j_{\text{max}}+1$ eigenvalues $\tilde{\lambda}_0, \tilde{\lambda}_1, \ldots, \tilde{\lambda}_{j_{\text{max}}}$ by solving the Schrödinger equation

$$-u''(z) + \tilde{V}(z)u(z) = \tilde{\lambda}_j u(z), \tag{4.68}$$

subject to normalizable boundary conditions, $u^{(-)}(\pm z_0) = 0$. We are using $u^{(+)}$ and $u^{(-)}$ to denote the normalizable and non-normalizable components to mode functions; see (4.33).

[27] As discussed above, if we have access to a spectrum associated with a bulk scalar field with $m^2 \leq 0$, there is no need for a second spectrum. We can therefore skip step 10, and solve the ODE (4.59) imposing that the scale factor is symmetric and has the correct asymptotics (4.60).

5. Define $\bar{\Delta} \equiv \sqrt{\alpha + 1/4}$. For $0 \leq j \leq j_{\text{max}}$ compute $\tilde{u}_j(z)$ by solving

$$\tilde{u}_j''(z) = \left[\tilde{V}(z) - \lambda_j\right]\tilde{u}_j(z), \tag{4.69}$$

subject to the initial conditions

$$\tilde{u}_j^{(+)}(-z_0) = \frac{1}{2\bar{\Delta}}, \tag{4.70}$$

$$\tilde{u}_j^{(-)}(-z_0) = 0. \tag{4.71}$$

6. For $0 \leq j \leq j_{\text{max}}$, obtain $\omega'(\lambda_j)$ from (4.58).

7. For $0 \leq j \leq j_{\text{max}}$, define $\tilde{y}_j(z) \equiv 2\frac{\tilde{u}_j(-z)-(-1)^j\tilde{u}_j(z)}{\omega'(\lambda_j)}$.

8. Determine $u_0, u_1, \ldots, u_{j_{\text{max}}}$ by solving the system of equations

$$u_j''(z) = \left(\tilde{V}(z) + \sum_{i=0}^{j_{\text{max}}}\left[\tilde{y}_i(z)u_i(z)\right]' - \lambda_j\right)u_j(z) \tag{4.72}$$

subject to the boundary conditions

$$u_j^{+}(-z_0) = \frac{1}{2\bar{\Delta}}, \tag{4.73}$$

$$u_j^{-}(-z_0) = 0. \tag{4.74}$$

9. Obtain the potential by setting

$$V(z) = \tilde{V}(z) + \frac{1}{2}\sum_{j=0}^{j_{\max}} \Big(\big[\tilde{y}_j(z)u_j(z)\big]' + \big[\tilde{y}_j(-z)u_j(-z)\big]' \Big). \tag{4.75}$$

Here we have ensured by hand that the reconstructed $V(z)$ is symmetric, since this is not automatically true for finite $j_{\max}$.[28]

10. Repeat steps 1-9 to reconstruct the potential associated with the second spectrum. Now we have reconstructed two potentials, $V_1(z)$ and $V_2(z)$, from the respective asymptotic spectra. The value of the scale factor at the center of the wormhole is then given by

$$\tilde{a}(0) = \tilde{a}_0 \equiv \sqrt{\left|\frac{V_1(0) - V_2(0)}{\alpha_1 - \alpha_2}\right|} \tag{4.76}$$

where $\tilde{a}(z) = a(z)/L$.

11. Compute the wormhole scale factor by solving

$$\begin{cases} \tilde{a}''(z) + (\alpha - 2)\tilde{a}^3(z) - V(z)\tilde{a}(z) = 0 \\ \tilde{a}(0) = \tilde{a}_0 \\ \tilde{a}'(0) = 0 \end{cases} \tag{4.77}$$

12. Finally, if one is interested in the corresponding FRW scale factor, it can be obtained by analytic continuation. Numerically this can be approximated by flipping the sign of every

[28]We would like the approximate potential to be symmetric so that the resulting scale factor in the wormhole picture is symmetric and thus the analytically continued scale factor in the cosmology picture is real.

other non-zero term in the Taylor expansion of $\tilde{a}(z)$ around $z = 0$. Namely,

$$\tilde{a}_{\text{FRW}}(t) \approx \sum_n \frac{(-1)^{n/2}}{n!} \frac{d^{2n}\tilde{a}(z)}{dz^{2n}}\Big|_{z=0} t^{2n}. \tag{4.78}$$

4.3.5 Numerical example of wormhole reconstruction

In this subsection we provide an explicit example of implementation of the reconstruction algorithm summarized in Section 4.3.4. The scale factor we wish to reconstruct has the analytic form[29]

$$\tilde{a}(z) = \frac{1}{z_0 + z} + \frac{1}{z_0 - z} + 2\cos\left(\frac{2\pi z}{z_0}\right) \tag{4.79}$$

where we set $z_0 = 1$. As a first step, we need to compute the asymptotic spectra of two potentials $V_1(z)$ and $V_2(z)$ of the form

$$V(z) = \frac{a''(z)}{a(z)} + m^2L^2a^2(z) \tag{4.80}$$

for two different choices of mL, and the first few eigenvalues of the same potentials, i.e. $\lambda_j^{(1)}$, $\lambda_j^{(2)}$ for $j < j_{max}$. This data will serve as input for the reconstruction procedure. Our choices of masses is $m_1L = 1/2$, $m_2L = 3/2$, and we choose $j_{\text{max}} = 50$, i.e. we reconstruct the potentials from their first 51 eigenvalues. The first step in our algorithm is to fit the asymptotic spectra as in equation (4.39) (see Figure 4.2). Using equations (4.44), (4.45), (4.46) and (4.47), this yields

[29] In this explicit example we did not include non-perturbative terms for the sake of numerical efficiency. Note that this scale factor does not have any specific physical meaning, and in particular it does not analytically continue to a Big Bang-Big Crunch cosmological scale factor. However, it is simple enough for the reconstruction to not be computationally too expensive, while its behavior is non-trivial enough to make the reconstruction example significant.

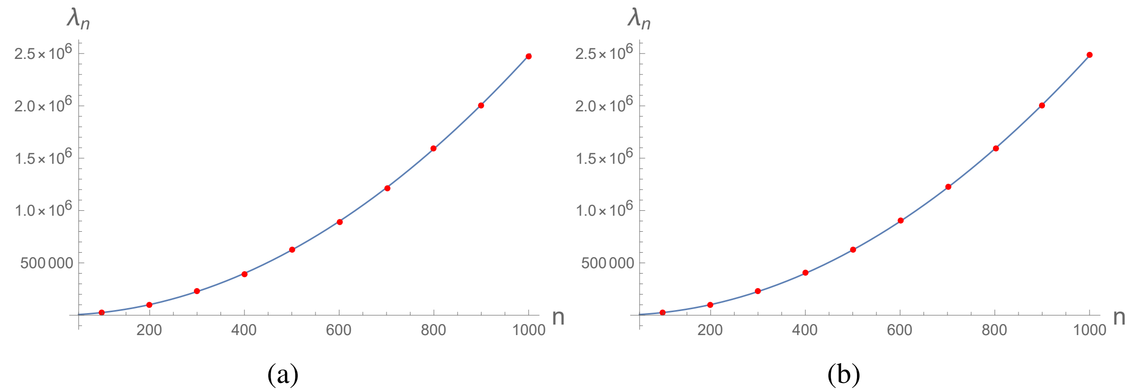

Figure 4.2: Asymptotic spectra generated by the potentials (4.80) for $\tilde{a}(z)$ given by (4.79). The fitted data also include all eigenvalues with $j \in [80, 99]$ and $j \in [901, 999]$, omitted in the plots. (a) $mL = 1/2$. The result of the fit is $Z_1 = 2.467401$, $A_1 = 10.270160$, $B_1 = -3.737523$, $C_1 = 39.926397$. (b) $mL = 3/2$. The result of the fit is $Z_2 = 2.467401$, $A_2 = 12.934720$, $B_2 = 6.267183$, $C_2 = 36.382785$.

$z_0 = 1$ for both spectra and the parameters of the test potentials (4.38):

$$\begin{aligned} &\alpha_1 = 2.250097, \qquad \beta_1 = -3.737523, \qquad c_1 = 33.996971; \\ &\alpha_2 = 4.249159, \qquad \beta_2 = 6.267183, \qquad c_2 = 21.274552. \end{aligned} \tag{4.81}$$

We can then compute the first 51 eigenvalues of the two test potentials defined as in (4.38), and apply the rest of the algorithm described in Section 4.3.4 to reconstruct the two potentials $V_1(z)$ and $V_2(z)$ from their spectra. Plots of the reconstructed potentials, together with the respective test potentials (4.38) and the exact potentials computed directly from the scale factor (4.79) are reported in Figure 4.3. The reconstructed potentials match the exact potentials up to corrections of order $1/j_{max} \sim 10^{-2}$, as expected.

We have now completed steps 1-9 of the reconstruction algorithm of Section 4.3.4 for two spectra, and reconstructed the two potentials $V_1(z)$ and $V_2(z)$ to good accuracy. The last two steps allow us to obtain the wormhole scale factor from such potentials. First, we must obtain the initial condition $\tilde{a}(0) = \tilde{a}_0$ as in equation (4.67). We could do this by directly subtracting $V_1^{rec}(0)$

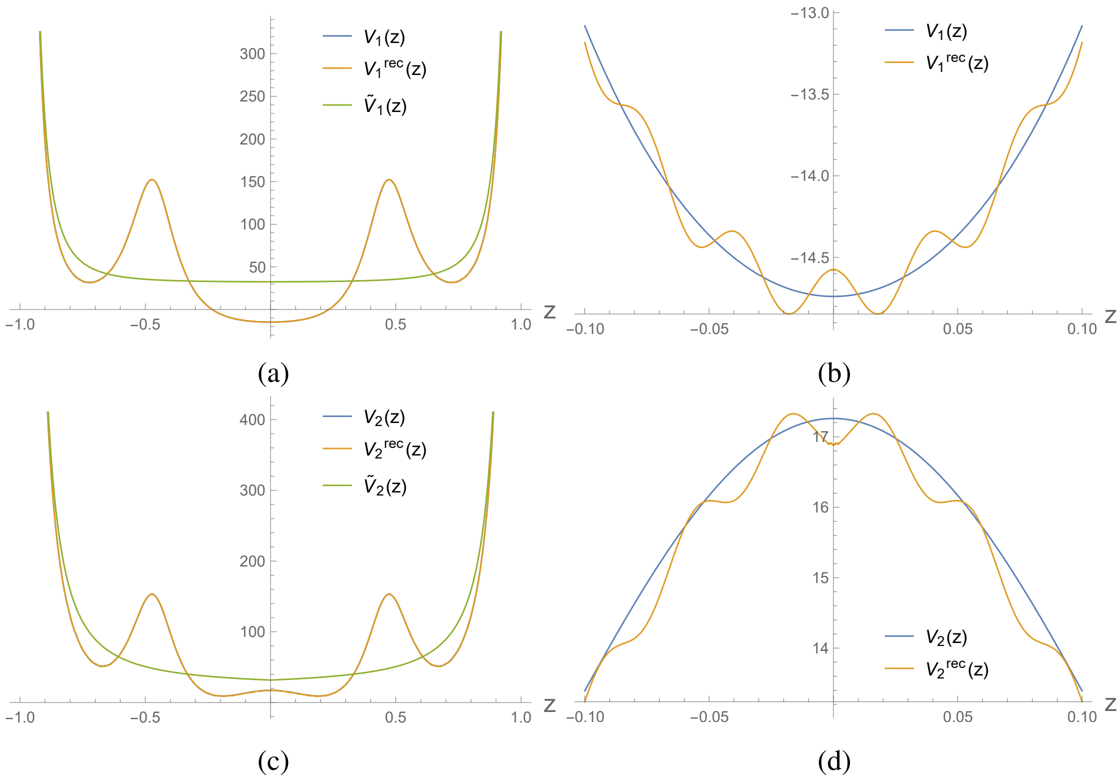

Figure 4.3: True potentials $V_i(z)$ (computed by equation (4.80) with $\tilde{a}(z)$ given by (4.79)), reconstructed potentials $V_i^{rec}(z)$, and test potentials $\tilde{V}_i(z)$ (given by equation (4.38) with parameters (4.81)) as a function of z. (a) $V_1(z)$, $V_2^{rec}(z)$, and $\tilde{V}_1(z)$ for $mL = 1/2$. (b) Detail of $V_1(z)$ and $V_1^{rec}(z)$ around $z = 0$ for $mL = 1/2$. As expected, the reconstructed potential is a good approximation to the true potential up to corrections of order $1/j_{max} \sim 10^{-2}$. (c) $V_2(z)$, $V_2^{rec}(z)$, and $\tilde{V}_2(z)$ for $mL = 3/2$. (d) Detail of $V_2(z)$ and $V_2^{rec}(z)$ around $z = 0$ for $mL = 3/2$. As expected, the reconstructed potential is a good approximation to the true potential up to corrections of order $1/j_{max} =\sim 10^{-2}$.

from $V_2^{rec}(0)$, which would already allow us to obtain the initial condition to good accuracy, and obtain a good reconstruction of the wormhole scale factor. However, note that the reconstructed potentials have an oscillating behavior around $z = 0$, because we only used a finite amount of eigenvalues to perform the reconstruction (see Figure 4.3). Therefore, we can further improve the accuracy of the initial condition by averaging $V_1^{rec}(z)$ and $V_2^{rec}(z)$ over one oscillation period around $z = 0$, and then using such average values in place of $V_1^{rec}(0)$, $V_2^{rec}(0)$ in (4.67). Using this procedure and the values (4.81) of α_1 and α_2, we obtain $\tilde{a}_0 = 3.989952$, where the exact value is $\tilde{a}_0^{true} = 4$ (note that the error is again of order $1/j_{max}$, as expected). Finally, we can solve the ODE (4.59) for either $V_1(z)$ or $V_2(z)$ with initial conditions $\tilde{a}(0) = \tilde{a}_0$, $\tilde{a}'(0) = 0$, and obtain the wormhole scale factor. The numerically reconstructed $\tilde{a}_{rec}(z)$ is reported in Figure 4.4 along with the exact scale factor (4.79). The two agree with very good accuracy, up to corrections of order $1/j_{max}$.

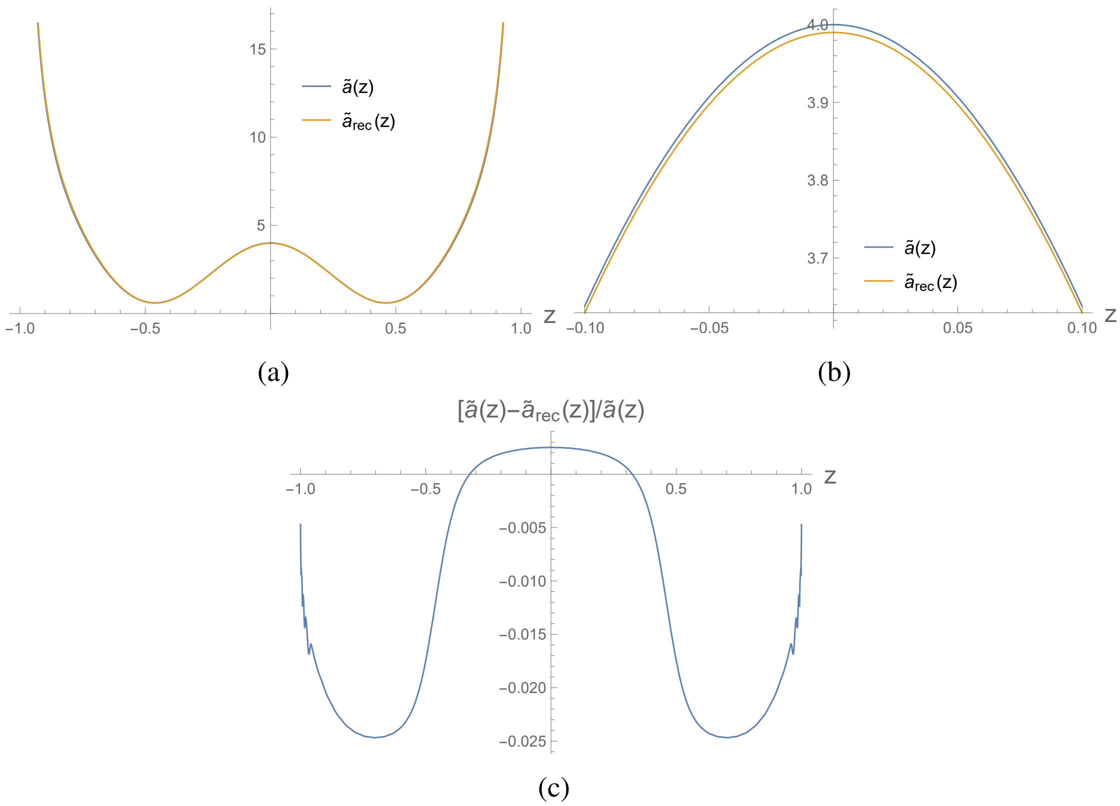

Figure 4.4: True scale factor $\tilde{a}(z)$ (given by equation (4.79)) and reconstructed scale factor $\tilde{a}_{rec}(z)$ as a function of z. (a) The scale factors are almost indistinguishable at large scales. (b) Detail around the center of the wormhole at $z = 0$. (c) Discrepancy between the true scale factor and the reconstructed scale factor, quantified by $[\tilde{a}(z) - \tilde{a}_{rec}(z)]/\tilde{a}(z)$. As expected, the reconstruction is accurate up to corrections of order $1/j_{max} \sim 10^{-2}$.

4.3.6 Scale factor from heavy correlators

In the previous sections we have shown how to reconstruct the wormhole geometry given certain information about the dual confining gauge theory. In particular we found that the reconstruction is possible if we are given two sets of microscopic correlators, associated with 3D CFT scalar operators $\mathcal{O}_1$ and $\mathcal{O}_2$ of different scaling dimensions. The duals of these operators are scalar fields of different masses living in the wormhole geometry. So far we have not assumed anything about the masses of these scalar fields, i.e. we have made no restrictions on the dimensions of the microscopic operators.

However, we will now see that the situation is much simpler if we have access to the two-point correlator of a heavy operator $\mathcal{O}$, i.e. an operator with a large scaling dimension. Namely we will find that a knowledge of this correlator is sufficient to reconstruct the wormhole geometry; there is no need for additional information from a different operator.

The key observation which allows for such a simplification is to note that for a scalar field of large mass m the spatial two-point function in the wormhole is given approximately by

$$\langle\phi(x)\phi(y)\rangle \sim e^{-mL(x,y)}, \tag{4.82}$$

where L is the geodesic distance between x and y. Via the extrapolate dictionary, this leads to a spatial two-point function

$$\langle\mathcal{O}(w)\mathcal{O}(0)\rangle \sim e^{-mL(w)} \tag{4.83}$$

for the heavy operator $\mathcal{O}$ dual to the field ϕ, where L is the regulated length of the geodesic. See [184] for a review. Since geodesics are manifestly associated with the geometry of the spacetime, it seems plausible that a knowledge of various geodesic lengths via the correlators of $\mathcal{O}$ is enough information to explicitly reconstruct the wormhole. We will now show that this is indeed the case. The discussion is similar to [263] though our final approach is somewhat different and we get a more explicit result.

Let us begin by expressing the wormhole metric in the form

$$ds^2 = A^2(z)dz^2 + B^2(z)dx_\mu dx^\mu. \tag{4.84}$$

This can be mapped to the familiar conformally flat gauge by changing to a coordinate $\tilde{z}$ defined by $Adz = Bd\tilde{z}$. Letting x be one of the spatial coordinates of the field theory, we have that spatial geodesics $z(x)$ lying in the $z - x$ plane are determined by extremizing the action

$$S = \int dz \sqrt{A^2(z) + B^2(z)\left(\frac{dx}{dz}\right)^2}\,. \tag{4.85}$$

The conserved quantity associated with translation invariance in the x direction is

$$p_x = \frac{\partial \mathcal{L}}{\partial x'} = \frac{B^2(z)}{\sqrt{A^2(z)\left(\frac{dz}{dx}\right)^2 + B^2(z)}}. \tag{4.86}$$

While the action itself (giving the length of a geodesic) diverges, the variation of the action with respect to one of the endpoints is finite. We recall that the variation of the action about an on shell configuration with respect to an endpoint variation δx_i in the direction x_i can be expressed as

$$\delta S = p_i \delta x_i\ . \tag{4.87}$$

Taking x_i to be the direction x we find

$$\frac{\delta S}{\delta x} = p_x. \tag{4.88}$$

For geodesics with two endpoints at the same asymptotic boundary separated by w, there will be some deepest point $z_*(w)$ to which the geodesic penetrates. At this point, $dz/dx = 0$, so from (4.86) we have that $p_x = B(z_*)$. Thus, we have the relation

$$B(z_*) = \frac{\delta S}{\delta x} \equiv S_1(w). \tag{4.89}$$

The right side here can be computed from CFT data. Namely, the regulated version of the geodesic length S is given by $L(w)$ and so using the heavy correlator (4.83) we obtain

$$S_1(w) = -\frac{1}{m}\frac{d}{dw}\ln\langle\mathcal{O}(w)\mathcal{O}(0)\rangle. \tag{4.90}$$

Now, using $p_x = B(z_*)$ and (4.86) gives us an equation for dx/dz which can be integrated along half the geodesic curve to obtain another relation between w and z_*. Namely

$$w/2 = \int_{z_\infty}^{z_*} dz \frac{A(z)}{B^2(z)} \frac{1}{\sqrt{\frac{1}{B^2(z_*)} - \frac{1}{B^2(z)}}}, \tag{4.91}$$

where z_∞ is the asymptotic value of the coordinate z.[30] By a choice of gauge, we can take $B(z)$ to be any convenient function. In this case, the CFT data $S_1(w)$ and the known function $B(z)$ can be used in equation (4.89) to write w on the left side of (4.91) as some function of z_*. The equation (4.91) can then be understood as an integral equation (specifically, a weakly singular Volterra equation of the first kind) for the remaining undetermined metric function $A(z)$.

[30]This assumes that z increases toward the interior. Otherwise the limits of integration would be reversed.

The integral equation

$$f(s) = \int_a^s \frac{y(t)dt}{\sqrt{g(s) - g(t)}} \tag{4.92}$$

for $y(t)$ has solution

$$y(s) = \frac{1}{\pi} \frac{d}{ds} \left[\int_a^s dt \frac{f(t)g'(t)}{\sqrt{g(s) - g(t)}} \right]. \tag{4.93}$$

Applying this to our case, we have that

$$A(z) = -\frac{1}{\pi} B^2(z) \frac{d}{dz} \left[\int_{z_\infty}^z d\hat{z} \frac{w(\hat{z}) B(z) B'(\hat{z})}{B^2(\hat{z}) \sqrt{B^2(\hat{z}) - B^2(z)}} \right] \tag{4.94}$$

Via this equation and (4.89), we are able to fully determine the metric in terms of the heavy microscopic two-point function.

We can make things more explicit by choosing the function $B(z)$ to be equal to $S_1(z)$. In this case, from (4.89) we have

$$S_1(z_*) = S_1(w), \tag{4.95}$$

so we have $z_* = w$. Thus, our choice of B corresponds to taking the z coordinate of a point in the wormhole to be the width of a CFT interval whose geodesic penetrates to that point. Then, from (4.94) we have

$$A(w) = -\frac{1}{\pi} S_1^2(w) \frac{d}{dw} \left[\int_0^w d\hat{w} \frac{\hat{w} S_1(w) S_1'(\hat{w})}{S_1^2(\hat{w}) \sqrt{S_1^2(\hat{w}) - S_1^2(w)}} \right], \tag{4.96}$$

and the metric is given by

$$ds^2 = A^2(w) dw^2 + S_1^2(w) dx_\mu dx^\mu. \tag{4.97}$$

In this way, we have explicitly expressed the metric in terms of the microscopic data encoded in the function $S_1(w)$ via equation (4.90).

The form (4.97) of the reconstructed metric suggests the change of variables

$$\mu(w) = -\frac{1}{\pi}\left[\int_0^w d\hat{w}\frac{\hat{w}S_1(w)S_1'(\hat{w})}{S_1^2(\hat{w})\sqrt{S_1^2(\hat{w})-S_1^2(w)}}\right] . \tag{4.98}$$

In terms of this radial coordinate, we have simply

$$ds^2 = S_1^4(w(\mu))d\mu^2 + S_1^2(w(\mu))dx_\mu dx^\mu . \tag{4.99}$$

4.3.7 Metric from entanglement entropy

Via a very similar analysis, we could also extract the metric from the entanglement entropy for a strip-shaped subsystem of one of the 3D CFTs.[31]

We consider the entanglement entropy of a strip of width w in one of the 3D CFTs. We assume that the result is well approximated by the area of a RT surface in the dual 4D traversable wormhole.[32]

The entanglement entropy has the usual UV divergence but also an IR divergence due to the infinite volume of the strip. We consider the quantity

$$s_1(w) = \frac{d}{dw}s(w) \tag{4.100}$$

[31]To be precise, we should also include some part of the 4D CFT here, but since this has many fewer local degrees of freedom, we expect that the precise choice if this region shouldn't matter too much.

[32]This expectation could be modified significantly if the volume of the internal space present in the UV-complete realization of our setup changes with radial position.

where $s(w)$ is the entanglement entropy per unit of length of the strip. In this case, it will be convenient to take the metric as

$$ds^2 = \frac{A^2(z)}{B(z)}dz^2 + B(z)dx_\mu dx^\mu \ , \tag{4.101}$$

where A and B are in general different than the similarly named functions in Section 4.3.6. With this choice, the expression for the action determining the extremal surface trajectory is precisely the same as the expression (4.85) that we used in the previous section. Precisely the same analysis then tells us that if we choose $B(z) = s_1(z)$, such that z is identified with w (i.e. the width of a strip whose RT surface barely reaches our point z^*), then the remaining metric function is

$$A(w) = -\frac{1}{\pi}s_1^2(w)\frac{d}{dw}\left[\int_0^w d\hat{w}\frac{\hat{w}s_1(w)s_1'(\hat{w})}{s_1^2(\hat{w})\sqrt{s_1^2(\hat{w})-s_1^2(w)}}\right]. \tag{4.102}$$

However, differently from Section 4.3.6, the final metric is

$$ds^2 = \frac{A^2(w)}{s_1(w)}dw^2 + s_1(w)dx_\mu dx^\mu. \tag{4.103}$$

In this case, a change of variables analogous to (4.98) with $S_1 \to s_1$ gives

$$ds^2 = s_1^3(w(\mu))d\mu^2 + s_1(w(\mu))dx_\mu dx^\mu. \tag{4.104}$$

4.4 Discussion

In this paper we have investigated the relationship between observables in a bulk theory with an AdS planar eternal traversable wormhole background geometry and observables in the corresponding dual confining microscopic theory. We have studied what properties of the microscopic theory can be deduced from the existence of a bulk dual wormhole, and, conversely, how the wormhole geometry can be reconstructed from observables in the microscopic theory.

The presence of the wormhole determines specific properties of the dual microscopic theory: spectrum of massive particles, existence of a massless sector, properties of two-point functions, and entanglement structure. In particular, the behavior of bulk quantum scalar and gauge fields implies the existence of a discrete spectrum of massive scalar and vector particles, along with a massless sector (associated with bulk gauge fields).

On the other hand, certain observables in the microscopic confining theory (two-point functions of two 3D CFT scalar operators with different scaling dimensions, correlators of 3D CFT operators with large scaling dimensions, and entanglement entropies of subregions of the microscopic theory) allow one to reconstruct the dual wormhole geometry. A central result of the paper is the explicit algorithm we derived to reconstruct the wormhole metric from two-point functions of 3D CFT scalar operators.

Finally, although the results just outlined are interesting in their own right, we would like to also emphasize two consequences they have on the Big Bang-Big Crunch FRW cosmologies related to our wormhole theory by double analytic continuation [2, 8, 9].

First, the existence of a massless sector in the dual confining theory implies the existence of long-range correlations in its ground state, which was not obvious a priori. In the bulk effective field theory, this translates to correlations at every scale in the wormhole background along the non-compact directions. Since the $z = t = 0$ codimension-2 surface is left invariant by the double analytic continuation relating the wormhole to the FRW cosmological universe [2, 9], this fact implies the existence of correlations at every scale in the cosmology at the (late) time-symmetric point where the universe stops expanding and starts re-collapsing. Therefore, the special state of the cosmology at the time-symmetric point (defined by the Euclidean path integral described in [2]) has built-in correlations even between regions that are never in causal contact at any point in the cosmological evolution. This feature helps to solve the cosmological horizon problem in terms of the properties of the underlying microscopic theory, without the need for inflation [2, 9].

Second, as we have already pointed out, the slicing duality implies that the FRW metric can be obtained from microscopic confining gauge theory observables by reconstructing the wormhole geometry, and then analytically continuing the resulting scale factor. Note that, if we do not make use of the slicing duality, the FRW universe is encoded in a very complex way into the physics of a specific highly excited state of only the microscopic 4D auxiliary degrees of freedom coupling the two 3D CFTs [1, 2, 5, 8]. In fact, in a doubly holographic setup, where the auxiliary degrees of freedom are also holographic, the cosmology can be understood as living on an end-of-the-world (ETW) brane behind the horizon of a 5D black hole [1, 5]. Without relying on double holography, the cosmology can be seen as an "entanglement island" associated with large subregions of the 4D auxiliary system [2]. In both interpretations, reconstructing the cosmological evolution using observables in the excited state of the 4D auxiliary system requires computing expectation values of extremely complicated field theory operators[33]. Nonetheless, by means of

[33]It has been shown in [5] that the entanglement entropy at early times of sufficiently large subregions of the boundary field theory can probe the cosmological scale factor. In fact, the RT surface associated with such subregions penetrates the black hole horizon and ends on the ETW brane, in analogy with the analysis of Hartman and Maldacena [143].

the slicing duality, the cosmological evolution can be probed by reconstructing the corresponding wormhole geometry using confining field theory observables as simple as the spectrum of massive particles or two-point functions of operators with large scaling dimension, and then analytically continuing the scale factor. This fact shows explicitly how the slicing duality introduced in [2,8] allows one to relatively easily reconstruct holographic cosmologies which would naively be extremely complex to probe.

Acknowledgements

We would like to thank Rodrigo A. Silva and Wucheng Zhang for helpful discussions and comments. This work is supported in part by the National Science and Engineering Research Council of Canada (NSERC) and in part by the Simons foundation via a Simons Investigator Award and the "It From Qubit" collaboration grant. PS is supported by an NSERC C-GSD award. SA is partially supported by a Leon A. Herreid Science Graduate Fellowship Award. This work is partially supported by the U.S. Department of Energy, Office of Science, Office of Advanced Scientific Computing Research, Accelerated Research for Quantum Computing program "FAR-QC" (SA) and by the AFOSR under grant number FA9550-19-1-0360 (BS).

Chapter 5: $\Lambda < 0$ accelerating cosmologies with AdS wormhole continuations

Authors:[1] *Stefano Antonini, Petar Simidzija, Brian Swingle, Mark Van Raamsdonk, Chris Waddell.*

Abstract: A large class of $\Lambda < 0$ cosmologies have big-bang / big crunch spacetimes with time-symmetric backgrounds and asymptotically AdS Euclidean continuations suggesting a possible holographic realization. We argue that these models generically have time-dependent scalar fields, and these can lead to realistic cosmologies at the level of the homogeneous background geometry, with an accelerating phase prior to the turnaround and crunch. We first demonstrate via explicit effective field theory examples that models with an asymptotically AdS Euclidean continuation can also exhibit a period of accelerated expansion without fine tuning. We then show that certain significantly more tuned examples can give predictions arbitrarily close to a ΛCDM model. Finally, we demonstrate via an explicit construction that the potentials of interest can arise from a superpotential, thus suggesting that these solutions may be compatible with an underlying supersymmetric theory.

[1]Originally published as *Accelerating cosmology from $\Lambda < 0$ gravitational effective field theory*, e-Print: 2212.00050 (accepted for publication, JHEP), [4]. The appendices of the paper are reported in Appendix D.

5.1 Introduction

In this paper, we consider the viability of models of cosmology based on gravitational effective theories associated to a dual CFT via the AdS/CFT correspondence. These EFTs have a negative extremum in their scalar potential (the negative cosmological constant, $\Lambda < 0$) with an associated stable AdS solution. But they also have cosmological solutions of FRW form, including flat big bang matter/radiation cosmologies. Naively, these wouldn't be realistic because of the negative cosmological constant. However, we will argue via examples that in the solutions that are most likely to have a holographic description, there will generically be time-dependent scalar fields whose potential energy can give rise to an accelerating phase in the cosmology without significant fine-tuning. We will show further that the resulting scale factor evolution can be realistic.

The initial motivation to study cosmological models based on EFTs with holographic duals is the goal of finding a complete quantum gravity for *some* four-dimensional big bang cosmology, realistic or not. Since some solutions of these $\Lambda < 0$ effective theories have a known microscopic description via holography, it is plausible that holographic tools may play a role in coming up with a microscopic description of the cosmological solutions as well.[2]

There is a strong hint for how holography might play a role: cosmological solutions with $\Lambda < 0$ and some combination of matter and radiation are time-symmetric big-bang / big-crunch spacetimes whose analytic continuation are real geometries with asymptotically AdS regions for Euclidean time $\tau \to \pm\infty$; following [13] we will refer to these geometries as wormholes (see [264] for an early study of accelerating cosmologies in similar setups). This suggests a picture

[2]On the other hand, it is presently much less clear how models with a positive cosmological constant can be given a microscopic description; see [97, 98, 100–102, 107, 109, 110, 218] for various approaches.

where the Euclidean theory is defined holographically via a pair of 3D CFTs and observables in the cosmology are related by analytic continuation to observables in this Euclidean theory. We have suggested a possible framework for this description in [1,2,5,8,9], but we will not assume this in the present paper.[3]

The existence of dual CFTs associated to the asymptotically AdS regions in the Euclidean solution suggests that the solutions will often also have non-trivial scalar fields [2, 10]. Scalars with $m^2 < 0$ will be present in the effective field theory in the fairly generic situation that the CFTs have relevant scalar operators.[4] These scalar fields vanish at the asymptotically AdS boundary, but in the most generic asymptotically AdS solutions, the $m^2 < 0$ scalars turn on as we move away from the boundary. This is associated with RG flow in the dual CFT. The radial dependence of the scalar field in the wormhole translates to a time-dependence of the scalar field in the cosmology.

The main goal of this paper is to show that these scalar fields can naturally give rise to an accelerating period in the cosmology, and that in some cases, the acceleration can be realistic, with the cosmological scale factor matching arbitrarily well with the scale factor of conventional models that provide a good fit to observational data.[5]

A typical potential for a scalar field associated with a relevant CFT operator is shown in Figure 5.1 (left). The negative m^2 gives the quadratic decrease in V for small ϕ, while the eventual increase is due to the interaction terms that would typically be present; for example, a higher-order polynomial potential should eventually be positive and growing if the EFT is stable.

In the Euclidean solution, the evolution of the scalar field from the middle of the wormhole

[3] Possible holographic constructions must address the factorization puzzle [13]; suggested resolutions include considering an ensemble of CFTs or a direct interaction between the CFTs [7, 13, 221].

[4] Recall that the scalar masses are related to operator dimensions by $m^2 L^2_{\text{AdS}} = \Delta(\Delta - 3)$.

[5] See [265] for an early study of accelerating negative Λ cosmologies compatible with data.

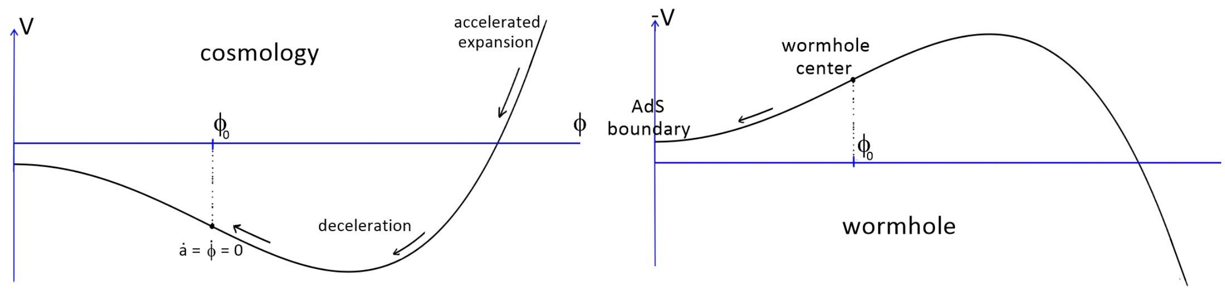

Figure 5.1: Evolution of the scalar field in a typical potential in the cosmology and its Euclidean continuation.

to the AdS boundary corresponds to the damped motion of a particle in the potential $-V$ with damping constant $3a'/a \equiv 3(da/d\tau)/a$. In order for this extremum to be associated with a stable AdS solution, we must satisfy the Breitenlohner-Freedmann bound $V'' > -9/(4L_{AdS}^2)$, which turns out to correspond to the fact that the motion of the scalar field towards the extremum is overdamped. Thus, the simplest evolution of the scalar in the wormhole is a simple monotonic evolution from a lower value of the potential (i.e. a higher value of $-V$) at the middle to the higher extremal value at the boundaries, as shown in Figure 5.1 (right).

In the cosmology, the value of the scalar at the time-symmetric point is the same as the value of the scalar at the middle of the Euclidean wormhole. The evolution back towards the big bang or forwards towards the big crunch corresponds to the anti-damped motion of the scalar in the potential V, initially moving in the direction towards the positive part of the potential. In many cases, the scalar will reach the positive region of the potential before the scale factor goes to zero, so part of the cosmological evolution has positive dark energy.

This opens up the possibility that some of these $\Lambda < 0$ models might exhibit an accelerating phase (as we have argued in [2,9]). To check this, we study various explicit examples in Section 5.2. We first verify that solutions based on the scalar evolution shown in Figure 5.1 can lead to periods of accelerated expansion in the cosmology without excessive fine-tuning. We find examples of simple potentials that give rise to acceleration for generic values of their parameters, meaning in a codimension zero region of the parameter space.

Next, we check that by taking an appropriately chosen potential, we can find models with acceleration where the scale factor is arbitrarily close to ΛCDM or wCDM models for the past evolution. These models are finely tuned, but we include them as a demonstration that the framework can in principle give results consistent with observations. For realistic cosmology, we want to match observations, not ΛCDM, and this requirement allows a much broader class of potentials. We return to this point in the discussion.

If the effective field theory describing cosmology is related to some underlying CFT, an interesting possibility is that this CFT and the corresponding effective theory is supersymmetric,[6] and that this supersymmetry is broken in the cosmology by the time-dependent scalar field expectation value. The physics of such a model is surely very complicated. If the underlying effective theory is some gauged supergravity, the scalar expectation value would break gauge symmetry and supersymmetry, and the low energy effective field theory relevant to the cosmology would arise via RG flow in which various fields would become strongly coupled (as in QCD). We will not attempt to understand any of these things here, but ask instead a fairly naive question: can the scalar potentials giving rise to realistic time-symmetric cosmologies with asymptotically AdS Euclidean continuations arise from a superpotential in a supersymmetric effective field theory? In Section 5.3, we find that the answer is yes, providing an algorithm to construct a superpotential that yields the right behavior of the scalar potential for the range of scalar field values present in the cosmological solutions.

[6]It has been conjectured that holographic CFTs with standard dual gravitational effective field theories must be supersymmetric [266], though this is not proven or widely accepted.

The results of this paper are explorations to see what is possible at the level of effective field theory; we have not attempted to investigate whether the detailed potentials giving rise to realistic cosmological backgrounds can arise from microscopic constructions in string theory. But the fact that $\Lambda < 0$ effective theories are not immediately ruled out suggests that cosmological models with asymptotically AdS continuations (and thus potential holographic descriptions) have a chance of being realistic. We discuss various directions for further investigation in Section 5.4.

5.2 Accelerating cosmologies from asymptotically AdS Euclidean geometries

Throughout this paper, we will consider spatially flat cosmological solutions

$$ds^2 = -dt^2 + a(t)^2 d\vec{x}^2 \tag{5.1}$$

of $\Lambda < 0$ effective field theories. For simplicity, we will consider models with a single scalar field with potential $V(\phi)$. Allowing matter and radiation, the equations of motion are

$$\ddot{\phi} + 3H\dot{\phi} + \frac{dV}{d\phi} = 0\,, \qquad H^2 = \frac{8\pi G}{3}\left[\frac{1}{2}\dot{\phi}^2 + V(\phi) + \frac{\rho_R}{a^4} + \frac{\rho_M}{a^3}\right]\,, \tag{5.2}$$

where $H = \dot{a}/a$.

The solutions we are interested in are time-symmetric and arise via analytic continuation from real Euclidean solutions

$$ds^2 = d\tau^2 + a_E(\tau)^2 d\vec{x}^2 \tag{5.3}$$

For the Euclidean solution, the equations of motion are

$$\phi_E'' + 3H_E\phi_E' - \frac{dV}{d\phi_E} = 0\,, \qquad H_E^2 = \frac{8\pi G}{3}\left[\frac{1}{2}(\phi_E')^2 - V(\phi_E) - \frac{\rho_R}{a_E^4} - \frac{\rho_M}{a_E^3}\right]\,, \tag{5.4}$$

where $a_E(\tau) = a(i\tau)$, $\phi_E(\tau) = \phi(i\tau)$, and $H_E(\tau) = H(i\tau)$.

We would like to find potentials $V(\phi)$ and solutions $a(t), \phi(t)$ with the following properties:

- The scale factor evolution matches observational constraints, including a recent phase of accelerated expansion
- The solution is time-reversal symmetric about a recollapse point.
- The analytic continuation of the solution (taking $t \to i\tau$ where $t = 0$ is the recollapse point) is asymptotically AdS for $\tau = \pm\infty$.
- The scalar field satisfies the Breitenlohner-Freedman (BF) bound $V'' > -9/(4L_{AdS}^2)$ at the two asymptotic AdS boundaries in the Euclidean solution.

5.2.1 Constraints on the potential

There are a variety of constraints on the scalar potential V coming from these requirements.

First consider the solution in Lorentzian time (we will refer to this as the "cosmology picture"). In order to have a time-symmetric solution, $a(t)$ and $\phi(t)$ must be even functions (taking $t = 0$ to be the recollapse time, so that our present era corresponds to negative times) with $\dot{a}(0) = 0$ and $\dot{\phi}(0) = 0$. The Friedmann equation shows that the potential must be negative at this time-symmetric point, since $H = 0$ here and V must cancel the remaining (positive) sources of energy density.

The scalar evolution equation is that of a particle in a potential with damping $3H$ which is positive during the expanding phase. In order for the scalar field to have zero time derivative at the time-symmetric point, this particle must stop at $t = 0$, and this is only possible if it is ascending the potential just prior to $t = 0$. Thus, going forward from the present time, the scalar field must descend from positive to negative values of the potential and then rise and stop at some ϕ_0, passing through some minimum along the way.

In the Euclidean continuation (we will refer to this as the "wormhole picture" since the solutions have two asymptotically AdS boundaries connected by an interior), the evolution equations are given in (5.4). Since $\ddot{a}(t = 0) < 0$, we have $a_E''(\tau = 0) > 0$. For a solution that is asymptotically AdS as $\tau \to \pm\infty$, a must behave as $e^{H_{AdS}|\tau|}$ for large $|\tau|$, so the simplest possibility is that a is monotonically increasing from $\tau = 0$ towards each boundary. In this case, the evolution of ϕ towards the boundary is the same as the damped motion of a particle in potential $-V$. The scalar ϕ should approach a constant as $\tau \to \pm\infty$, so the inverted potential $-V$ should have a minimum here. Without loss of generality, we will take such a minimum to be located at $\phi = 0$.

Thus, the simplest possibility for the shape of the overall potential is that shown in Figure 5.1 with the evolution in the cosmology picture and the wormhole picture covering different regions of the potential as shown. We have argued in the introduction that this shape is natural for effective field theories associated with holographic CFTs.

A final constraint comes from requiring that the AdS solution which describes the two asymptotic regions is stable to scalar perturbations. This requires that the scalar field mass (the second derivative of the potential) satisfies the BF bound

$$\left.\frac{d^2V}{d\phi^2}\right|_{\phi=0} \geq \frac{9}{4}V(0), \tag{5.5}$$

where we chose units such that $8\pi G/3 = 1$, in which $V(0) = -1/L_{AdS}^2$. The condition (5.5) also ensures that the scaling dimensions of the corresponding operator in the dual microscopic theory is real as required for a unitary quantum field theory.

This bound turns out to have a simple implication for the scalar evolution towards the extremum at $\phi = 0$. First notice that, in order to ensure the existence of the AdS asymptotic regions in the wormhole picture, the scalar potential energy term must be the dominant contribution on the right-hand side of the Euclidean Friedmann equation (5.4) as $\tau \to \pm\infty$. This implies $H(\tau) \to H_{AdS} \equiv \sqrt{-V(0)}$ as $\tau \to \pm\infty$. By inspecting the scalar field evolution equation in (5.4) it is then immediate to conclude that the BF bound (5.5) is equivalent to the condition for the scalar field motion to be overdamped in the vicinity of the extremum of the potential at $\phi = 0$. Therefore, moving from the center of the wormhole towards the asymptotic boundaries, the scalar field will simply evolve from $\phi = \phi_0$ to $\phi = 0$, settling at the minimum of the inverted potential $-V$ without any oscillation occurring in the asymptotic region.

To summarize, starting from the present value of the scalar potential, we require that it decreases to negative values and then increases to an extremum with a negative value, where the second derivative of the potential at the extremum satisfies (5.5).

5.2.2 Existence and genericity of an accelerating phase

Starting with a potential satisfying these constraints, we can look for solutions with the desired properties.

As initial conditions at the symmetric point $t = \tau = 0$, we can take[7]

$$\phi(0) = \phi_0, \qquad a(0) = 1 \tag{5.6}$$

with vanishing derivatives $\dot{a}(0) = a'(0) = \dot{\phi}(0) = \phi'(0) = 0$. The matter and radiation densities are constrained via the Friedmann equation at $t = 0$ as

$$\rho_R + \rho_M = -V(\phi_0) \ . \tag{5.7}$$

In the approximation where radiation can be neglected (valid for most of the cosmological history and everywhere in the wormhole solution), the matter density is fixed by $V(\phi_0)$, so the solution is fully specified by ϕ_0, the scalar field value at $t = 0$.

We would first like to check that it's possible to have an accelerating phase of cosmology before the recollapse without significant fine-tuning of the potential. Evolving backward in time from the recollapse point in the cosmology picture, the scalar field evolution corresponds to antidamped motion in the potential V; it is natural that the scalar reaches positive values of the potential, however this does not immediately imply an accelerating phase. Such a phase further requires the positive scalar potential to dominate over all other sources of energy density. This

[7] In this convention, a will be less than one at the present time for examples applicable to realistic cosmology, but we can rescale $a(t) \to a(t)/a(t_0)$ to give the scale factor corresponding to the conventions of Sections 5.2.3 and 5.2.4.

doesn't always happen: it may be that the growth of matter density, radiation density, or scalar kinetic energy outpaces the increase in scalar potential as $a \to 0$ or that the scale factor decreases to zero (i.e. we reach the big bang) before the potential energy dominates. Thus, it is not true that we get an accelerating phase for all potentials of the type shown in Figure 5.1 and all initial conditions.

On the other hand, it is not difficult to find examples of potentials and initial conditions that do give rise to acceleration. Here we study a simple example of a potential that satisfies all of our criteria and exhibits acceleration over a significant fraction of the combined parameter space of potential parameters and the initial condition ϕ_0. For just this subsection, we restrict to a simplified model with only radiation and scalar field contributions to the stress tensor; we set the matter contribution to zero for the purposes of this demonstration.

We consider a potential that is even about the AdS extremum $\phi = 0$ with mass $m^2 = -9/4$ at the BF bound,

$$V(\phi) = -1 - \frac{9}{8}\phi^2 + V_{\text{int}}(\phi) \ . \tag{5.8}$$

In order to make the potential bounded from below and take positive values for larger ϕ, we include terms at higher order in ϕ^2. We have found that simply adding a ϕ^4 term does not give solutions with an accelerating phase. Instead, we consider a one-parameter family of even interaction potentials

$$V_{\text{int}}(\phi) = e^{g\phi^2} - g\phi^2 - 1 \tag{5.9}$$

where the last two terms are subtracted off to give an interaction potential starting at order ϕ^4.

We consider solutions for various model parameters g and initial condition ϕ_0. These solutions are obtained by numerically integrating the coupled scalar and Friedmann equations starting

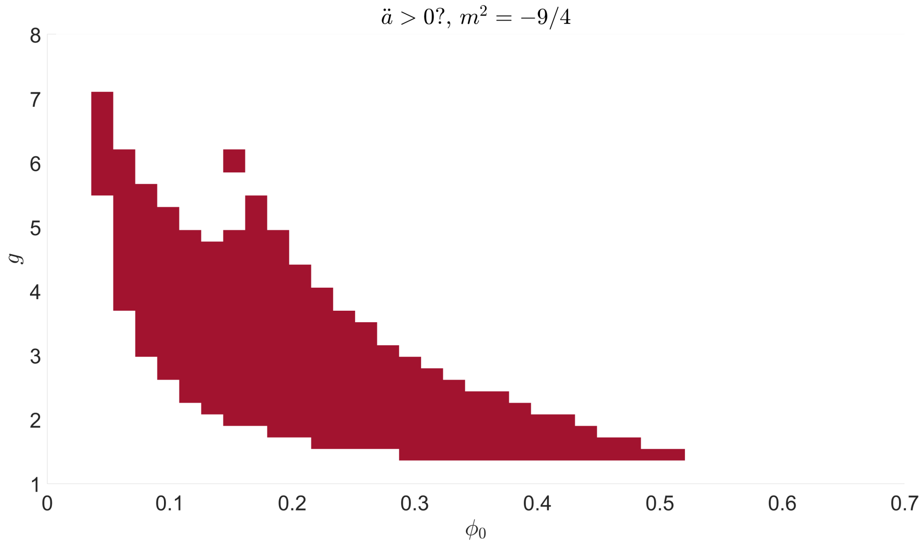

Figure 5.2: Space of model parameter g and initial condition ϕ_0 for the exponential potential of (5.8) and (5.9). Solutions of the equations of motion (5.2) and (5.4) with parameter g and initial condition ϕ_0 contained in the red region exhibit an accelerating phase.

from the turning point where $\phi = \phi_0$ and $H = \dot{\phi} = 0$. We set $\rho_M = 0$ and determine the value of ρ_R from $V(\phi_0)$ using (5.2). The system is numerically integrated back in time towards the big bang, then we numerically check if a given solution has a numerically detectable period of accelerated expansion.

In Figure 5.2, we show the space of parameters (g, ϕ_0) that leads to a period of accelerated expansion in the cosmology picture before the recollapse. We see that a significant region of the space where the parameters are of order 1 yields an accelerating phase. Thus, cosmological acceleration can be obtained without significant fine-tuning of the model or initial conditions.

We can also consider how the mass of the field affects the allowed parameter space. In Figure 5.3 we show the evolution of the parameter space exhibiting accelerated expansion as m^2 becomes less negative. We see that accelerated expansion becomes rapidly less generic as m^2 increases. Conversely, we have also observed that if m^2 is allowed to go below the BF bound, then a period of acceleration becomes more generic. Qualitatively, this is because the slope of

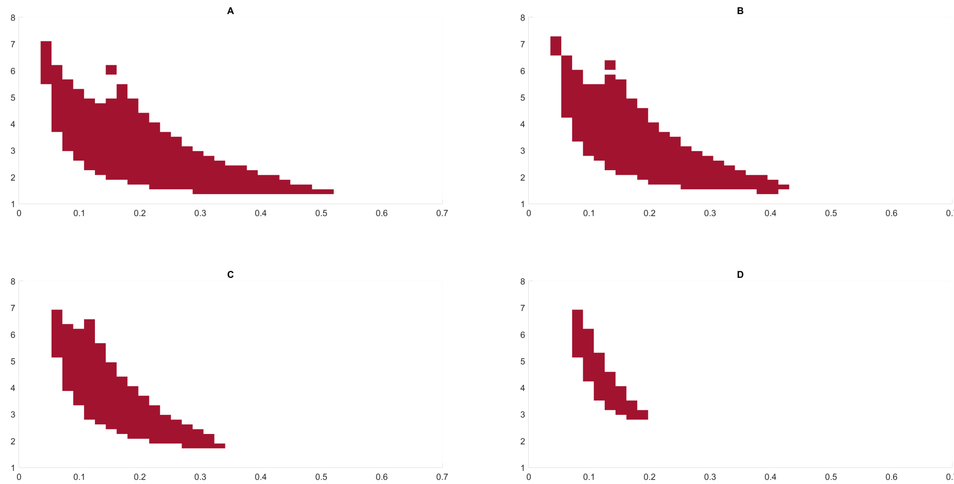

Figure 5.3: Panel (A) is the same as Figure 5.2 with $m^2 = -9/4$. Panels (B), (C), and (D) correspond to masses $m^2 = -8/4$, $m^2 = -7/4$, and $m^2 = -6/4$, respectively. Clearly it becomes much less generic to have a period of accelerated expansion as m^2 increases.

the potential near the turning point (which in the present model is controlled mostly by the value of the mass) must be steep enough for the anti-damped scalar field to quickly gain kinetic energy as we evolve back towards the big bang (or forward towards the big crunch). This is necessary for the scalar field to reach the positive region of the potential before the scale factor vanishes.

There is no particular physical significance to the form of the potential we have chosen; below, we will see that the exponentially increasing behavior of the potential for large ϕ is not necessary to obtain acceleration.

5.2.3 An example matching flat ΛCDM

As a first example of a phenomenologically realistic cosmology based on the framework introduced in [2, 9], we study potentials able to reproduce to good accuracy the ΛCDM model. These are potentials satisfying all the properties outlined above and having a nearly flat positive region.

For our numerical analysis it is useful to work in units such that $8\pi G/3 = 1$ and to introduce rescaled variables

$$\tilde{t} = H_0 t, \qquad \Omega_i = \frac{\rho_i^{now}}{H_0^2}, \qquad \tilde{H} = \frac{H}{H_0}, \qquad \tilde{V}(\phi) = \frac{V(\phi)}{H_0^2}\ , \tag{5.10}$$

where ρ_i^{now} are the energy densities at the present time. The equations of motion then read

$$\ddot{\phi} + 3\tilde{H}\dot{\phi} + \frac{d\tilde{V}}{d\phi} = 0\ , \qquad \tilde{H}^2 = \frac{1}{2}\dot{\phi}^2 + \tilde{V}(\phi) + \frac{\Omega_R}{a^4} + \frac{\Omega_M}{a^3} \tag{5.11}$$

in the cosmology picture, and

$$\phi_E'' + 3\tilde{H}_E\phi_E' - \frac{d\tilde{V}}{d\phi_E} = 0\ , \qquad \tilde{H}_E^2 = \frac{1}{2}(\phi_E')^2 - \tilde{V}(\phi_E) - \frac{\Omega_R}{a_E^4} - \frac{\Omega_M}{a_E^3} \tag{5.12}$$

in the wormhole picture, where overdots and primes now represent derivatives with respect to rescaled time variables. With this choice, both the Lorentzian time $\tilde{t} = H_0 t$ and the Euclidean time $\tilde{\tau} = H_0\tau$ are measured in units of the Hubble time $1/H_0$. We also adopt the convention $a(\tilde{t}_0) = 1$ where $\tilde{t}_0 < 0$ is the present time. This implies that at the time-symmetric point the initial condition for the scale factor is $a(0) = a_0 > 1$. The $\tilde{t}/\tilde{\tau}$ derivatives of a and ϕ vanish at the symmetric point $\tilde{t} = \tilde{\tau} = 0$. Given a value for the density parameters Ω_R and Ω_M and a choice of a_0, the initial condition for the scalar field is determined by the Friedmann equation at $\tilde{t} = 0$:

$$\frac{\Omega_R}{a_0^4} + \frac{\Omega_M}{a_0^3} = -\tilde{V}(\phi_0)\ . \tag{5.13}$$

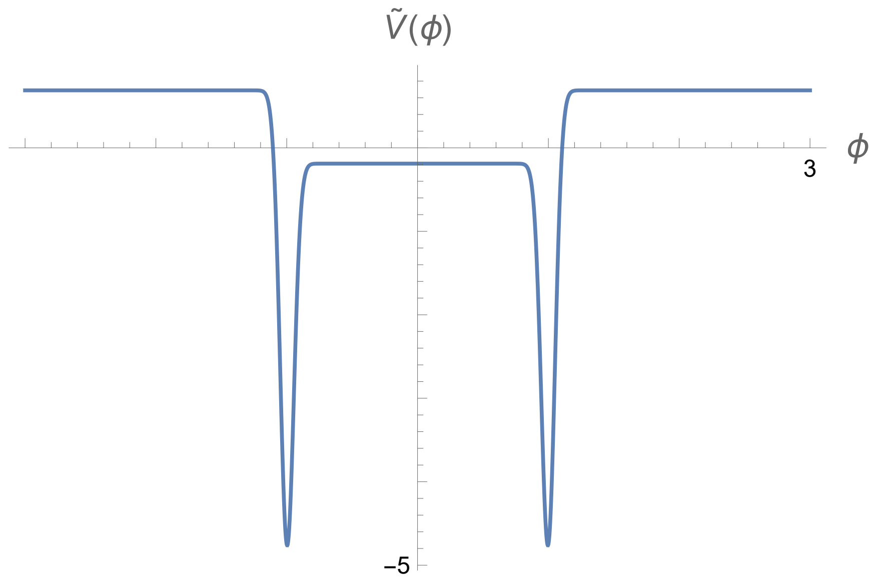

Figure 5.4: An example of the potential (5.14). A fixes the value of $\tilde{V} > 0$ at the plateau, B the value of $\tilde{V}(0)$, i.e. the negative cosmological constant in the asymptotically AdS regions of the wormhole solution. C, X, Δ determine the depth, location, and width of the deep valleys present in the potential.

Let us now consider a five-parameter family of potentials given by

$$\tilde{V}(\phi) = \tilde{V}_0(\phi) + \tilde{V}_0(-\phi) - B \tag{5.14}$$

where

$$\tilde{V}_0(\phi) = \frac{A-B}{2}\mathrm{erf}\left(\frac{\phi - X}{\Delta}\right) + C\exp\left[-\left(\frac{\phi - X}{\Delta}\right)^2\right] + \frac{A+B}{2}. \tag{5.15}$$

and erf is the error function. An example of the potential (5.14) is plotted in Figure 5.4. The parameter $A > 0$ fixes the height of the plateau for large values of ϕ and determines the value of the positive vacuum energy driving the accelerated expansion in the cosmology picture, while $B < 0$ gives the value of the negative cosmological constant in the asymptotic AdS regions in the wormhole picture. The parameters $C < 0$, $X > 0$ and $\Delta > 0$ determine the depth, location, and width of the deep valleys present in the potential, respectively. In order to reproduce the

ΛCDM model, the value of A must match the value of the positive vacuum energy observed in our universe.

We can then study solutions of the cosmology and wormhole equations of motion (5.11) and (5.12) with potential given by equations (5.14) and (5.15). We choose the values for the cosmological parameters obtained by the *Planck* 2018 collaboration using TT, TE, EE + lowE + lensing + BAO data [90]:

$$\Omega_R = 9.18 \times 10^{-5}, \qquad \Omega_M = 0.311, \qquad \Omega_\Lambda = 0.6889 \tag{5.16}$$

where Ω_Λ is the density parameter associated with the vacuum energy today. We further choose the initial condition $a_0 = 2$ for the scale factor at the time-symmetric point, while the scalar field initial condition ϕ_0 is determined by equation (5.13) once the five parameters of the potential are fixed.[8] In our numerical solutions depicted in Figures 5.5, 5.6, and 5.8, they are taken to be

$$A = 0.6889, \qquad B = -0.03, \qquad C = -5, \qquad X = 1, \qquad \Delta = 0.0726775778709 \tag{5.17}$$

yielding $\phi_0 = 0.817319$.

Cosmological solution

By an appropriate fine-tuning of the potential's parameters (see Appendix D.1) leading to the values (5.17), the cosmological evolution reproduces to very good accuracy the one predicted by the corresponding ΛCDM solution between the early universe and the present day $\tilde{t} = \tilde{t}_0$, see

[8] We remind that the initial conditions for the cosmology and wormhole pictures are the same. Note also that in general there are multiple solutions of equation (5.13). As we have explained above, we are interested in a solution such that ϕ_0 is in between a minimum and a maximum of the potential.

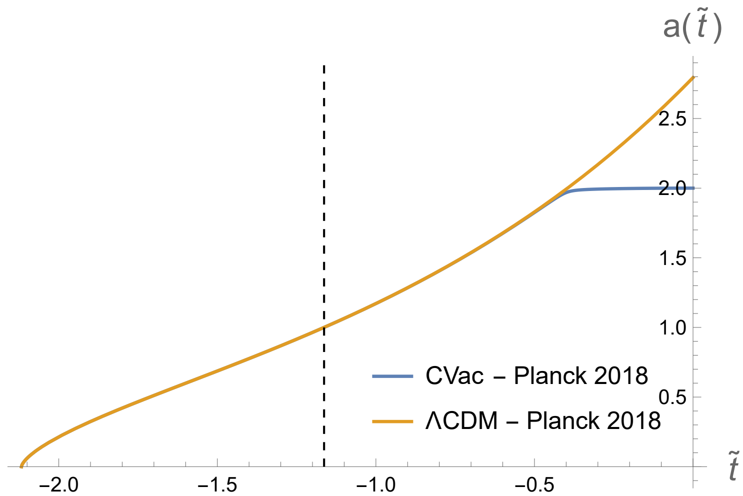

Figure 5.5: Scale factor evolution for the cosmological solution obtained using the *Planck* cosmological parameters (5.16) (denoted by "CVac"). The potential parameters are given in equation (5.17). The scale factor for the corresponding ΛCDM solution is also depicted. The two scale factors are indistinguishable until the present day $\tilde{t} = \tilde{t}_0 = -1.16342$ (where $a(\tilde{t}_0) = 1$) — indicated by the black dashed line — and beyond. Deviations in our solution from the ΛCDM behavior become evident at late times as the universe approaches the turning point at $\tilde{t} = 0$. The contraction phase in our solution, not depicted here, can be obtained by time-reversal.

Figure 5.5. For $\tilde{t} > \tilde{t}_0$, the potential energy eventually decreases and becomes negative as the scalar field rolls down the potential, while the kinetic energy K_ϕ increases. Finally, the scalar kinetic energy decreases and vanishes as we reach the time-symmetric point $\tilde{t} = 0$ (where we impose our initial conditions for both the cosmological and the wormhole solutions). See Figure 5.6.

As a consistency check, we verified that the luminosity distance

$$d_L(z) = \frac{1}{H_0 a(t)} \int_{\tilde{t}}^{\tilde{t}_0} \frac{dt'}{a(t')}\,, \qquad 1 + z = \frac{1}{a(t)} \tag{5.18}$$

computed from our solution[9] agrees with the Pantheon+SH0ES type Ia supernova (SN Ia) data [267]. In particular, we found that the luminosity distance in our solution is indistinguishable

[9]For the solution obtained using the *Planck* cosmological parameters (5.16) we can use the value of H_0 measured by *Planck*, i.e. $H_0^{planck} = 67.66$ km s^{-1} Mpc^{-1}.

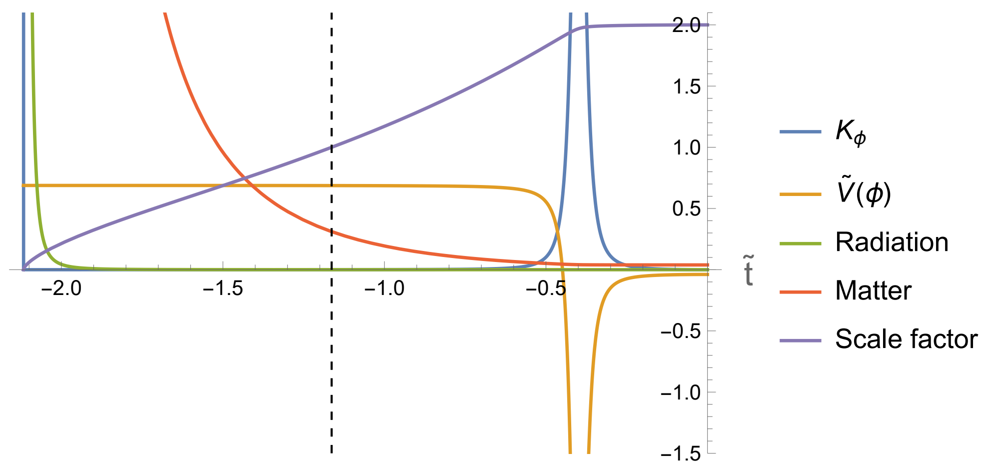

Figure 5.6: Scalar field kinetic and potential energies, radiation contribution Ω_R/a^4, matter contribution Ω_M/a^3, and scale factor $a(\tilde{t})$ as a function of time $\tilde{t}$ for the expansion phase of our cosmological solution obtained using the *Planck* cosmological parameters (5.16). The potential parameters are given in equation (5.17). The contraction phase can be obtained by time-reversal. The black dashed line indicates the present day $\tilde{t} = \tilde{t}_0 = -1.16342$ for which $a(\tilde{t}_0) = 1$. K_ϕ is negligible for most of the evolution until the present day. The universe undergoes a radiation-dominated and a matter-dominated era before the current potential energy-dominated era. In the future, the potential energy will decrease and the kinetic energy increase and become dominant as the scalar field rolls down the potential. Finally, the kinetic energy vanishes as the universe reaches its turning point at $\tilde{t} = 0$, where initial conditions for our numerical solutions are imposed.

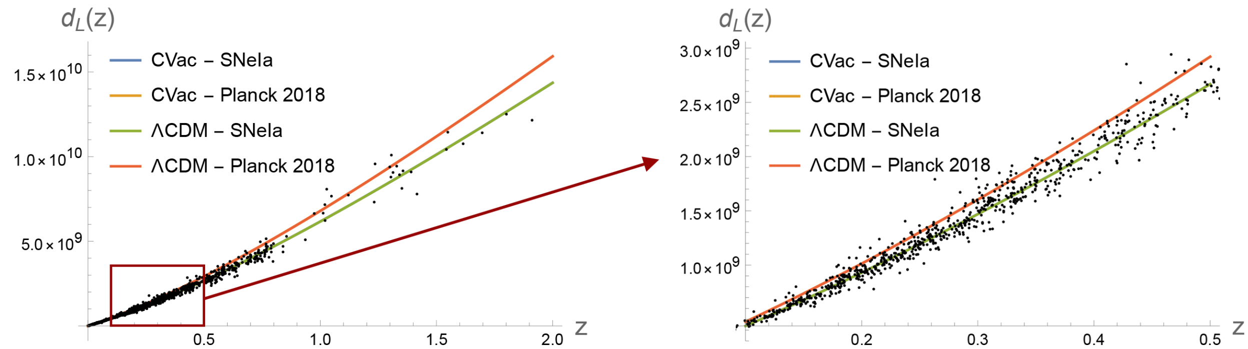

Figure 5.7: Luminosity distance $d_L(z)$ computed for two solutions involving rolling scalars (denoted by "CVac") and their corresponding ΛCDM solutions. For the *Planck* 2018 solution, the cosmological parameters are given in equation (5.16), the potential parameters in equation (5.17), and we used $H_0^{Planck} = 67.66$ km s^{-1} Mpc^{-1} [90]. For the SNeIa solution, the cosmological parameters are given by[10] $\Omega_R = 9.96\times10^{-5}$, $\Omega_M = 0.338$, $\Omega_\Lambda = 0.662$, $H_0^{SN} = 73.4$ km s^{-1} Mpc^{-1} [269], and the potential parameters are $A = 0.662$, $B = -0.03$, $C = -5$, $X = 1$, $\Delta = 0.0716914850735$; this yields $\phi_0 = 0.824448$. The Pantheon+SH0ES experimental data are also depicted [267]. Our cosmological solutions and their corresponding ΛCDM solutions are indistinguishable, meaning that our model matches supernovae data as well as the ΛCDM model. Notice that the solutions generated using *Planck* 2018 cosmological parameters are in tension with data, while the ones generated using cosmological parameters derived from supernovae observations agree with data: this is a manifestation of the Hubble tension.

from the one generated by the corresponding ΛCDM solution in the range of redshifts z covered by the SNIa data, see Figure 5.7. Therefore, our model fits the data as well as the ΛCDM model. Due to the well-known Hubble tension issue [268], this also implies that the solution obtained using the *Planck* 2018 parameters (5.16) is in tension with supernovae data. We also studied a solution generated using cosmological parameters obtained from supernovae observations [269], which clearly matches data much better. Whether specific realizations of our models could help solve the Hubble tension is an interesting open question that we plan to investigate in future work.

Wormhole solution

First, we remark that the potential under consideration with the parameters (5.17) used in our numerical analysis satisfies the BF bound (5.5). As a result of the scalar field's overdamped motion described above, the scale factor in the wormhole solution $a_E(\tilde{\tau})$ increases away from the wormhole center, the matter and radiation terms are suppressed as $\tilde{\tau}$ increases or decreases from $\tilde{\tau} = 0$, and the scalar kinetic energy K_ϕ becomes negligible as $\phi_E \to 0$ (see Figure 5.8, right panel). Therefore, for $\tilde{\tau} \to \pm\infty$ the solution approaches pure AdS with vacuum energy density parameter given by $\Omega_\Lambda = 3\tilde{V}(0) = 3B$. As a consequence, the scale factor takes the asymptotic form $a(\tilde{\tau}) \to \exp(\sqrt{-B}\tilde{\tau})$ as $\tau \to \pm\infty$ and the Hubble parameter approaches a constant value $\tilde{H}(\tilde{\tau}) \to \tilde{H}_\infty = \sqrt{-B}$ (see Figure 5.8, left panel). These results confirm the existence, within the class of models introduced in [2, 9], of well-defined wormhole solutions associated with cosmological solutions able to reproduce to arbitrary accuracy the predictions of the ΛCDM model.

We would like to point out that, from a top-down point of view, there is reason to be skeptical about the existence of the type of potentials studied in this subsection on the grounds of Swampland conjectures. In particular, the de Sitter conjecture [219, 270, 271] would appear to rule out potentials with very flat regions such as the ones introduced in equations (5.14) and (5.15). Nonetheless, this class of nearly-flat potentials is a useful starting point for our discussion. Indeed, the present analysis suggests that sufficient fine-tuning allows us to reproduce arbitrarily well the predictions of the ΛCDM model between the early universe and the present time while preserving the existence of a wormhole solution with the scalar field satisfying the BF bound at the two asymptotic AdS boundaries. A similar conclusion remains valid for a more general class of potentials, as we will see in the next subsection.

[10] In the late stages of this manuscript's preparation a revised version of [269] was announced, with a slight correction of the best fits for the cosmological parameters, yielding $\Omega_M = 0.334 \pm 0.018$ and $\Omega_\Lambda = 0.666 \pm 0.018$. This difference is irrelevant for the purposes of the present paper.

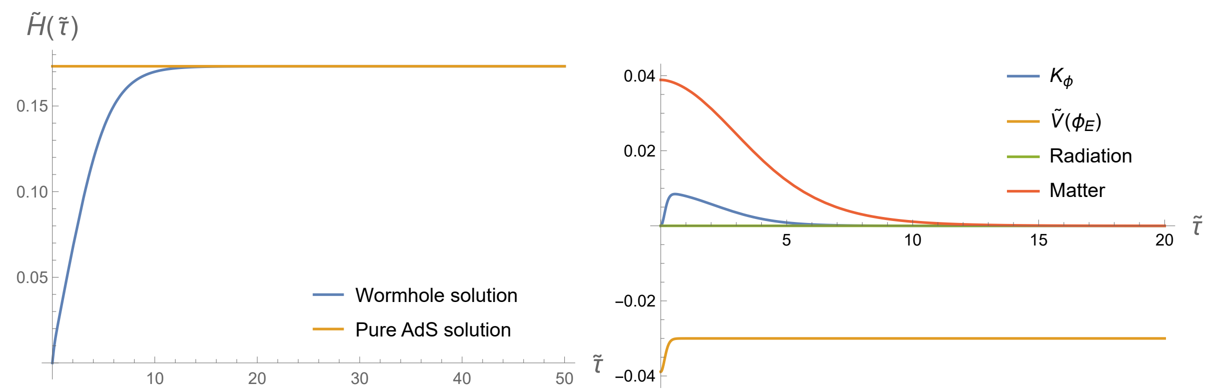

Figure 5.8: Wormhole solution from the center of the wormhole towards the asymptotic boundary at $\tilde{\tau} = \infty$, obtained using the *Planck* cosmological parameters (5.16). The potential parameters are given in equation (5.17). The evolution from the center of the wormhole towards the other asymptotic boundary at $\tilde{\tau} = -\infty$ is obtained by reflection symmetry around $\tilde{\tau} = 0$. (Left) Hubble parameter as a function of the coordinate $\tilde{\tau}$. The value of the Hubble parameter for the corresponding pure AdS solution $\tilde{H}_\infty = \sqrt{B}$ is also depicted. In the asymptotic region $\tilde{\tau} \to \infty$ the wormhole solution approaches pure AdS. (Right) Scalar field kinetic and potential energies, radiation contribution Ω_R/a_E^4, and matter contribution Ω_M/a_E^3 as a function of the coordinate $\tilde{\tau}$ along the wormhole direction. As we move towards the AdS asymptotic boundary (i.e. as we increase $\tilde{\tau}$), the overdamped scalar field approaches its value $\phi_E = 0$ at the AdS boundary and its kinetic energy vanishes. The radiation and matter contributions are suppressed as the scale factor increases, and in the asymptotic region the negative scalar potential energy $\tilde{V}(0)$ is dominant: the solution approaches an AdS vacuum solution.

5.2.4 An example matching flat wCDM

Though we have considered a flat potential to make direct contact with the ΛCDM model, such tuning of the scalar potential is not at all necessary, and we can consider a broader class of models consistent with direct observations of Ω_M and the scale factor $a(t)$, which may involve scalar evolution over a range of potential values $\Delta V/V = O(1)$.

For concreteness, we consider the spatially flat wCDM model,[11] since direct constraints on the cosmological parameters for these models from type Ia supernova observations, using the Pantheon+SH0ES data set, are provided in [269]. We recall that this model consists of modifying the dark energy contribution in the ΛCDM model, by replacing the cosmological constant with a perfect fluid governed by the equation of state $\rho = wp$, with w constant. The corresponding Hubble expansion is given by

$$H(z) = H_0\sqrt{\Omega_M(1+z)^3 + \Omega_\Lambda(1+z)^{3(1+w)}}\,, \tag{5.19}$$

where Ω_Λ is the density parameter for the dark energy, so that $\Omega_\Lambda = 1 - \Omega_M$ with the assumption of spatial flatness. The constraints on the parameters of this model from [269] are

$$H_0 = (73.5 \pm 1.1)\,\mathrm{km}\cdot\mathrm{s}^{-1}\cdot\mathrm{Mpc}^{-1}\,, \quad \Omega_M = 0.309^{+0.063}_{-0.069}\,, \quad w = -0.90 \pm 0.14\,. \tag{5.20}$$

We can reproduce the evolution of the wCDM cosmology over an arbitrarily large range of redshifts using our scalar field model. With the assumption that only a single scalar field is relevant to the cosmological evolution, we can actually deduce the potential associated with this

[11] We neglect radiation in this subsection.

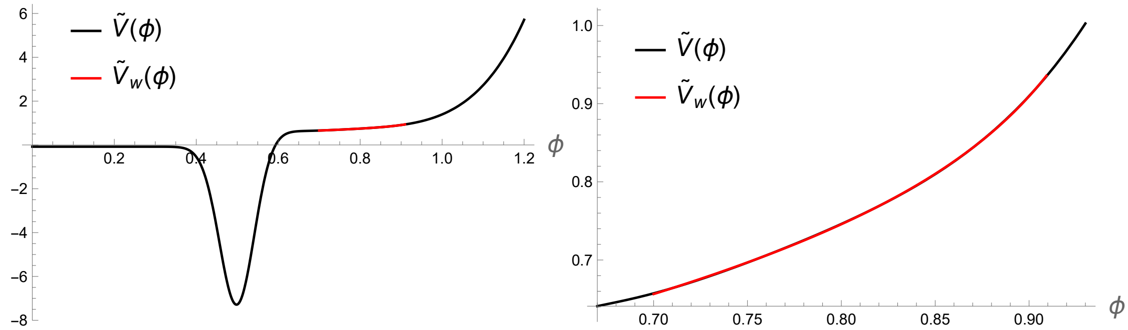

Figure 5.9: Rescaled potentials for the model $V(\phi)$ and reconstruction $V_w(\phi)$, where the region of the latter probed by the scalar field in the range $z \in (z_{\text{min}}, z_{\text{max}})$ is shown. The righthand plot is a close-up on this region. The precise form of the model $V(\phi)$ can be found in Appendix D.2.

scalar field given $a(t)$ and Ω_M. The kinetic energy can be expressed as

$$K(t) \equiv \frac{1}{2}\dot{\phi}^2 = -\frac{1}{8\pi G}\dot{H} - \frac{3}{16\pi G}\Omega_M H_0^2 \frac{1}{a^3} \ , \tag{5.21}$$

and we can take the square root and integrate, to obtain

$$\phi(t) = \phi(t_0) + \int_{t_0}^{t} d\hat{t} \sqrt{-\frac{1}{4\pi G}\dot{H}(\hat{t}) - \frac{3}{8\pi G}\Omega_M H_0^2 \frac{1}{a^3(\hat{t})}}. \tag{5.22}$$

Similarly, the potential energy is

$$V(t) = \frac{1}{8\pi G}\dot{H} + \frac{3}{8\pi G}H^2 - \frac{3}{16\pi G}\Omega_M H_0^2 \frac{1}{a^3} \ . \tag{5.23}$$

We can alternatively express these in terms of the redshift z and adopt the rescaled quantities introduced in the previous subsection, obtaining

$$\begin{aligned} \phi(z) &= \phi_0 + \int_0^z dz' \, \frac{\sqrt{\frac{1}{4\pi G}(1+z')\tilde{H}(z')\tilde{H}'(z') - \frac{3}{8\pi G}(1+z')^3\Omega_M}}{(1+z')\tilde{H}(z')} \\ \tilde{V}(z) &= -\frac{1}{8\pi G}(1+z)\tilde{H}(z)\tilde{H}'(z) + \frac{3}{8\pi G}\tilde{H}(z)^2 - \frac{3}{16\pi G}(1+z)^3\Omega_M \ . \end{aligned} \tag{5.24}$$

We may then substitute the rescaled version of the Hubble expansion from equation (5.19) into these expressions.

In the scalar field model, the effective equation of state parameter is given by

$$w = \frac{\frac{1}{2}\dot{\phi}^2 - V}{\frac{1}{2}\dot{\phi}^2 + V} \,. \tag{5.25}$$

For a general scalar theory, w will be redshift dependent, but with appropriate choice of scalar potential, we may recover solutions for which w is approximately constant over an arbitrarily large range of redshifts. We denote by $V_w(\phi)$ the scalar potential reconstructing the wCDM model for all $z > 0$. For the best-fit parameters of wCDM listed above, we show part of the reconstructed potential $\tilde{V}_w(\phi) = V_w(\phi)/H_0$ in Figure 5.9.

Since the Pantheon+SH0ES data used to deduce the cosmological parameter constraints probe only redshifts in the range $z \in (z_{\text{min}}, z_{\text{max}})$ with $z_{\text{min}} \approx 10^{-3}$ and $z_{\text{max}} \approx 2.26$, we are free to consider any scalar potential $V(\phi)$ which coincides with $V_w(\phi)$ in the region over which the scalar solution evolves in this range of redshifts. In Figure 5.9, we also plot a rescaled scalar potential $\tilde{V}(\phi) = V(\phi)/H_0$ agreeing with $\tilde{V}_w(\phi)$ in the appropriate range, but that satisfies the "UV constraints" necessary for the existence of an analytic continuation of the cosmological solution to an asymptotically AdS wormhole. The precise form of the potential $\tilde{V}(\phi)$, as well as our method for constructing the potential and the appropriate initial conditions for the cosmological solution, are given in Appendix D.2. In the left panel of Figure 5.10, we plot the equation of state evolution $w(z)$ extracted directly from the time-symmetric cosmological solutions in the model with potential $\tilde{V}(\phi)$, confirming that they reproduce that of the wCDM model with the desired precision, while in the right panel of Figure 5.10 we confirm that the analytic continuation of

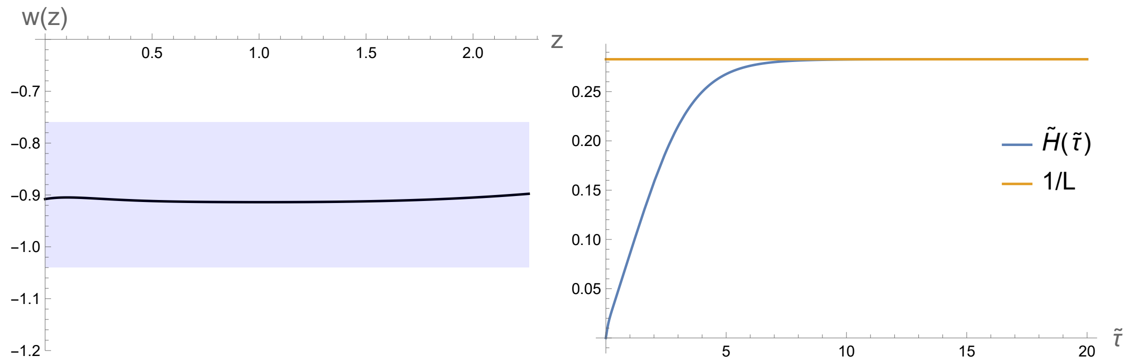

Figure 5.10: (Left) Equation of state parameter w versus redshift z for time-symmetric solutions to the model $\tilde{V}(\phi)$, with shaded region given by the Pantheon+SH0ES constraint. (Right) Euclidean evolution of $\tilde{H}(\tilde{\tau})$, with $\frac{1}{L} \equiv \sqrt{-V(0)}$ plotted for reference. In the asymptotic region $\tilde{\tau} \to \infty$ the wormhole solution approaches pure AdS, as expected. The precise form of the potential $\tilde{V}(\phi)$ can be found in Appendix D.2.

these solutions have AdS asymptotics.

We emphasize that, while we have only aimed here to reproduce the wCDM model over the region $z \in (z_{\text{min}}, z_{\text{max}})$ where it has been constrained by SNe Ia data, we could recover the same model over an arbitrarily large redshift interval through suitable choice of the scalar potential.

5.3 Supersymmetric models

In our discussion so far, we have considered an effective gravitational field theory involving scalar fields with dynamics controlled by an effective potential V. We have shown that such a theory could describe the background dynamics of our Universe while also admitting a Euclidean continuation suggestive of a dual CFT description.

The most well-understood examples of gravitational theories which are dual to CFTs are supersymmetric. It is thus interesting to ask whether there exist supersymmetric theories whose effective low energy descriptions contain scalar fields with potentials V, which give rise to effective cosmological dynamics. In these examples, supersymmetry could be broken by the time-dependent scalar field expectation value. Note that here we will not be concerned with whether the supersymmetric theories under consideration have explicitly known CFT duals. Instead we simply wish to understand whether supersymmetry is consistent with the restricted class of scalar potentials which we have considered so far.

We will consider $\mathcal{N} = 1$ supergravity and restrict to considering only the gravity and scalar sectors; presumably one can consistently set the gravitino and chiral fermions to zero in solutions to the full equations of motion. We follow the notation of [186] and we set $8\pi G_{\rm N} = \kappa^2 = 1$ in this section.

The n_c scalar fields ϕ^i of $\mathcal{N} = 1$ supergravity are bottom components of chiral multiplets, such that the theory has bosonic Lagrangian

$$\mathcal{L} = \frac{1}{2}R - K_{i\bar{j}}\partial_\mu \phi^i \partial^\mu \bar{\phi}^{\bar{j}} - V_W(\phi, \bar{\phi}) \,, \tag{5.26}$$

where $K_{i\bar{j}} = \partial_i \bar{\partial}_{\bar{j}} K$ is the Kähler metric arising from a Kähler potential K, and V_W is the scalar potential

$$V_W = e^K \left(K^{i\bar{j}} D_i W D_{\bar{j}} \bar{W} - 3|W|^2 \right) \,, \qquad D_i W = \partial_i W + K_i W \,, \tag{5.27}$$

defined in terms of the superpotential W.

For simplicity we will consider the case of a single chiral multiplet, $n_c = 1$, and set the Kähler potential to the canonical form $K(\phi, \bar{\phi}) = \bar{\phi}\phi$. Theories with more general Kähler potentials and more chiral multiplets may also be interesting to consider. In our case the scalar potential is given by

$$V_W(\phi) = e^{\phi\bar{\phi}} \left(|W'(\phi) + \bar{\phi}W(\phi)|^2 - 3|W(\phi)|^2 \right). \tag{5.28}$$

A specification of W is part of the specification of the supersymmetric theory, with the only restriction on W being that it is a holomorphic function of ϕ. Thus we would like to know whether it is possible to choose W such that V_W is a scalar potential like the ones considered in previous sections, i.e. which gives rise to effective cosmological dynamics.

The scalar field ϕ arising from the supersymmetric theory is a complex field, which we can decompose into two real fields as $\phi = \phi_R + i\phi_I$. Thus V_W is a (real) potential of two real fields, ϕ_R and ϕ_I, whose dynamics will in general be coupled — the trajectory of ϕ in the complex plane will generally involve motion in both the ϕ_R and ϕ_I directions.

However, although it is certainly possible that the low energy effective field theory describing our Universe contains multiple real scalar fields, in the previous sections we have shown that a single field with potential V is sufficient for the cosmology to be in quantitative agreement with measurements of the scale factor, while still admitting an asymptotically AdS Euclidean continuation. Thus we might hope that we can find a potential V_W such that the dynamics in the ϕ plane is one-dimensional, for example such that ϕ rolls down the real axis, with $\phi_I = 0$ for all times. Moreover we would like $V_W(\phi_R) = V(\phi_R)$, so that the remaining scalar degree of freedom ϕ_R provides us with the desired cosmological evolution.

We will now show that, even with this restriction that ϕ_I effectively decouples from the dynamics, given any cosmological potential $V(\phi_R)$ it is possible to find a superpotential $W(\phi)$ such that $V_W(\phi_R)$ is, to an arbitrarily good approximation, equal to $V(\phi_R)$ within a given fixed region. Furthermore, in this construction W will be holomorphic everywhere provided that V is. Since the cosmological potentials which we considered in previous sections are generically holomorphic everywhere, this construction will produce holomorphic superpotentials W which give rise to realistic effective cosmological dynamics with Euclidean AdS asymptotics.

Constructing the superpotential

In our construction $W(\phi_R)$ will be real, in which case Eq. (5.28) for $\phi = \phi_R$ reads

$$V_W(\phi_R) = e^{\phi_R^2}\left([W'(\phi_R) + \phi_R W(\phi_R)]^2 - 3W^2(\phi_R)\right). \tag{5.29}$$

This is a nonlinear ODE for W and cannot be solved in closed form. To obtain a linear equation, write

$$V_W(\phi_R) = e^{\phi_R^2}\left(W' + (\phi_R + \sqrt{3})W\right)\left(W' + (\phi_R - \sqrt{3})W\right). \tag{5.30}$$

Now let $f(\phi_R)$ be some function, which we define shortly, and consider the linear ODE

$$W'(\phi_R) + (\phi_R - \sqrt{3})W(\phi_R) = f(\phi_R). \tag{5.31}$$

The general solution is the sum of a homogeneous plus inhomogeneous piece,

$$W(\phi_R) = CG(\phi_R) + G(\phi_R)\int_0^{\phi_R} du \frac{f(u)}{G(u)}, \tag{5.32}$$

where C is an arbitrary integration constant, and the homogeneous piece is given by

$$G(\phi_R) = \exp\left(-\frac{1}{2}\phi_R^2 + \sqrt{3}\phi_R\right). \tag{5.33}$$

Substituting this solution for W into (5.30) we obtain the scalar potential

$$V_W(\phi_R) = \tilde{V}(\phi_R)\left(1 + \frac{\tilde{V}(\phi_R)e^{-2\sqrt{3}\phi_R}}{12C^2} + \frac{1}{2\sqrt{3}C^2}\int_0^{\phi_R} du\, \tilde{V}(u)e^{-2\sqrt{3}u}\right). \tag{5.34}$$

where we have defined

$$\tilde{V}(\phi_R) \equiv 2\sqrt{3}Ce^{\phi_R^2}f(\phi_R)G(\phi_R). \tag{5.35}$$

Because we are free to choose f, we are effectively free to choose $\tilde{V}$. We can thus require $V_W(\phi_R) = V(\phi_R)$ and solve (5.34) for $\tilde{V}$. Although this cannot be done in closed form, we can obtain a series approximation for $\tilde{V}$ in powers of $1/C^2$. Notice that C is an arbitrary constant, and so it can be chosen large enough to be a good expansion parameter; we will discuss this in more detail below. Namely, writing

$$\tilde{V}(\phi_R) = \tilde{V}_0(\phi_R) + \frac{1}{C^2}\tilde{V}_2(\phi_R) + \frac{1}{C^4}\tilde{V}_4(\phi_R) + \dots, \tag{5.36}$$

it is possible to recursively solve the equation $V_W(\phi_R) = V(\phi_R)$ for the $\tilde{V}_n$. The first two terms in the expansion are

$$\tilde{V}_0(\phi_R) = V(\phi_R), \tag{5.37}$$

$$\tilde{V}_2(\phi_R) = -\frac{V(\phi_R)}{2\sqrt{3}}\left(\frac{e^{-2\sqrt{3}\phi_R}V(\phi_R)}{2\sqrt{3}} + \int_0^{\phi_R} du\, V(\phi_R)e^{-2\sqrt{3}u}\right), \tag{5.38}$$

and expressions for higher order terms can be straightforwardly obtained by recursion. Substituting (5.35) into (5.32) we obtain the superpotential in terms of $\tilde{V}$,

$$W(\phi_R) = CG(\phi_R)\left(1 + \frac{1}{2\sqrt{3}C^2}\int_0^{\phi_R} du\, \tilde{V}(u)e^{-2\sqrt{3}u}\right), \tag{5.39}$$

and using the series expansion for $\tilde{V}$ in terms of V, we can, perturbatively in powers of $1/C^2$, write the superpotential W in terms of the cosmological potential V:

$$W(\phi_R) = CG(\phi_R)\left[1 + \frac{1}{2\sqrt{3}C^2}\int_0^{\phi_R} du\, V(u)e^{-2\sqrt{3}u} + \mathcal{O}\left(C^{-4}\right)\right]. \tag{5.40}$$

Truncating the expansion

If we use the full expression for $W(\phi_R)$ derived above, including all corrections in powers of $1/C^2$, then we would expect to find an exact equality $V_W(\phi_R) = V(\phi_R)$ for all values of ϕ_R. Of course, it is not possible to work with the infinite series of terms. Instead we can truncate the series expansion of W at n terms, obtaining the truncated superpotential, which we denote W_n. For example, W_2 is obtained by keeping two terms in the expansion,

$$W_2(\phi_R) = CG(\phi_R)\left(1 + \frac{1}{2\sqrt{3}C^2}\int_0^{\phi_R} du\, V(u)e^{-2\sqrt{3}u}\right), \tag{5.41}$$

which results in the scalar potential

$$V_{W_2}(\phi_R) = V(\phi_R)\left(1 + \frac{V(\phi_R)e^{-2\sqrt{3}\phi_R}}{12C^2} + \frac{1}{2\sqrt{3}C^2}\int_0^{\phi_R} du\, V(u)e^{-2\sqrt{3}u}\right). \tag{5.42}$$

Recall that C appeared simply as an undetermined integration constant, and we are free to set it to any value whatsoever. Therefore we have the somewhat unusual freedom to set our expansion parameter $1/C$, and thus the terms truncated in going from W to W_2, as small as we like. In terms of the potentials, given any value of ϕ_R we can make $V_{W_2}(\phi_R)$ arbitrarily close to the cosmological potential $V(\phi_R)$. In other words, as we take C large V_{W_2} converges pointwise to $V(\phi_R)$. If we restrict to values of ϕ_R in any compact subset of the real line, then the convergence is uniform within this subset. Thus we have successfully managed to embed any scalar potential V — including cosmological potentials — into a supersymmetric theory, to an arbitrary degree of accuracy.

In Fig. 5.11 we illustrate with a simple example the deviation of V_{W_2} from V for various values of C. Notice that $V_{W_2}(\phi_R)$ is in excellent agreement with $V(\phi_R)$ for $\phi_R > 0$, but for a fixed value of C the agreement breaks down for negative enough values of ϕ_R. This is because the exponential factor in the integrand in (5.41) suppresses the contribution of the subleading term for positive values of ϕ_R, but enhances this same contribution for negative ϕ_R. This effect can be traced back to us choosing to set the second bracketed factor in (5.30) equal to f. Had we chosen to set the first factor equal to f, the same analysis would result in an approximation $V_{W_2}(\phi_R)$ of $V(\phi_R)$ which is accurate for all $\phi_R < 0$, but breaks down for ϕ_R positive enough. Since throughout this paper we have worked with the convention that the scalar field rolls along the positive real axis, it makes sense to consider, as we have done, the construction which gives

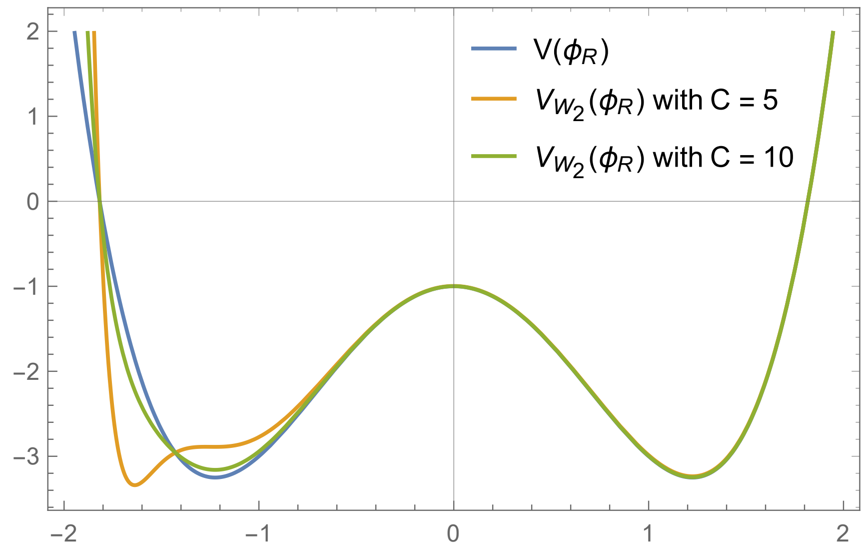

Figure 5.11: Comparison of $V(\phi_R) = -1 - 3\phi_R^2 + \phi_R^4$ and the potential $V_{W_2}(\phi_R)$ given by equation (5.42), obtained from the truncated superpotential W_2 given by equation (5.41).

an accurate approximation $V_{W_2}(\phi_R) \approx V(\phi_R)$ for positive ϕ_R. Nevertheless, by taking C large enough, we can make $V_{W_2}(\phi_R)$ arbitrarily close to $V(\phi_R)$ for ϕ_R greater than any real ϕ_R^*.

Maximum at $\phi_R = 0$

One potential issue with the truncated potential $V_{W_2}(\phi_R)$ is that it is not symmetric with respect to $\phi_R \to -\phi_R$; see Fig. 5.11. Despite this, from (5.42) we find

$$V'_{W_2}(\phi_R) = V'(\phi_R)\left(1 + \frac{2V(\phi_R)e^{-2\sqrt{3}\phi_R}}{12C^2} + \frac{1}{2\sqrt{3}C^2}\int_0^{\phi_R} du\, V(u)e^{-2\sqrt{3}u}\right), \tag{5.43}$$

and hence $V'_{W_2}(0) = 0$ if $V'(0) = 0$. Thus, although $V_{W_2}(\phi_R)$ is not symmetric, it does have a local maximum at $\phi_R = 0$, allowing for the asymptotically AdS solution $\phi_R = 0$ in the Euclidean continuation. Therefore it is not a problem that $V_{W_2}(\phi_R)$ is not symmetric.

Dynamics of a complex ϕ

So far we have restricted the complex field $\phi = \phi_R + i\phi_I$ to the real line, i.e. we have set $\phi_I = 0$. This has allowed us to explicitly construct the superpotential $W_2(\phi_R)$, which gives a scalar potential $V_{W_2}(\phi_R)$ that is arbitrarily close to the cosmological potential $V(\phi_R)$. Analytically continuing away from the real axis, we obtain the superpotential $W_2(\phi)$ as a function of complex ϕ. Notice from (5.41) that if $V(\phi)$—the analytic continuation of the cosmological potential $V(\phi_R)$—is analytic in some simply connected region of the complex plane containing $\phi = 0$, then $W_2(\phi)$ is analytic in this same region. The cosmological potentials considered in previous sections were analytic everywhere, and so the corresponding superpotential is also analytic everywhere.

The superpotential $W_2(\phi)$ defines a scalar potential $V_{W_2}(\phi)$ for complex values of ϕ via Eq. (5.28),

$$V_{W_2}(\phi) = e^{\phi\bar{\phi}} \left(|W_2'(\phi) + \bar{\phi} W_2(\phi)|^2 - 3|W_2(\phi)|^2 \right) . \tag{5.44}$$

Notice that $V_{W_2}(\phi)$ is not holomorphic even if $W_2(\phi)$ is. In fact, $V_{W_2}(\phi)$ is real for all ϕ, and so it cannot be holomorphic. Thus instead of thinking of $V_{W_2}(\phi)$ as a function of a single complex variable ϕ, it makes more sense to think of it as a (real) function of two real variables, ϕ_R and ϕ_I.

By construction we have ensured that $V_{W_2}(\phi)$ restricted to the real axis is approximately equal to the cosmological potential $V(\phi_R)$. An important question is: if at some initial time the values of ϕ and $\dot{\phi}$ are both real (i.e. $\phi_I = 0 = \dot{\phi}_I$), then does ϕ remain real (i.e. does ϕ_I remain zero) throughout its dynamical evolution? In other words we are asking whether the imaginary component of ϕ decouples, leaving only a single real scalar degree of freedom to source the cosmological dynamics.

To answer this, suppose that ϕ is spatially homogeneous and consider the equation of motion for the fields ϕ_R and ϕ_I with potential $V_{W_2}(\phi_I, \phi_R)$,

$$\ddot{\phi}_i + 3H\dot{\phi}_i + \partial_i V_{W_2} = 0. \tag{5.45}$$

Since $W_2(\phi)$ is analytic in the complex plane and real on the real axis, it can be shown that $\overline{W_2(\phi)} = W_2(\bar{\phi})$.[12] Equation (5.44) then implies that $V_{W_2}(\bar{\phi}) = V_{W_2}(\phi)$ which implies that $\partial V_{W_2}/\partial\phi_I$ is identically zero on the real axis. Therefore if ϕ_I and $\dot{\phi}_I$ vanish at some initial time, they vanish for all times; if ϕ starts rolling along the real axis, it stays on the real axis. Hence we are able to construct any effective single field cosmological model, such as those discussed in previous sections, by starting with a supersymmetric Lagrangian.

Stability

Having shown that $\phi_I = 0 = \dot{\phi}_I$ initially implies vanishing ϕ_I for all times, i.e. ϕ_I decouples from ϕ_R, it is important to ask whether the dynamics of ϕ_R is stable against small perturbations which make ϕ_I or $\dot{\phi}_I$ nonzero. Such perturbations will inevitably spontaneously occur due to quantum fluctuations, so it is crucial to consider their effects.

To determine the effects of such small perturbations away from real values of ϕ, we must evaluate $\partial^2 V_W/\partial\phi_I^2$ for $\phi_I = 0$. If this is positive, the potential $V_{W_2}(\phi)$ curves upwards as

[12] Proof: Since $W_2(\phi)$ is analytic $W_2(\phi) = W_2(\phi_R + i\phi_I) = \sum_{n=0}^{\infty} \frac{1}{n!} W_2^{(n)}(\phi_R)(\phi - \phi_R)^n$. Since $W_2(\phi_R)$ is real $\overline{W_2^{(n)}}(\phi_R) = W_2^{(n)}(\phi_R)$. Hence $\overline{W_2(\phi)} = \sum_{n=0}^{\infty} \frac{1}{n!} W_2^{(n)}(\phi_R)(\bar{\phi} - \phi_R)^n = W_2(\bar{\phi})$.

ϕ moves away from the real axis, and thus the motion along the real axis is stable to small perturbations.

Equation (5.44) gives $V_{W_2}(\phi)$ for all complex values of ϕ. Setting $\phi = \phi_R + i\phi_I$ and differentiating, we find

$$\left.\frac{\partial^2 V_{W_2}}{\partial \phi_I^2}\right|_{\phi_I=0} = 8e^{2\sqrt{3}\phi_R}C^2 + F_0(\phi_R) + \frac{F_2(\phi_R)}{C^2}, \tag{5.46}$$

where $F_0(\phi)$ and $F_2(\phi)$ are analytic functions (which depend on V) and are thus bounded on any compact set $I \subset \mathbb{R}$. Therefore, since the leading term in this expansion is positive, it is always possible to take C large enough so that $\partial^2 V_{W_2}/\partial\phi_I^2|_{\phi_I=0} > 0$ for any $\phi_R \in I$.[13] In this case the dynamics of ϕ_R along the real axis is guaranteed to be stable under fluctuations in the imaginary directions, and so even at the level of perturbations the field ϕ_I decouples from the dynamics of ϕ_R.[14] Thus we truly have a single field cosmological model, starting from a supersymmetric Lagrangian.

5.4 Outlook

In this paper, we have argued that accelerated expansion is generic (i.e. arises without fine tuning) in $\Lambda < 0$ cosmologies arising from asymptotically AdS Euclidean wormholes, for simple scalar potentials with a form that is natural in theories with a dual CFT. We found that there exist models of this type which can match ΛCDM to high accuracy at the level of background geometry, so the framework can give realistic cosmologies. We found that the scalar potential in

[13]Recall that taking C large is the same limit which ensures $V_{W_2}(\phi_R) \approx V(\phi_R)$ in the first place.

[14]Note that the dynamics is also stable in the double analytically continued (Lorentzian wormhole) picture [2], because $\partial^2 V_{W_2}/\partial\phi_I^2 > 0$ trivially satisfies the BF bound, while $\partial^2 V_{W_2}/\partial\phi_R^2$ satisfies the BF bound by construction.

these examples can arise from a superpotential, so the effective field theory can potentially have a supersymmetric point for $\phi = 0$. There are many directions for further study.

Direct reconstruction of the potential

The class of models considered in this paper make at least two generic predictions: that one should have a dynamical scalar field contributing to the energy density of the universe and that the universe should eventually begin to decelerate. With this in mind, it is interesting to consider direct measurements of the scale factor from supernova observations and search for evidence of an evolving scalar field. In principle, the scalar potential in a single field model can be reconstructed directly from knowledge of the scale factor $a(t)$ and Ω_M when radiation can be ignored. The explicit expressions given in equations (5.22) and (5.23) define $V(\phi)$ parametrically. However, Ω_M (the present day matter contribution to the energy density) is not well constrained by direct observation, and the reconstruction of $V(\phi)$ for given Ω_M is quite sensitive to small changes in $a(t)$. As a result, there is actually considerable freedom in the form of the potential that can be consistent with data, and thus considerable room for the types of models considered here.[15] Plausibly, the type of fine-tuning that we required to match ΛCDM precisely will not be required if the goal is to provide a good fit with direct obserations of the scale factor. We will discuss these issues along with a more complete analysis of the supernova data in a forthcoming paper [272]. We note that it is particularly interesting at present to consider models that go beyond ΛCDM given the Hubble tension [268].

[15] One example of this flexibility is highlighted in Figure 5.9 which shows in red a potential with significant variation that provides a good fit to the low redshift measurements of the scale factor.

Including fluctuations in a realistic effective field theory model

In this paper, we have focused entirely on the evolution of the homogeneous background. We found that there are effective theories which are compatible both with the cosmological history obtained from ΛCDM or wCDM and with having a stable asymptotically AdS analytic continuation. It is very interesting to understand whether these effective theories are also capable of reproducing the observed spectrum of fluctuations in the CMB. One question we would particularly like to understand is whether primordial inflation is required or if the existence of the analytic continuation is already enough to give a sensible spectrum of fluctuations.

We also want to understand if the scalar potentials we are considering could have other phenomenological effects. For example, considering fluctuations around a very flat potential raises the prospect of a new long-ranged scalar-mediated force. One can also ask if scalar particles would be produced in any appreciable quantity and, if so, could such particles form a component of dark matter? These are issues that must be addressed to claim a fully realistic model, quite apart from objections to flat potentials arising from Swampland conjectures.

Towards a microscopic construction

Here we have focused exclusively on effective theories, but it remains an important open question to find concrete microscopic realizations of these big bang / big crunch cosmologies with a holographic dual. In the search for such constructions, it makes sense to again back off of demanding a fully realistic model. Instead, we can ask if relatively simple models can be found, perhaps corresponding to a pure radiation scenario or a scenario with a relatively simple scalar potential exhibiting some period of acceleration.

It is also interesting to further explore the issue of supersymmetric effective theories. Here we showed that a superpotential can be constructed to match any potential we devise, but presumably not all such superpotentials arise from a UV-complete and supersymmetric microscopic theory.

Acknowledgements

We acknowledge support from the U.S. Department of Energy grant DE-SC0009986 (B.G.S.), the U.S. Department of Energy, Office of Science, Office of Advanced Scientific Computing Research, Accelerated Research for Quantum Computing program "FAR-QC" (S.A.), the National Science and Engineering Research Council of Canada (NSERC) and the Simons foundation via a Simons Investigator Award and the "It From Qubit" collaboration grant.

Chapter 6: Discussion

In this dissertation I described the progress my collaborators and I made in the last few years in obtaining a description of $\Lambda < 0$ cosmologies within the holographic framework for quantum gravity. I first reported in Chapter 2 the results obtained within the holographic braneworld cosmology approach. The main advantage of this approach is that it is a more conventional holographic system, in which a 4D BCFT is dual to a 5D bulk spacetime, with the 4D cosmology living on an end-of-the-world brane. As we have discussed in Chapter 1, the presence of the 5D bulk allows us to understand more directly the relationship between cosmological observables and observables in the microscopic dual theory, leading to a more intuitive understanding of the holographic setup. However, this approach also presents some limitations: the loss of the 4D effective cosmological description in the early and late universe due to gravity delocalization; the constraints on the cosmological EFT deriving from the embedding in the higher dimensional spacetime, which make it complicated—at least in the simplest models—to obtain a phenomenologically realistic cosmology; the extreme difficulty of probing the cosmological physics (which sits behind a black hole horizon) from the dual theory.

On the other hand, the holographic wormhole cosmology approach—which was the subject of Chapters 3, 4, and 5—is more general and includes the holographic braneworld cosmology as a special case, as we have explained in Section 1.5. Within this approach, the limitations of the holographic braneworld cosmology models outlined above do not arise: the 4D EFT is expected to be valid until the early and late universe; it is possible to obtain more generic cosmological spacetimes by considering various bulk fields (as long as they respect the symmetry of the setup and other constraints guaranteeing the existence of a dual description, see Section 1.4), including cosmologies admitting a phase of accelerated expansion and possibly matching experimental observations; the slicing duality provides a way to probe cosmological physics from the dual theory in a much simpler way. Additionally, this approach can also give an interesting perspective on naturalness puzzles and the existence of entanglement islands in cosmology. The price to pay for these advantages is a less conventional holographic dual construction—in which 3D holographic CFTs are coupled by 4D non-holographic degrees of freedom—and the need to show the existence and stability of Euclidean wormhole saddles in the gravitational Euclidean path integral dual to the microscopic Euclidean path integral of interest. If the Lorentzian wormhole picture is also taken into account, the occurrence of enhanced negative vacuum energies able to support the wormhole in these bulk setups must be justified too.

These lines of research have been developed only in recent years and, although they show several promising features I have emphasized in this dissertation, much work is still required in order to obtain a full description of a realistic cosmology within holography. I will therefore conclude this dissertation by briefly outlining some of the possible future directions for research in this area and some related speculations.

6.1 Future directions

Holographic braneworld cosmology approach

Possible future directions in the holographic braneworld cosmology approach include:

- Generalizing our constructions to setups involving ETW branes with non-constant stress-energy tensors. For example, one could consider a brane action including a 4D Einstein-Hilbert term along the lines of [118], or include scalar fields localized on the brane. This could help achieving more generic cosmological universes, possibly undergoing phases of accelerated expansion, also within the holographic braneworld cosmology approach.

- Understanding whether well-defined solutions supporting gravity localization can be obtained in more generic setups beyond the specific one considered in Chapter 2. For example having more complicated forms for the brane stress-energy tensor as suggested above could help achieve gravity localization.

- Finding specific examples of microscopic BCFT constructions dual to the holographic braneworld cosmology setups of our interest. This would provide a UV-complete, fully quantum description of a gravitational system involving a cosmological spacetime.

- Generalizing the framework to different spatial topologies (flat and hyperbolic) and study in more detail how an effective 4D EFT on the brane arises when "integrating out" the bulk degrees of freedom. This would allow us to describe more classes of cosmological models within the holographic braneworld cosmology framework and could also help us make contact between our two approaches. One interesting related direction could be the construction of a doubly-holographic description of the Lorentzian traversable wormhole picture arising in the holographic wormhole cosmology approach.

Holographic wormhole cosmology approach

Possible future directions in the holographic wormhole cosmology approach include:

- Building specific examples of the microscopic "sandwich theory" dual to our bulk setup. As suggested in [8] and discussed in Chapter 3, these could involve two 3D superconformal field theories (SCFT) coupled to a 4D SCFT (such as $\mathcal{N} = 4$ SYM) on $\mathbb{R}^3 \times I$, with supersymmetry partially preserved by the coupling at each boundary of the interval, but fully broken in the full sandwich theory. It would also be interesting to build bulk string-theoretic setups reducing to our semiclassical bulk EFT in the appropriate limit. These could be given by brane-antibrane systems giving rise to a connected brane, which would represent the Euclidean wormhole, see [8] for a proposal in this direction. The construction of such microscopic models is a key step which will need to be taken in order to obtain a full quantum gravitational description of cosmology within our approach.

- Given a microscopic Euclidean path integral, showing that the dual bulk gravitational Euclidean path integral admits a stable saddle given by a Euclidean wormhole of the desired form. In other words, showing that the semiclassical Einstein's equations for the bulk EFT dual to specific sandwich theories admit wormhole solutions, and that such solutions are stable. This problem is connected to the discussion about the existence and stability of Euclidean wormhole saddles of the gravitational Euclidean path integral connecting multiple AdS boundaries, see for example [167].

- Understanding what are the general requirements that need to be satisfied by the bulk EFT to obtain enhanced negative vacuum energies able to support the Lorentzian traversable wormhole solutions. Examples are known [157, 158] in which such large negative energies arise when specific boundary conditions are imposed at the AdS boundaries—which means at the intersection between the bulk EFT coupled to gravity living on the wormhole background and the non-gravitational auxiliary degrees of freedom living on spatial $\mathbb{R}^2 \times I$. It would be interesting to understand whether such enhancement occurs generically for given classes of boundary conditions.

- As a follow-up of the previous direction and given bulk EFTs able to support the Lorentzian traversable wormhole, understanding whether there are generic common features in the vacuum expectation values of the stress-energy tensor of such EFTs (which source semi-classical Einstein's equations). Thanks to the slicing duality, understanding what behaviors of these vacuum expectation values are possible in the wormhole picture can help us determine what type of cosmological universes we can expect to arise in the cosmology picture.

- Finding other scalar potentials (possibly more natural and with a smaller number of parameters) able to support a scale factor evolution matching cosmological data. It would also be interesting to understand whether similar scalar potentials arise naturally within the holographic description we are interested in.

- Studying cosmological correlators within our framework. It would be interesting to understand what properties of cosmological correlators does our construction predict, and in particular whether scale invariance of cosmological perturbations is already built into the special state for the cosmology prepared by the gravitational Euclidean path integral without the need of primordial inflation. One way to approach this problem could be to study vacuum correlators in the Lorentzian wormhole picture and understand their generic features arising from the specific wormhole geometry the EFT lives on, and then obtain cosmological correlators by double analytic continuation.

- Considering generalizations of our constructions to topologies of the 3-manifold different from $\mathbb{R}^3$ (for instance a sphere or a hyperbolic space). This could help us describe a wider variety of cosmological spacetimes within our holographic wormhole cosmology approach, make contact with the holographic braneworld cosmology approach, and understand what constraints does the presence of a Euclidean wormhole with non-flat cross section impose on such cosmologies.

- Understanding how a classical "arrow of time" can emerge in our time-symmetric cosmologies from the full quantum-mechanical wavefunction [249]. One interesting possibility, different from the "forward" and "backward" bases interpretation suggested in Chapter 3, is that the wavefunction of the universe defined à la Hartle-Hawking by our gravitational Euclidean path integral has different classical branches, with some branches being "forward-moving" and some branches being "backward-moving" [7].

- Finally, understanding whether our framework contains features which could help us solve other phenomenological puzzles of the standard model of cosmology such as the Hubble tension [268], and whether it can teach us, possibly in its UV-complete realizations, new lessons about interpretational puzzles of theoretical quantum cosmology, for example the meaning of the wavefunction of the universe (which is related to the question about the emergence of the arrow of time described above), the nature of the cosmological singularity, and the measure problem [273].

Appendix A: Technical details of the results reported in Chapter 2

Authors:[1] *Stefano Antonini, Brian Swingle.*

A.1 Euclidean action and Einstein-Maxwell equations

The total Euclidean action for the bulk spacetime is given by

$$I_{bulk} = -\frac{1}{16\pi G}\int_{\mathcal{M}} d^{d+1}x\sqrt{g}(R - 2\Lambda - 4\pi G F_{\mu\nu}F^{\mu\nu}) + I_{GHY} + I^{em}_{bound} \tag{A.1}$$

where $\mathcal{M}$ is the $(d+1)$-dimensional spacetime manifold, g is the determinant of the bulk metric, R is the Ricci scalar, $\Lambda = -d(d-1)/(2L^2_{AdS})$ is the cosmological constant, I_{GHY} is the Gibbons-Hawking-York term for the asymptotic boundary and

$$I^{em}_{bound} = -\int_{\partial\mathcal{M}_\infty} d^dx\sqrt{\gamma}F^{\mu\nu}\tilde{n}_\mu A_\nu \tag{A.2}$$

with γ determinant of the metric induced on the asymptotic boundary $\partial\mathcal{M}_\infty$ and $\tilde{n}_\mu$ dual vector normal to the boundary. The term I^{em}_{bound} is needed [201–203] because we keep the charge fixed instead of the potential when we vary the action (A.1). This choice is preferable since we are

[1]Originally published as Supplementary Material of *Cosmology at the end of the world*, Nature Phys. 16 (2020) 8, 881-886, [1]. Also available in the appendices of e-Print: 1907.06667.

interested in controlling the charge in order to approach the extremal black hole case and obtain a sensible Euclidean solution for a near-critical brane. Additionally, the dual (pure) CFT state, will be a fixed charge state. The electromagnetic potential (in Lorentzian signature, t Lorentzian time[2]) $A_\mu = (A_t, \vec{0})$ for a point charge in the origin reads:

$$A_t = \sqrt{\frac{d-1}{8\pi G(d-2)}}\left(\frac{Q}{r^{d-2}} - \frac{Q}{r_+^{d-2}}\right) \tag{A.3}$$

where we chose the outer (event) horizon of the black hole $r = r_+$ to be the zero-potential surface and Q is the charge parameter of the black hole, related to the point charge $\tilde{Q}$ (charge of the black hole) by [144, 202, 203]

$$Q = \sqrt{\frac{8\pi G}{(d-1)(d-2)}}\frac{\tilde{Q}}{V_{d-1}} \tag{A.4}$$

with V_{d-1} volume of the $(d-1)$-dimensional unit sphere. The electromagnetic tensor is standardly defined as $F_{\mu\nu} = \partial_\mu A_\nu - \partial_\nu A_\mu$. The action for the End-of-the-World brane is reported in equation (2.2), where I^{em}_{ETW} has the same form (A.2) of the electromagnetic boundary term for the asymptotic boundary, with $\gamma \to h$ and n_μ dual vector normal to the ETW brane. The extrinsic curvature appearing there is defined as

$$K_{ab} = \nabla_\mu n_\nu \mathrm{e}^\mu_a \mathrm{e}^\nu_b, \qquad \mathrm{e}^\mu_a = \frac{dx^\mu}{dy^a}. \tag{A.5}$$

A variation of the total action for the bulk and the brane leads to a set of three equations: equation (2.5) (describing the motion of the brane in the bulk spacetime and obtained by imposing

[2] In Euclidean signature the electromagnetic potential differs by a $-i$ factor: $A_\tau = -iA_t$ with τ Euclidean time. Note that all the quantities of our interest in the following involve the contraction of two A_τ with the 00-component of the Euclidean metric (which is defined with a $-$ sign with respect to the Lorentzian one). Therefore, the Lorentzian and Euclidean versions of such quantities take exactly the same form.

Neumann boundary conditions at the brane, according to the AdS/BCFT prescription [11, 12]), the Einstein-Maxwell equations for the bulk

$$R_{\mu\nu} - \frac{1}{2}g_{\mu\nu}(R - 2\Lambda) = 8\pi G T^{bulk}_{\mu\nu} \tag{A.6}$$

with $R_{\mu\nu}$ Ricci tensor, and the Maxwell equation

$$\nabla_\mu F^{\mu\nu} = 0. \tag{A.7}$$

The bulk stress-energy tensor appearing in equation (A.6) is the electromagnetic stress-energy tensor:

$$T^{bulk}_{\mu\nu} = g^{\rho\sigma} F_{\mu\rho} F_{\nu\sigma} - \frac{1}{4} g_{\mu\nu} F_{\rho\sigma} F^{\rho\sigma}. \tag{A.8}$$

The static and spherically symmetric metric reported in equation (2.3) is a solution of the Einstein-Maxwell equations (A.6) and the mass parameter μ appearing in equation (2.4) (which is valid only for $d > 2$) is related to the ADM mass of the black hole by

$$\mu = \frac{8\pi G M}{(d-1)V_{d-1}}. \tag{A.9}$$

In order to approach, in our numerical analysis, the extremal black hole case for a fixed event horizon size by controlling the Cauchy horizon radius it is useful to express the mass and the charge parameters in terms of r_+ and r_-:

$$\mu = \frac{L_{AdS}^2 \left[r_+^{2(d-2)} - r_-^{2(d-2)} \right] + r_+^{2d-2} - r_-^{2d-2}}{2L_{AdS}^2 (r_+^{d-2} - r_-^{d-2})}; \tag{A.10}$$

$$Q^2 = r_+^{d-2} r_-^{d-2} \left[\frac{L_{AdS}^2 \left(r_+^{d-2} - r_-^{d-2} \right) + r_+^d - r_-^d}{L_{AdS}^2 \left(r_+^{d-2} - r_-^{d-2} \right)} \right]. \tag{A.11}$$

It is also convenient to eliminate the mass parameter from the expression of the $\tau\tau$ component of the metric $f(r)$:

$$f(r) = 1 + \frac{r^2}{L_{AdS}^2} - \frac{r_+^{d-2}}{r^{d-2}} \left(1 + \frac{r_+^2}{L_{AdS}^2} \right) + \frac{Q^2}{r^{d-2}} \left(\frac{1}{r^{d-2}} - \frac{1}{r_+^{d-2}} \right) \tag{A.12}$$

which can be rewritten, using the adimensional coordinates introduced in Section 2.4, in a form more functional for the gravity localization analysis

$$f(y) = \frac{\left[y^4 + \left(\gamma^2 + 1 \right) y^2 - \gamma^2 q^2 \right] \left(y^2 - 1 \right)}{\gamma^2 y^4}. \tag{A.13}$$

For completeness, we report here also the form of the $\tau\tau$ component of the metric for the BTZ charged black hole (i.e. for $d = 2$) as a function of the ADM mass M and the charge of the black hole $\tilde{Q}$, in units such that $G_3 = 1/8$ [147]:

$$f(r) = \frac{r^2}{L_{AdS}^2} - M - \tilde{Q}^2 \ln \left(\frac{r}{L_{AdS}} \right). \tag{A.14}$$

Finally, the Ricci scalar for a spherically symmetric metric of the form (3) takes in general the form

$$R = -\frac{r^2 f''(r) + 2r(d-1)f'(r) + (d-1)(d-2)f(r) - (d-1)(d-2)}{r^2}. \tag{A.15}$$

Substituting equation (2.4), we obtain, for $d > 2$

$$R = -\frac{d(d+1)}{L_{AdS}^2} - \frac{(d-3)(d-2)Q^2}{r^{2d-2}}. \tag{A.16}$$

Note that we made use of the AdS/BCFT prescription first introduced by Takayanagi [11], which is suitable for ETW branes, to define our action principle. In such a formulation, the variation of the action leads to Einstein equations for the bulk without a delta contribution proportional to the tension of the brane on the right-hand side. The equations of motion for the brane are then obtained directly from the action principle (by imposing Neumann boundary conditions at the brane), instead of the Israeli junction conditions (the latter approach is employed, for instance, in ref [114]). Starting from this well-established formulation, the Ricci scalar has no contribution at the position of the brane proportional to the brane tension.

A.2 Euclidean analysis - details

In order to avoid a conical singularity, the Euclidean time τ must be periodic with periodicity given by

$$\beta = \frac{2\pi}{k_g}. \tag{A.17}$$

k_g is the surface gravity, which for the static and spherically symmetric black holes reads

$$k_g = \left.\frac{f'(r)}{2}\right|_{r=r_H} \tag{A.18}$$

where r_H is the event horizon radius. For a Reissner-Nordström black hole $r_H = r_+$. Using equation (A.12), for $d > 2$ we find the Euclidean periodicity

$$\beta = \frac{4\pi L_{AdS}^2 r_+^{2d-3}}{(d-2)L_{AdS}^2\left[r_+^{2(d-2)} - Q^2\right] + dr_+^{2d-2}}. \tag{A.19}$$

The spherically symmetric ETW brane can be parametrize with $r = r(\tau)$. Analogously to the AdS-Schwarzschild case [5], the one-form dual to the unit vector normal to the brane is given by

$$n_\mu = N(-r', 1, \mathbf{0}), \qquad\qquad N = \sqrt{\frac{f(r)}{f^2(r) + (r')^2}} \tag{A.20}$$

with $r' = dr/d\tau$. The metric induced on the brane reads

$$\begin{aligned} h_{\tau\tau} &= f(r) + \frac{(r')^2}{f(r)}; \\ h_{\phi_i\phi_i} &= g_{\phi_i\phi_i} \qquad i = 1, .., d-1 \end{aligned} \tag{A.21}$$

where ϕ_i are the coordinates on the sphere directions. Using $e^\mu_\tau = (1, r', 0)$, the definition of the extrinsic curvature (A.5) and equation (A.20), the components of the extrinsic curvature read:

$$K_{\tau\tau} = -e^\mu_\tau n_\nu \nabla_\mu e^\nu_\tau = N\left[\frac{3f'(r)}{2f(r)}(r')^2 - r'' + \frac{f(r)f'(r)}{2}\right]; \tag{A.22}$$

$$K_{\phi_i\phi_i} = \frac{Nf(r)}{r} h_{\phi_i\phi_i} \tag{A.23}$$

where $r' = dr/d\tau$ and $r'' = d^2r/d\tau^2$. Then the $\tau\tau$ component of equation (2.5) leads to equation (2.6), that we report here:

$$\frac{dr}{d\tau} = \pm \frac{f(r)}{Tr} \sqrt{f(r) - T^2 r^2}. \tag{A.24}$$

The $+$ $(-)$ sign corresponds to the contracting (expanding) phase. Indeed, as it is clear from Figure 2.2, for $T > 0$ during the contraction the Euclidean time decreases (clockwise) from $\tau = -\tau_0$ to $\tau = -\beta/2$, therefore the $dr/d\tau > 0$; during the expansion the time decreases from $\tau = \beta/2$ to $\tau = \tau_0$, and $dr/d\tau < 0$. Note that choosing $T < 0$ corresponds to picking the opposite normal vector to the brane, i.e. to retaining the red-shaded part of the geometry in Figure 2.2 [5, 133]. More precisely, since the portion of Euclidean boundary retained in our geometry is on the right, choosing $T < 0$ means to consider a solution analogous to the one in Figure 2.2, but reflected with respect to a vertical line passing through the centre of the Euclidean circle (i.e. the $\tau = \pm\beta/4$ line). The initial condition will now be $r(\tau = 0) = r_0$. Note that the signs in equation (A.24) corresponding to the expanding and contracting phase remain the same, because we did not include the absolute value for the tension. Naturally, the preparation time will be defined differently for $T < 0$: $\tau_0 = \Delta\tau$ [133]. This reasoning can also be understood in terms of the geometrical interpretation of the tension. Indeed, let $u_\mu = C(-f(r), -r', \mathbf{0})$ with $C = [f(r)(f^2(r) + (r')^2)]^{-1/2}$ be the unit vector tangent to the brane and $v_\mu = (0, -1/\sqrt{f(r)}, \mathbf{0})$ the inward-directed unit vector normal to the asymptotic boundary. Then $\cos\theta \equiv u \cdot v \sim \sqrt{1 - T^2}$ close to the boundary ($r \gg L_{AdS}, r_+$), where θ is the angle between u and v. Therefore, $T = \sin\theta$: the tension gives the angle of incidence of the brane with the asymptotic boundary [5, 12].

Choosing opposite values of the tension means having opposite angles of incidence of the brane with the boundary, i.e. choosing one solution or its counterpart symmetric with respect to the $\tau = \pm\beta/4$ axis. As we pointed out, in this paper we only focus our attention on the positive tension case.

It is easy to show that, if equation (A.24) is satisfied, the other components of equation (2.5) are identically fulfilled. Indeed, using equations (A.23) and (A.24), the $\phi_i\phi_i$ components of equation (2.5) lead to

$$r''(t) = f(r)\left[\frac{3}{2}\frac{f(r)f'(r)}{T^2r^2} - f'(r) - \frac{f^2(r)}{T^2r^3}\right]. \tag{A.25}$$

But this equation can also be obtained by deriving equation (A.24) and substituting again r' with the right hand side of equation (A.24). Therefore, if equation (A.24) holds, the acceleration equation (A.25) is automatically fulfilled.

The minimum radius r_0 is defined by the largest zero of the RHS of equation (A.24), i.e. by the largest solution of the equation

$$f(r) = T^2r^2, \tag{A.26}$$

as discussed in Section 2.2. For a vanishing tension, clearly $r_0 = r_+$. Indeed, the two solutions of equation (A.26) are $r_0^- = r_-$ and $r_0^+ = r_+$, because $f(r_+) = f(r_-) = 0$ by definition of horizon. Since $f(r) > 0$ only when $r < r_-$ or $r > r_+$, for $0 < T < 1/L_{AdS}$ equation (A.26) can have solutions only for $r < r_-$ or $r > r_+$. In particular, we note that $f(0) = \infty$ and $f(r_-) = 0$, meaning that there is always a solution for $r < r_-$, which we label r_0^-. Additionally, given that

$f(r_+) = 0$ and $f(r) \sim r^2/L_{AdS}^2$ for $r \to \infty$, the condition $T < 1/L_{AdS}$ guarantees that there is always a solution of equation (A.26) for $r > r_+$ as well, that we label r_0^+. The latter is the largest solution, and is therefore the minimum radius of the brane r_0. We remark that, in the Euclidean picture, the brane always stays outside the event horizon.

A numerical evaluation shows that the ratio r_0/r_+ increases when the tension increases. In particular, if the black hole is big (meaning $r_+ \gg L_{AdS}$), it is possible to obtain a very large ratio r_0/r_+ by approaching the critical value of the tension (see Figure 2.3 panel (b)). If the black hole is small, the ratio is never large, preventing gravity localization on the brane. Since

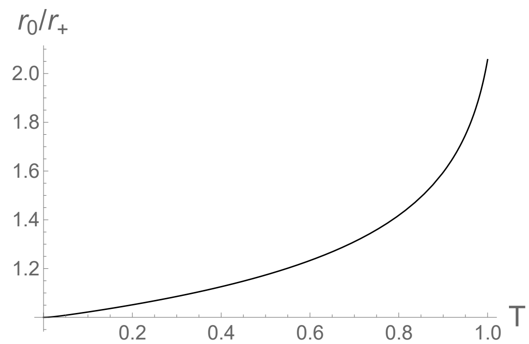

Figure A.1: Minimum brane radius - Small black hole. The minimum radius of the brane r_0 grows with the tension T, but it never becomes much larger than the black hole horizon. $d = 4$, $r_+ = 1$, $r_- = 0.99$, $L_{AdS} = 1$.

we are interested in time-symmetric solutions with a positive-tension brane, we can require the brane to reach its minimum radius for $\tau = \pm\beta/2$, defining $r_0 = r(\tau = \pm\beta/2)$. Up to a constant $\beta/2$ (which cancels out when adding up the Euclidean times necessary for the expanding and the contracting phases), the brane locus is given by

$$\tau(r) = \int_{r_0}^{r} d\hat{r} \frac{T\hat{r}}{f(\hat{r})\sqrt{f(\hat{r}) - T^2\hat{r}^2}}. \tag{A.27}$$

The total Euclidean time necessary for the brane to go from $r = r_0$ to $r = \infty$, i.e. to cover half of its trajectory, is

$$\Delta\tau = \int_{r_0}^{\infty} dr \frac{Tr}{f(r)\sqrt{f(r) - T^2 r^2}}. \tag{A.28}$$

The Euclidean preparation time τ_0 is given by the residual Euclidean periodicity:

$$\tau_0 = \frac{\beta - 2\Delta\tau}{2} = \frac{2\pi L_{AdS}^2 r_+^{2d-3}}{(d-2)L_{AdS}^2\left(r_+^{2(d-2)} - Q^2\right) + dr_+^{2d-2}} - \Delta\tau. \tag{A.29}$$

For a critical brane we obtain:

$$\Delta\tau_{crit} = \frac{1}{L_{AdS}} \int_{r_0}^{\infty} dr \frac{r}{\left(1 + \frac{r^2}{L_{AdS}^2} - \frac{2\mu}{r^{d-2}} + \frac{Q^2}{r^{2(d-2)}}\right)\sqrt{1 - \frac{2\mu}{r^{d-2}} + \frac{Q^2}{r^{2(d-2)}}}} \tag{A.30}$$

and this expression is logarithmically divergent at infinity. For $T > T_{crit}$, the square root $\sqrt{f(r) - T^2r^2}$ becomes imaginary for large values of r. Thus, $\Delta\tau$, and therefore the preparation time τ_0, are well defined only for $T < T_{crit}$.

Our numerical evaluation shows that, given a value for the outer horizon radius r_+ and for the brane tension $T < T_{crit}$, it is always possible to obtain a positive preparation time (i.e. a sensible Eucliden solution, and a dual description in terms of an Euclidean-time-evolved charged boundary state of a CFT living on the boundary of the right asymptotic region of the black hole) by increasing the size of the inner horizon radius r_-, which means by increasing the charge of the black hole. For $T \to T_{crit}$, we need $r_- \to r_+$ in order to retain a sensible Euclidean solution, i.e. the black hole must approach extremality. This feature guarantees that, for a large black hole sufficiently close to extremality, we can find a sensible Euclidean solution with the minimum radius of the brane (which is the maximum radius in Lorentzian signature) consistently larger than the black hole event horizon. As we have pointed out, this is a necessary condition in order to achieve gravity localization on the brane. In the AdS-Schwarzschild case, which is the $Q \to 0$ limit of our analysis, this result is clearly impossible to obtain. Therefore, for an uncharged black hole gravity localization and positive preparation time mututally exclude each other, and a holographic braneworld cosmology picture is not feasible. [5]

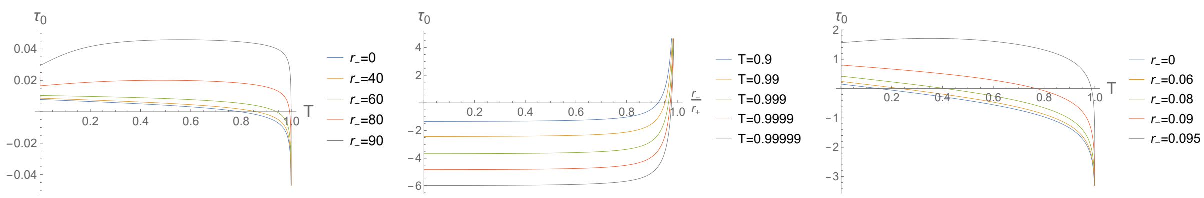

(a) (b) (c)

Figure A.2: Preparation time. (a) Large black hole case. Approaching the extremal black hole (r_-, and therefore the charge, increasing from bottom to top), τ_0 is positive for a larger range of values for the tension T. $d = 4$, $r_+ = 100$, $L_{AdS} = 1$. (b)-(c) Small black hole case. The behaviour is similar to the large black hole case (the analogous of (b) is reported in Figure 2.3(a)). $d = 4$, $r_+ = 0.1$, $L_{AdS} = 1$.

A.3 Action comparison

In order to understand if the non-extremal AdS-RN solution we studied is dominant in the Euclidean path integral, we must compare its on-shell action with other possible phases contributing to the path integral. The dominant phase will be the one with smallest action. As we have already pointed out, we will focus our attention on the fixed charge case. This choice corresponds to a canonical ensemble, where the temperature and the charge are held fixed. Note that this implies that (differently from the fixed potential case) the variation of the potential does not vanish on the boundary. For this reason, we need to add the electromagnetic boundary terms (A.2) for the asymptotic boundary and the brane to the action. For fixed charge, the other possible phase is represented by the extremal AdS-RN black hole with the same charge as the corresponding non-extremal solution (for a complete treatment of the AdS-RN phase structure for fixed charge and fixed potential without the ETW brane see refs. [202, 203]). The CFT state corresponding to the fixed charge ensemble is the Euclidean-time-evolved boundary state with fixed charge reported in equation (2.1). It is clear that the two Euclidean solutions contributing to the gravity path integral dual to the state (2.1) must have the same charge and the same preparation time τ_0. We will use this property in order to match the two geometries in the asymptotic region, procedure needed in order to regularize the Euclidean action and compare the two actions. [5, 202, 203] We will now briefly review some useful properties of the extremal AdS-RN black hole.

Extremal AdS-RN black hole

For the extremal AdS-Reissner-Nordström black hole, the two solutions r_+ and r_- of $f_e(r) = 0$ coincide, defining the extremal horizon radius r_e. Therefore, also the relationship $f_e'(r)|_{r=r_e} = 0$ must hold. By requiring the two conditions to be satisfied, we obtain for the extremal mass and charge parameters:

$$2\mu_e = 2r_e^{d-2} + \frac{2d-2}{d-2}\frac{r_e^d}{L_{AdS}^2}; \tag{A.31}$$

$$Q_e^2 = r_e^{2d-4} + \frac{d}{d-2}\frac{r_e^{2d-2}}{L_{AdS}^2}. \tag{A.32}$$

We remark how, by fixing the charge of the black hole, the extremal horizon radius is uniquely determined.

Another important feature of the extremal black hole is that, since $f_e'(r)|_{r=r_e} = 0$, the Euclidean periodicity (A.17) diverges, i.e. the temperature of the extremal black hole vanishes. Nonetheless, it has been demonstrated [149, 202, 203] that an arbitrary Euclidean periodicity can be chosen for the extremal RN black hole without running into a conical singularity. Physically, this means that an extremal RN black hole can be in thermodynamic equilibrium with a thermal bath at an arbitrary temperature. In the following we will use this feature, fixing a total Euclidean periodicity β_e for the extremal black hole that will be determined by matching the geometries of the non-extremal and the extremal black holes in the asymptotic regions. Given β_e, the extremal horizon radius r_e and the expression (A.32) for the extremal charge, the same Euclidean analysis carried out in Appendix A.1 can be applied to the extremal case.

Before explicitly evaluating the difference of the two Euclidean actions for the non-extremal and extremal black holes, one more remark is needed. In general, the phase structure is more complicated than the one we are going to study. In particular, for a given small charge $Q < Q_{crit}$ and some range of temperatures, three different non-extremal black holes with the same temperature but different horizon radius can exist [202]. Indeed, for $Q < Q_{crit}$, there exist turning points for the Euclidean periodicity β as a function of the external horizon r_+, which disappear for $Q > Q_{crit}$. The critical charge can be obtained from the condition $\partial_{r_+}\beta = 0 = \partial^2_{r_+}\beta$, and reads [202]:

$$Q^2_{crit} = \frac{1}{(d-1)(2d-3)} \left[\frac{(d-2)^2}{d(d-1)}\right] L^{2d-4}_{AdS}. \tag{A.33}$$

The coexistence of different non-extremal black holes implies the necessity of studying which one of them has the smallest action, before a comparison with the extremal case can be made. To do so, we should fix an Euclidean periodicity β and a charge Q, find the different corresponding values of r_+ and compare the actions for each of them.

Nonetheless, since, as we have already pointed out, we are interested in solutions involving near-critical branes, and this requires to have a large black hole near extremality in order to have a positive preparation time, we are safely into the region where only one non-extremal phase exists [202]. Note that the parameter we want to fix is the preparation time τ_0, which is meaningful in the dual CFT, and not the Euclidean periodicity β. But for $Q > Q_{crit}$, a numerical analysis shows that, given a tension T, when $\tau_0 > 0$ it is in a one-to-one correspondence with β. In other words, fixing Q, T and β or fixing Q, T and τ_0 is completely equivalent for the region of parameters of our interest, and there is only one possible non-extremal phase for each choice of parameters. Therefore, we are allowed to choose r_+ and r_- independently, and a tension T (this is equivalent to choose a tension T, a charge Q and a preparation time τ_0) and compare directly the resulting action with the corresponding extremal action with the same charge.

Bulk action

Let us evaluate the three terms of the bulk action (A.1) separately in the non-extremal case. First, using equation (A.3)[3], the only non vanishing components of the electromagnetic tensor are $F_{\tau r} = -F_{r\tau}$, and we obtain

$$F_{\mu\nu}F^{\mu\nu} = -\frac{(d-1)(d-2)}{4\pi G}\frac{Q^2}{r^{2d-2}}. \tag{A.34}$$

Using equation (A.15) for the Ricci scalar, the relationship between Λ and L_{AdS}, and noting that $\sqrt{g} = r^{d-1}$, the first term of the bulk action reads

$$I_{bulk}^{(1)} = \frac{dV_{d-1}}{8\pi G L_{AdS}^2}\int dr d\tau r^{d-1} - \frac{(d-2)V_{d-1}Q^2}{8\pi G}\int dr d\tau \frac{1}{r^{d-1}}. \tag{A.35}$$

[3]Using equation (A.3), we must raise the indices with the Lorentzian metric, computing $F_{\mu\nu}F^{\mu\nu}$ in the Lorentzian case. As we have pointed out, this yields exactly the same result that we would get using the Euclidean version of the electromagnetic potential $A_\tau = -iA_t$ and raising the indices with the Euclidean metric. In other words, $F_{\mu\nu}F^{\mu\nu}$ is unchanged under Wick's rotation. The same is true for the combination $F^{\mu\nu}n_\mu A_\nu$ appearing in the electromagnetic boundary term.

Recalling that part of the Euclidean geometry is cut off by the ETW brane parametrized by $\tau(r)$, we can rewrite this integral as the integral in the entire spacetime minus the excised part. In order to avoid divergences, we must also introduce a cut-off R in the asymptotic region. After a few steps, the result turns out to be

$$\begin{aligned} I_{bulk}^{(1)} =& \frac{V_{d-1}}{8\pi G L_{AdS}^2}\left[\beta(R^d - r_+^d) - 2\left(r^d\tau(r)\right)\Big|_{r_0}^{R} + 2\int_{r_0}^{R} dr r^d \frac{\partial\tau}{\partial r}\right] \\ &+ \frac{V_{d-1}Q^2}{8\pi G}\left[\beta\left(\frac{1}{R^{d-2}} - \frac{1}{r_+^{d-2}}\right) - 2\left(\frac{\tau(r)}{r^{d-2}}\right)\Bigg|_{r_0}^{R} + 2\int_{r_0}^{R} dr \frac{1}{r^{d-2}}\frac{\partial\tau}{\partial r}\right] \end{aligned} \tag{A.36}$$

where β is given by equation (A.19).

The Gibbons-Hawking-York term I_{GHY} gives a vanishing contribution to the action difference for asymptotically AdS spacetimes [202, 203, 274] and therefore we can neglect it. The electromagnetic boundary term finally reads

$$I_{bound}^{em} = -\frac{(d-1)V_{d-1}Q^2\tau_0}{4\pi G}\left(\frac{1}{R^{d-2}} - \frac{1}{r_+^{d-2}}\right). \tag{A.37}$$

Brane action

Tracing equation (2.5) we obtain

$$K - (d-1)T = T. \tag{A.38}$$

Parametrizing again the brane with $\tau(r)$, and using equation (A.24), the determinant of the metric induced on the brane reads:

$$\sqrt{h} = \pm \frac{1}{T} f(r) r^{d-2} \frac{\partial \tau}{\partial r} \tag{A.39}$$

where the $+$ $(-)$ sign is for the contracting (expanding) phase. Considering the contributions of both these two phases and using the expression (A.20) for the dual vector normal to the brane, the total action for the ETW brane reads

$$\begin{aligned} I_{ETW} =& - \frac{V_{d-1}}{4\pi G} \int_{r_0}^{R} dr f(r) r^{d-2} \frac{\partial \tau}{\partial r} \\ &+ \frac{(d-1)V_{d-1}Q^2}{4\pi G r_+^{d-2}} \tau(r) \Big|_{r_0}^{R} - \frac{(d-1)V_{d-1}Q^2}{4\pi G} \int_{r_0}^{R} dr \frac{1}{r^{d-2}} \frac{d\tau}{dr}. \end{aligned} \tag{A.40}$$

Action difference

Using the definition (A.27), we note that $\tau(r_0) = 0$. Additionally, $\lim_{R\to\infty} \tau(R) = \Delta\tau$ and $\beta - 2\Delta\tau = 2\tau_0$. Since, after subtracting the extremal action from the non-extremal one, we will take the limit $R \to \infty$, for simplicity of notation we will substitute now $\tau(R) \to \Delta\tau$ and $\beta - 2\tau(R) \to 2\tau_0$, even if the limit has not been taken yet. Using the above cited relationships, the total action for the non-extremal black hole can be cast in the form

$$\begin{aligned} I_{tot} =& \frac{V_{d-1}}{8\pi G L_{AdS}^2} \left\{ 2\tau_0 R^d - \beta r_+^d - \frac{2(d-2)L_{AdS}^2 Q^2}{R^{d-2}} \tau_0 + \frac{(d-2)L_{AdS}^2 Q^2}{r_+^{d-2}} \beta \right. \\ &\left. + 2 \int_{r_0}^{R} dr \left[\left(r^d - \frac{(d-2)L_{AdS}^2 Q^2}{r^{d-2}} - L_{AdS}^2 r^{d-2} f(r) \right) \frac{\partial \tau}{\partial r} \right] \right\}. \end{aligned} \tag{A.41}$$

We must now subtract from this action the equivalent action for the extremal black hole after matching the geometries in the asymptotic region, and then take the limit $R \to \infty$. The total action for the extremal black hole is given by equation (A.41) where all the quantities are substituted by their extremal counterparts ($r_+ \to r_e$, $\tau_0 \to \tau_0^e$, $\beta \to \beta_e$, $r_0 \to r_0^e$, $f(r) \to f_e(r)$, $Q \to Q_e$). As we have already mentioned, the Euclidean analysis carried out for the non extremal black hole is still valid by substituting $r_+ \to r_e$, and the total Euclidean periodicity β_e can be chosen arbitrarily [149]. Since we are interested in the fixed charge case, we can choose a charge, which will be the same for both the black holes ($Q = Q_e$), using equation (A.11) and selecting values for the outer and inner horizon radii (r_+ and r_-) of the non-extremal black hole. The extremal horizon radius r_e is then uniquely determined by equation (A.32). Therefore r_e can be written as a function of r_+ and r_- only. We will use this feature in our numerical analysis.

The choice of the (arbitrary) Euclidean periodicity for the extremal black hole is determined by the matching of the two geometries in the asymptotic region. In particular, we must match the proper Euclidean preparation times in the asymptotic region (i.e. for $r = R$):

$$2\tau_0\sqrt{f(R)} = 2\tau_0^e\sqrt{f_e(R)}. \tag{A.42}$$

At lowest order in $1/R$, equation (A.42) gives

$$\tau_0^e \sim \tau_0(1 + A) \tag{A.43}$$

where we have defined:

$$A = \frac{L_{AdS}^2}{R^d}(\mu_e - \mu) = \frac{L_{AdS}^2}{R^d}\left(r_e^{d-2} + \frac{d-1}{d-2}\frac{r_e^d}{L_{AdS}^2} - \frac{r_+^{d-2}}{2} - \frac{r_+^d}{2L_{AdS}^2} - \frac{Q^2}{2r_+^{d-2}}\right). \tag{A.44}$$

We emphasize that, at the asymptotic boundary (i.e. for $R \to \infty$), $\tau_0^e = \tau_0$, as we expect for two geometries dual to the state (2.1). The total Euclidean periodicity for the extremal black hole can then be set to be

$$\beta_e = 2\tau_0^e + 2\Delta\tau_e = 2\tau_0(1+A) + 2\Delta\tau_e \tag{A.45}$$

where $\Delta\tau_e$ is defined in perfect analogy with the non-extremal case. Using equation (A.45) and the matching condition (A.43) and taking the limit $R \to \infty$, after some manipulation the difference between the non-extremal and the extremal action finally takes the form

$$\begin{aligned}
\Delta I \equiv & \frac{8\pi G L_{AdS}^2}{V_{d-1}} \lim_{R\to\infty} (I - I_{ext}) = \\
& - \frac{2r_e^d \tau_0}{d-2} - 2L_{AdS}^2 r_e^{d-2}\tau_0 + L_{AdS}^2 r_+^{d-2}\tau_0 + r_+^d\tau_0 - \beta r_+^d + \frac{L_{AdS}^2 Q^2 \tau_0}{r_+^{d-2}} \\
& + 2r_e^d \Delta\tau_e + \frac{(d-2)L_{AdS}^2 Q^2 \beta}{r_+^{d-2}} - \frac{2(d-2)L_{AdS}^2 Q^2 \tau_0}{r_e^{d-2}} - \frac{2(d-2)L_{AdS}^2 Q^2 \Delta\tau_e}{r_e^{d-2}} \\
& - 2L_{AdS}^2 \int_{r_0^e}^{r_0} dr \left\{ \left[-r^{d-2} + r_e^{d-2}\left(1 + \frac{r_e^2}{L_{AdS}^2}\right) + \frac{Q^2}{r_e^{d-2}} - \frac{(d-1)Q^2}{r^{d-2}} \right] \frac{Tr}{f_e(r)\sqrt{f_e(r) - T^2 r^2}} \right\} \\
& + 2L_{AdS}^2 \int_{r_0}^{\infty} dr \left\{ \left[-r^{d-2} + r_+^{d-2}\left(1 + \frac{r_+^2}{L_{AdS}^2}\right) + \frac{Q^2}{r_+^{d-2}} - \frac{(d-1)Q^2}{r^{d-2}} \right] \frac{Tr}{f(r)\sqrt{f(r) - T^2 r^2}} \right. \\
& \left. - \left[-r^{d-2} + r_e^{d-2}\left(1 + \frac{r_e^2}{L_{AdS}^2}\right) + \frac{Q^2}{r_e^{d-2}} - \frac{(d-1)Q^2}{r^{d-2}} \right] \frac{Tr}{f_e(r)\sqrt{f_e(r) - T^2 r^2}} \right\} .
\end{aligned} \tag{A.46}$$

When such a difference is negative, the non-extremal black hole phase has smaller action and is therefore dominant in the ensemble.

A numerical evaluation shows that, for $d = 4$ and for a range of parameters such that the Euclidean solution for the non-extremal black hole is sensible (i.e. $\tau_0 > 0$), ΔI is always negative. Therefore, differently from the AdS-Schwarzschild case [5], when the non-extremal AdS-RN solution admits a dual CFT description, it is also always dominant in the gravity path integral.

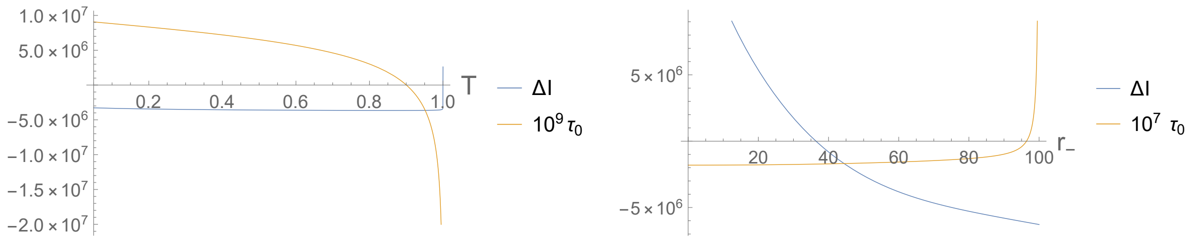

(a) (b)

Figure A.3: Action difference - Large black hole. Results for four spatial dimensions ($d = 4$). We set the outer horizon radius to be $r_+ = 100$, with the AdS length given by $L_{AdS} = 1$. (a) We chose $r_- = 50$ for the inner horizon radius. When the tension T is not too close to its critical value $T_{crit} = 1/L_{AdS} = 1$, the preparation time τ_0 is positive (i.e. the solution is Euclidean-sensible) and the action difference ΔI is negative, meaning that the non-extremal phase is always dominant in the path integral. (b) For a near-critical brane (we chose a value $T = 0.99999 \sim T_{crit}$ for the brane tension), when the black hole is sufficiently close to extremality (i.e. $r_- \to r_+$), the preparation time τ_0 becomes positive, and therefore the Euclidean solution is sensible. The non-extremal phase is already dominant in the ensemble (i.e. the action difference ΔI is negative) well before it happens. The same properties hold also for the small black hole case.

A.4 Lorentzian analysis and braneworld cosmology - details

The initial condition for the real time evolution is given by the $\tau = 0, \pm\beta/2$ slice of the Euclidean geometry, where the brane reaches its minimum radius r_0. The time coordinate is analytically continued $\tau \to -it$, with t Schwarzschild time. Further time evolution will be in Lorentzian signature. The brane locus is then given by

$$t(r) = \int_{r_0}^{r} d\hat{r} \frac{T\hat{r}}{f(\hat{r})\sqrt{T^2\hat{r}^2 - f(\hat{r})}}. \tag{A.47}$$

We explained that, in the Lorentzian case, the range of the radial coordinate is $r_0^- < r_0 < r_0^+ \equiv r_0$. Let us now focus on the Friedmann equation (considered in equation (2.8)) describing the evolution of the brane in terms of its proper time λ. By defining $L(r) = \ln r$ and $L_+ = L(r_+)$, it can be rewritten as

$$\dot{L}^2 + V(L) = T^2 \tag{A.48}$$

where

$$V[L(r)] = \frac{f(r)}{r^2}. \tag{A.49}$$

In this new coordinate, the motion of the brane can be regarded as the one of a particle with energy T^2 in the presence of a potential $V(L)$. The potential (A.49) naturally vanishes for $r = r_+$ and $r = r_-$. It has a local maximum and a local minimum in r_M and r_m respectively. For the local minimum $r_- < r_m < r_+$ and $V[L(r_m)] < 0$, while for the local maximum $r_M > r_+$ and $V[L(r_M)] > 1/L^2_{AdS} = T^2_{crit}$. Additionally $\lim_{r\to\infty} V[L(r)] = T^2_{crit}$, while $\lim_{r\to 0} V[L(r)] = \infty$. The latter behaviour confirms that the brane radius cannot vanish, i.e. the brane undergoes a bounce for a minimum radius r_0^-. Differently from the small black hole case ($r_+ \lesssim L_{AdS}$), in the large black hole case ($r_+ \gg L_{AdS}$) the minimum of the potential is $V[L(r_m)] \sim 0$ and its local maximum is $V[L(r_M)] \sim T^2_{crit}$, the latter meaning that the value of the potential at the peak is almost indistinguishable from its asymptotic value. As an example we report in Figure A.4 a plot of the potential $V[L(r)]$ as a function of the radius of the brane r in the small and in the large black hole cases.

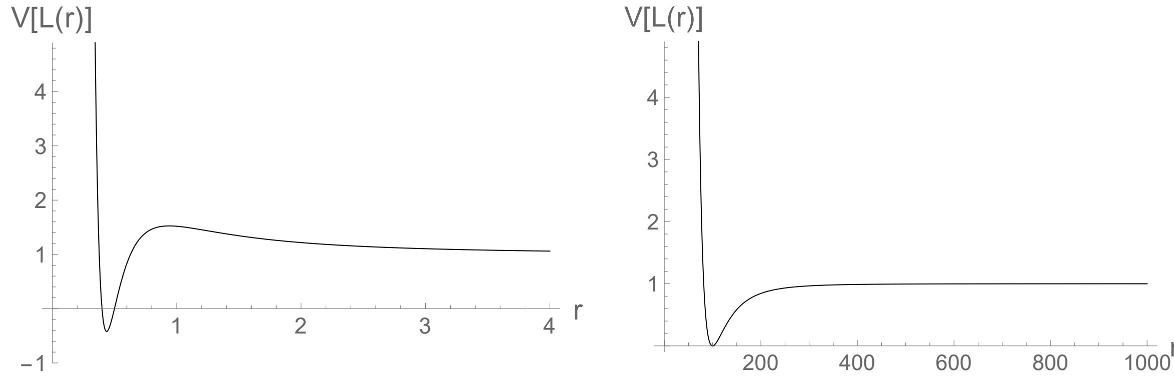

(a) (b)

Figure A.4: Potential $V[L(r)]$. (a) Small black hole case. The peak at $r = r_M$ is particularly evident. $d = 4$, $r_+ = 0.5$, $r_- = 0.4$, $L_{AdS} = 1$. (b) Large black hole case. r_M is very large and the value of the potential at the peak is almost indistinguishable from the asymptotic value. $d = 4$, $r_+ = 100$, $r_- = 99.9$, $L_{AdS} = 1$.

The brane trajectory will be determined by the value of its tension (i.e. the energy of the particle). In particular, analogously to the AdS-Schwarzschild case [5], we can distinguish in general five different cases:

1. $\mathbf{T^2} > \mathbf{V[L(r_M)]}$. The equation $f(r_0) = T^2 r_0^2$ has only one positive solution (r_0^-), which is by definition the position of the brane at $\lambda = 0$ (where λ is the brane proper time). Therefore, the brane radius decreases from $r = \infty$ to $r = r_0^-$ for negative time and then increases monotonically from $r = r_0^-$ to $r = \infty$ for positive time.

2. $\mathbf{T^2} = \mathbf{V[L(r_M)]}$. The brane has constant radius $r = r_M$. This corresponds to an Einstein static universe.

3. $\mathbf{T^2_{crit}} < \mathbf{T^2} < \mathbf{V[L(r_M)]}$ **- Large r branch.** The equation $f(r_0) = T^2 r_0^2$ admits three solutions. In particular, if we order such solutions as $r_0^{(3)} > r_0^{(2)} > r_0^{(1)}$, the quantity $\sqrt{T^2 r^2 - f(r)}$ is real for $r > r_0^{(3)}$ and for $r_0^{(1)} < r < r_0^{(2)}$. Thus, for large r, the behaviour

is similar to the first case, with the brane trajectory starting from $r = \infty$, shrinking to $r = r_0^{(3)}$ for $\lambda = 0$ and expanding again to $r = \infty$.

4. $\mathbf{T^2_{crit} < T^2 < V[L(r_M)]}$ **- Small r branch.** This is the same situation as in the previous case, but with $r_0^{(1)} < r < r_0^{(2)}$. The brane expands from $r = r_0^{(1)}$ to $r = r_0^{(2)}$ at $\lambda = 0$, and contracts again to $r = r_0^{(1)}$.

5. $\mathbf{T^2 < T^2_{crit}}$. In this case, as we have already pointed out, the equation $f(r_0) = T^2 r_0^2$ has two solutions, r_0^+ and r_0^-. The brane expands from $r = r_0^-$, emerges from the horizon, reaches its maximum radius $r = r_0^+$ for $\lambda = 0$, and shrinks again to $r = r_0^-$. This trajectory is completed in a finite amount of proper time, as we will see.

We remark that, as we have pointed out, our Euclidean analysis is feasible only for $T < T_{crit}$, condition needed to have a well-defined preparation time τ_0. Therefore only the last situation is of interest for our analysis. Nonetheless, a continuously expanding brane with $T > T_{crit}$ (first and third case) implies, from a braneworld cosmology point of view, a 4-dimensional Friedmann universe with a positive cosmological constant, which undergoes for late times a de Sitter expanding phase. This cosmological scenario is clearly more in accordance with the behaviour of our observed universe with respect to the Big Bounce cosmology of the last case. Therefore, an interesting future development of this work could be its extension to over-critical branes, which probably requires a different class of CFT states in the dual theory.

Focusing on the last case, a few final remarks are worth of attention. First, the choice of the sign of the tension T determines which vector normal to the brane we are considering [133], i.e. which one of the two sides of the brane we are retaining. The choice $T > 0$ corresponds to a Lorentzian geometry which contains the complete right asymptotic region and part of the left one, ending on the ETW brane (see Figure 2.1). Additionally, the total brane proper time needed to complete the trajectory from r_0^- to r_0^+ and back is given by

$$\lambda_{tot} = 2 \int_{r_0^-}^{r_0^+} d\hat{r} \frac{1}{\sqrt{T^2 \hat{r}^2 - f(\hat{r})}} \tag{A.50}$$

and is clearly finite. This expression is the one used in Table 2.1 in order to quantify the portion of the trajectory of the brane where the adiabatic approximation is reliable. Finally, from the definition of proper time, we find

$$\dot{t} = \frac{dt}{d\lambda} = \pm \frac{Tr}{f(r)}. \tag{A.51}$$

Referring again to Figure 2.1, $f(r)$ has a definite (negative) sign in region II ($r_- < r < r_+$). This feature implies that the Schwarzschild time is monotonic with respect to the proper time during the brane trajectory in that region. Thus, if in the contraction phase the brane crossed the outer horizon, for instance, from the left asymptotic region I' (i.e. it crossed the line $r = r_+$, $t = -\infty$), it must cross the inner horizon to the right internal region III (i.e. it must cross the line $r = r_-$, $t = \infty$), cutting off completely the left internal region. As far as we know, this was first noted in ref. [151]. The existence of the minimum radius r_0^-, where the brane reverses again its motion, suggests that, gluing together more spacetime patches as in Figure 1, we can obtain a cyclical Big Bounce cosmology (with the caveat that gravity is not always localized on the brane during the trajectory). However, it is not clear if the effective semiclassical analysis we used to derive the brane trajectory is reliable when the brane is close to or inside the inner horizon. Indeed, the instability of the Cauchy horizon against even small excitations of bulk fields implies that curvature sigularities may appear [151], preventing a smooth evolution of the brane trajectory.

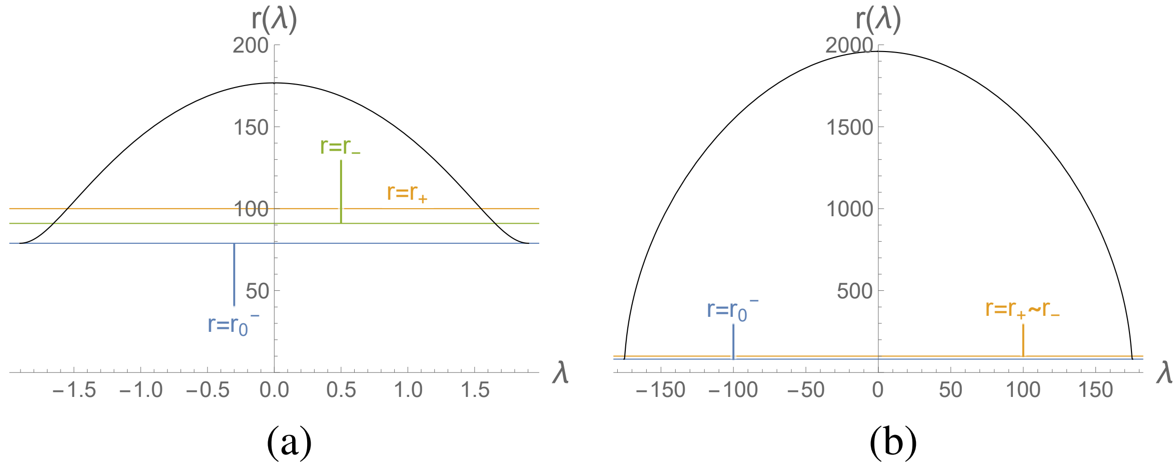

Figure A.5: Proper brane trajectory $\mathbf{r}(\lambda)$. Results for four spatial dimensions ($d = 4$), where we chose the AdS length to be $L_{AdS} = 1$. (a) Brane radius $r(\lambda)$ as a function of the brane proper time λ for a subcritical brane of tension $T = 0.89$. During its trajectory, the brane radius expands to a maximum value r_0 larger than the black hole outer horizon $r_+ = 100$, and shrinks to a minimum value r_0^- smaller than the black hole inner horizon $r_- = 91$. (b) For larger values of the brane tension ($T = 0.99999 \sim T_{crit} = 1/L_{AdS} = 1$) and a near-extremal black hole ($r_+ = 100$, $r_- = 99.9$), the maximum radius of the brane r_0 is larger, and the inversion at the minimum radius r_0^- becomes sharper. In both cases the brane trajectory resembles the one qualitatively described in Figure 2.1.

A.5 Gravity Localization and trapping coefficient method

Before clarifying the technical details of the gravity localization analysis, let us qualitatively understand what conditions we expect to be necessary in order to obtain an effective 4-dimensional description of gravity on the ETW brane.

1. The radius of the brane must be much larger than the event horizon size and the AdS radius: $r_b \gg r_+, L_{AdS}$. Since gravity in a 5-dimensional spacetime is unavoidably influenced by the presence of the fifth dimension, a 4-dimensional description of gravity is achievable only in a region where the gravitational effects directed along the fifth dimension and due to the presence of the black hole are weak. If the brane is too close to the black hole horizon, the gravitational attraction of the black hole is strong and a graviton localized on

the brane will certainly "leak" in the fifth dimension, eventually falling into the black hole horizon. On the other hand, if the brane is far enough from the black hole horizon and deep in the asymptotically AdS region ($r_b \gg L_{AdS}$), we recover a setup very similar to Randall-Sundrum II (RS II) model, with the brane embedded in a region of the spacetime which is nearly AdS. Thus we can expect to recover, at least locally, gravity localized on the brane. It is somehow surprising that gravity localization is lost if the radius of the brane is too large, as we will see.

2. The time scale of the motion of the brane must be much smaller than the time scale of oscillation of a graviton: $1/H \ll t_o$. This condition is needed to treat the motion of the brane as adiabatic with respect to gravitational perturbations. In other words, under this condition we can consider the brane as effectively static during the propagation of a graviton. As we will see, this assumption turns out to be pivotal in our analysis. Indeed, in the case of a moving brane, it is non trivial to define a boundary condition for the graviton wavefunction at the position of the brane.

3. $\frac{[r'(t)]^2}{f(r)} \ll f(r)$ or equivalently $\frac{[y'(t)]^2}{f(y)} \ll f(y)$. It is clear looking at the definition of the brane proper time that this condition guarantees that the properties of the graviton are interpreted, up to a constant redshift factor $\sqrt{f(r_b)} = \sqrt{f(y_b)}$, in the same way by a bulk observer (from the perspective of which we develop our analysis) and by an observer comoving with the brane.

We remark that, differently from the AdS-Schwarzschild case, if the black hole is large, the first condition can be satisfied for part of the brane trajectory while still retaining a positive preparation time, provided that the brane is near-critical and the black hole near-extremal.

The presence of the black hole unavoidably alters the RS II model, therefore we expect gravity localization to be only a local phenomenon, and valid only for a limited range of time.

A.5.1 TT perturbations and Schrödinger equation

The first step to find the Schrödinger equation reported in Section 2.4 is to derive the linearized Einstein equations about the AdS-RN background. Since we are considering only the tensor component of the metric perturbation, the perturbations of the electromagnetic field (which couple only to the scalar and the vector perturbations of the metric [206]) can be neglected. Therefore, the only terms arising from the perturbation of the electromagnetic stress-energy tensor will be the ones linear in the metric perturbation and with an unperturbed electromagnetic field. For a transverse-traceless (TT) perturbation (i.e. one that satisfies $\delta g^{\mu}_{\mu} = 0 = \nabla^{\mu}\delta g_{\mu\nu}$) the linearized Einstein equations read

$$\delta R_{\mu\nu} = \left(\frac{2}{d-1}\Lambda + \frac{(d-2)Q^2}{r^{2d-2}}\right)\delta g_{\mu\nu} \tag{A.52}$$

with

$$\delta R_{\mu\nu} = -\frac{1}{2}\Box_{d+1}\delta g_{\mu\nu} + R_{\rho\mu\sigma\nu}\delta g^{\rho\sigma} - \frac{1}{2}R_{\mu\rho}\delta g^{\rho}_{\nu} - \frac{1}{2}R_{\nu\rho}\delta g^{\rho}_{\mu} \equiv \Delta_L \delta g_{\mu\nu} \tag{A.53}$$

where $\Box_{d+1}$ is the $(d+1)$-dimensional covariant d'Alembertian, $R_{\mu\nu\rho\sigma}$ is the Riemann tensor and Δ_L is the Lichnerowicz operator.

Introducing the adimensional coordinates discussed in Section 2.4 (that we will use in the rest of this section), using the explicit expression for the Christoffels and the components of the Riemann and Ricci tensors and defining the covariant Laplacian Δ_{d-1} on the unit $(d-1)$-sphere, after a long calculation the spatial components (all the other components are identically satisfied) of equation (A.52) can be recast in the form

$$
\begin{aligned}
-\frac{1}{f(y)}\partial_{\tilde{t}}^2\delta g_{kl} + f(y)\partial_y^2\delta g_{kl} + \left[f'(y) - \frac{(5-d)f(y)}{y}\right]\partial_y\delta g_{kl} + \frac{1}{y^2}\Delta_{d-1}\delta g_{kl} \\
+2\left[\frac{2f(y)}{y^2} - \frac{d-1}{y^2}\right]\delta g_{kl} = \left[\frac{2d}{\gamma^2} - \frac{2(d-2)q^2}{y^{2d-2}}\right]\delta g_{kl}.
\end{aligned}
\tag{A.54}
$$

We can now decompose the metric perturbation in terms of the tensor harmonics on the unit $(d-1)$-sphere (defined in Section 2.4):

$$
\delta g_{kl} = \sum_k y^{\frac{5-d}{2}}\phi_k(\tilde{t}, y)\mathbb{T}_{kl}^{(k)} \tag{A.55}
$$

and introduce the tortoise coordinate $dr^* = dy/f(y)$, in terms of which the horizon of the black hole is mapped to $r^* \to -\infty$ and the asymptotic boundary to a finite value $r^* = r^*_\infty$. Equation (A.54) reduces then to a wave equation for each of the modes $\phi_k(\tilde{t}, y)$:

$$
-\partial_{\tilde{t}}^2\phi_k(\tilde{t}, y) = -\partial_{r^*}^2\phi_k(\tilde{t}, y) + V_k\left[y(r^*)\right]\phi_k(\tilde{t}, y) \tag{A.56}
$$

where the potential $V_k\left[y(r^*)\right]$ is given by equation (2.10) and is in accordance with the results of ref [206]. In the frequency domain, equation (A.56) finally takes the form of the Schrödinger equation (2.9), which encodes the effects of the radial extra dimension on a transverse-traceless graviton.

By finding the expression of the tortoise coordinate r^* as a function of the adimensional radial coordinate y in the limit of large y, it is easy to show that the potential (2.10) diverges at the asymptotic boundary as $V(r^*) \sim 15/[4(r^*_\infty - r^*)^2]$. This behaviour is very similar to the one typical of the RS II potential [34, 35, 111]. On the other hand, at the black hole horizon ($r^* \to -\infty$) the potential vanishes exponentially: $V(r^*) \sim \exp(2k_g r^*)$ where k_g is the above defined surface gravity of the black hole. Since the normalizable zero-graviton mode bound on the brane present in the RS II model is a marginally bound mode, and since our potential vanishes exponentially while RS's one exhibited a power-law behaviour deep into the bulk, we cannot expect to find a normalizable bound mode as well. But the presence of the brane still allows the existence of a quasi-bound mode, with complex frequency $\omega = \bar{\omega} + i\Gamma/2$, very well localized close to the brane. Its finite lifetime (determined by the imaginary part of the frequency $\Gamma/2$) implies that it will stay on the brane for an interval of time, after which it will eventually leak into the bulk black hole.

Up to this point, we only studied the perturbed Einstein equations, without taking into account the presence of the ETW brane. To study the evolution of a TT graviton living on the brane, and to understand whether or not it is possible for this graviton to remain bound on the brane at least locally and for a reasonable amount of time, we need to enforce a boundary condition for the graviton wavefunction at the position of the brane. At each instant of time, the brane is effectively a hypersurface at fixed y (i.e. at fixed r^*), therefore the previous analysis can be applied to study a gravitational perturbation on the brane. In particular, the Schrödinger equation allows us to understand if the graviton is bound on the brane or if it necessarily leaks into the bulk. If the brane is expanding or contracting, it is not clear how to implement such a boundary condition. But if the time scale of the perturbation is much smaller than the time scale of the motion of the brane, the linearization of equation (2.5) provides the boundary condition needed. In other words, we must work under an adiabatic approximation for the motion of the brane with respect to the time scale of the perturbation, so that we can approximately consider the ETW brane to be static at $y = y_b$, or $r^* = r^*_b$. Additionally, since all the calculations will be carried out in the bulk coordinates assuming the brane to be static, in order for an observer comoving with the brane to interpret correctly the graviton, we must also verify that the redshift between the bulk coordinates and the comoving coordinates on the brane is compatible with the assumption of a static brane. From the definition of proper time, this means that $y'^2 \ll f^2(y)$ must hold.

Equation (2.5) can be traced and rewritten as

$$K_{ab} = \tilde{T} h_{ab} \tag{A.57}$$

where $\tilde{T} = r_+ T$ and the extrinsic curvature is computed using the adimensional coordinates. For a static brane, the normal dual vector is given by $n_\mu = \delta_{\mu,y}/\sqrt{f(y)}$ and $e^\mu_a = \delta^\mu_a$. Linearizing equation (A.57) and using the decomposition (A.55) of the metric perturbation, we obtain the (Neumann) boundary condition at the brane

$$\partial_y \psi_{k,\omega}\Big|_{y=y_b} = \frac{4\tilde{T}y - (5-d)\sqrt{f(y)}}{2y\sqrt{f(y)}} \psi_{k,\omega}\Bigg|_{y=y_b}. \tag{A.58}$$

Using the condition $y'^2 \ll f^2(y)$, equation (2.6) guarantees that $f(y) \sim \tilde{T}^2 y^2$. The latter result and the definition of the tortoise coordinate finally lead to the boundary condition reported in Section 2.4, i.e.

$$\partial_{r^*} \psi_{k,\omega}\Big|_{r^*=r^*_b} = \frac{(d-1)\sqrt{f\left[y(r^*)\right]}}{2y(r^*)} \psi_{k,\omega}\Bigg|_{r^*=r^*_b}. \tag{A.59}$$

As we have already discussed, imposing this boundary condition is equivalent to add to the potential (2.10) a negative delta term, which "traps" the graviton, allowing gravity localization. Before reviewing the trapping coefficient method introduced in ref. [199] and give more details about our numerical results, we remark that in the small black hole case ($\gamma \gtrsim 1$) the potential (2.10) presents a peak for $r^* \sim 0$ before diverging at $r^* = r^*_\infty$ (see Figure A.6). This feature disappears for large black holes. If the brane radius was able to reach values consistently larger than the position of the peak, it would have implied not only the presence of a quasi-bound zero mode, but also the existence of "overtones" [199] trapped in the resonance cavity between the peak and the brane position. Nonetheless, as we have already shown, in the small black hole case the ratio between the maximum brane radius and the horizon of the black hole cannot be large, implying that no quasi-bound modes exist. Therefore, the small black hole case is not of our interest and we will focus our attention on the $\gamma \ll 1$ case.

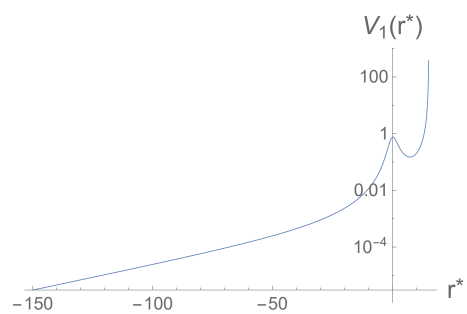

Figure A.6: Potential $V_k[y(r^*)]$ - Small black hole. $r_+ = 0.1$, $r_- = 0.099$, $L_{AdS} = 1$, $l = k = 1$. The potential diverges for $r^*_\infty = 15.3$ and vanishes exponentially at the horizon $r^* \to -\infty$. Differently from the large black hole case (see Figure 2.4), the potential exhibits a peak for $r^* \sim 0$.

A.5.2 Trapping coefficient method

The quasi-normal modes, already studied in ref. [199] for the Schwarzschild-AdS spacetime in the presence of a static brane, are modes with a finite lifetime determined by the imaginary part of the frequency $\Gamma/2$ and purely infalling boundary condition at the black hole horizon, i.e. $\psi_{k,\omega} \sim \exp(i\omega r^*)$ for $r^* \to -\infty$. This finite lifetime can be understood as a probability of tunneling through the potential barrier from the delta potential at the position of the brane toward the black hole horizon. The absence of the resonant cavity in the potential (2.10) for the large black hole case implies that only one resonant mode, supported by the attractive delta potential, exists, that we will call quasi-bound mode. Our analysis is based on the trapping coefficient method introduced in ref. [199], that we will review and apply to the AdS-Reissner-Nordström case.

Since the potential vanishes approaching the horizon, the wavefunction in that region must take the form of a plane wave:

$$\psi_{k,\omega}(r^*) \sim \frac{1}{2} A_h \mathrm{e}^{-i\delta(\omega)} \left[\mathrm{e}^{-i\omega r^*} + S(\omega)\mathrm{e}^{i\omega r^*}\right] \tag{A.60}$$

where $S(\omega) = \mathrm{e}^{2i\delta(\omega)}$ is the scattering matrix and $\delta(\omega)$ is the scattering phase shift. The black hole horizon is located at $r^* = -\infty$, and we want purely infalling solutions, therefore in that limit $\psi_{k,\omega}$ must be a left-moving plane wave. Since we are imposing two boundary conditions (equation (A.59) at the brane and the pure infalling one at the horizon), we expect to find a discrete set of solutions to the Schrödinger equation (the quasi-normal modes), corresponding to a discrete set of frequencies ω_n. By considering complex frequencies, we can obtain the purely infalling solutions by requiring the scattering matrix to have a pole at the quasi-normal mode frequencies ω_n[4]. It can be shown [199, 275] that the leading order Laurent expansion of $S(\omega)$ is given by:

$$S(\omega) \sim \mathrm{e}^{2i\delta_0(\omega)} \frac{\omega - \omega_n^*}{\omega - \omega_n} \tag{A.61}$$

where $\delta_0(\omega)$ is a slowly varying real function of ω. Using the definition $\omega_n = \bar{\omega}_n + i\Gamma_n/2$, the

[4]In the large black hole case, only one mode, supported by the attractive delta potential, will be present in the spectrum. In the following we will then drop the n index, understood to take the value $n = 0$.

scattering phase shift can be expressed as:

$$\delta(\omega) \sim \delta_0(\omega) + \arcsin\left[\frac{\Gamma_n}{\sqrt{4(\omega-\bar{\omega}_n)^2+\Gamma_n^2}}\right]. \tag{A.62}$$

For real ω and if Γ_n is small with respect to $\bar{\omega}_n$, $\delta(\omega)$ varies of a value which is approximately π when ω is varied across the real part of the resonance frequency, flipping the sign of the wave-function (A.60). We can now define the trapping coefficient

$$\eta(\omega) \equiv \frac{A_b}{A_h} \tag{A.63}$$

where A_b is the magnitude of the wavefunction $\psi_{k,\omega}$ at the brane and A_h its magnitude at the horizon of the black hole (effectively, in a region where the potential is almost vanishing). Intuitively, since we expect the quasi-bound mode to be almost localized on the brane due to the presence of the attractive delta potential at $r^* = r_b^*$, the trapping coefficient will present a peak at the frequency of the quasi-bound mode. In the case of a normalizable bound mode (with vanishing imaginary part of the frequency), clearly the wavefunction would vanish at the horizon, giving an infinite trapping coefficient. For a purely infalling solution we can write in general [199]:

$$\psi_{k,\omega}(r^*) = N(\omega)\begin{cases} A_h \Re\left[\mathrm{e}^{i\delta(\omega)}\mathrm{e}^{i\omega r^*}\right] & r^* \to -\infty \\ \\ R(\omega)\Re\left[\mathrm{e}^{i\delta(\omega)}\mathrm{e}^{i\theta(\omega)}\right] = -R(\omega)\sin\left(\delta(\omega)+\theta(\omega)-\frac{\pi}{2}\right) \equiv A_b & r^* = r_b^* \end{cases} \tag{A.64}$$

where $\Re$ indicates the real part and $R(\omega)$ and $\theta(\omega)$ are slowly-varying functions of the frequency. For every frequency ω we can choose the normalization $N(\omega)$ of the wavenfunction such that

$A_b = 1$, and of course the trapping coefficient will be unchanged. This allows us to set $\psi(r_b^*) = 1$ in our numerical analysis, obtaining:

$$\psi_{k,\omega}(r^*) = \begin{cases} -\frac{A_h}{R(\omega)\sin\left(\delta(\omega)+\theta(\omega)-\frac{\pi}{2}\right)}\Re\left[\mathrm{e}^{i\delta(\omega)}\mathrm{e}^{i\omega r^*}\right] = -\frac{1}{\eta(\omega)}\Re\left[\mathrm{e}^{i\delta(\omega)}\mathrm{e}^{i\omega r^*}\right] & r^* \to -\infty \\ 1 & r^* = r_b^* \end{cases} \tag{A.65}$$

where the trapping coefficient therefore reads:

$$\eta(\omega) = \frac{R(\omega)\sin\left(\delta(\omega)+\theta(\omega)-\frac{\pi}{2}\right)}{A_h}. \tag{A.66}$$

If the relation

$$\delta_0(\omega) + \theta(\omega) \sim \frac{\pi}{2}, \frac{3\pi}{2} \tag{A.67}$$

holds, the square of the trapping coefficient takes the form:

$$\xi(\omega) \equiv \eta^2(\omega) \sim \frac{R^2(\omega)}{A_h^2}\frac{\Gamma_n^2}{4(\omega-\bar{\omega}_n)^2+\Gamma_n^2}. \tag{A.68}$$

This Lorentzian (Breit-Wigner) peak is centred at the real part of the frequency of the quasi-bound mode, while its half-width at half-maximum $\Gamma/2$ gives the imaginary part of the frequency, and therefore the lifetime of the mode. If the condition (A.67) is not satisfied, the shape of the peak is more complicated. Nonetheless, at least for the zero mode of our interest, it has been shown that the condition (A.67) holds in a good approximation [199] and our numerical analysis confirms this result. We mention here the possibility of refining such an approximation by subtracting from the plot of $\xi(\omega)$ as a function of the frequency a baseline function accounting for the slow variation of $\delta_0(\omega)$ and $\theta(\omega)$ with the frequency. For our purposes, such a procedure (which leads to some difficulties due to the arbitrariness of the choice of the baseline [199]), turns out to be not necessary. It is therefore possible, in a reasonable approximation, to find the real and imaginary parts of the frequencies of the quasi-bound mode (we remind that for the large black hole case we expect only the $n = 0$ mode to be present, supported by the negative delta potential at the position of the brane) using the following procedure (trapping coefficient method):

1. Compute numerically a family of solutions of the Schrödinger equation (2.9), parametrized by real-valued frequencies ω and with boundary condition (A.59), requiring also $\psi_{k,\omega}(r_b^*) = 1$;

2. Find numerically the maximum of the wavefunction in the region where the potential is almost vanishing (i.e. near the horizon) for a range of values of ω;

3. Plot the square of the inverse of these maxima as a function of ω: a peak will be present at the real part of the frequency of the (purely infalling) quasi-normal mode;

4. Eventually subtract a baseline function;

5. Fit the data with the Breit-Wigner distribution (A.68) to find real and imaginary parts of the frequency of the quasi bound mode.

A.5.3 Numerical results

We will find the real and imaginary parts of the frequency and the height of the peak R/A_h for three sizes of the black hole: $r_+ = 10, 100, 10000$ (with $L_{AdS} = 1$ and r_- such that the black holes are near extremality), corresponding to $\gamma = 0.1, 0.01, 0.0001$ respectively. For each case we will consider different positions y_b for the brane and values for the angular momentum l. The results of the fits are reported in Table A.1.

γ	y_b	l	r_-	R/A_h	$\bar{\omega}$	Γ	ω_{GR}
0.1	17.34	1	9.99	68.22	17.22	0.7354	17.32
0.1	17.34	5	9.99	61.41	58.93	0.9186	59.16
0.01	17.34	1	99.9	71.51	168.2	67.22	173.2
0.01	34.62	1	99.9	202.5	147.5	16.86	173.2
0.01	60.22	1	99.9	464.8	71.70	5.580	173.2
0.01	63	1	99.9	499.2	52.40	5.060	173.2
0.01	66	1	99.9	528.8	12.56	4.835	173.2
0.01	66.15	1	99.9	~ 519.6	~ 4	~ 5	173.2
0.01	17.34	5	99.9	70.74	586.4	68.55	591.6
0.01	30.00	5	99.9	160.9	585.0	23.09	591.6
0.01	34.62	5	99.9	199.5	583.6	17.28	591.6
0.01	99.94	5	99.9	980.9	530.5	2.081	591.6
0.01	60.00	10	99.9	447.8	$1.084 \cdot 10^3$	5.984	$1.095 \cdot 10^3$
0.01	120.0	20	99.9	$1.229 \cdot 10^3$	$2.074 \cdot 10^3$	1.587	$2.098 \cdot 10^3$
0.001	17.34	5	999	~ 73	$\sim 4 \cdot 10^3$	$\sim 5 \cdot 10^3$	$5.916 \cdot 10^3$
0.0001	34.82	100	9900	203.2	$4.181 \cdot 10^5$	$1.737 \cdot 10^5$	$1.010 \cdot 10^6$
0.0001	34.82	1000	9900	180.9	$9.955 \cdot 10^6$	$2.097 \cdot 10^5$	$1.001 \cdot 10^7$
0.0001	34.82	10000	9900	160.9	$9.993 \cdot 10^7$	$2.552 \cdot 10^5$	$1.000 \cdot 10^8$

Table A.1: Quasi-bound modes. Results of the numerical analysis based on the trapping coefficient method. We set the AdS radius to be $L_{AdS} = 1$. In the first column we report the size of the black hole $\gamma = L_{AdS}/r_+$, in the second column the position of the brane in adimensional coordinates $y_b = r_b/r_+$, in the third column the angular momentum l, in the fourth column the value of the inner horizon radius r_-. In the fifth, sixth and seventh column we show the results of the Breit-Wigner fits of the squared trapping coefficient: the amplitude R/A_h of the trapping coefficient and the real ($\bar{\omega}$) and imaginary ($\Gamma/2$) parts of the frequency of the quasi-bound mode, respectively. In the last column we show the expected frequency ω_{GR} of a 4-dimensional perturbation of an Einstein static universe. The fitted values for $\gamma = 0.01$, $y_b = 66.15$, $l = 1$ and for $\gamma = 0.001$, $y_b = 17.34$, $l = 5$ are purely indicative. We remark that for each set of parameters reported above it is possible to choose a tension T for the brane such that the corresponding y_b is, for instance, the turning point of the brane, while the corresponding Euclidean solutions are sensible ($\tau_0 > 0$) and dominant in the gravity path integral ($\Delta I < 0$).

From our analysis the following picture emerges (we remind that $\gamma = L_{AdS}/r_+$ and $y_b = r_b/r_+$):

- For fixed γ and l, increasing the distance of the brane y_b the real part of the frequency $\bar{\omega}$ decreases and the peak of the square of the trapping coefficient ξ becomes sharper and higher, indicating that the imaginary part of the frequency $\Gamma/2$ decreases as well and gravity localization is more efficient. This is evident from the data reported in Table 2.1 (where $t_o = 1/\bar{\omega}$ and $t_d = 2/\Gamma$). But if the brane is very far, $\bar{\omega}$ approaches zero. When it happens, the peak becomes broader (indicating $\Gamma \sim \bar{\omega}$) and is not approximable with a Lorentzian curve anymore. At this point, the peak is very high, indicating a short-lived (large ratio between imaginary and real part of the frequency) but very well localized quasi-bound state. After that, for even farther brane, the quasi-bound mode is no more present (there is no peak, and the trapping coefficient never becomes very big). Additionally, for low values of the angular momentum l, the real part of the frequency obtained is not in accordance with the one expected from a 4-dimensional perturbation of an Einstein static universe (given by $\omega_{GR} = \sqrt{f(y_b) \cdot (l+2)l}/y_b$) [199], even when the brane is far and the peak is narrow. For higher values of l instead, i.e. for smaller scale perturbations, the GR expected value and the one obtained numerically are closer. We report here the data showing these behaviours only in the $\gamma = 0.01$ case, but we verified that the same analysis applies also for $\gamma = 0.1, 0.0001$ as well as in the small black hole case. The smaller is the black hole, the farther is the position of the brane where gravity localization is lost. We remark how this behaviour is in contradiction with the conclusions of ref. [199], where it is argued that the real part of the frequency approaches a constant value and the RS II normalizable bound zero-graviton mode is recovered in the far brane limit. However, it is worth noting that the loss of localization for the small black hole case, which is the one mainly studied in ref. [199], occurs for a position of the brane much farther than the ones explored in Figure 11 of ref. [199]

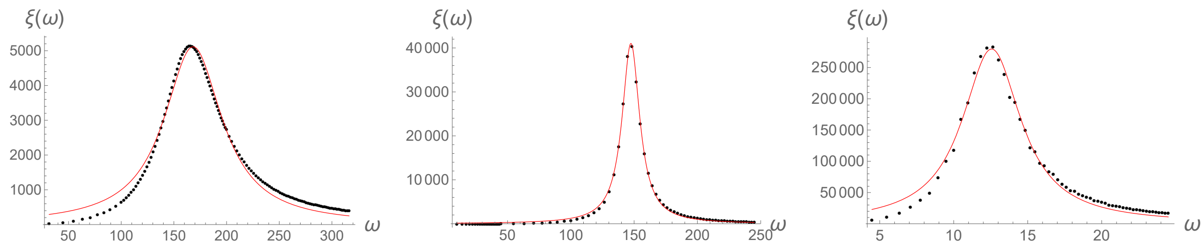

(a) (b) (c)

Figure A.7: Delocalization for far brane. $d = 4$, $r_+ = 100$ ($\gamma = 0.01$), $r_- = 99.9$, $L_{AdS} = 1$, $l = 1$. For fixed black hole size and angular momentum, if the brane is too far from the horizon gravity localization is lost. (a) $y_b = 17.34$. If the brane is not far enough from the horizon, the peak of the squared trapping coefficient is not well approximated by the Lorentzian profile and gravity localization is not very efficient. (b) $y_b = 34.62$. When the brane is farther, gravity localization is more efficient and the peak of the squared trapping coefficient is Lorentzian. (c) $y_b = 66$. If the brane is too far from the horizon, the peak becomes broad, the mode is short-lived and gravity is no more localized.

- For fixed l and y_b, decreasing γ (i.e. increasing the size of the black hole) the real part of the frequency grows and the peak becomes broader, indicating a shorter-lived quasi-bound mode. The Lorentzian approximation of the peak is also less precise. At the same time, we remind that the same maximum radius of the brane $y_b^{max} = r_0/r_+$ is reached for a smaller value of the tension T if the black hole is larger.

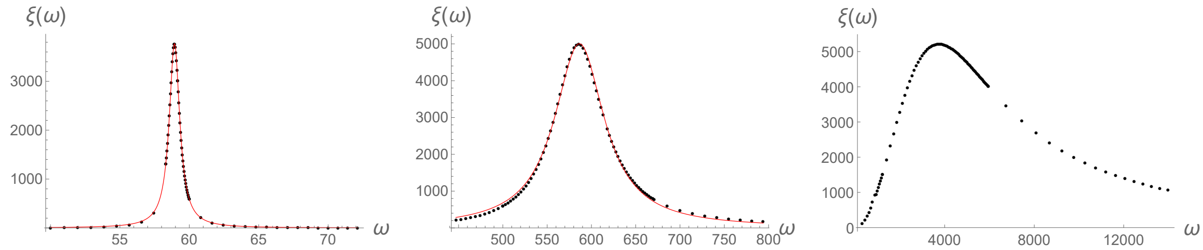

(a) (b) (c)

Figure A.8: Delocalization for large black holes. $d = 4$, $r_-/r_+ = 0.99$, $L_{AdS} = 1$, $y_b = 17.34$, $l = 5$, (a) $\gamma = 0.1$, (b) $\gamma = 0.01$ and (c) $\gamma = 0.001$. Increasing the size of the black hole for fixed angular momentum and radius of the brane, the peak of the squared trapping coefficient is broader and not well approximated by the Lorentzian profile: gravity localization becomes less efficient.

- Holding γ and y_b fixed and increasing the angular momentum l the real part of the frequency grows. In the small black hole case, we verified that the imaginary part of the frequency decreases, exactly in the same way as it was described in ref. [199] Differently, in the large black hole case, the imaginary part grows, but much slower than the real part. The peaks are therefore narrower and the ratio between the imaginary and the real part decreases. At the same time, since the imaginary part of the frequency increases, the height of the peaks decreases with increasing l, indicating that, even if they are able to undergo a larger number of oscillations before decaying, these smaller-scale modes have a shorter lifetime than the larger-scale ones (even if localization is still very efficient). These characteristics can be observed comparing the peaks for different values of l in all the three cases, but are particularly evident in the very large black hole cases $\gamma = 0.0001$. We remark that even for a very far brane, which does not support localization of gravity for instance for $l = 1$, increasing the angular momentum the quasi-bound state is recovered. For example, for $\gamma = 0.01$ and $l = 1$ the quasi bound state is lost for $y_b \sim 66$, but for $l = 5$ it is still present when the brane radius is $y_b = 99.94$.

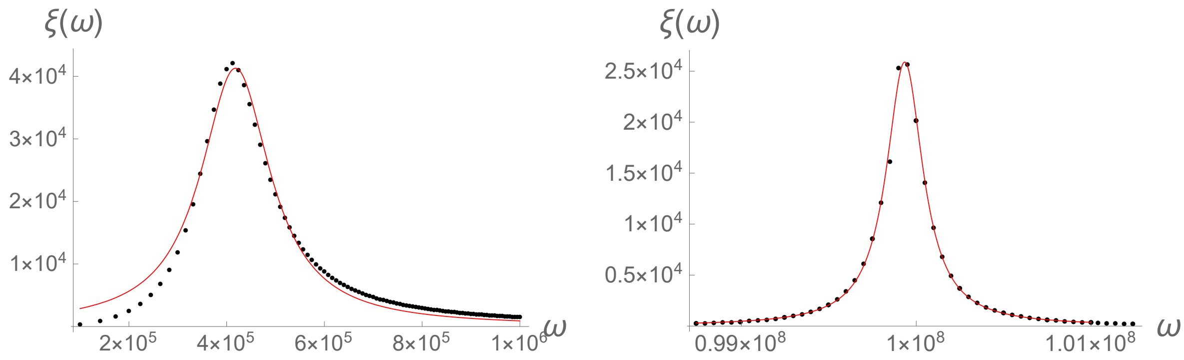

(a) (b)

Figure A.9: Localization for small scales. $d = 4$, $L_{AdS} = 1$, $r_+ = 10000$ ($\gamma = 0.0001$), $r_- = 9900$, $y_b = 34.62$, (a) $l = 100$ and (b) $l = 10000$. For fixed radius of the brane and size of the black hole, increasing the angular momentum (i.e. decreasing the scale of the perturbation) the peak of the squared trapping coefficient is better approximated by the Lorentzian profile and gravity localization becomes more efficient.

- Keeping the size of the black hole and the scale of the perturbation constant while increasing the brane radius, i.e. increasing l and y_b of the same factor holding γ fixed, the peak becomes narrower and gravity localization more efficient: remaining on a local enough scale, if the brane is farther we are in a setup more similar to the RS II scenario.

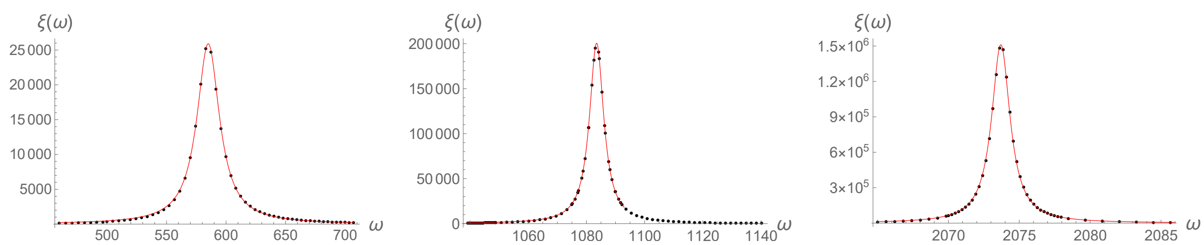

(a) (b) (c)

Figure A.10: Localization for far brane and small scales. $d = 4$, $L_{AdS} = 1$, $r_+ = 100$ ($\gamma = 0.01$), $r_- = 99.9$. (a) $l = 5$, $y_b = 30$. (b) $l = 10$, $y_b = 60$. (c) $l = 20$, $y_b = 120$. For fixed black hole size, increasing the angular momentum and the radius of the brane of the same factor, the mode is longer-lived and gravity localization becomes more efficient.

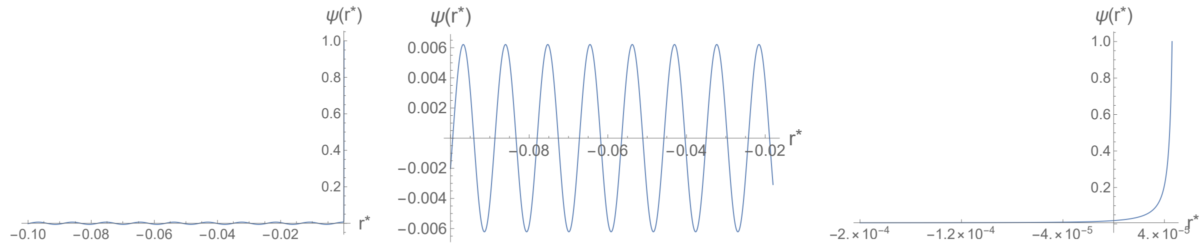

Figure A.11: Example of quasi-bound mode wavefunction. $d = 4$, $L_{AdS} = 1$, $r_+ = 100$ ($\gamma = 0.01$), $r_- = 99.9$, $l = 5$, $y_b = 30$. (a) Quasi-bound mode wavefunction. (b) Detail of the oscillatory behaviour near the horizon. (c) Detail of the growth near the brane.

A.5.4 Time scales and adiabatic approximation

As we pointed out in Section 2.4, the three time scales that we must compare in order to verify that the adiabatic approximation we used is reliable are the oscillation time $t_o = 1/\bar{\omega}$, the decay time $t_d = 2/\Gamma$ and the quantity

$$T_H = \frac{y(t)}{y'(t)} = \frac{\tilde{T}y^2}{f(y)\sqrt{\tilde{T}^2y^2 - f(y)}}, \tag{A.69}$$

which in comoving coordinates would correspond to the Hubble time of the braneworld cosmology, and that we will call for semplicity "Hubble time". If $t_o \ll T_H$ for a given radius of the brane $y = y_b$, the adiabatic approximation holds. We remark that the Hubble time does not depend on the angular momentum l. Thus, since increasing l the real part of the frequency increases and the oscillation time t_o decreases, for higher values of l it is easier to satisfy the adiabatic approximation condition. Additionally, as we have explained, the relation

$$\frac{[y'(t)]^2}{f^2(y)} = \frac{\tilde{T}^2y^2}{\tilde{T}^2y^2 - f(y)} \ll 1 \tag{A.70}$$

must hold as well at $y = y_b$. We remind that $\tilde{T} = r_+ T$. In Section 2.4 we have shown that, for $l = 10$, $\gamma = 0.01$, $r_+ = 100$, $r_- = 99.9$ and $T = 0.999999999$ it is possible to obtain $t_d \gg T_H \gg t_o$ for a large part of the brane trajectory, meaning that the adiabatic approximation is reliable and that it breaks down (and therefore our analysis loses its meaning) before the graviton leaks into the bulk. Additionally, the condition (A.70) is always satisfied when the adiabatic approximation holds. For completeness we report in Figure A.12 a plot of these quantities as a function of the position of the brane for the data reported in Table 2.1.

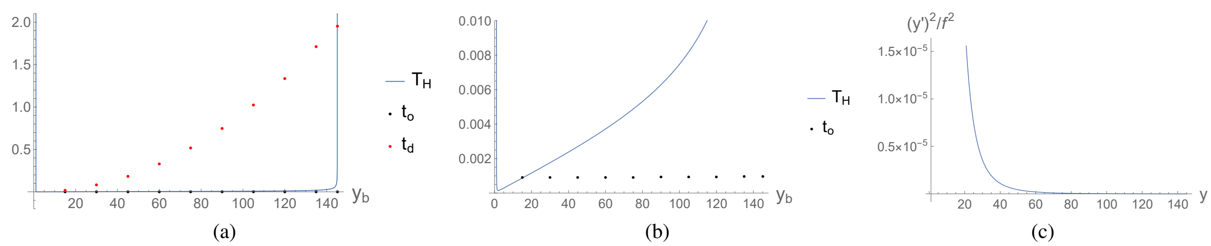

Figure A.12: Time scales comparison for data in Table 2.1. $d = 4$, $L_{AdS} = 1$, $r_+ = 100$ ($\gamma = 0.01$), $r_- = 99.9$, $l = 10$, $T = 0.999999999$. (a) Hubble time T_H, oscillation time t_o and decay time t_d as a function of the brane radius y_b. (b) Detail of Hubble time T_H and oscillation time t_o only. (c) Ratio $[y'(t)]^2/f^2(y)$. The adiabatic approximation is reliable for at least part of the brane trajectory considered, as discussed in Section 2.4. The condition $[y'(t)]^2/f^2(y) \ll 1$ is also satisfied.

For the same size and charge of the black hole but with $l = 1$ and $T = 0.99999993325$ (the maximum radius of the brane is $y_0 = r_0/r_+ = 66.15$), using the results reported in Table A.1, we find that the adiabatic approximation is never reliable (i.e. $T_H < t_o$) during the trajectory of the brane (see Figure A.13). It clearly holds at the turning point y_0, where the Hubble time diverges, but there the quasi-bound mode is extremely short-lived ($\bar{\omega}$ and Γ are of the same order). The condition (A.70) is still satisfied for a large part of the brane trajectory. This problem sums up with the discordance between the expected 4-dimensional value of the frequency ω_{GR} and the one obtained numerically in the $l = 1$ case. Even if for smaller black holes (for instance in the

$\gamma = 0.1$ case) close to the turning point the adiabatic approximation can hold also for $l = 1$, we can conclude that an effective 4-dimensional description of gravity localized on the brane is obtained more easily and for a larger amount of brane proper time when the value of the angular momentum l is higher. This result, together with the observation that our analysis is valid only on a time scale smaller than the Hubble time and that the quasi-bound mode is not stable, confirms our expectation to find gravity localization only locally and for a finite amount of time.

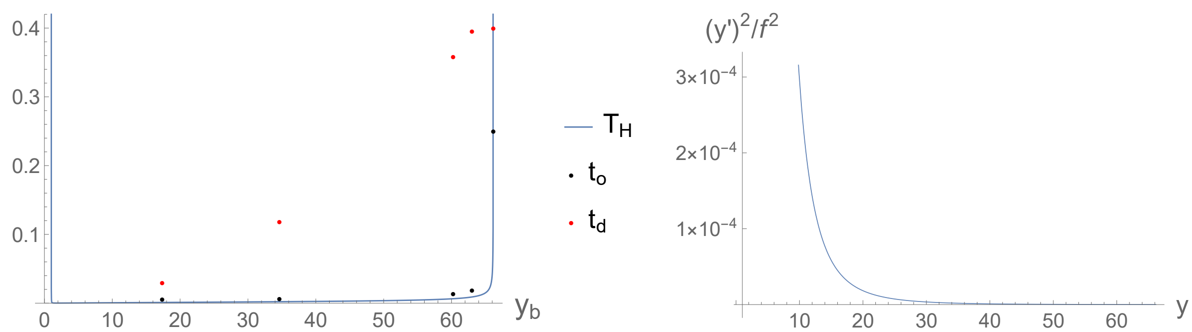

(a) (b)

Figure A.13: Time scales comparison for data in Table A.1. $d = 4$, $L_{AdS} = 1$, $r_+ = 100$ ($\gamma = 0.01$), $r_- = 99.9$, $l = 1$, $T = 0.99999993325$. (a) Hubble time T_H, oscillation time t_o and decay time t_d. (b) Ratio $[y'(t)]^2/f^2(y)$. The adiabatic approximation is clearly not reliable for the parameters considered. The condition $[y'(t)]^2/f^2(y) \ll 1$ is still satisfied.

Appendix B: Technical details of the results reported in Chapter 3

Authors:[1] *Stefano Antonini, Petar Simidzija, Brian Swingle, Mark Van Raamsdonk.*

B.1 States from sliced Euclidean path integrals

In this appendix, we review the construction of Lorentzian states from slicing Euclidean path integrals.

Consider a Euclidean quantum field theory on a space M such that the background and the theory are refection-symmetric about some surface A which divides M into two equivalent parts $M_{\pm}$. The partition function of this Euclidean theory can be defined by the path integral

$$Z = \int_M [d\phi] e^{-S_E} \; , \tag{B.1}$$

where S_E is the Euclidean action for the theory. We can use this path integral to define a particular state of the field theory degrees of freedom on the surface A. The wavefunctional for this state is

$$\Psi_A[\phi_0] = \frac{1}{Z^{\frac{1}{2}}} \int_{M_-}^{\phi(A)=\phi_0} [d\phi] e^{-S_E} \; , \tag{B.2}$$

[1]Originally published in the appendices of *Cosmology from the vacuum*, JOURNAL CITATION, e-Print: 2203.11220, [2].

so the probability amplitude for a particular field configuration ϕ_0 is a sum over all field configurations on M_- with the fields on A set to ϕ_0. Observables in this state at time 0 are computed by inserting operators on the surface A in the original path integral. More generally, certain time-dependent observables for this state in the associated Lorentzian quantum field theory are related by analytic continuation to observables in the Euclidean quantum field theory.

In the special case where M has a non-compact direction with a translation symmetry and A is a surface that divides the space in half perpendicular to this direction, the state Ψ_A is the vacuum state of the associated Lorentzian quantum field theory (which has a time-independent Hamiltonian in this case). The reason is that the vacuum state can be defined, up to normalization, as $\lim_{\beta\to\infty} e^{-\beta H}|\Psi_0\rangle$ (where $|\Psi_0\rangle$ is any state that has overlap with the vacuum) and the path integral version of this expression is the sliced Euclidean path integral we have described.

B.2 Cosmological equations in conformal coordinates

For some applications, it is useful to consider the evolution equations that determine the background cosmology and wormhole spacetimes in conformal coordinates in which the metric is a scaled version of Minkowski space.

Background geometry and stress-energy tensor: conformal time

In the cosmology picture, the background metric with conformal time is

$$ds^2 = \hat{a}^2(\eta)(-d\eta^2 + dw^2 + dx_i dx_i)\ . \tag{B.3}$$

Here $\hat{a}(\eta) = a(t)$ and t and η are related by $d\eta/dt = a^{-1}(t)$. In these coordinates, the stress-energy tensor is

$$T^{\eta\eta} = \frac{\hat{\rho}(\eta)}{\hat{a}^2(\eta)}, \quad T^{ij} = \frac{\hat{p}(\eta)}{\hat{a}^2(\eta)}\delta^{ij}, \quad T^{ww} = \frac{\hat{p}(\eta)}{\hat{a}^2(\eta)} \tag{B.4}$$

where $\hat{\rho}(\eta) = \rho(t)$ and $\hat{p}(\eta) = p(t)$.

In these coordinates the Friedmann equation gives

$$\frac{1}{\hat{a}^4}\left(\frac{d\hat{a}}{d\eta}\right)^2 + \frac{1}{L^2} = \frac{8\pi G}{3}\hat{\rho} \tag{B.5}$$

and the conservation equation is

$$\dot{\hat{\rho}} = -\frac{3}{\hat{a}}\frac{d\hat{a}}{d\eta}(\hat{\rho} + \hat{p}) \tag{B.6}$$

Wormhole picture: conformal distance coordinates

It will also be convenient to describe the wormhole in terms of a conformal distance coordinate z, in terms of which the metric is

$$ds^2 = \hat{a}_E^2(z)(dz^2 - d\zeta^2 + dx_i dx_i) \ . \tag{B.7}$$

The scale factor $\hat{a}_E(z)$ is related to $\hat{a}(\eta)$ by analytic continuation $\eta^2 \leftrightarrow -z^2$.

In these coordinates, the range of z is finite, $z \in [-z_0, z_0]$. The coordinate locations $\pm z_0$ correspond to the asymptotically AdS boundaries; the scale factor $\hat{a}_E(z)$ has simple poles at these locations.

The stress-energy tensor in this picture is

$$T^{zz} = -\frac{\hat{\rho}_E(z)}{\hat{a}_E^2(z)}, \quad T^{\zeta\zeta} = -\frac{\hat{p}_E(z)}{\hat{a}_E^2(z)}, \quad T^{ij} = \frac{\hat{p}_E(z)}{\hat{a}_E^2(z)}\delta^{ij} \tag{B.8}$$

where $\hat{\rho}_E$ and $\hat{p}_E$ are related to ρ and p by analytic continuation $\eta^2 \leftrightarrow -z^2$.

The analog of the Friedmann equation in this picture is

$$-\frac{1}{\hat{a}_E^4}\left(\frac{d\hat{a}_E}{dz}\right)^2 + \frac{1}{L^2} = \frac{8\pi G}{3}\hat{\rho}_E \tag{B.9}$$

and the conservation equation is

$$\frac{d\hat{\rho}_E}{dz} = -\frac{3}{\hat{a}_E}\frac{d\hat{a}_E}{dz}(\hat{\rho}_E + \hat{p}_E). \tag{B.10}$$

B.3 Requirement of negative integrated null energy in the wormhole picture

The requirement of negative null energy at the midpoint of the wormhole can be extended to a requirement for integrated null energy between the two asymptotically AdS boundaries [276].

Considering the expression

$$N \equiv 8\pi G \int d\lambda T_{\mu\nu}\frac{dx^\mu}{d\lambda}\frac{dx^\nu}{d\lambda}\ . \tag{B.11}$$

and taking $x(\lambda)$ to be a null geodesic between the two asymptotically AdS boundaries with λ the affine parameter, we find

$$N = 8\pi G \int \frac{dz}{\hat{a}_E^2(z)} T_{++}(z) = 8\pi G \int dz T^{--}(z) \ . \tag{B.12}$$

Using Einstein's equations, we have that

$$8\pi G T_{++} = R_{++} = 4 \left(\frac{\hat{a}_E'}{\hat{a}_E} \right)^2 - 2 \frac{\hat{a}_E''}{\hat{a}_E} \ . \tag{B.13}$$

Then we can check that

$$\begin{aligned} N &= 2 \int dz \left\{ \frac{d}{dz} \left[\frac{1}{\hat{a}_E} \frac{d}{dz} \frac{1}{a} \right] - \left[\frac{d}{dz} \frac{1}{\hat{a}_E} \right]^2 \right\} \\ &= - \int_{-z_0}^{z_0} dz \left[\tfrac{d}{dz} \tfrac{1}{\hat{a}_E} \right]^2 < 0 \ , \end{aligned} \tag{B.14}$$

where $\pm z_0$ are the locations of the two asymptotically AdS boundaries. Near these points, $1/\hat{a}_E(z)$ behaves as $C(z_0 \mp z)$, so the total derivative term in the first line term vanishes.

We conclude that the null energy integrated from one side of the wormhole to the other as in (B.11) must be negative. This is not possible for any ordinary matter satisfying the null energy condition, but it is possible for the vacuum energy of quantum fields, and this is the situation we are considering.

B.4 Negative Casimir energies in quantum field theory

In this appendix, we briefly recall a few relevant aspects of negative Casimir energies in quantum field theory.

Negative energies with a periodic direction

Consider any quantum field theory on $\mathbb{R}^{3,1}$ that is conformal in the UV (including UV-free theories). If we consider this quantum field theory at finite temperature, the energy density relative to the vacuum state at temperatures much higher than any other scale will behave as

$$T_{00} = c_T T^4 \tag{B.15}$$

where c_T gives some measure of the number of UV degrees of freedom. The full stress-energy tensor in this high-temperature limit will be approximately traceless (again because of the UV CFT), so we will have

$$T_{ij} = \frac{1}{3}\delta_{ij} c_T T^4 \ . \tag{B.16}$$

The thermal state of this CFT may be constructed by considering the Euclidean version of the quantum field theory with a Euclidean time direction that is periodic, with anti-periodic boundary conditions for fermions. The thermal density matrix for the original theory can be obtained by slicing the Euclidian path integral at some Euclidean time along the thermal circle.[2]

We can slice this same path integral perpendicular to one of the $\mathbb{R}^3$ directions to define the vacuum state of the field theory on $\mathbb{R}^2 \times S^1$ with antiperiodic boundary conditions for fermions on the S^1.

The Casimir stress-energy tensor for this vacuum state (i.e. the stress-energy relative to its value on Minkowski space) is directly related to the thermal stress-energy tensor above, since both are obtained by inserting an operator into the Euclidean path integral that defines these two

[2]Alternatively, we can slice the path integral into two pieces at a pair of times on opposite sides of the circle to define the thermofield double state.

states.

Specifically, if τ is the periodic coordinate and η is the time coordinate in the theory with a periodic direction, we have

$$\begin{aligned} T^{Cas}_{\tau\tau} &= -c_T \frac{1}{\beta^4} \\ T^{Cas}_{\eta\eta} &= -\frac{1}{3} c_T \frac{1}{\beta^4} \\ T^{Cas}_{ij} &= \delta_{ij} \frac{1}{3} c_T \frac{1}{\beta^4} \end{aligned}$$

Thus, we have a negative energy density $T^{Cas}_{\eta\eta}$ and a negative null energy in the periodic direction of $T_{++} = T_{--} = -4/3 c_T \beta^{-4}$.

These energy densities can be made arbitrarily negative by taking the length β of the periodic direction to be small.

Enhanced negative energies in systems with boundaries

In order to support the wormhole geometries that could give rise to realistic cosmology, we need negative energy that extends over a spatial region that is much larger than the scale of the negative energy itself. A naive way to construct this would be to take this quantum field theory state from the example above, consider the reduced state on a subsystem $\tau \in (0, \beta - \epsilon)$ of the periodic direction, and try to purify this in a system where the τ direction has a larger extent.

It is impossible to purify this system to a translation-invariant state of a quantum field theory on Minkowski space, since the averaged null energy condition (ANEC) [277, 278] says that integral of T_{++} over a complete null geodesic must be non-negative. So in any purification on Minkowski, we must have regions of positive null-energy surrounding this region of negative null energy. However, we are not aware of any restriction on the width of a region where T_{++} is bounded above by a certain negative value. The holographic models of [8, 157], which have interfaces that create a finite spatial extent for the CFT, provide examples to suggest that there is no such restriction. It would be interesting to understand whether even weakly coupled quantum field theories can exist in states with a negative energy much larger than the geometrical scale (distance between interfaces/boundaries) for the right choice of boundary physics.

Appendix C: Technical details of the results reported in Chapter 4

Authors:[1] *Stefano Antonini, Petar Simidzija, Brian Swingle, Mark Van Raamsdonk.*

C.1 Quantization of a gauge field in the wormhole background

Consider the action[2] for a gauge field in our wormhole background[3]:

$$S_{gauge} = -\frac{1}{4}\int d^4x\sqrt{-g}F_{IJ}F^{IJ} \tag{C.1}$$

leading to the equations of motion (which, together with the Bianchi identity for F_{IJ}, provide the four Maxwell's equations)

$$\partial_I\left(\sqrt{-g}F^{IJ}\right) = 0. \tag{C.2}$$

In our four-dimensional wormhole, these can be recast in the form

$$\eta^{IK}\partial_I\partial_K A_J - \partial_J\left(\eta^{IK}\partial_I A_K\right) = 0 \tag{C.3}$$

[1]Originally published in the appendices of *Can one hear the shape of a wormhole?*, JHEP 09 (2022) 241, e-Print: 2207.02225, [3].

[2]In general, a boundary term dependent on the choice of boundary conditions is present in the action. We omit here, see [262]

[3]In this appendix we will use latin indices $I, J = 0, 1, 2, 3$ to indicate 4D components, and greek indices $\mu, \nu = 0, 1, 2$ for 3D components t, x, y.

where η_{IJ} is the 4D Minkowski metric. Note that, as a result of the conformal invariance of the gauge field action in 4D, the equations of motion have no dependence on the wormhole scale factor $a(z)$. With a slight abuse of notation, in the rest of this appendix we will raise and lower indices using the Minkowski metric, rather than the wormhole metric $g_{IJ} = 1/a^2(z)\eta_{IJ}$. We will work in Lorenz gauge

$$\partial^I A_I = 0 \tag{C.4}$$

in which the equations of motion decouple, reducing to four independent Klein-Gordon equations for a massless field in flat spacetime.

C.1.1 Boundary conditions

For simplicity of notation, we define here $\ell = 2z_0$ and shift $z \to z - z_0$ such that the two boundaries are located at $z = 0, \ell$. The behavior of the gauge field near the two boundaries is given by[4]

$$\begin{aligned} A_I(x, z \sim 0) &\sim \alpha_I^{(L)}(x)(1 + ...) + z\beta_I^{(L)}(x)(1 + ...) \\ A_I(x, z \sim \ell) &\sim \alpha_I^{(R)}(x)(1 + ...) + (\ell - z)\beta_I^{(R)}(x)(1 + ...) \end{aligned} \tag{C.5}$$

where the dots indicate terms of higher order in z and $\ell - z$ for the left and right boundaries respectively. We must now specify a set of boundary conditions. We will do so for the μ components of the gauge field; we will see that the Lorenz gauge condition then uniquely determines the boundary condition for A_z. There are two standard choices for the boundary conditions [258–262]: at each boundary we can either fix $\alpha_\mu(x)$ (Dirichlet boundary conditions), or fix $\beta_\mu(x)$ (Neumann

[4] The argument (x) stands for a dependence on the 3D coordinates t, x, y only.

boundary conditions), up to a (residual) gauge transformation[5]. For later convenience, let us introduce a deformation term in the dual CFT action, given by

$$I_d = i \int d^3x O_\mu^{(\alpha)}(x) J^\mu(x), \tag{C.6}$$

where the role of $O_\mu^{(\alpha)}(x)$ and $J_\mu(x)$ depends on the choice of boundary conditions and will be clarified below.

Imposing Dirichlet boundary conditions, which can be reformulated in a gauge-invariant way by fixing $F_{\mu\nu}|_\partial$, the boundary value $\alpha_\mu(x)$ becomes a non-dynamical source $O_\mu^{(\alpha)}(x)$ in the dual 3D CFT living on the corresponding boundary, which couples to a global conserved current $J^\mu(x)$ with dimension $\Delta = 2$, as in equation (C.6). The one-point function of $J_\mu(x)$ is related to the coefficient $\beta_\mu(x)$ of the subleading term of the gauge field at the boundary. This leads to the "standard quantization", where the CFT path integral computes the generating functional $Z[O^{(\alpha)}] = \langle \exp\left(i \int d^3x O_\mu^{(\alpha)}(x) J^\mu(x)\right)\rangle$ with fixed sources $O_\mu^{(\alpha)}(x) = \alpha_\mu(x)$. Note that, since the current J^μ is conserved, the generating functional is insensitive to a gauge transformation $\alpha_\mu \to \alpha_\mu + \partial_\mu \lambda$, which shows explicitly why we can fix α_μ up to a gauge transformation. In the corresponding bulk theory, the part of the gauge field giving rise to the subleading boundary term proportional to $\beta_\mu(x)$ is quantized. The boundary limit of its bulk correlators are dual to boundary correlators of the current $J_\mu(x)$.

The second choice, whose gauge-invariant form is given by fixing $F_{\mu z}|_\partial$[6], leaves the value

[5]The Dirichlet and Neumann boundary conditions are sometimes referred to as "magnetic" and "electric" boundary conditions, because they correspond to fixing $F_{\mu\nu}$ and $F_{\mu z}$ at the boundary, respectively (although this nomenclature is somewhat improper, z being a spatial direction).

[6]As we will see below, the gauge-invariant form of the boundary conditions is not completely equivalent to just fixing $\beta_\mu(x)$. In fact, differently from the Dirichlet case, fixing $\beta_\mu(x)$ and then imposing the Lorenz gauge condition (C.4) does not completely determine a boundary condition for A_z. On the other hand, the (physically meaningful) gauge-invariant condition fixes the boundary conditions for A_z completely. As far as the μ component of the gauge

$\alpha_\mu(x)$ of the gauge field at the boundary free to fluctuate. This must then be identified with the expectation value of a boundary vector operator $\langle O_\mu^{(\alpha)}(x)\rangle$ of dimension $\Delta = 1$. In the CFT path integral, we must integrate over the field $O_\mu^{(\alpha)}(x)$. $J_\mu(x)$ appearing in (C.6) must now be regarded as an external source, determined by the value of $\beta_\mu(x)$, which is now fixed.[7] This leads to the "alternative quantization", where the CFT path integral computes a generating functional $Z[J] = \langle \exp\left(i\int d^3x O_\mu^{(\alpha)}(x)J^\mu(x)\right)\rangle$ with fixed sources $J_\mu(x)$ determined by $\beta_\mu(x)$. Once again, the generating functional is invariant under gauge transformations. In the bulk theory, the part of the gauge field giving rise to the leading boundary term $O_\mu^{(\alpha)}(x)$ is quantized. For additional discussion on these points, see [258–262].

So far we did not make any assumption about the relationship between boundary conditions at the left ($z = 0$) and right ($z = \ell$) boundaries. Since the microscopic construction dual to our traversable wormhole is reflection symmetric and involves two copies of the same 3D CFT [2], we will assume that boundary conditions at the two boundaries are the same: either we fix $\alpha_\mu^{(L)}(x), \alpha_\mu^{(R)}(x)$ (i.e. $F_{\mu\nu}|_{z=0,\ell}$), or we fix $\beta_\mu^{(L)}(x), \beta_\mu^{(R)}(x)$ (i.e. $F_{\mu z}|_{z=0,\ell}$). Note that, in more general settings, different boundary conditions can be chosen at the two boundaries. The boundary conditions for A_z, which we will derive using the Lorenz gauge condition, also need to be the same at the two boundaries. Therefore, we can write in general

$$A_I(x,z) = A_I^{(1)}(x,z) + A_I^{(2)}(x,z) \tag{C.7}$$

field is concerned, the two boundary conditions are equivalent.

[7] Note that in the classical case the field $O_\mu^{(\alpha)}(x)$ has no kinetic term in the dual CFT's lagrangian. Therefore, from equation (C.6), the equations of motion for $O_\mu^{(\alpha)}(x)$ imply $\langle J^\mu\rangle = 0$, constraining the value of $\beta_\mu(x)$ to zero [258]. In general, quantum corrections can introduce a kinetic term [258], allowing arbitrary values of the current, and therefore of $\beta_\mu(x)$.

where

$$\begin{aligned}
&A_I^{(1)}(x, z \sim 0) \sim \alpha_I^{(L)}(x), \qquad && A_I^{(1)}(x, z \sim \ell) \sim \alpha_I^{(R)}(x) \\
&A_I^{(2)}(x, z \sim 0) \sim z\beta_I^{(L)}(x), \qquad && A_I^{(2)}(x, z \sim \ell) \sim (\ell - z)\beta_I^{(R)}(x)
\end{aligned} \tag{C.8}$$

where we omitted subleading corrections in z and $\ell - z$. The standard quantization corresponds then to fixing $A_\mu^{(1)}(x, z)$ at $z = 0, \ell$, and quantizing $A_\mu^{(2)}(x, z)$. The alternative quantization corresponds to fixing the value of $A_\mu^{(2)}(x, z)/z$ at $z = 0$ and $A_\mu^{(2)}(x, z)/(\ell - z)$ at $z = \ell$, and quantizing $A_\mu^{(1)}(x, z)$. We can then write $A_I^{(1)}(x, z)$ and $A_I^{(2)}(x, z)$ in the general form

$$\begin{aligned}
A_I^{(1)}(x, z) &= \sum_{n=0}^{\infty} \int \frac{dk_x dk_y}{2\pi\sqrt{\ell}\sqrt{\omega_n}\sqrt{1+\delta_{n,0}}} \left[\varepsilon_I^{(1)}(k_x, k_y, \rho_n)\cos(\rho_n z)\mathrm{e}^{-i(\omega_n t - k_x x - k_y y)} + c.c.\right] \\
A_I^{(2)}(x, z) &= \sum_{n=1}^{\infty} \int \frac{dk_x dk_y}{2\pi\sqrt{\ell}\sqrt{\omega_n}} \left[\varepsilon_I^{(2)}(k_x, k_y, \rho_n)\sin(\rho_n z)\mathrm{e}^{-i(\omega_n t - k_x x - k_y y)} + c.c.\right]
\end{aligned} \tag{C.9}$$

where the factor $\sqrt{1+\delta_{n,0}}$ is necessary to guarantee the normalization of the $n = 0$ mode, $\omega_n = \sqrt{k_x^2 + k_y^2 + \rho_n^2}$, $\rho_n = n\pi/\ell$ is the momentum in the z direction (whose discrete values are determined by the requirement of having the same kind of boundary conditions (Dirichlet or Neumann) at the two boundaries), and ϵ_I is the polarization 4-vector.

The gauge field (C.7) must satisfy the Lorenz gauge condition (C.4). Using the expansion (C.9), the Lorenz gauge condition takes the form

$$\begin{cases}
i\varepsilon_\mu^{(1)}k^\mu + \varepsilon_z^{(2)}\rho_n = 0 \\
i\varepsilon_\mu^{(2)}k^\mu - \varepsilon_z^{(1)}\rho_n = 0.
\end{cases} \tag{C.10}$$

Fixing Dirichlet (Neumann) boundary conditions on A_μ corresponds to fixing the polarization vectors $\varepsilon_\mu^{(1)}$ ($\varepsilon_\mu^{(2)}$) up to a residual gauge transformation $\varepsilon_\mu^{(1)} \to \varepsilon_\mu^{(1)} + C_1 k_\mu$ ($\varepsilon_\mu^{(2)} \to \varepsilon_\mu^{(2)} + C_2 k_\mu$).

The condition (C.10) then implies that, for Dirichlet boundary conditions on A_μ, all the $\varepsilon_z^{(2)}$ are also fixed up to a residual gauge transformation $\varepsilon_z^{(2)} \to \varepsilon_z^{(2)} + i\rho_n$. In other words, $\beta_z(x)$ (the subleading part of A_z at the boundary) is fixed: Neumann boundary conditions are imposed on A_z.

On the other hand, for Neumann boundary conditions on A_μ, all the $\varepsilon_z^{(1)}$ with $n \geq 1$ are fixed up to a gauge transformation by the condition (C.10), while $\varepsilon_z^{(1)}(k_x, k_y, \rho_0)$ is unconstrained. However, it is easy to show that, choosing the correct gauge-invariant boundary condition (i.e. fixing $F_{\mu z}|_{z=0,\ell}$ instead of $\beta_\mu(x)$ only), $\varepsilon_z^{(1)}(k_x, k_y, \rho_0)$ is also constrained. Therefore, the second choice of boundary condition is given by Neumann on A_μ and Dirichlet on A_z.

Now that we have specified an appropriate set of boundary conditions at the two boundaries, we can proceed to the quantization of the bulk gauge field. In the following, we will keep referring to Dirichlet and Neumann boundary conditions as determined by the boundary condition imposed on A_μ.

C.1.2 Dirichlet boundary conditions: standard quantization

For Dirichlet boundary conditions on A_μ and Neumann on A_z, the field we must quantize is given by

$$A_\mu^D(x,z) = A_\mu^{(2)}(x,z), \qquad\qquad A_z^D(x,z) = A_z^{(1)}(x,z) \tag{C.11}$$

where $A_I^{(1,2)}$ are defined in equation (C.9). The Lorenz condition does not fix the gauge completely. In particular, we have a residual gauge freedom

$$A_I^D \to A_I^D + \partial_I \lambda_D \tag{C.12}$$

where we can write

$$\lambda_D = \sum_{n=1}^{\infty} \int \frac{dk_x dk_y}{2\pi\sqrt{\ell}} C_D(k_x, k_y, \rho_n) \sin(\rho_n z) \mathrm{e}^{-i(\omega_n t - k_x x - k_y y)} \tag{C.13}$$

where $C_D(k_x, k_y, \rho_n)$ can be chosen arbitrarily. We can use such residual gauge freedom to set $\varepsilon_z^{(1)}(k_x, k_y, \rho_n) = 0$ for all $n \geq 1$. Note that $\varepsilon_z^{(1)}(k_x, k_y, \rho_0)$ cannot be set to zero by such a residual gauge transformation. Normalization for the resulting 3D massless scalar field imposes $\varepsilon_z^{(1)}(k_x, k_y, \rho_0) = 1$. The Lorenz gauge condition then reduces to $\varepsilon_\mu^{(2)} k^\mu = 0$, which removes one degree of freedom in the μ components of the gauge field. We can define an orthonormal basis of polarization 3-vectors $\{\epsilon_\mu^{(j)}\}|_{j=a,b}$ satisfying such condition:

$$\begin{aligned}
\tilde{\epsilon}_\mu^{(a)}(k, \rho_n) &= \frac{1}{\sqrt{k_x^2 + k_y^2}}(0, -k_y, k_x) \\
\tilde{\epsilon}_\mu^{(b)}(k, \rho_n) &= \frac{1}{\rho_n\sqrt{k_x^2 + k_y^2}}(-(k_x^2 + k_y^2), \omega_n k_x, \omega_n k_y)
\end{aligned} \tag{C.14}$$

with $n \geq 1$. We are now left with only physical degrees of freedom and can finally quantize the field:

$$\begin{aligned}
\hat{A}_\mu^D &= \sum_{n=1}^{\infty} \int \frac{dk_x dk_y}{2\pi\sqrt{\omega_n}\sqrt{\ell}} \sum_{j=a,b} \left[\tilde{\varepsilon}_\mu^{(j)}(k, \rho_n) \sin(\rho_n z) \mathrm{e}^{-(i\omega_n t - k_x x - k_y y)} \hat{a}_{k,\rho_n}^{(j)} + h.c.\right] \\
\hat{A}_z^D &= \int \frac{dk_x dk_y}{2\pi\sqrt{2\omega_0}\sqrt{\ell}} \left[\mathrm{e}^{-(i\omega_0 t - k_x x - k_y y)} \hat{a}_k + h.c.\right]
\end{aligned} \tag{C.15}$$

where the creation and annihilation operators $\hat{a}$, $\hat{a}^\dagger$ satisfy the canonical commutation relations. For the physical interpretation of this result, see Section 4.2.3.

C.1.3 Neumann/electric boundary conditions: alternative quantization

For Neumann boundary conditions, where we fix $F_{\mu z}|_{z=0,\ell}$, the field we must quantize is

$$A^N_\mu(x,z) = A^{(1)}_\mu(x,z), \qquad\qquad A^N_z(x,z) = A^{(2)}_z(x,z). \tag{C.16}$$

The residual gauge freedom is now given by

$$A^N_I \to A^N_I + \partial_I \lambda_N \tag{C.17}$$

with

$$\lambda_N = \sum_{n=0}^{\infty} \int \frac{dk_x dk_y}{2\pi\sqrt{\ell}} C_N(k_x,k_y,\rho_n)\cos(\rho_n z)\mathrm{e}^{-i(\omega_n t - k_x x - k_y y)}. \tag{C.18}$$

Using this residual gauge freedom, we can set $\varepsilon^{(2)}_z(k,\rho_n) = 0$ for all $\rho_n \geq 1$, and $\varepsilon^{(1)}_0(k,\rho_0) = 0$. After fixing the residual gauge, the Lorenz condition reduces to $\varepsilon^{(1)}_\mu k^\mu = 0$. For all the modes with $n \geq 1$, we can use the basis of polarization vectors (C.14). Now we also have to define an additional polarization vector for the $n = 0$ mode of A^N_μ. Having set $\varepsilon^{(1)}_0(k,\rho_0) = 0$, the Lorenz gauge condition for this mode reads $k^i \varepsilon^{(1)}_i(k,\rho_0) = 0$ with $i = 1,2$. The unique unit vector satisfying such condition is

$$\tilde{\varepsilon}^{(0)}_\mu(k) = \frac{1}{\sqrt{k_x^2 + k_y^2}}(0, -k_y, k_x). \tag{C.19}$$

Now that all the non-physical degrees of freedom have been eliminated, we can quantize the field:

$$\begin{aligned}\hat{A}_\mu^N &= \int \frac{dk_x dk_y}{2\pi\sqrt{2\omega_0}\sqrt{\ell}} \left[\tilde{\varepsilon}_\mu^{(0)}(k)\mathrm{e}^{-(i\omega_0 t - k_x x - k_y y)}\hat{a}_k^{(j)} + h.c.\right] \\ &+ \sum_{n=1}^{\infty} \int \frac{dk_x dk_y}{2\pi\sqrt{\omega_n}\sqrt{\ell}} \sum_{j=a,b} \left[\tilde{\varepsilon}_\mu^{(j)}(k,\rho_n)\cos(\rho_n z)\mathrm{e}^{-(i\omega_n t - k_x x - k_y y)}\hat{a}_{k,\rho_n}^{(j)} + h.c.\right].\end{aligned} \tag{C.20}$$

For the physical interpretation of this result, see Section 4.2.3.

C.2 Derivation of the asymptotic spectrum

Consider the Schrödinger equation with the "test" potential

$$\tilde{V}(z) \equiv \frac{\alpha}{(z_0 - |z|)^2} + \frac{\beta}{z_0 - |z|} + c \tag{C.21}$$

The potential (C.21) is simple enough that we can explicitly compute the asymptotic form of its normalizable spectrum, $\tilde{\lambda}_j$. Indeed, a simple rescaling of z reduces the corresponding Schrödinger equation to a Whittaker's differential equation, whose solution is well known [279]. First, we note the basic result from Sturm-Liouville theory that since the potential $\tilde{V}(z)$ is even, the normalizable eigenfunctions alternate between even functions ($u_0, u_2, \dots$) and odd functions ($u_1, u_3, \dots$). Let us consider the odd eigenfunctions, which are defined, up to normalization, by the condition $u(0) = 0$. The solution to the Schrödinger equation with this "initial" condition at $z = 0$ can be obtained from the solution of the Whittaker's differential equation by an appropriate rescaling of z [279]. The general solution is given by the linear combination

$$u_{\text{odd}}(z,\tilde{\lambda}) = C_1 M_{x,\frac{\mu}{2}}\left(i2(z_0 - |z|)\sqrt{\tilde{\lambda} - c}\right) + C_2 M_{x,-\frac{\mu}{2}}\left(i2(z_0 - |z|)\sqrt{\tilde{\lambda} - c}\right) \tag{C.22}$$

where $M_{x,\frac{\mu}{2}}(y)$ is related to the confluent hypergeometric function of the first kind ${}_1F_1(a;b;y)$ by

$$M_{x,\frac{\mu}{2}}(y) = y^{\frac{1+\mu}{2}} \mathrm{e}^{-\frac{y}{2}} {}_1F_1\left(\frac{1+\mu}{2} - x; 1+\mu; y\right) \tag{C.23}$$

and we identified

$$x = \frac{i\beta}{2\sqrt{\tilde{\lambda} - c}}; \qquad \mu = 2\bar{\Delta}; \qquad y = i2(z_0 - |z|)\sqrt{\tilde{\lambda} - c} \tag{C.24}$$

where $\bar{\Delta} = \sqrt{1+4\alpha}/2$. The first term in the linear combination (C.22) corresponds to the normalizable component of the eigenfunctions, while the second term is the non-normalizable component. Since we are interested in the normalizable spectrum of the potential (C.21), we set $C_2 = 0$.

Then the odd normalizable eigenvalues $\tilde{\lambda}_j$, $j = 1, 3, 5...$, are given by values of $\tilde{\lambda}$ that solve the odd condition $u_{odd}(0, \tilde{\lambda}_j) = 0$.[8] Since we are interested in the asymptotic spectrum, we want to look for solutions $\{\tilde{\lambda}_j\}$ of the odd condition with $\tilde{\lambda}_j \gg 1$. Therefore, we can set $z = 0$ and find the form of the normalizable eigenfunction (first term in equation (C.22)) in the limit of large $\tilde{\lambda}$. Defining $x = i\tau$, $y = i\zeta$ and assuming $\tau \in \mathbb{R}^+$, $\zeta \in \mathbb{R}\backslash\{0\}$, $\mu \in \mathbb{R}$, the function $M_{i\tau,\frac{\mu}{2}}(i\zeta)$

[8]For $-1/4 < a < 0$ the non-normalizable modes also vanish at $z = z_0$. To avoid this difficulty, here we are assuming that $a > 0$. The results for the case $a < 0$ follow by analytic continuation.

has the following asymptotic expansion for large ζ [279]:

$$M_{i\tau,\frac{\mu}{2}}(i\zeta) \sim \frac{2\Gamma(1+\mu)\exp\left[\frac{\pi}{2}\left(\tau+i\frac{1+\mu}{2}\right)\right]\mathrm{sgn}(\zeta)}{\left|\Gamma\left(\frac{1+\mu}{2}\pm i\tau\right)\right|}\cdot$$

$$\left\{\cos\left[-\tau\log|\zeta|+\frac{\zeta}{2}+\delta-\frac{\pi}{4}(1+\mu)\mathrm{sgn}(\zeta)\right]\sum_{k=0}^{N}\frac{\left(\frac{\tau^2}{\zeta}\right)^k}{k!}\frac{\cos\left[\sum_{r=1}^{k}(\phi_r^{(+)}+\phi_r^{(-)})-\frac{\pi}{2}k\right]}{\prod_{r=1}^{k}\left(\sin\phi_r^{(+)}\sin\phi_r^{(-)}\right)}\right.$$

$$\left.-\sin\left[-\tau\log|\zeta|+\frac{\zeta}{2}+\delta-\frac{\pi}{4}(1+\mu)\mathrm{sgn}(\zeta)\right]\sum_{k=1}^{N}\frac{\left(\frac{\tau^2}{\zeta}\right)^k}{k!}\frac{\sin\left[\sum_{r=1}^{k}(\phi_r^{(+)}+\phi_r^{(-)})-\frac{\pi}{2}k\right]}{\prod_{r=1}^{k}\left(\sin\phi_r^{(+)}\sin\phi_r^{(-)}\right)}\right\} \tag{C.25}$$

where $\Gamma(x)$ is the Euler gamma function, and δ, $\phi_r^{(\pm)}$ are given by

$$\delta=-\frac{i}{2}\log\left[\frac{\Gamma\left(\frac{1+\mu}{2}+i\tau\right)}{\Gamma\left(\frac{1+\mu}{2}-i\tau\right)}\right]; \qquad \tan\phi_r^{(\pm)}=\frac{\tau}{r+\frac{-1\pm\mu}{2}}. \tag{C.26}$$

Keeping only terms up to order $1/\sqrt{\tilde{\lambda}-c}$ in equation (C.25), we get (up to an irrelevant multiplicative factor)

$$\begin{aligned} M_{i\tau,\frac{\mu}{2}}(i\zeta) \sim & \cos\left[-\tau\log|\zeta|+\frac{\zeta}{2}+\delta-\frac{\pi}{4}(1+\mu)\mathrm{sgn}(\zeta)\right] \\ & +\frac{1-\mu^2}{4\zeta}\sin\left[-\tau\log|\zeta|+\frac{\zeta}{2}+\delta-\frac{\pi}{4}(1+\mu)\mathrm{sgn}(\zeta)\right]+\mathcal{O}\left(\frac{1}{\tilde{\lambda}-c}\right). \end{aligned} \tag{C.27}$$

The discrete set of asymptotic odd eigenvalues $\{\tilde{\lambda}_j\}$ (for odd values of $j \gg 1$) we are looking for is determined by the zeros of equation (C.27). Using equation (C.24), such zeros are given by the $\tilde{\lambda}$'s satisfying

$$\sqrt{\tilde{\lambda}-c} = -\frac{\alpha}{2z_0^2\sqrt{\tilde{\lambda}-c}} + \frac{\beta}{2z_0\sqrt{\tilde{\lambda}-c}}\log\left(2z_0\sqrt{\tilde{\lambda}-c}\right) + \frac{i}{2z_0}\log\left[\frac{\Gamma\left(\Delta_+ + \frac{i\beta}{2\sqrt{\tilde{\lambda}-c}}\right)}{\Gamma\left(\Delta_+ - \frac{i\beta}{2\sqrt{\tilde{\lambda}-c}}\right)}\right]$$
$$+\frac{\pi}{2z_0}(\Delta_+ + 2n - 1) \tag{C.28}$$

with $\Delta_+ = (1+2\bar{\Delta})/2$ and $n = 1, 2, 3....$ Substituting the expansion ansatz

$$\sqrt{\tilde{\lambda}-c} = a_1 n + a_2 \log n + a_3 + a_4\frac{\log n}{n} + \frac{a_5}{n} + \mathcal{O}\left(\frac{1}{n^2}\right) \tag{C.29}$$

into equation (C.28) and expanding the right hand side up to order $1/n$ yields the values of the $\{a_i\}_{i=1,\ldots,5}$. Solving equation (C.29) for $\tilde{\lambda}$ and identifying $n = (j+1)/2$ with j odd, we finally obtain the expression for the asymptotic spectrum:

$$\tilde{\lambda}_j \sim \left(\frac{\pi}{2z_0}\right)^2 j^2 + \left(\frac{\pi}{2z_0}\right)^2 2\Delta_+ j + \frac{\beta}{z_0}\log(j)$$
$$+\left(\frac{\pi}{2z_0}\right)^2\left(\Delta_+^2 - \frac{4\alpha}{\pi^2}\right) + \frac{\beta}{z_0}\left[\log(\pi) - \psi(\Delta_+)\right] + c, \tag{C.30}$$

where $\psi(x)$ is the digamma function. Although we have derived this expansion for j odd, it can immediately be extended also to even values of j, yielding the full asymptotic spectrum (4.39).

C.3 Proof of lemma

Here we prove the lemma used in the reconstruction algorithm in Section 4.3.2.

Lemma 2 *For any L^2 integrable function $f(z)$ on $z \in (-z_0, z_0)$ the following identity holds:*

$$f(z) = \sum_{j=0}^{\infty} \frac{\tilde{v}_j(z) \int_{-z_0}^{z} dy\, u_j(y) f(y) + \tilde{u}_j(z) \int_{z}^{z_0} dy\, v_j(y) f(y)}{\omega'(\lambda_j)}. \tag{C.31}$$

Proof. Let $f(z)$ be an L^2 integrable function. We define

$$\Phi(z, \lambda) \equiv \frac{\tilde{v}(z, \lambda) \int_{-z_0}^{z} dy\, u(y, \lambda) f(y) + \tilde{u}(z, \lambda) \int_{z}^{z_0} dy\, v(y, \lambda) f(y)}{\omega(\lambda)}. \tag{C.32}$$

Notice that this is well-defined because $u(y, \lambda)$ is integrable at the left boundary, while $v(y, \lambda)$ is integrable at the right boundary. Now consider the contour integral

$$\frac{1}{2\pi i} \int_{\Gamma} d\lambda\, \Phi(z, \lambda), \tag{C.33}$$

where Γ is a large circle in the complex λ plane, whose radius we take to infinity. In this limit, we can evaluate the contour integral in two different ways. First, directly by the residue theorem we find

$$\frac{1}{2\pi i} \int_{\Gamma} d\lambda\, \Phi(z, \lambda) = \sum_{j=0}^{\infty} \frac{\tilde{v}_j(z) \int_{-z_0}^{z} dy\, u_j(y) f(y) + \tilde{u}_j(z) \int_{z}^{z_0} dy\, v_j(y) f(y)}{\omega'(\lambda_j)}, \tag{C.34}$$

where λ_j are eigenvalues of (4.32) with normalizable boundary conditions, and where we define $u_j(z) \equiv u(z, \lambda_j)$, $\tilde{u}_j(z) \equiv \tilde{u}(z, \lambda_j)$, and similarly for the vs.

Alternatively, we can evaluate the above contour integral by first going to the limit of large $|\lambda|$ (since we are taking the radius of the contour Γ to infinity) before using the residue theorem. As we discussed, in the limit $|\lambda| \to \infty$ we can effectively replace $V(z)$ with $\tilde{V}(z)$, and hence

$u \to \tilde{u}$, $v \to \tilde{v}$ and $\omega(\lambda) \to \tilde{\omega}(\lambda) \equiv -\tilde{u}^{-}(z_0, \lambda)$. Using the residue theorem we thus obtain

$$\frac{1}{2\pi i}\int_{\Gamma} d\lambda\, \Phi(z,\lambda) = \sum_{j=0}^{\infty} \frac{\tilde{V}_j(z)\int_{-z_0}^{z} dy\, \tilde{U}_j(y) f(y) + \tilde{U}_j(z)\int_{z}^{z_0} dy\, \tilde{V}_j(y) f(y)}{\tilde{\omega}'(\tilde{\lambda}_j)}, \tag{C.35}$$

where $\tilde{U}_j$ and $\tilde{V}_j$ are solutions of the following initial value problems on $z \in (-z_0, z_0)$

$$\tilde{U}_j : \begin{cases} \tilde{U}_j''(z) = \big[\tilde{V}(z) - \tilde{\lambda}_j\big]\tilde{U}_j(z) \\ \tilde{U}_j^{(+)}(-z_0) = \frac{1}{2\bar{\Delta}} \\ \tilde{U}_j^{(-)}(-z_0) = 0 \end{cases} \qquad \tilde{V}_j : \begin{cases} \tilde{V}_j''(z) = \big[\tilde{V}(z) - \tilde{\lambda}_j\big]v_j(z) \\ \tilde{V}_j^{(+)}(+z_0) = \frac{1}{2\bar{\Delta}} \\ \tilde{V}_j^{(-)}(+z_0) = 0 \end{cases} . \tag{C.36}$$

Hence $\tilde{U}_j$ and $\tilde{V}_j$ must both be proportional to the j-th normalizable eigenfunction of $u''(z) = \big[\tilde{V}(z) - \lambda\big]u(z)$. Since $\tilde{V}(z)$ is $\mathbb{Z}_2$ symmetric, these eigenfunctions have a parity $(-1)^j$, and thus $\tilde{U}_j(z) = (-1)^j\tilde{V}_j(z)$. Additionally, by using the explicit form C.22 for the normalizable eigenfunctions, it can be verified by direct calculation that $\tilde{\omega}'(\tilde{\lambda}_j) = (-1)^j||U_j||^2$, where $||\cdot||^2$ denotes the L^2-norm, i.e. the norm associated with the Sturm-Liouville inner product. It was in order to obtain this identity that we chose the normalization factor $1/2\bar{\Delta}$ for the normalizable modes in Eqs. (4.48) and (4.49). Therefore (C.35) gives

$$\frac{1}{2\pi i}\int_{\Gamma} d\lambda\, \Phi(z,\lambda) = \sum_{j=0}^{\infty} \frac{\tilde{U}_j(z)\int_{-z_0}^{z_0} dy\, \tilde{U}_j(y) f(y)}{||U_j||^2}, \tag{C.37}$$

which is precisely the Sturm-Liouville expansion of $f(z)$. Comparing with (C.34) we obtain the identity

$$f(z) = \sum_{j=0}^{\infty} \frac{\tilde{v}_j(z) \int_{-z_0}^{z} dy\, u_j(y) f(y) + \tilde{u}_j(z) \int_{z}^{z_0} dy\, v_j(y) f(y)}{\omega'(\lambda_j)}, \tag{C.38}$$

which completes the proof. $\square$

Appendix D: Technical details of the results reported in Chapter 5

Authors:[1] *Stefano Antonini, Petar Simidzija, Brian Swingle, Mark Van Raamsdonk, Chris Waddell.*

D.1 Fine-tuning potentials with a flat region

In this appendix we explain how the parameters of potentials with a flat region of the form (5.14)-(5.15) must be chosen and fine-tuned to reproduce the ΛCDM cosmological evolution between the early universe and the present day.

In order to have a phase of accelerated expansion in the cosmological evolution, the positive potential energy at the plateau (which is fixed by observational data to be $A = \Omega_\Lambda$) must be dominant over every other term on the right-hand side of the Friedmann equation. This implies that the scalar field's kinetic energy K_ϕ must be very small when the field reaches the plateau. Evolving backwards in time from the time-symmetric point $\tilde{t} = 0$ in the cosmology picture, the scalar field behaves like an anti-damped particle. Therefore, intuitively, an accelerated expansion can take place only if $|B| \ll |A|$ — where B sets the value of $V(0)$. In this way, for an appropriately fine-tuned potential, the scalar field just barely makes it up to the plateau and the kinetic energy does not become dominant until very close to the Big Bang (or Big Crunch, if we evolve

[1] Originally published in the appendices of *Accelerating cosmology from $\Lambda < 0$ gravitational effective field theory*, JOURNAL CITATION, e-Print: 2212.00050, [4].

forward in time from the time-symmetric point).

Next, we must require that the BF bound (5.5) is satisfied. This can be achieved by choosing the value of X to be large enough that the deep valleys are not too close to the maximum at $\phi = 0$, so that $(d^2\tilde{V}/d\phi^2)|_{\phi=0}$ is suppressed. However, X must not be too large, otherwise the cosmological evolution will reach the Big Bang singularity before the scalar field can reach the valleys (and then the plateau): in this case, no accelerated expansion phase occurs.

Moreover, the (negative) parameter C — which controls the depth of the valleys — must be large enough that the scalar field acquires sufficient kinetic energy in its anti-damped motion to reach the positive plateau. But it cannot be too large, or the kinetic energy will be large when the scalar reaches the plateau and no accelerated phase can take place. We remark that no particular fine-tuning has been carried out so far on the parameters: we just identified the general criteria to choose the parameters B, C and X in order for an accelerated expansion to be possible and for the BF bound to be satisfied (we remind that A is fixed by data). The specific choice of their values is arbitrary and irrelevant for the sake of reproducing the ΛCDM evolution.

Finally, we fine-tune the value of Δ[2] to allow the scalar field to reach the plateau with a very small kinetic energy. This yields a phase of accelerated expansion, and will allow us to reproduce the ΛCDM cosmological evolution between the early universe and the present day.

Note that, as we evolve backwards in time towards the Big Bang, the scalar field's kinetic energy will eventually become dominant. Our goal is to reproduce as best as possible the results of the ΛCDM model, in which there is no such term in the Friedmann equation, between the early universe and the present day. More precisely, an important criterion for the feasibility of these models is that we should not have a significant departure from ΛCDM between the

[2]Note that we could have instead fixed a value of Δ and fine-tuned the parameter C.

present time and the time of Big Bang Nucleosynthesis (BBN) (which roughly occurs in the range of temperatures $T \sim 10^9 - 10^{10}$ K), otherwise the abundances of various elements could vary appreciably from those experimentally observed. These temperatures correspond to scale factors which are between 10^{-9} and 10^{-10} times smaller than the current value of the scale factor $a(\tilde{t}_0) = 1$. We can therefore ask whether it is possible to tune our model with a rolling scalar such that the scalar field's kinetic energy is a subdominant contribution in the cosmological Friedmann equation for $10^{-10} \lesssim a(\tilde{t}) \leq 1$. In other words, we would like to determine whether the kinetic energy dominance can be pushed sufficiently early in time that it would not impact the predictions of BBN.

By appropriately fine-tuning the parameter Δ we were able to push the crossover between the early kinetic-energy-dominated era and the radiation-dominated era to $\tilde{t} = \tilde{t}^*$ with $\tilde{t}^* - \tilde{t}_{BB} = \mathcal{O}(10^{-13})$ (where $\tilde{t}_{BB}$ corresponds to the Big Bang) in our numerical solutions, corresponding to $a(\tilde{t}^*) = \mathcal{O}(10^{-7})$. We were not able to reach the desired value $a(\tilde{t}^*) = \mathcal{O}(10^{-10})$ because of numerical precision issues related to the excessively small time steps needed, but there is no a priori obstacle in pushing the kinetic-energy-dominated era arbitrarily close to the cosmological singularity.

By implementing this fine-tuning procedure after choosing the *Planck* 2018 cosmological parameters (5.16) and the initial condition $a_0 = 2$, we obtained the set of parameters (5.17) used in our numerical analysis. The same procedure was also used to fine-tune the potential for the solution employing SNIa-derived cosmological parameters depicted in Figure 5.7.

D.2 Scalar potential for wCDM model

For completeness, we provide some details related to the analysis in Section 5.2.4.

To construct a scalar potential $V(\phi)$ agreeing with $V_w(\phi)$ in a suitable region, permitting cosmological solutions which satisfy observational constraints from SNe Ia and have asymptotically AdS Euclidean continuations, we proceed as follows:

1. Determine the redshift dependence of the scalar field $\phi_w(z)$ and potential $V_w(z)$ for the given wCDM model,[3] in the region $z \in (z_{\text{min}}, z_{\text{max}})$ where type Ia supernova data have been used to constrain cosmological parameters. We have the freedom to choose the value $\phi_w(0) \equiv \phi_0$ and the sign of $\phi'_w(0)$; we will take both to be positive. Note however that the present scalar kinetic energy is fixed to

$$\frac{1}{2}\dot{\phi}_w(z=0)^2 = \frac{1}{8\pi G}H_0 H'(0) - \frac{3}{16\pi G}H_0^2\Omega_M \equiv K_0\,. \tag{D.1}$$

2. Evaluate $\phi_w(z)$ and $V_w(z)$ for a large sample $\{z_i\}$ of redshifts in the interval $(z_{\text{min}}, z_{\text{max}})$, to obtain an array of pairs $\{(\phi_w^{(i)}, V_w^{(i)})\}$.

3. Choose a model $V(\phi;\{p\},q)$, with parameters $\{p\}$ and q, satisfying:

    - $V(0;\{p\},q) < 0$
    - $-\frac{9}{4} < \frac{V''(0;\{p\},q)}{|V(0;\{p\},q)|} < 0$
    - $V(\phi;\{p\},q)$ behaves as a polynomial for $\phi \gtrsim \phi(z=0)$.

[3] The Hubble expansion $H(z)$ for the wCDM model is given in equation (5.19), using the parameters recorded in Section 5.2.4. The redshift dependence of the scalar $\phi(z)$ and potential $V(z)$ may then be computed from $H(z)$ using equation (D.2).

In our case, the model has a Gaussian trough between $\phi = 0$ and $\phi = \phi_0$, with a height controlled by the parameter q.

4. Apply the "shooting method" to determine parameters $\{p\}$ and q for which the model has a time-symmetric solution with the correct scalar kinetic energy K_0 at $z = 0$:

   - For various choices of q, use the array $\{(\phi_w^{(i)}, V_w^{(i)})\}$ to determine the best-fit parameters $\{p_{\text{fit}}(q)\}$.

   - Solve the equations of motion for $a(t), \phi(t)$ for the best-fit models $V(\phi; \{p_{\text{fit}}(q)\}, q)$ with each choice of q to determine for which value q_* there exists a future time t for which $\dot{a}(t) = \dot{\phi}(t) = 0$; this determines the model for which the solution has a moment of time symmetry. We use initial conditions $\phi(t_0) = \phi_0$, $\dot{\phi}(t_0) = -\sqrt{2K_0}$, and $a(t_0) = 1$.

5. As a check, evaluate the solution to the model $V(\phi; \{p_{\text{fit}}(q_*)\}, q_*)$ with time-symmetric initial conditions, and verify that the equation of state $w(z)$ behaves appropriately for $z \in (z_{\text{min}}, z_{\text{max}})$, and that the Euclidean continuation has AdS asymptotics.

It will frequently be useful to work with quantities rescaled by the Hubble parameter H_0, as defined in Section 5.2.3.

We observe that the procedure outlined above has significant freedom in the choice of model $V(\phi)$; since our goal is merely to demonstrate the existence of a scalar potential satisfying the list of criteria outlined in the main text, it suffices to construct a specific example.

Constructing an example

We first deduce the redshift dependence of the scalar field $\phi_w(z)$ and the rescaled potential $\tilde{V}_w(z)$ from the rescaled Hubble expansion $\tilde{H}(z)$ for the wCDM model, using

$$\begin{aligned} \phi_w(z) &= \phi_0 + \int_0^z dz' \, \frac{\sqrt{\frac{1}{4\pi G}(1+z')\tilde{H}(z')\tilde{H}'(z') - \frac{3}{8\pi G}(1+z')^3\Omega_M}}{(1+z')\tilde{H}(z')} \\ \tilde{V}_w(z) &= -\frac{1}{8\pi G}(1+z)\tilde{H}(z)\tilde{H}'(z) + \frac{3}{8\pi G}\tilde{H}(z)^2 - \frac{3}{16\pi G}(1+z)^3\Omega_M \, . \end{aligned} \tag{D.2}$$

We also deduce the present time-derivative $\dot{\phi}(\tilde{t}_0)$, where the overdot denotes a derivative with respect to the rescaled time coordinate; in units $\frac{8\pi G}{3} = 1$, we find for the wCDM model

$$\dot{\phi}_w(\tilde{t}_0) = -0.2628687886 \, . \tag{D.3}$$

Next, we choose as our model function

$$\begin{aligned} \tilde{V}(\phi; A, B, C, \Delta, X, \mathbf{V}) &= \tilde{V}_0(\phi; \ldots) + \tilde{V}_0(-\phi; \ldots) \\ \tilde{V}_0(\phi; \ldots) &= \frac{A-B}{2}\text{erf}\left(\frac{\phi - X}{\Delta}\right) + C\exp\left(-\frac{(\phi-X)^2}{\Delta^2}\right) \\ &\quad + \left(\sum_{k=1}^{4} \frac{V_k}{k!}(\phi - X)^k\right)\left(1 + \text{erf}\left(\frac{\phi - X}{\Delta}\right)\right) + \frac{A}{2} \, . \end{aligned} \tag{D.4}$$

This is similar to the asymptotically flat potential introduced in Section 5.2.3 to reproduce the ΛCDM model, though we have effectively replaced the flat region with a polynomial.

We will choose to situate the present time at $\phi_0 = 0.7$, the trough in the potential at roughly $X = 0.5$, the width $\Delta = 0.06$, and to take $B = -0.08$, which fixes the potential at $\phi = 0$ to this value; we choose these values for concreteness, though one could proceed analogously for many suitable choices of these quantities. Our choices are motivated by the facts that (1) having the trough join suitably to the polynomial piece of the potential requires $(\phi_0 - X)$ to be a few multiples of Δ, and (2) B should be sufficiently large in absolute value that we avoid recollapse in the wormhole picture. The parameter C, controlling the depth of the trough, is the parameter that we will vary for the shooting method.

With these choices, we proceed to apply the shooting method, solving the equation (5.11) with initial conditions $a(t_0) = 0, \phi(t_0) = \phi_0, \dot{\phi}(t_0) = -0.2628687886$, for various choices of C and best-fit (A, V_1, V_2, V_3, V_4). Our procedure yields, to our working precision, the parameters $C = -7.80623080636$ and

$$\begin{gathered} A = 1.13258420902349\,, \quad V_1 = -4.21938633468535\,, \quad V_2 = 50.3190576443637\,, \\ V_3 = -370.514499837809\,, \quad V_4 = 1408.97547041725\,. \end{gathered} \tag{D.5}$$

We plot the corresponding potential $V(\phi)$, as well as $V_w(\phi)$, in Figure 5.9 of the main text. We find that the moment of time symmetry occurs at rescaled time $\tilde{t}$ with

$$\tilde{t} - \tilde{t}_0 = 0.5712956836\,, \tag{D.6}$$

at which time the scale factor and scalar field are given by

$$a(\tilde{t}) = 1.41641139203233\,, \quad \phi(\tilde{t}) = 0.358665688585761\,. \tag{D.7}$$

To check our results, we can solve both the Lorentzian and Euclidean equations of motion (5.11) and (5.12) for the model with scalar potential $V(\phi)$, assuming time-symmetric initial conditions at

$$\phi = 0.358665688585761\;, \tag{D.8}$$

the location suggested by equation (D.7). Assuming that the present time $\tilde{t}_0$ satisfies $a(\tilde{t}_0) = 1$, we can extract the redshift dependence of the equation of state parameter $w(z)$ over the range $z \in (z_{\text{min}}, z_{\text{max}})$ using equation (5.25), and verify that it is approximately constant and equal to the Pantheon+SH0ES value $w = -0.90 \pm 0.14$; we show this in Figure 5.10 in the main text. We can also verify that the Euclidean solution is asymptotically AdS by plotting the rescaled "Euclidean Hubble expansion" $H(\tau)$ and observing that it approaches a constant value, as also shown in Figure 5.10 in the main text.

Bibliography

[1] Stefano Antonini and Brian Swingle. Cosmology at the end of the world. *Nature Phys.*, 16(8):881–886, 2020. arXiv:1907.06667 [hep-th].

[2] Stefano Antonini, Petar Simidzija, Brian Swingle, and Mark Van Raamsdonk. Cosmology from the vacuum. *Under review (JHEP)*, 3 2022. arXiv:2203.11220 [hep-th].

[3] Stefano Antonini, Petar Simidzija, Brian Swingle, and Mark Van Raamsdonk. Can one hear the shape of a wormhole? *JHEP*, 09:241, 2022. arXiv:2207.02225 [hep-th].

[4] Stefano Antonini, Petar Simidzija, Brian Swingle, Mark Van Raamsdonk, and Chris Waddell. Accelerating cosmology from $\Lambda < 0$ gravitational effective field theory. *Accepted for publication (JHEP)*, 11 2022. arXiv:2212.00050 [hep-th].

[5] Sean Cooper, Moshe Rozali, Brian Swingle, Mark Van Raamsdonk, Christopher Waddell, and David Wakeham. Black hole microstate cosmology. *Journal of High Energy Physics*, 2019(7):1–70, 2019.

[6] Stefano Antonini and Brian Swingle. Holographic boundary states and dimensionally reduced braneworld spacetimes. *Phys. Rev. D*, 104(4):046023, 2021. arXiv:2105.02912 [hep-th].

[7] Mark Van Raamsdonk. Comments on wormholes, ensembles, and cosmology. *JHEP*, 12:156, 2021. arXiv:2008.02259 [hep-th].

[8] Mark Van Raamsdonk. Cosmology from confinement? *JHEP*, 03:039, 2022. arXiv:2102.05057 [hep-th].

[9] Stefano Antonini, Petar Simidzija, Brian Swingle, and Mark Van Raamsdonk. Cosmology as a holographic wormhole. *Accepted for publication (Phys. Rev. Lett.)*, 6 2022. arXiv:2206.14821 [hep-th].

[10] Mark Van Raamsdonk. Cosmology without time-dependent scalars is like quantum field theory without RG flow. 11 2022. arXiv:2211.12611 [hep-th].

[11] Tadashi Takayanagi. Holographic Dual of BCFT. *Phys. Rev. Lett.*, 107:101602, 2011. arXiv:1105.5165 [hep-th].

[12] Mitsutoshi Fujita, Tadashi Takayanagi, and Erik Tonni. Aspects of AdS/BCFT. *JHEP*, 11:043, 2011. arXiv:1108.5152 [hep-th].

[13] Juan Martin Maldacena and Liat Maoz. Wormholes in AdS. *JHEP*, 02:053, 2004. arXiv:hep-th/0401024.

[14] Juan Martin Maldacena. The Large N limit of superconformal field theories and supergravity. *Int. J. Theor. Phys.*, 38:1113–1133, 1999. arXiv:hep-th/9711200 [hep-th], [Adv. Theor. Math. Phys.2,231(1998)].

[15] S. S. Gubser, Igor R. Klebanov, and Alexander M. Polyakov. Gauge theory correlators from noncritical string theory. *Phys. Lett.*, B428:105–114, 1998. arXiv:hep-th/9802109 [hep-th].

[16] Edward Witten. Anti-de Sitter space and holography. *Adv. Theor. Math. Phys.*, 2:253–291, 1998. arXiv:hep-th/9802150 [hep-th].

[17] Ofer Aharony, Steven S. Gubser, Juan Martin Maldacena, Hirosi Ooguri, and Yaron Oz. Large N field theories, string theory and gravity. *Phys. Rept.*, 323:183–386, 2000. arXiv:hep-th/9905111 [hep-th].

[18] Veronika E. Hubeny. The AdS/CFT Correspondence. *Class. Quant. Grav.*, 32(12):124010, 2015. arXiv:1501.00007 [gr-qc].

[19] Mark Van Raamsdonk. Lectures on Gravity and Entanglement. In *Proceedings, Theoretical Advanced Study Institute in Elementary Particle Physics: New Frontiers in Fields and Strings (TASI 2015): Boulder, CO, USA, June 1-26, 2015*, pages 297–351, 2017.

[20] J. D. Bekenstein. Black holes and the second law. *Lett. Nuovo Cim.*, 4:737–740, 1972.

[21] Jacob D. Bekenstein. Black holes and entropy. *Phys. Rev. D*, 7:2333–2346, Apr 1973.

[22] Jacob D. Bekenstein. Generalized second law of thermodynamics in black hole physics. *Phys. Rev. D*, 9:3292–3300, 1974.

[23] Jacob D. Bekenstein. A Universal Upper Bound on the Entropy to Energy Ratio for Bounded Systems. *Phys. Rev. D*, 23:287, 1981.

[24] S. W. Hawking. Black hole explosions. *Nature*, 248:30–31, 1974.

[25] S. W. Hawking. Particle Creation by Black Holes. *Commun. Math. Phys.*, 43:199–220, 1975. [Erratum: Commun.Math.Phys. 46, 206 (1976)].

[26] S. W. Hawking. Black Holes and Thermodynamics. *Phys. Rev. D*, 13:191–197, 1976.

[27] Raphael Bousso. A Covariant entropy conjecture. *JHEP*, 07:004, 1999. arXiv:hep-th/9905177.

[28] Raphael Bousso, Horacio Casini, Zachary Fisher, and Juan Maldacena. Proof of a Quantum Bousso Bound. *Phys. Rev. D*, 90(4):044002, 2014. arXiv:1404.5635 [hep-th].

[29] Raphael Bousso, Zachary Fisher, Stefan Leichenauer, and Aron C. Wall. Quantum focusing conjecture. *Phys. Rev. D*, 93(6):064044, 2016. arXiv:1506.02669 [hep-th].

[30] Gerard 't Hooft. Dimensional reduction in quantum gravity. *Conf. Proc.*, C930308:284–296, 1993. arXiv:gr-qc/9310026 [gr-qc].

[31] Charles B. Thorn. Reformulating string theory with the 1/N expansion. In *The First International A.D. Sakharov Conference on Physics*, 5 1991.

[32] Leonard Susskind. The World as a hologram. *J. Math. Phys.*, 36:6377–6396, 1995. arXiv:hep-th/9409089 [hep-th].

[33] Raphael Bousso. The Holographic principle. *Rev. Mod. Phys.*, 74:825–874, 2002. arXiv:hep-th/0203101.

[34] Lisa Randall and Raman Sundrum. Large mass hierarchy from a small extra dimension. *Phys. Rev. Lett.*, 83:3370–3373, Oct 1999.

[35] Lisa Randall and Raman Sundrum. An alternative to compactification. *Phys. Rev. Lett.*, 83:4690–4693, Dec 1999.

[36] Ahmed Almheiri, Raghu Mahajan, Juan Maldacena, and Ying Zhao. The Page curve of Hawking radiation from semiclassical geometry. *JHEP*, 03:149, 2020. arXiv:1908.10996 [hep-th].

[37] Dominik Neuenfeld. Homology conditions for RT surfaces in double holography. *Class. Quant. Grav.*, 39(7):075009, 2022. arXiv:2105.01130 [hep-th].

[38] Andreas Karch, Haoyu Sun, and Christoph F. Uhlemann. Double holography in string theory. *JHEP*, 10:012, 2022. arXiv:2206.11292 [hep-th].

[39] Mehmet Demirtas, Manki Kim, Liam McAllister, Jakob Moritz, and Andres Rios-Tascon. Small cosmological constants in string theory. *JHEP*, 12:136, 2021. arXiv:2107.09064 [hep-th].

[40] Mehmet Demirtas, Manki Kim, Liam McAllister, Jakob Moritz, and Andres Rios-Tascon. Exponentially Small Cosmological Constant in String Theory. *Phys. Rev. Lett.*, 128(1):011602, 2022. arXiv:2107.09065 [hep-th].

[41] P. Di Francesco, P. Mathieu, and D. Senechal. *Conformal Field Theory*. Graduate Texts in Contemporary Physics. Springer-Verlag, New York, 1997.

[42] Igor R. Klebanov and Giuseppe Torri. M2-branes and AdS/CFT. *Int. J. Mod. Phys. A*, 25:332–350, 2010. arXiv:0909.1580 [hep-th].

[43] Lorenz Eberhardt and Matthias R. Gaberdiel. String theory on AdS_3 and the symmetric orbifold of Liouville theory. *Nucl. Phys. B*, 948:114774, 2019. arXiv:1903.00421 [hep-th].

[44] Edward Witten. AdS / CFT correspondence and topological field theory. *JHEP*, 12:012, 1998. arXiv:hep-th/9812012.

[45] Subir Sachdev. Holographic metals and the fractionalized Fermi liquid. *Phys. Rev. Lett.*, 105:151602, 2010. arXiv:1006.3794 [hep-th].

[46] Juan Maldacena and Douglas Stanford. Remarks on the Sachdev-Ye-Kitaev model. *Phys. Rev. D*, 94(10):106002, 2016. arXiv:1604.07818 [hep-th].

[47] Horatiu Nastase. Introduction to Supergravity. 12 2011. arXiv:1112.3502 [hep-th].

[48] Jan de Boer, Erik P. Verlinde, and Herman L. Verlinde. On the holographic renormalization group. *JHEP*, 08:003, 2000. arXiv:hep-th/9912012.

[49] Jan de Boer. The Holographic renormalization group. *Fortsch. Phys.*, 49:339–358, 2001. arXiv:hep-th/0101026.

[50] Masafumi Fukuma, So Matsuura, and Tadakatsu Sakai. Holographic renormalization group. *Prog. Theor. Phys.*, 109:489–562, 2003. arXiv:hep-th/0212314.

[51] Ofer Aharony. The NonAdS / nonCFT correspondence, or three different paths to QCD. In *NATO Advanced Study Institute and EC Summer School on Progress in String, Field and Particle Theory*, pages 3–24, 12 2002.

[52] Joshua Erlich. An Introduction to Holographic QCD for Nonspecialists. *Contemp. Phys.*, 56(2):159–171, 2015. arXiv:1407.5002 [hep-ph].

[53] Sophia K. Domokos, Robert Bell, Trinh La, and Patrick Mazza. A Pedagogical Introduction to Holographic Hadrons. 6 2021. arXiv:2106.13136 [hep-th].

[54] Phil Saad, Stephen H. Shenker, and Douglas Stanford. JT gravity as a matrix integral. 3 2019. arXiv:1903.11115 [hep-th].

[55] Daniel Harlow and Douglas Stanford. Operator Dictionaries and Wave Functions in AdS/CFT and dS/CFT. 2011. arXiv:1104.2621 [hep-th].

[56] L. Susskind and Edward Witten. The Holographic Bound in Anti-de Sitter Space. pages 1–10, 1998. arXiv:9805114 [hep-th].

[57] Tom Banks, Michael R. Douglas, Gary T. Horowitz, and Emil J. Martinec. AdS dynamics from conformal field theory. 8 1998. arXiv:hep-th/9808016.

[58] Shinsei Ryu and Tadashi Takayanagi. Aspects of Holographic Entanglement Entropy. *JHEP*, 08:045, 2006. arXiv:hep-th/0605073 [hep-th].

[59] Shinsei Ryu and Tadashi Takayanagi. Holographic derivation of entanglement entropy from AdS/CFT. *Phys. Rev. Lett.*, 96:181602, 2006. arXiv:hep-th/0603001 [hep-th].

[60] Aitor Lewkowycz and Juan Maldacena. Generalized gravitational entropy. *JHEP*, 08:090, 2013. arXiv:1304.4926 [hep-th].

[61] Veronika E. Hubeny, Mukund Rangamani, and Tadashi Takayanagi. A Covariant holographic entanglement entropy proposal. *JHEP*, 07:062, 2007. arXiv:0705.0016 [hep-th].

[62] Aron C. Wall. Maximin Surfaces, and the Strong Subadditivity of the Covariant Holographic Entanglement Entropy. *Class. Quant. Grav.*, 31(22):225007, 2014. arXiv:1211.3494 [hep-th].

[63] Thomas Faulkner, Aitor Lewkowycz, and Juan Maldacena. Quantum corrections to holographic entanglement entropy. *JHEP*, 11:074, 2013. arXiv:1307.2892 [hep-th].

[64] Netta Engelhardt and Aron C. Wall. Quantum Extremal Surfaces: Holographic Entanglement Entropy beyond the Classical Regime. *JHEP*, 01:073, 2015. arXiv:1408.3203 [hep-th].

[65] Douglas Stanford and Leonard Susskind. Complexity and Shock Wave Geometries. *Phys. Rev.*, D90(12):126007, 2014. arXiv:1406.2678 [hep-th].

[66] Adam R. Brown, Daniel A. Roberts, Leonard Susskind, Brian Swingle, and Ying Zhao. Holographic Complexity Equals Bulk Action? *Phys. Rev. Lett.*, 116(19):191301, 2016. arXiv:1509.07876 [hep-th].

[67] Adam R. Brown, Hrant Gharibyan, Geoff Penington, and Leonard Susskind. The Python's Lunch: geometric obstructions to decoding Hawking radiation. *JHEP*, 08:121, 2020. arXiv:1912.00228 [hep-th].

[68] Brian Swingle. Entanglement Renormalization and Holography. *Phys. Rev.*, D86:065007, 2012. arXiv:0905.1317 [cond-mat.str-el].

[69] Mark Van Raamsdonk. Building up spacetime with quantum entanglement. *Gen. Rel. Grav.*, 42:2323–2329, 2010. arXiv:1005.3035 [hep-th], [Int. J. Mod. Phys.D19,2429(2010)].

[70] Juan Maldacena and Leonard Susskind. Cool horizons for entangled black holes. *Fortsch. Phys.*, 61:781–811, 2013. arXiv:1306.0533 [hep-th].

[71] Ahmed Almheiri, Xi Dong, and Daniel Harlow. Bulk Locality and Quantum Error Correction in AdS/CFT. *JHEP*, 04:163, 2015. arXiv:1411.7041 [hep-th].

[72] Daniel Harlow. TASI Lectures on the Emergence of Bulk Physics in AdS/CFT. *PoS*, TASI2017:002, 2018. arXiv:1802.01040 [hep-th].

[73] Fernando Pastawski, Beni Yoshida, Daniel Harlow, and John Preskill. Holographic quantum error-correcting codes: Toy models for the bulk/boundary correspondence. *JHEP*, 06:149, 2015. arXiv:1503.06237 [hep-th].

[74] Patrick Hayden, Sepehr Nezami, Xiao-Liang Qi, Nathaniel Thomas, Michael Walter, and Zhao Yang. Holographic duality from random tensor networks. *Journal of High Energy Physics*, 2016(11):1–56, 2016.

[75] Chris Akers, Netta Engelhardt, Geoff Penington, and Mykhaylo Usatyuk. Quantum Maximin Surfaces. *JHEP*, 08:140, 2020. arXiv:1912.02799 [hep-th].

[76] Ahmed Almheiri, Thomas Hartman, Juan Maldacena, Edgar Shaghoulian, and Amirhossein Tajdini. Replica Wormholes and the Entropy of Hawking Radiation. *JHEP*, 05:013, 2020. arXiv:1911.12333 [hep-th].

[77] Geoff Penington, Stephen H Shenker, Douglas Stanford, and Zhenbin Yang. Replica wormholes and the black hole interior. *Journal of High Energy Physics*, 2022(3):1–87, 2022.

[78] S. W. Hawking. Breakdown of Predictability in Gravitational Collapse. *Phys. Rev. D*, 14:2460–2473, 1976.

[79] Geoffrey Penington. Entanglement Wedge Reconstruction and the Information Paradox. *JHEP*, 09:002, 2020. arXiv:1905.08255 [hep-th].

[80] Ahmed Almheiri, Netta Engelhardt, Donald Marolf, and Henry Maxfield. The entropy of bulk quantum fields and the entanglement wedge of an evaporating black hole. *JHEP*, 12:063, 2019. arXiv:1905.08762 [hep-th].

[81] Hong Zhe Chen, Robert C. Myers, Dominik Neuenfeld, Ignacio A. Reyes, and Joshua Sandor. Quantum Extremal Islands Made Easy, Part I: Entanglement on the Brane. 6 2020. arXiv:2006.04851 [hep-th].

[82] Hong Zhe Chen, Robert C. Myers, Dominik Neuenfeld, Ignacio A. Reyes, and Joshua Sandor. Quantum Extremal Islands Made Easy, Part II: Black Holes on the Brane. *JHEP*, 12:025, 2020. arXiv:2010.00018 [hep-th].

[83] Juan Hernandez, Robert C. Myers, and Shan-Ming Ruan. Quantum extremal islands made easy. Part III. Complexity on the brane. *JHEP*, 02:173, 2021. arXiv:2010.16398 [hep-th].

[84] Guglielmo Grimaldi, Juan Hernandez, and Robert C. Myers. Quantum extremal islands made easy. Part IV. Massive black holes on the brane. *JHEP*, 03:136, 2022. arXiv:2202.00679 [hep-th].

[85] Martin Bojowald. Quantum cosmology: a review. *Rept. Prog. Phys.*, 78:023901, 2015. arXiv:1501.04899 [gr-qc].

[86] C. L. Bennett et al. Nine-Year Wilkinson Microwave Anisotropy Probe (WMAP) Observations: Final Maps and Results. *Astrophys. J. Suppl.*, 208:20, 2013. arXiv:1212.5225 [astro-ph.CO].

[87] G. Hinshaw et al. Nine-Year Wilkinson Microwave Anisotropy Probe (WMAP) Observations: Cosmological Parameter Results. *Astrophys. J. Suppl.*, 208:19, 2013. arXiv:1212.5226 [astro-ph.CO].

[88] Publications of the *Planck* collaboration. `https://www.cosmos.esa.int/web/planck/publications`.

[89] Steven Weinberg. *Cosmology*. OUP Oxford, 2008.

[90] N. Aghanim et al. Planck 2018 results. VI. Cosmological parameters. *Astron. Astrophys.*, 641:A6, 2020. arXiv:1807.06209 [astro-ph.CO], [Erratum: Astron.Astrophys. 652, C4 (2021)].

[91] J. Alberto Vázquez, Luis E. Padilla, and Tonatiuh Matos. Inflationary cosmology: from theory to observations. *Rev. Mex. Fis. E*, 17(1):73–91, 2020. arXiv:1810.09934 [astro-ph.CO].

[92] P. J. E. Peebles and Bharat Ratra. Cosmology with a Time Variable Cosmological Constant. *Astrophys. J. Lett.*, 325:L17, 1988.

[93] Bharat Ratra and P. J. E. Peebles. Cosmological Consequences of a Rolling Homogeneous Scalar Field. *Phys. Rev. D*, 37:3406, 1988.

[94] Shinji Tsujikawa. Quintessence: A Review. *Class. Quant. Grav.*, 30:214003, 2013. arXiv:1304.1961 [gr-qc].

[95] Leandros Perivolaropoulos and Foteini Skara. Challenges for ΛCDM: An update. *New Astron. Rev.*, 95:101659, 2022. arXiv:2105.05208 [astro-ph.CO].

[96] Kevin J. Ludwick. The viability of phantom dark energy: A review. *Mod. Phys. Lett. A*, 32(28):1730025, 2017. arXiv:1708.06981 [astro-ph.CO].

[97] Andrew Strominger. The dS / CFT correspondence. *JHEP*, 10:034, 2001. arXiv:hep-th/0106113.

[98] Mohsen Alishahiha, Andreas Karch, Eva Silverstein, and David Tong. The dS/dS correspondence. *AIP Conf. Proc.*, 743(1):393–409, 2004. arXiv:hep-th/0407125.

[99] Xi Dong, Eva Silverstein, and Gonzalo Torroba. De Sitter Holography and Entanglement Entropy. *JHEP*, 07:050, 2018. arXiv:1804.08623 [hep-th].

[100] Victor Gorbenko, Eva Silverstein, and Gonzalo Torroba. dS/dS and $T\overline{T}$. *JHEP*, 03:085, 2019. arXiv:1811.07965 [hep-th].

[101] Evan Coleman, Edward A. Mazenc, Vasudev Shyam, Eva Silverstein, Ronak M. Soni, Gonzalo Torroba, and Sungyeon Yang. De Sitter microstates from T$\overline{T}$ + Λ_2 and the Hawking-Page transition. *JHEP*, 07:140, 2022. arXiv:2110.14670 [hep-th].

[102] Leonard Susskind. Black Holes Hint Towards De Sitter-Matrix Theory. 9 2021. arXiv:2109.01322 [hep-th].

[103] Leonard Susskind. De Sitter Holography: Fluctuations, Anomalous Symmetry, and Wormholes. *Universe*, 7(12):464, 2021. arXiv:2106.03964 [hep-th].

[104] Leonard Susskind. Entanglement and Chaos in De Sitter Space Holography: An SYK Example. *JHAP*, 1(1):1–22, 2021. arXiv:2109.14104 [hep-th].

[105] Edgar Shaghoulian and Leonard Susskind. Entanglement in De Sitter space. *JHEP*, 08:198, 2022. arXiv:2201.03603 [hep-th].

[106] Sabrina Pasterski. Lectures on celestial amplitudes. *Eur. Phys. J. C*, 81(12):1062, 2021. arXiv:2108.04801 [hep-th].

[107] Ben Freivogel, Veronika E. Hubeny, Alexander Maloney, Robert C. Myers, Mukund Rangamani, and Stephen Shenker. Inflation in AdS/CFT. *JHEP*, 03:007, 2006. arXiv:hep-th/0510046 [hep-th].

[108] Xi Dong, Bart Horn, Shunji Matsuura, Eva Silverstein, and Gonzalo Torroba. FRW solutions and holography from uplifted AdS/CFT. *Phys. Rev. D*, 85:104035, 2012. arXiv:1108.5732 [hep-th].

[109] Souvik Banerjee, Ulf Danielsson, Giuseppe Dibitetto, Suvendu Giri, and Marjorie Schillo. Emergent de Sitter Cosmology from Decaying Anti–de Sitter Space. *Phys. Rev. Lett.*, 121(26):261301, 2018. arXiv:1807.01570 [hep-th].

[110] Paul McFadden and Kostas Skenderis. Holography for Cosmology. *Phys. Rev. D*, 81:021301, 2010. arXiv:0907.5542 [hep-th].

[111] Andreas Karch and Lisa Randall. Locally localized gravity. *JHEP*, 05:008, 2001. arXiv:hep-th/0011156.

[112] Andreas Karch and Lisa Randall. Open and closed string interpretation of SUSY CFT's on branes with boundaries. *JHEP*, 06:063, 2001. arXiv:hep-th/0105132 [hep-th].

[113] Andreas Karch and Lisa Randall. Localized gravity in string theory. *Phys. Rev. Lett.*, 87:061601, 2001. arXiv:hep-th/0105108.

[114] Antonio Padilla. *Brane world cosmology and holography*. PhD thesis, Durham U., 2002.

[115] James P. Gregory and Antonio Padilla. Exact brane world cosmology induced from bulk black holes. *Class. Quant. Grav.*, 19:4071–4083, 2002. arXiv:hep-th/0204218 [hep-th].

[116] Moshe Rozali, James Sully, Mark Van Raamsdonk, Christopher Waddell, and David Wakeham. Information radiation in BCFT models of black holes. *JHEP*, 05:004, 2020. arXiv:1910.12836 [hep-th].

[117] Mark Van Raamsdonk and Chris Waddell. Finding $\mathrm{AdS}^5 \times \mathrm{S}^5$ in 2+1 dimensional SCFT physics. *JHEP*, 11:145, 2021. arXiv:2109.04479 [hep-th].

[118] Chris Waddell. Bottom-up holographic models for cosmology. *JHEP*, 09:176, 2022. arXiv:2203.03096 [hep-th].

[119] Seamus Fallows and Simon F. Ross. Constraints on cosmologies inside black holes. *JHEP*, 05:094, 2022. arXiv:2203.02523 [hep-th].

[120] Juan Martin Maldacena. Eternal black holes in anti-de Sitter. *JHEP*, 04:021, 2003. arXiv:hep-th/0106112 [hep-th].

[121] Hirosi Ooguri and Lev Spodyneiko. New Kaluza-Klein instantons and the decay of AdS vacua. *Phys. Rev. D*, 96(2):026016, 2017. arXiv:1703.03105 [hep-th].

[122] Iñaki García Etxebarria, Miguel Montero, Kepa Sousa, and Irene Valenzuela. Nothing is certain in string compactifications. *JHEP*, 12:032, 2020. arXiv:2005.06494 [hep-th].

[123] Giuseppe Dibitetto, Nicolò Petri, and Marjorie Schillo. Nothing really matters. *JHEP*, 08:040, 2020. arXiv:2002.01764 [hep-th].

[124] Edward Witten. Instability of the Kaluza-Klein Vacuum. *Nucl. Phys.*, B195:481–492, 1982.

[125] Petr Horava and Edward Witten. Heterotic and type I string dynamics from eleven-dimensions. *Nucl. Phys. B*, 460:506–524, 1996. arXiv:hep-th/9510209.

[126] Petr Horava and Edward Witten. Eleven-dimensional supergravity on a manifold with boundary. *Nucl. Phys. B*, 475:94–114, 1996. arXiv:hep-th/9603142.

[127] Stefano Antonini, Gregory Bentsen, ChunJun Cao, Jonathan Harper, Shao-Kai Jian, and Brian Swingle. Holographic measurement and bulk teleportation. *JHEP*, 12:124, 2022. arXiv:2209.12903 [hep-th].

[128] Werner Israel. Singular hypersurfaces and thin shells in general relativity. *Il Nuovo Cimento B (1965-1970)*, 44(1):1–14, 1966.

[129] G. W. Gibbons and S. W. Hawking. Action Integrals and Partition Functions in Quantum Gravity. *Phys. Rev.*, D15:2752–2756, 1977.

[130] James W. York, Jr. Conformatlly invariant orthogonal decomposition of symmetric tensors on Riemannian manifolds and the initial value problem of general relativity. *J. Math. Phys.*, 14:456–464, 1973.

[131] Chris Clarkson and Sanjeev S. Seahra. Braneworld resonances. *Class. Quant. Grav.*, 22:3653–3688, 2005. arXiv:gr-qc/0505145 [gr-qc].

[132] Claudia de Rham. Massive Gravity. *Living Rev. Rel.*, 17:7, 2014. arXiv:1401.4173 [hep-th].

[133] Ahmed Almheiri, Alexandros Mousatov, and Milind Shyani. Escaping the interiors of pure boundary-state black holes. *JHEP*, 02:024, 2023. arXiv:1803.04434 [hep-th].

[134] John L. Cardy. Boundary Conditions, Fusion Rules and the Verlinde Formula. *Nucl. Phys.*, B324:581–596, 1989.

[135] Ian Affleck and Andreas W. W. Ludwig. Universal noninteger 'ground state degeneracy' in critical quantum systems. *Phys. Rev. Lett.*, 67:161–164, 1991.

[136] John L. Cardy. Boundary conformal field theory. 2004. arXiv:hep-th/0411189 [hep-th].

[137] Pasquale Calabrese and John Cardy. Entanglement entropy and conformal field theory. *J. Phys.*, A42:504005, 2009. arXiv:0905.4013 [cond-mat.stat-mech].

[138] Ioanna Kourkoulou and Juan Maldacena. Pure states in the SYK model and nearly-AdS_2 gravity. 2017. arXiv:1707.02325 [hep-th].

[139] Kyriakos Papadodimas and Suvrat Raju. An Infalling Observer in AdS/CFT. *JHEP*, 10:212, 2013. arXiv:1211.6767 [hep-th].

[140] Kyriakos Papadodimas and Suvrat Raju. State-Dependent Bulk-Boundary Maps and Black Hole Complementarity. *Phys. Rev.*, D89(8):086010, 2014. arXiv:1310.6335 [hep-th].

[141] Netta Engelhardt, Geoff Penington, and Arvin Shahbazi-Moghaddam. A world without pythons would be so simple. *Class. Quant. Grav.*, 38(23):234001, 2021. arXiv:2102.07774 [hep-th].

[142] Chris Akers, Netta Engelhardt, Daniel Harlow, Geoff Penington, and Shreya Vardhan. The black hole interior from non-isometric codes and complexity. 7 2022. arXiv:2207.06536 [hep-th].

[143] Thomas Hartman and Juan Maldacena. Time evolution of entanglement entropy from black hole interiors. *Journal of High Energy Physics*, 2013(5), 2013. arXiv:1303.1080.

[144] Goncalo A. S. Dias and Jose P. S. Lemos. Hamiltonian thermodynamics of d-dimensional ($d >= 4$) Reissner-Nordstrom anti-de Sitter black holes with spherical, planar, and hyperbolic topology. *Phys. Rev.*, D79:044013, 2009. arXiv:0901.0278 [gr-qc].

[145] Yang Huang, Dao-Jun Liu, and Xin-Zhou Li. Superradiant instability of D-dimensional Reissner-Nordström-anti-de Sitter black hole mirror system. *Int. J. Mod. Phys.*, D26(13):1750141, 2017. arXiv:1606.00100 [gr-qc].

[146] P. P. Avelino, A. J. S. Hamilton, C. A. R. Herdeiro, and M. Zilhao. Mass inflation in a D dimensional Reissner-Nordstrom black hole: a hierarchy of particle accelerators? *Phys. Rev.*, D84:024019, 2011. arXiv:1105.4434 [gr-qc].

[147] Jafar Sadeghi and Vahid Reza Shajiee. Quantum Tunneling from the Charged Non-Rotating BTZ Black Hole with GUP. *Eur. Phys. J. Plus*, 132(3):132, 2017. arXiv:1605.04595 [hep-th].

[148] B. Gouteraux. *Black-Hole Solutions to Einstein's Equations in the Presence of Matter and Modifications of Gravitation in Extra Dimensions*. PhD thesis, Orsay, LPT, 2010.

[149] Amit Ghosh and P. Mitra. Temperatures of extremal black holes. 1995. arXiv:gr-qc/9507032 [gr-qc].

[150] R. Penrose. Gravitational collapse: The role of general relativity. *Riv. Nuovo Cim.*, 1:252–276, 1969.

[151] Jordan L. Hovdebo and Robert C. Myers. Bouncing brane worlds go crunch! *JCAP*, 0311:012, 2003. arXiv:hep-th/0308088 [hep-th].

[152] Pierre-Henri Chavanis. Cosmology with a stiff matter era. *Phys. Rev.*, D92(10):103004, 2015. arXiv:1412.0743 [gr-qc].

[153] Anindya K. Biswas and Sudipta Mukherji. Holography and stiff matter on the brane. *JHEP*, 03:046, 2001. arXiv:hep-th/0102138 [hep-th].

[154] Daniel Harlow and Hirosi Ooguri. Symmetries in quantum field theory and quantum gravity. *Commun. Math. Phys.*, 383(3):1669–1804, 2021. arXiv:1810.05338 [hep-th].

[155] Yiming Chen, Victor Gorbenko, and Juan Maldacena. Bra-ket wormholes in gravitationally prepared states. *JHEP*, 02:009, 2021. arXiv:2007.16091 [hep-th].

[156] Ben Freivogel, Victor Godet, Edward Morvan, Juan F. Pedraza, and Antonio Rotundo. Lessons on Eternal Traversable Wormholes in AdS. *JHEP*, 07:122, 2019. arXiv:1903.05732 [hep-th].

[157] Alex May, Petar Simidzija, and Mark Van Raamsdonk. Negative energy enhancement in layered holographic conformal field theories. *Journal of High Energy Physics*, 2021(8):1–24, 2021.

[158] Brian Swingle and Mark Van Raamsdonk. Enhanced Negative Energy with a Massless Dirac Field. 12 2022. arXiv:2212.02609 [hep-th].

[159] Nima Arkani-Hamed, Jacopo Orgera, and Joseph Polchinski. Euclidean wormholes in string theory. *JHEP*, 12:018, 2007. arXiv:0705.2768 [hep-th].

[160] Jordan S. Cotler, Guy Gur-Ari, Masanori Hanada, Joseph Polchinski, Phil Saad, Stephen H. Shenker, Douglas Stanford, Alexandre Streicher, and Masaki Tezuka. Black Holes and Random Matrices. *JHEP*, 05:118, 2017. arXiv:1611.04650 [hep-th], [Erratum: JHEP 09, 002 (2018)].

[161] Phil Saad, Stephen H. Shenker, and Douglas Stanford. A semiclassical ramp in SYK and in gravity. 6 2018. arXiv:1806.06840 [hep-th].

[162] Douglas Stanford and Edward Witten. JT gravity and the ensembles of random matrix theory. *Adv. Theor. Math. Phys.*, 24(6):1475–1680, 2020. arXiv:1907.03363 [hep-th].

[163] Donald Marolf and Henry Maxfield. Transcending the ensemble: baby universes, spacetime wormholes, and the order and disorder of black hole information. *JHEP*, 08:044, 2020. arXiv:2002.08950 [hep-th].

[164] Phil Saad, Stephen Shenker, and Shunyu Yao. Comments on wormholes and factorization. 7 2021. arXiv:2107.13130 [hep-th].

[165] Phil Saad, Stephen H. Shenker, Douglas Stanford, and Shunyu Yao. Wormholes without averaging. 3 2021. arXiv:2103.16754 [hep-th].

[166] Andreas Blommaert, Luca V. Iliesiu, and Jorrit Kruthoff. Gravity factorized. *JHEP*, 09:080, 2022. arXiv:2111.07863 [hep-th].

[167] Donald Marolf and Jorge E. Santos. AdS Euclidean wormholes. *Class. Quant. Grav.*, 38(22):224002, 2021. arXiv:2101.08875 [hep-th].

[168] Jordan Cotler and Kristan Jensen. Wormholes and black hole microstates in AdS/CFT. *JHEP*, 09:001, 2021. arXiv:2104.00601 [hep-th].

[169] J.B. Hartle and S.W. Hawking. Wave Function of the Universe. *Adv. Ser. Astrophys. Cosmol.*, 3:174–189, 1987.

[170] Ping Gao, Daniel Louis Jafferis, and Aron Wall. Traversable Wormholes via a Double Trace Deformation. *JHEP*, 12:151, 2017. arXiv:1608.05687 [hep-th].

[171] Juan Maldacena, Douglas Stanford, and Zhenbin Yang. Diving into traversable wormholes. *Fortsch. Phys.*, 65(5):1700034, 2017. arXiv:1704.05333 [hep-th].

[172] Juan Maldacena and Xiao-Liang Qi. Eternal traversable wormhole. 4 2018. arXiv:1804.00491 [hep-th].

[173] Juan Maldacena, Alexey Milekhin, and Fedor Popov. Traversable wormholes in four dimensions. 7 2018. arXiv:1807.04726 [hep-th].

[174] Raphael Bousso and Elizabeth Wildenhain. Gravity/ensemble duality. *Phys. Rev. D*, 102(6):066005, 2020. arXiv:2006.16289 [hep-th].

[175] Thomas Hartman, Yikun Jiang, and Edgar Shaghoulian. Islands in cosmology. *JHEP*, 11:111, 2020. arXiv:2008.01022 [hep-th].

[176] Raphael Bousso and Elizabeth Wildenhain. Islands in closed and open universes, 2022.

[177] Peter Breitenlohner and Daniel Z Freedman. Positive energy in anti-de sitter backgrounds and gauged extended supergravity. *Physics letters B*, 115(3):197–201, 1982.

[178] Peter Breitenlohner and Daniel Z Freedman. Stability in gauged extended supergravity. *Annals of physics*, 144(2):249–281, 1982.

[179] T. S. Bunch and P. C. W. Davies. Quantum Field Theory in de Sitter Space: Renormalization by Point Splitting. *Proc. Roy. Soc. Lond. A*, 360:117–134, 1978.

[180] Edward Witten. Anti-de Sitter space, thermal phase transition, and confinement in gauge theories. *Adv. Theor. Math. Phys.*, 2:505–532, 1998. arXiv:hep-th/9803131 [hep-th], [,89(1998)].

[181] B. M. Levitan and M. G. Gasymov. Determination of a Differential Equation by Two of its Spectra. *Russian Mathematical Surveys*, 19(2):R01, April 1964.

[182] Ole H. Hald. The inverse Sturm-Liouville problem with symmetric potentials. *Acta Mathematica*, 141(none):263 – 291, 1978.

[183] Mark Kac. Can one hear the shape of a drum? *The american mathematical monthly*, 73(4P2):1–23, 1966.

[184] Thomas Faulkner, Min Li, and Huajia Wang. A modular toolkit for bulk reconstruction. *JHEP*, 04:119, 2019. arXiv:1806.10560 [hep-th].

[185] Adam G. Riess et al. A Comprehensive Measurement of the Local Value of the Hubble Constant with 1 km s^{-1} Mpc^{-1} Uncertainty from the Hubble Space Telescope and the SH0ES Team. *Astrophys. J. Lett.*, 934(1):L7, 2022. arXiv:2112.04510 [astro-ph.CO].

[186] Senarath de Alwis, Jan Louis, Liam McAllister, Hagen Triendl, and Alexander Westphal. Moduli spaces in AdS_4 supergravity. *JHEP*, 05:102, 2014. arXiv:1312.5659 [hep-th].

[187] Leonard Susskind. The World as a hologram. *J. Math. Phys.*, 36:6377–6396, 1995. arXiv:hep-th/9409089 [hep-th].

[188] Kyriakos Papadodimas and Suvrat Raju. An Infalling Observer in AdS/CFT. *JHEP*, 10:212, 2013. arXiv:1211.6767 [hep-th].

[189] Kyriakos Papadodimas and Suvrat Raju. State-Dependent Bulk-Boundary Maps and Black Hole Complementarity. *Phys. Rev.*, D89(8):086010, 2014. arXiv:1310.6335 [hep-th].

[190] Kyriakos Papadodimas and Suvrat Raju. Remarks on the necessity and implications of state-dependence in the black hole interior. *Phys. Rev.*, D93(8):084049, 2016. arXiv:1503.08825 [hep-th].

[191] Daniel Harlow. Aspects of the Papadodimas-Raju Proposal for the Black Hole Interior. *JHEP*, 11:055, 2014. arXiv:1405.1995 [hep-th].

[192] Pierre Binetruy, Cedric Deffayet, and David Langlois. Nonconventional cosmology from a brane universe. *Nucl. Phys.*, B565:269–287, 2000. arXiv:hep-th/9905012 [hep-th].

[193] Steven S. Gubser. AdS / CFT and gravity. *Phys. Rev.*, D63:084017, 2001. arXiv:hep-th/9912001 [hep-th].

[194] Ivo Savonije and Erik P. Verlinde. CFT and entropy on the brane. *Phys. Lett.*, B507:305–311, 2001. arXiv:hep-th/0102042 [hep-th].

[195] Erik P. Verlinde. On the holographic principle in a radiation dominated universe. 2000. arXiv:hep-th/0008140 [hep-th].

[196] Heliudson Bernardo and Horatiu Nastase. Holographic cosmology from ”dimensional reduction” of $\mathcal{N} = 4$ SYM vs. $\mathrm{AdS}_5 \times \mathrm{S}^5$. *JHEP*, 12:025, 2019. arXiv:1812.07586 [hep-th].

[197] Neven Bilic. Randall-Sundrum versus holographic cosmology. *Phys. Rev.*, D93(6):066010, 2016. arXiv:1511.07323 [gr-qc].

[198] Sanjeev S. Seahra, Chris Clarkson, and Roy Maartens. Delocalization of brane gravity by a bulk black hole. *Class. Quant. Grav.*, 22:L91–L102, 2005. arXiv:gr-qc/0504023 [gr-qc].

[199] Chris Clarkson and Sanjeev S. Seahra. Braneworld resonances. *Class. Quant. Grav.*, 22:3653–3688, 2005. arXiv:gr-qc/0505145 [gr-qc].

[200] Tomas Andrade, Sebastian Fischetti, Donald Marolf, Simon F. Ross, and Moshe Rozali. Entanglement and correlations near extremality: CFTs dual to Reissner-Nordström AdS_5. *JHEP*, 04:023, 2014. arXiv:1312.2839 [hep-th].

[201] S. W. Hawking and Simon F. Ross. Duality between electric and magnetic black holes. *Phys. Rev. D*, 52:5865–5876, Nov 1995.

[202] Andrew Chamblin, Roberto Emparan, Clifford V. Johnson, and Robert C. Myers. Charged ads black holes and catastrophic holography. *Phys. Rev. D*, 60:064018, Aug 1999.

[203] Piyabut Burikham and Chatchai Promsiri. The Mixed Phase of Charged AdS Black holes. *Adv. High Energy Phys.*, 2016:5864672, 2016. arXiv:1408.2694 [hep-th].

[204] William Cottrell, Ben Freivogel, Diego M. Hofman, and Sagar F. Lokhande. How to Build the Thermofield Double State. *JHEP*, 02:058, 2019. arXiv:1811.11528 [hep-th].

[205] John Martyn and Brian Swingle. Product Spectrum Ansatz and the Simplicity of Thermal States. *Phys. Rev. A*, 100(3):032107, 2019. arXiv:1812.01015 [cond-mat.str-el].

[206] Hideo Kodama and Akihiro Ishibashi. Master equations for perturbations of generalized static black holes with charge in higher dimensions. *Prog. Theor. Phys.*, 111:29–73, 2004. arXiv:hep-th/0308128 [hep-th].

[207] Veronika E. Hubeny, Mukund Rangamani, and Tadashi Takayanagi. A Covariant holographic entanglement entropy proposal. *JHEP*, 07:062, 2007. arXiv:0705.0016 [hep-th].

[208] Marco Chiodaroli, Eric D'Hoker, and Michael Gutperle. Simple Holographic Duals to Boundary CFTs. *JHEP*, 02:005, 2012. arXiv:1111.6912 [hep-th].

[209] Saul Perlmutter, Goldhaber Aldering, Gerson Goldhaber, RA Knop, Peter Nugent, Patricia G Castro, Susana Deustua, Sebastien Fabbro, Ariel Goobar, Donald E Groom, et al. Measurements of ω and λ from 42 high-redshift supernovae. *The Astrophysical Journal*, 517(2):565, 1999.

[210] Adam G Riess, Alexei V Filippenko, Peter Challis, Alejandro Clocchiatti, Alan Diercks, Peter M Garnavich, Ron L Gilliland, Craig J Hogan, Saurabh Jha, Robert P Kirshner, et al. Observational evidence from supernovae for an accelerating universe and a cosmological constant. *The Astronomical Journal*, 116(3):1009, 1998.

[211] R. R. Caldwell, Rahul Dave, and Paul J. Steinhardt. Cosmological imprint of an energy component with general equation of state. *Phys. Rev. Lett.*, 80:1582–1585, 1998. arXiv:astro-ph/9708069.

[212] Shao-Jiang Wang. Electroweak relaxation of cosmological hierarchy. *Phys. Rev. D*, 99(2):023529, 2019. arXiv:1810.06445 [hep-th].

[213] Gen Ye and Yun-Song Piao. Is the Hubble tension a hint of AdS phase around recombination? *Phys. Rev. D*, 101(8):083507, 2020. arXiv:2001.02451 [astro-ph.CO].

[214] Koushik Dutta, Ruchika, Anirban Roy, Anjan A. Sen, and M. M. Sheikh-Jabbari. Beyond ΛCDM with low and high redshift data: implications for dark energy. *Gen. Rel. Grav.*, 52(2):15, 2020. arXiv:1808.06623 [astro-ph.CO].

[215] Luca Visinelli, Sunny Vagnozzi, and Ulf Danielsson. Revisiting a negative cosmological constant from low-redshift data. *Symmetry*, 11(8):1035, 2019. arXiv:1907.07953 [astro-ph.CO].

[216] Anjan A. Sen, Shahnawaz A. Adil, and Somasri Sen. Do cosmological observations allow a negative λ?, 2021.

[217] Rodrigo Calderón, Radouane Gannouji, Benjamin L'Huillier, and David Polarski. Negative cosmological constant in the dark sector? *Phys. Rev. D*, 103(2):023526, 2021. arXiv:2008.10237 [astro-ph.CO].

[218] T. Banks and W. Fischler. An Holographic cosmology. 11 2001. arXiv:hep-th/0111142.

[219] Georges Obied, Hirosi Ooguri, Lev Spodyneiko, and Cumrun Vafa. De Sitter Space and the Swampland. 6 2018. arXiv:1806.08362 [hep-th].

[220] Ulf H. Danielsson and Thomas Van Riet. What if string theory has no de Sitter vacua? *Int. J. Mod. Phys. D*, 27(12):1830007, 2018. arXiv:1804.01120 [hep-th].

[221] P. Betzios, E. Kiritsis, and O. Papadoulaki. Euclidean Wormholes and Holography. *JHEP*, 06:042, 2019. arXiv:1903.05658 [hep-th].

[222] Alexander Maloney and Edward Witten. Averaging over Narain moduli space. *JHEP*, 10:187, 2020. arXiv:2006.04855 [hep-th].

[223] Nima Afkhami-Jeddi, Henry Cohn, Thomas Hartman, and Amirhossein Tajdini. Free partition functions and an averaged holographic duality. *JHEP*, 01:130, 2021. arXiv:2006.04839 [hep-th].

[224] Jordan Cotler and Kristan Jensen. AdS_3 gravity and random CFT. *JHEP*, 04:033, 2021. arXiv:2006.08648 [hep-th].

[225] Juan Maldacena and Leonard Susskind. Cool horizons for entangled black holes. *Fortsch. Phys.*, 61:781–811, 2013. arXiv:1306.0533 [hep-th].

[226] Mark Van Raamsdonk. Evaporating Firewalls. *JHEP*, 11:038, 2014. arXiv:1307.1796 [hep-th].

[227] Petar Simidzija and Mark Van Raamsdonk. Holo-ween. *JHEP*, 12:028, 2020. arXiv:2006.13943 [hep-th].

[228] Mark Van Raamsdonk. Building up spacetime with quantum entanglement II: It from BC-bit. 2018. arXiv:1809.01197 [hep-th].

[229] Alex Hamilton, Daniel N. Kabat, Gilad Lifschytz, and David A. Lowe. Local bulk operators in AdS/CFT: A Boundary view of horizons and locality. *Phys. Rev. D*, 73:086003, 2006. arXiv:hep-th/0506118.

[230] Zhi Wang, Zekun Xu, Shuyan Zhou, and Yang Zhou. Partial reduction and cosmology at defect brane. *JHEP*, 05:049, 2022. arXiv:2112.13782 [hep-th].

[231] Zhong-Ying Fan. On holographic braneworld cosmology. 6 2021. arXiv:2106.14376 [hep-th].

[232] Ahmed Almheiri. Holographic Quantum Error Correction and the Projected Black Hole Interior. 2018. arXiv:1810.02055 [hep-th].

[233] Xi Dong, Xiao-Liang Qi, Zhou Shangnan, and Zhenbin Yang. Effective entropy of quantum fields coupled with gravity. *Journal of High Energy Physics*, 2020(10):1–52, 2020.

[234] James B. Hartle, S. W. Hawking, and Thomas Hertog. Accelerated expansion from negative λ, 2012.

[235] Latham Boyle, Kieran Finn, and Neil Turok. C p t-symmetric universe. *Physical review letters*, 121(25):251301, 2018.

[236] Panos Betzios, Elias Kiritsis, and Olga Papadoulaki. Interacting systems and wormholes. *JHEP*, 02:126, 2022. arXiv:2110.14655 [hep-th].

[237] E. Antonyan, J.A. Harvey, and D. Kutasov. Chiral symmetry breaking from intersecting D-branes. *Nucl. Phys. B*, 784:1–21, 2007. arXiv:hep-th/0608177.

[238] Davide Gaiotto and Edward Witten. S-Duality of Boundary Conditions In N=4 Super Yang-Mills Theory. *Adv. Theor. Math. Phys.*, 13(3):721–896, 2009. arXiv:0807.3720 [hep-th].

[239] Eric D'Hoker, John Estes, and Michael Gutperle. Exact half-BPS Type IIB interface solutions. I. Local solution and supersymmetric Janus. *JHEP*, 06:021, 2007. arXiv:0705.0022 [hep-th].

[240] Eric D'Hoker, John Estes, and Michael Gutperle. Exact half-BPS Type IIB interface solutions. II. Flux solutions and multi-Janus. *JHEP*, 06:022, 2007. arXiv:0705.0024 [hep-th].

[241] Ofer Aharony, Leon Berdichevsky, Micha Berkooz, and Itamar Shamir. Near-horizon solutions for D3-branes ending on 5-branes. *Phys. Rev.*, D84:126003, 2011. arXiv:1106.1870 [hep-th].

[242] Benjamin Assel, Costas Bachas, John Estes, and Jaume Gomis. Holographic Duals of D=3 N=4 Superconformal Field Theories. *JHEP*, 08:087, 2011. arXiv:1106.4253 [hep-th].

[243] Constantin Bachas and Ioannis Lavdas. Massive Anti-de Sitter Gravity from String Theory. *JHEP*, 11:003, 2018. arXiv:1807.00591 [hep-th].

[244] Christoph F. Uhlemann. Islands and Page curves in 4d from Type IIB. *JHEP*, 08:104, 2021. arXiv:2105.00008 [hep-th].

[245] Massimo Porrati. Mass and gauge invariance 4. Holography for the Karch-Randall model. *Phys. Rev. D*, 65:044015, 2002. arXiv:hep-th/0109017.

[246] D. Z. Freedman, S. S. Gubser, K. Pilch, and N. P. Warner. Renormalization group flows from holography supersymmetry and a c theorem. *Adv. Theor. Math. Phys.*, 3:363–417, 1999. arXiv:hep-th/9904017.

[247] Jan Louis and Hagen Triendl. Maximally supersymmetric ads 4 vacua in n = 4 supergravity. *Journal of High Energy Physics*, 2014(10), Oct 2014.

[248] Parinya Karndumri. Holographic rg flows and symplectic deformations of n= 4 gauged supergravity. *Physical Review D*, 105(8):086009, 2022.

[249] Don N. Page. Will Entropy Decrease if the Universe Recollapses? *Phys. Rev. D*, 32:2496, 1985.

[250] Ian Affleck and Michael Dine. A New Mechanism for Baryogenesis. *Nucl. Phys. B*, 249:361–380, 1985.

[251] Sean M Carroll. Quintessence and the rest of the world: suppressing long-range interactions. *Physical Review Letters*, 81(15):3067, 1998.

[252] Luca Amendola. Coupled quintessence. *Physical Review D*, 62(4):043511, 2000.

[253] Seamus Fallows and Simon F. Ross. Islands and mixed states in closed universes. *JHEP*, 07:022, 2021. arXiv:2103.14364 [hep-th].

[254] Ricardo Espíndola, Bahman Najian, and Dora Nikolakopoulou. Islands in FRW Cosmologies. 3 2022. arXiv:2203.04433 [hep-th].

[255] Raphael Bousso and Joseph Polchinski. Quantization of four form fluxes and dynamical neutralization of the cosmological constant. *JHEP*, 06:006, 2000. arXiv:hep-th/0004134.

[256] Tadakatsu Sakai and Shigeki Sugimoto. Low energy hadron physics in holographic QCD. *Prog. Theor. Phys.*, 113:843–882, 2005. arXiv:hep-th/0412141.

[257] Izrail Solomonovich Gradshteyn and Iosif Moiseevich Ryzhik. *Table of integrals, series, and products*. Academic press, 2014.

[258] Ofer Aharony, Donald Marolf, and Mukund Rangamani. Conformal field theories in anti-de Sitter space. *JHEP*, 02:041, 2011. arXiv:1011.6144 [hep-th].

[259] Eliot Hijano and Dominik Neuenfeld. Soft photon theorems from CFT Ward identites in the flat limit of AdS/CFT. *JHEP*, 11:009, 2020. arXiv:2005.03667 [hep-th].

[260] Edward Witten. SL(2,Z) action on three-dimensional conformal field theories with Abelian symmetry. In *From Fields to Strings: Circumnavigating Theoretical Physics: A Conference in Tribute to Ian Kogan*, pages 1173–1200, 7 2003.

[261] Ho-Ung Yee. A Note on AdS / CFT dual of SL(2,Z) action on 3-D conformal field theories with U(1) symmetry. *Phys. Lett. B*, 598:139–148, 2004. arXiv:hep-th/0402115.

[262] Donald Marolf and Simon F. Ross. Boundary Conditions and New Dualities: Vector Fields in AdS/CFT. *JHEP*, 11:085, 2006. arXiv:hep-th/0606113.

[263] Samuel Bilson. Extracting Spacetimes using the AdS/CFT Conjecture: Part II. *JHEP*, 02:050, 2011. arXiv:1012.1812 [hep-th].

[264] Brett McInnes. Answering a basic objection to bang / crunch holography. *JHEP*, 10:018, 2004. arXiv:hep-th/0407189.

[265] Rolando Cardenas, Tame Gonzalez, Yoelsy Leiva, Osmel Martin, and Israel Quiros. A model of the universe including dark energy accounted for by both a quintessence field and a (negative) cosmological constant. *Phys. Rev. D*, 67:083501, 2003. arXiv:astro-ph/0206315.

[266] Hirosi Ooguri and Cumrun Vafa. Non-supersymmetric AdS and the Swampland. *Adv. Theor. Math. Phys.*, 21:1787–1801, 2017. arXiv:1610.01533 [hep-th].

[267] Pantheon+SH0ES 2021/2022 data release. `https://pantheonplussh0es.github.io`.

[268] Eleonora Di Valentino, Olga Mena, Supriya Pan, Luca Visinelli, Weiqiang Yang, Alessandro Melchiorri, David F. Mota, Adam G. Riess, and Joseph Silk. In the realm of the Hubble tension—a review of solutions. *Class. Quant. Grav.*, 38(15):153001, 2021. arXiv:2103.01183 [astro-ph.CO].

[269] Dillon Brout et al. The Pantheon+ Analysis: Cosmological Constraints. *Astrophys. J.*, 938(2):110, 2022. arXiv:2202.04077 [astro-ph.CO].

[270] Sumit K. Garg and Chethan Krishnan. Bounds on Slow Roll and the de Sitter Swampland. *JHEP*, 11:075, 2019. arXiv:1807.05193 [hep-th].

[271] Hirosi Ooguri, Eran Palti, Gary Shiu, and Cumrun Vafa. Distance and de Sitter Conjectures on the Swampland. *Phys. Lett. B*, 788:180–184, 2019. arXiv:1810.05506 [hep-th].

[272] Mark Van Raamsdonk and Chris Waddell. Possible hints of decreasing dark energy from supernova data. 5 2023. arXiv:2305.04946 [astro-ph.CO].

[273] G. W. Gibbons and Neil Turok. The Measure Problem in Cosmology. *Phys. Rev. D*, 77:063516, 2008. arXiv:hep-th/0609095.

[274] Alexandre Yale. Simple counterterms for asymptotically AdS spacetimes in Lovelock gravity. *Phys. Rev.*, D84:104036, 2011. arXiv:1107.1250 [gr-qc].

[275] J. R. Taylor. *Scattering Theory*. New York: Wiley, 1972.

[276] G. J. Galloway, K. Schleich, D. M. Witt, and E. Woolgar. Topological censorship and higher genus black holes. *Phys. Rev. D*, 60:104039, 1999. arXiv:gr-qc/9902061.

[277] Thomas Faulkner, Robert G. Leigh, Onkar Parrikar, and Huajia Wang. Modular Hamiltonians for Deformed Half-Spaces and the Averaged Null Energy Condition. *JHEP*, 09:038, 2016. arXiv:1605.08072 [hep-th].

[278] Thomas Hartman, Sandipan Kundu, and Amirhossein Tajdini. Averaged Null Energy Condition from Causality. *JHEP*, 07:066, 2017. arXiv:1610.05308 [hep-th].

[279] David Colton. The confluent hypergeometric function. by herbert buchholz. springer-verlag, new york (1969). 238 pp. *Canadian Mathematical Bulletin*, 13(1):164–164, 1970.